Organically Functionalized Mesoporous Silica as a Support for Synthesis and Catalysis

by

Kevin Andrew McEleney

A thesis submitted to the Department of Chemistry
in conformity with the requirements for
the degree of Doctor of Philosophy

Queen's University
Kingston, Ontario, Canada
April 2009

Abstract

Mesoporous silicates are excellent materials for supported catalysis due to their ease of functionalization, tunable pore size and high surface areas. Mesoporous silicates have been utilized in a variety of applications such as drug delivery scaffolds and catalyst supports. Functionalization of the surface can be achieved by either grafting of alkoxy silanes or co-condensation of the organosilane with the inorganic silica source.

My research in this area can be divided into two components. In the first, we address the significant issue of metal contamination after reactions that are catalyzed by transition metals. In the second, we examine the design of new catalysts based on organic/inorganic composites.

Ruthenium catalyzed processes such as olefin metathesis or asymmetric hydrogenation, are often underutilized due to the difficulty of removing the ruthenium by-products. Attempts to remove ruthenium involve treating the solution with a scavenging reagent followed by silica chromatography. Often these scavenging agents are expensive phosphines or toxic agents like lead tetra-acetate. SBA-15 functionalized with aminopropyl triethoxysilane displays a high affinity for ruthenium. Furthermore, it can be utilized to remove ruthenium by-products from olefin metathesis or hydrogenation reactions without the need for silica chromatography.

We have also prepared sulfur-functionalized mesoporous silicates that have a high affinity for palladium. The materials after loading prove to be active catalysts for a variety of palladium catalyzed processes such as

Suzuki-Miyaura and Sonogashira couplings. The catalysts are recyclable with moderate loss of activity and structure, depending on the method of incorporation of the thiol. We have characterized the as-synthesized and used catalysts by nitrogen sorption, TEM, X-ray photoelectron spectroscopy (XPS) and a variety of homogeneity tests were performed on the catalysts.

Periodic mesoporous organosilicates (PMOs) are a well known class of inorganic-organic hybrid materials. The majority of PMOs prepared utilize simple organic bridges such as ethyl, phenyl or biphenyl. The use of a chiral organic bridging group, such as BINAP, allows the synthesis of chiral PMOs with possible applications in catalysis and separation science. The synthesis of a triethoxysilyl functionalized BINAP as well as its incorporation into PMO materials with 4,4'-bistriethoxysilyl biphenyl or tetraethylorthosilicate as co-silica sources are described.

Acknowledgements

When completing a task as monumental as a doctoral thesis, you inevitably become indebted to a number of people who lend you assistance along the way. For those who I may unwittingly leave out, a hearty thank you for sharing your wisdom and knowledge.

I would like to thank my supervisor Dr. Cathleen Crudden for taking a chance on a biochemist who no longer wanted to study biochemistry. My synthetic skills were limited when I joined your lab but I was grateful for the opportunity to learn. Your encouragement and guidance were invaluable to me in completing this work.

Over the course of my studies I have been taught by a number of talented individuals. I owe my choice of field to Dr. Walter Szarek, he taught me organic chemistry as an undergraduate and opened my eyes to the world of chemistry. I would not be writing this without his enthusiastic love of teaching and chemistry. I would also like to thank Dr. Hugh Horton for all of his time spent mentoring me and teaching me surface science.

Of course the heart of your interactions while a graduate student is with the members of your lab. To all of the people I have worked with over my studies a warm thank you for your efforts. You have taught me many things about being a chemist and about life. I would especially like to thank Stephanie MacQuarrie who was always there to encourage me when I thought that I would never finish this degree. I would also like to thank John Carran for all of our fruitful discussions. I have also had the pleasure of

supervising undergraduate student researchers; Larbi Benhabib, Darren Finnamore and Alex Goldberg during my degree. I want to thank each of you for your hard work, I take away fond memories of our shared time in the lab.

Chemistry is a multidisciplinary field and it is impossible to have expertise in all aspects. Thus I would like to thank all of the people who have lent their time to help me. In particular I would like to thank Dr. Francoise Sauriol for her assistance with my many questions about NMR. I would also like to thank NSERC and Queen's University for funding my research.

I didn't get to this point by myself, my family has always been there to support me and encourage my academic endeavors. I want to thank all of you for being there for me. I would like to dedicate my thesis to my Gran, Marion Graham, you always pushed me to be the best that I could be but never judged me when I failed. I only wish you were still here to enjoy this with me.

Finally, I want to thank my partner, Jennifer. You have helped me through this process more than you know. You were my motivation to stick to it. I can't thank you enough.

Statement of Originality

I hereby certify that all of the work described within this thesis is the original work of the author. Any published (or unpublished) ideas and/or techniques from the work of others are fully acknowledged in accordance with the standard referencing practices.

Kevin McEleney

April 2009

Table of Contents

Abstract ii

Acknowledgements iv

Statement of Originality vi

Table of Contents vii

List of Figures and Schemes x

List of Tables xvii

List of Abbreviations xix

Chapter 1: Introduction to Mesoporous Silica

1.1 Introduction 1

1.2 References 24

Chapter 2: Removal of Ruthenium Residues Using Amino-Functionalized SBA-15

2.1 Introduction 28

2.2 Results and Discussion 47

2.3 Conclusions 60

2.4 References 62

Chapter 3: Palladium Loaded Thiol-Functionalized SBA-15. Catalyst Activity, Reusability, and Stability

3.1 Introduction 65

3.2 Results and Discussion 80

3.2.1 Catalyst Preparation 81

3.2.2 Application to Various Coupling Reactions 85

3.2.3 SBA-15-SH-Pd in Semi-Hydrogenation Reactions 90

3.2.4 Mechanism of Action 93

3.2.5 Material Stability and Reusability 101

3.3 Conclusions 105

3.4 References 107

Chapter 4: X-Ray Photoelectron Spectroscopy Studies of SBA-15-SH-Pd

4.1 Introduction 110

4.2 Results and Discussion 115

4.3 Conclusions 126

4.4 References 127

Chapter 5: Preparation and Characterization of BINAP Functionalized Periodic Mesoporous Organosilica

5.1 Introduction 128

5.2 Results and Discussion 154

5.3 Conclusions 175

5.4 References 177

Chapter 6: Experimental Procedures

6.1 General Procedures 180

6.2 Experimental Procedures from Chapter 2 182

6.3 Experimental Procedures from Chapter 3 186

6.4 Experimental Procedures from Chapter 4 203

6.5 Experimental Procedures from Chapter 5 204

6.6 References 223

Appendix A: Tables of X-Ray Photoelectron Spectroscopy Data 224

References 228

Appendix B: Crystallography Data for 5,5'-Diiodo BINAPO 229

List of Figures and Schemes

Chapter 1: Introduction to Mesoporous Silica

Figure 1.1: TEM images of MCM-41 and MCM-48 3

Figure 1.2: Surfactants for synthesis of mesoporous materials 4

Figure 1.3: TEM images of SBA-15 and a platinum replica of SBA-15 5

Figure 1.4: Comparison of cooperative self assembly and liquid Crystal templating pathways 6

Figure 1.5: Representation of surfactant-silica interactions 8

Figure 1.6: Examples of IUPAC type I and type IV isotherms 11

Figure 1.7: Organosilanes for the functionalization of silica 14

Figure 1.8: Sulfonic acid functionalized silica, catalyzed addition of acetic acid to camphene 16

Figure 1.9: Base-catalyzed Knoevenagel condensation with silica 17

Figure 1.10: TBS functionalized silica for base catalyzed Michael addition 17

Figure 1.11: Rhodium-silica complex for bifunctional catalysis 18

Figure 1.12: Cinchona alkaloid functionalized silica for asymmetric Michael addition 19

Figure 1.13: Cinchona alkaloid functionalized silica for asymmetric dihydroxylation 19

Figure 1.14: Copper functionalized silica for azidiridation of styrene 20

Figure 1.15: Immobilized rhodium catalyst for hydrogenation 21

Figure 1.16: Immobilized salen complex for asymmetric hydrogenation of imines 21

Figure 1.17: Immobilized Mn-salen complexes for asymmetric epoxidation 22

Scheme 1.1: Functionalization of MCM-41 with ephedrine 20

Chapter 2: Removal of Ruthenium Residues Using Amino-Functionalized SBA-15

Figure 2.1: Comparison of classical and bifunctional mechanisms for hydrogenation of ketones 30

Figure 2.2: Application of asymmetric hydrogenation to pharmaceutical molecules 31

Figure 2.3: Shrock's molybdenum based metathesis catalyst 32

Figure 2.4: Ruthenium based olefin metathesis catalysts 33

Figure 2.5: Complex macrocycles formed by ring closing metathesis 33

Figure 2.6: Water soluble phosphine scavenger and poly ethylene glycol modified Ru catalyst employed by Grubbs 37

Figure 2.7: Polymer bound phosphine scavenging resin 38

Figure 2.8: Carbon monoxide poisoned metathesis catalyst and isocyanate for ruthenium remediation 39

Figure 2.9: Polymer supported metathesis catalyst 41

Figure 2.10: Metathesis catalysts immobilized through the NHC 42

Figure 2.11: Supported metathesis catalysts through anionic ligands 43

Figure 2.12: Monolith and silica supported metathesis catalysts 44

Figure 2.13: Alkoxyphenyl substituted metathesis catalyst 44

Figure 2.14: Metathesis catalysts with modified alkylidenes 45

Figure 2.15: Poly vinyl pyridine supported Grubbs third generation catalyst 46

Figure 2.16 Comparison of N and S based scavengers 48

Figure 2.17: Ligands employed for ruthenium removal 49

Figure 2.18: Nitrogen porosimetry of amino functionalized SBA-15 50

Figure 2.19: Scavenging of Grubbs generation I from THF 55

Figure 2.20: ^{1}H NMR of metathesis product 58

Scheme 2.1: Asymmetric hydrogenation of functionalized ketones 30

Equation 2.1: Olefin metathesis and remediation with Grubbs first generation catalyst 58

Equation 2.2: Asymmetric hydrogenation using Noyori's catalyst 60

Chapter 3: Palladium Loaded Thiol-Functionalized SBA-15. Catalyst Activity, Reusability, and Stability

Figure 3.1: Palladium catalyzed coupling reactions 65

Figure 3.2: Pharmaceuticals prepared by Suzuki-Miyaura coupling 66

Figure 3.3: Synthetic improvement by using Suzuki-Miyaura coupling 67

Figure 3.4: Pharmaceuticals prepared by Sonogashira coupling 67

Figure 3.5: Ionic gels for immobilization of palladium 70

Figure 3.6: Immobilized SCS pincer complex 71

Figure 3.7: Pyridyl-imine palladium complex 72

Figure 3.8: Palladacycle catalyst 72

Figure 3.9: Representation of a hot filtration test 74

Figure 3.10: Leaching and conversion during a Mizoroki-Heck reaction 76

Figure 3.11: Methoxy carbonylation of a vinyl halide 78

Figure 3.12: Three phase test used by Davies *et al.* 79

Figure 3.13: Nitrogen porosimetry of SBA-15-SH materials 82

Figure 3.14: TEM images of SBA-15-SH 82

Figure 3.15: TEM images of SBA-15-SH-Pd after catalysis in air 84

Figure 3.16: TEM images of SBA-15-SH-Pd after catalysis in argon 84

Figure 3.17: Pharmaceutical intermediates using palladium catalyzed coupling reactions 87

Figure 3.18: Potential chelation site for palladium in a calcium channel blocker precursor 89

Figure 3.19: Catalyst poisoning experiments 95

Figure 3.20: Illustration of catalyst poisoning 97

Figure 3.21: Recycling of Suzuki-Miyaura reaction in air 101

Figure 3.22: Effect of recycling on Pd leaching 102

Figure 3.23: Effect of recycling on pore structure 102

Figure 3.24: Comparison of stability of grafted and co condensed catalysts after use in the Suzuki-Miyaura reaction 103

Figure 3.25: Effect of recycling on pore structure of DPS-SBA-15-SH-Pd 104

Figure 3.26: Effect of recycling on pore structure of DMS-SBA-15-SH-Pd 105

Scheme 3.1: Synthesis of a YC-1 precursor 88

Scheme 3.2: Synthesis of a calcium channel blocker precursor 89

Scheme 3.3: Synthesis of an ABT-100 precursor 90

Scheme 3.4: Three phase test for Suzuki-Miyaura reaction 98

Scheme 3.5: Synthesis of immobilized aryl halide for three phase test 99

Scheme 3.6: Synthesis of immobilized aryl halide with no free amines 100

Equation 3.1: Test reaction for Suzuki-Miyaura coupling 83

Equation 3.2: Test reaction for Sonogashira coupling 86

Equation 3.3: Hydrogenation of diphenylacetylene 91

Chapter 4: X-Ray Photoelectron Spectroscopy Studies of SBA-15-SH-Pd

Figure 4.1: Chelated Pd(II) complexes 113

Figure 4.2: XPS and XAES spectra of C, Pd, S and Si from SBA-15-SH-Pd 116

Figure 4.3: Wagner chemical state plot for palladium 117

Figure 4.4: Expansion of Wagner plot for palladium 118

Figure 4.5: Wagner chemical state plot for sulfur 122

Figure 4.6: Expansion of Wagner plot for sulfur 123

Equation 4.1: Definition of Auger parameter 111

Equation 4.2: Relationship between Auger parameter and extra atomic relaxation 111

Equation 4.3: Contribution of ground state and relaxation energy differences to the difference in binding energy of two chemical species 111

Chapter 5: Preparation and Characterization of BINAP Functionalized Periodic Mesoporous Organosilica

Figure 5.1: Organic bridged polysilanes for materials synthesis 129

Figure 5.2: Cleavable bridging groups 130

Figure 5.3: Organometallic bridged silsesquioxane precursors 131

Figure 5.4: Crystallinity of the pore walls in phenylene PMO 135

Figure 5.5: Crystallinity of the pore walls in biphenylene PMO 136

Figure 5.6: Non-rigid PMO precursors 137

Figure 5.7: Chiral PMO precursors 138

Figure 5.8: Chiral surfactants for preparation of chiral silica 141

Figure 5.9: SEM image of helically twisted silica 142

Figure 5.10: Diastereomeric rotamers of amino acid based surfactant 143

Figure 5.11: SEM image of helical silica without chiral surfactant template 144

Figure 5.12: Restricted rotation of 2,2'-6,6' substituted biphenyl 145

Figure 5.13: Chiral biphenyl monomer 146

Figure 5.14: Circular dichroism spectra of chiral biphenyl PMOs 146

Figure 5.15: Polymeric BINOL and BINAP ligands 148

Figure 5.16: Polymeric BINOL ligand 149

Figure 5.17: Bifunctional BINOL-BINAP polymer 149

Figure 5.18: Substrate for tandem bifunctional catalysis with BINOL-BINAP polymer 150

Figure 5.19: Silica immobilized BINOL 151

Figure 5.20: Immobilized BINAP by electrostatics and hydrogen bonding 152

Figure 5.21: Silica Immobilized BINAP 153

Figure 5.22: Alternative methods for incorporating trialkoxysilane 160

Figure 5.23: Proposed 4,4'-disubsttuted BINAP monomer 161

Figure 5.24: Crystallographic representations of 5,5'-diiodo BINAPO 168

Figure 5.25: Nitrogen porosimetry of BINAPO/BiPh PMOs 170

Figure 5.26: TEM images of BINAPO/BiPh PMOs 171

Figure 5.27: Circular dichroism spectra of diiodo BINAPO 172

Figure 5.28: Circular dichroism spectra of BINAPO/BiPh PMOs 172

Figure 5.29: Nitrogen porosimetry of BINAPO/TEOS PMOs 173

Figure 5.30: Circular dichroism spectra of BINAPO/TEOS PMOs 174

Scheme 5.1: Decomposition of bridging methylene groups 132

Scheme 5.2: Photocatalyzed di-π-methane rearrangement 139

Scheme 5.3: Proposed synthesis of bis-silyl BINOL monomer 155

Scheme 5.4: Synthesis of 4,4'-Bis(triethoxysilyl)BINAPO 162

Scheme 5.5: Regioselective bromination of BINAPO 163

Scheme 5.6: Attempted Grignard synthesis from dibromo-BINAPO 164

Scheme 5.7: Direct synthesis of diiodo BINAPO 167

Scheme 5.8: Masuda reaction products for 5,5'-diiodo BINAPO 169

Equation 5.1: Preparation of propylsilyl functionalized BINOL monomer 156

Equation 5.2: Addition of siloxy groups by Grignard Functionalization 157

Equation 5.3: Direct metallation and siloxy functionalization of BINOL 157

Equation 5.4: Methoxy protection of BINOL 158

Equation 5.5: Siloxy functionalization of methoxy BINOL 159

Equation 5.6: Siloxy functionalization of p-bromoanisole 159

Equation 5.7: Aromatic Finkelstein reaction 165

Equation 5.8: Aromatic Finkelstein with dibromo BINAPO 165

Equation 5.9: Masuda reaction of 4,4'-diiodo BINAPO 166

List of Tables

Chapter 2: Removal of Ruthenium Residues Using Amino-Functionalized SBA-15

Table 2.1: Comparison of N and S based ruthenium scavengers in water 49

Table 2.2: Nitrogen porosimetry of ordered ruthenium scavengers 50

Table 2.3: Comparison of amine scavengers at low ruthenium concentrations 52

Table 2.4: Comparison of amine scavengers at high ruthenium concentrations 52

Table 2.5: Ruthenium scavenging from THF solutions 54

Table 2.6: Ruthenium scavenging from literature sources 56

Table 2.7: Ruthenium remediation from olefin metathesis with Grubbs first generation catalyst 59

Chapter 3: Palladium Loaded Thiol-Functionalized SBA-15. Catalyst Activity, Reusability, and Stability

Table 3.1: Suzuki-Miyaura coupling with SBA-15-SH-Pd 83

Table 3.2: Effect of S:Pd ratio on Suzuki-Miyaura coupling 85

Table 3.3: Sonogashira coupling with SBA-15-SH-Pd 86

Table 3.4: Hydrogenation of diphenylacetylene with supported palladium catalysts 91

Table 3.5: Summary of three phase test results 99

Table 3.6: Recycling studies with protected catalysts in an inert atmosphere 104

Chapter 5: Preparation and Characterization of BINAP Functionalized Periodic Mesoporous Organosilica

Table 5.1: Nitrogen porosimetry characterication of BINAPO/BiPh PMOs 170

Table 5.2: Nitrogen porosimetry characterication of BINAPO/TEOS PMOs 173

List of Abbreviations

α’	Auger parameter
Å	Ångstrom
Ac	acetyl
APTES	aminopropyl triethoxysilane
Ar	aryl
BE	binding energy
BET	Brunauer-Emmett-Teller
BINAP	2,2’-Bis(diphneylphosphino)-1,1’-binaphthyl
BINAPO	2,2’-Bis(diphneylphosphino)-1,1’-binaphthyl dioxide
BINOL	1,1’-binaphth-2,2’-diol
BiPh	biphenyl
BJH	Barrett-Joyner-Halenda
°C	degree Celsius
CD	circular dichroism
CM	cross methathesis
cod	cyclooctadiene
CP	cross polarization
CTAB	cetyl trimethyl ammonium bromide
CV	column volume
dba	dibenzylideneacetone
DCM	dichloromethane
DMF	dimethylformamide
DMS	dimethylsilyl
DMSO	dimethylsulfoxide
DPS	diphenylsilyl

ε	ground state energy
ee	enantiomeric excess
EISA	evaporation induced self assembly
EO	ethylene oxide
Et	ethyl
EtOAc	ethyl acetate
eV	electron volt
EXAFS	extended X-ray absorption fine structure
F127	Pluronic F127
h	hours
I	inorganic silica species
ICPMS	inductively coupled plasma mass spectrometry
^{i}Pr	isopropyl
IR	infrared
IUPAC	International Union of Pure and Applied Chemists
KE	kinetic energy
M41S	MCM-41 family of materials
MAS	magic angle spinning
MCM	Mobil composition of matter
Me	methyl
MeOH	methanol
Mes	2,4,6-trimethylbenzene
min	minute
MOM	methoxymethyl
MPTMS	mercaptopropyl trimethoxysilane
NHC	N-heterocyclic carbene
nm	nanometer

NMR	nuclear magnetic resonance
P123	Pluronics P123
PEG	poly ethylene glycol
Ph	phenyl
PhBpin	pinacol ester of phenyl boronic acid
PL-DETA	Polymer Labs diethylenetriamine
PL-EDA	Polymer Labs ethylenediamine
PMO	periodic mesoporous organosilica
PO	propylene oxide
ppb	parts per billion
ppm	parts per million
PS	poly styrene
psig	pounds per square inch gauge
PVPy	poly vinyl pyridine
Pyr	pyridine
Q_n	silicon bearing 4 oxygen and n Si-O-Si linkages
R_{ea}	extra atomic relaxation energy
RCM	ring closing metathesis
ROMP	ring opening metathesis polymerization
s	second
S	surfactant
SAM	self assembled monolayer
SBA	Santa Barbara amorphous type material
SBA-15-SH	thiol modified SBA-15
SBA-15-SH-Pd	thiol modified SBA-15 loaded with palladium
SEM	scanning electron microscopy
SiO_2	amorphous silica

T_n	silicon bearing 3 oxygen and n Si-O-Si linkages
TBD	1,5,7-triazabicyclo[4.4.0]dec-5-ene
^{t}Bu	tert-butyl
TEM	transmission electron microscopy
TEOS	tetraethylorthosilicate
TFA	trifluoroacetic acid
TGA-MS	thermogravimetric analysis mass spectrometry
THF	tetrahydrofuran
THMP	tris(hydroxymethyl)phosphine
TLC	thin layer chromatography
TMAPS	N-trimethoxysilylpropyl-N,N,N-trimethyl ammonium chloride
TMB	1,3,5 trimethylbenzene
TMOS	tetramethylorthosilicate
TMS	trimethylsilyl
TOF	turnover frequency
TON	turnover number
TPPO	triphenylphosphine oxide
Ts	*p*-toluenesulfonate
UV	ultraviolet
X	halide/counterion
XAE	X-ray induced Auger electron
XAES	X-ray induced Auger electron spectroscopy
XANES	X-ray absorption near edge structure
XP	X-ray photoelectron
XPS	X-ray photoelectron spectroscopy
XRD	X-ray diffraction

Chapter 1: Introduction to Mesoporous Silica

1.1 Introduction

The discovery of the M41S family of materials in the early 90s led to an explosion of research in the field of mesoporous silica[1,2]. Prior to this discovery, mesoporous solids were limited to materials that had irregularly spaced pores and broad pore size distributions[3,4]. Continued research into ordered porous silicas has allowed for the synthesis of materials with control of pore size, mesostructure and morphology. The ability to vary these properties is vital for application of these materials in fields such as sensing, optics, catalysis, adsorption, separation and host guest chemistry. Furthermore, these synthetic methods have been expanded to include a variety of other ordered materials including metal oxides other than silica[5-12], metal sulfides[13-15], metals[16-18], carbon[19-21] and hybrid organosilicas[22-26].

Mesoporous silicas were initially examined as replacements for zeolites, which are microporous aluminosilicates, whose pore sizes of up to 1.2 nm were too small for large molecules to enter. However, there are many differences between mesoporous silicas and zeolites. Zeolites are near perfect inorganic crystals based on an aluminosilicate tetrahedron. As the crystallinity of zeolites is very rigid, these materials have a high hydrothermal stability. Furthermore, there are almost no three-coordinate defect sites and therefore zeolites lack abundant surface hydroxyl groups. Mesoporous silicas on the other hand are based on a periodic arrangement of silicon oxides in

the walls with a lower degree of condensation in the walls leading to a greater number of surface hydroxyl groups. This leads to a less crystalline wall structure, which consequently lowers the hydrothermal stability of mesoporous silicas relative to zeolites. These surface hydroxyls are important for post synthesis functionalization as will be discussed later.

Mesoporous silicas can also be prepared under a wider range of synthesis conditions. Unlike zeolites that require aqueous conditions for synthesis, mesoporous silicas can be formed in organic solvents by evaporation induced self assembly (EISA). This has permitted the preparation of mesoporous silica thin films, monoliths and fibers. Moreover, mesoporous silicas have been prepared over a wide range of pH values from 0 to 12. Zeolites, on the other hand, can only be prepared in basic solutions[2]. Despite these differences, zeolites and mesoporous silicas have found differing and complementary applications in a variety of industries, with zeolites being used for applications requiring high stability and mesoporous silicas offering ease of functionalization and accessibility.

MCM-41, perhaps the most well known of the M41S family of silicas contains a two-dimensional hexagonally ordered pore network[1]. The porous structure is formed by the co-operative self-assembly of a cationic surfactant, usually cetyl-trimethylammonium bromide (CTAB), in the presence of a silica source under basic conditions. These conditions result in materials with high surface areas, large pore sizes and pore volumes. The pore sizes of these materials can be modified by altering the length of the alkyl tail of the

ammonium surfactant or by incorporating a swelling agent such as 1,3,5-trimethylbenzene (TMB) into the synthesis mixture[1]. In spite of its well-ordered structure, MCM-41 has low hydrothermal stability likely due to the thin, amorphous pore walls (~10 Å). The morphology of MCM-41 can be changed by hydrothermal treatment at 110 °C. This converts the 2D hexagonal arrangement of the pores into a cubic arrangement. The resulting material is MCM-48, which can also be synthesized by increasing the surfactant to silica molar ratio to greater than one (Figure 1.1)[1].

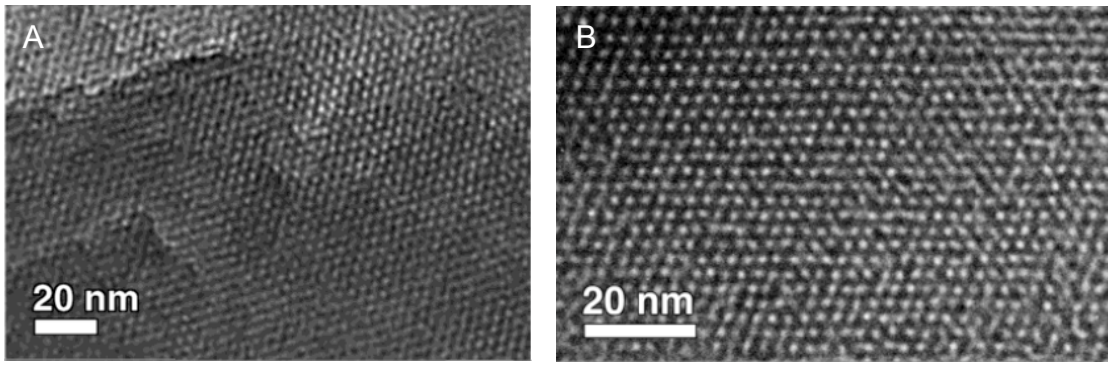

Figure 1.1: TEM images of MCM-41 (A) and MCM-48 (B). Reproduced from reference 27.

The range of surfactants that can be employed has since been expanded to include other cationic surfactants, anionic and nonionic surfactants (Figure 1.2). The cationic surfactants have high solubility and can be used to generate a variety of mesostructures[28-30]. They have been used in both acidic and basic syntheses but are expensive and toxic. Anionic surfactants have not been explored as extensively as other surfactant types, but they have shown promise as templates for mesoporous materials[31].

Nonionic surfactants have been widely used to generate a multitude of mesostructures[32-34] due to their low cost and low toxicity.

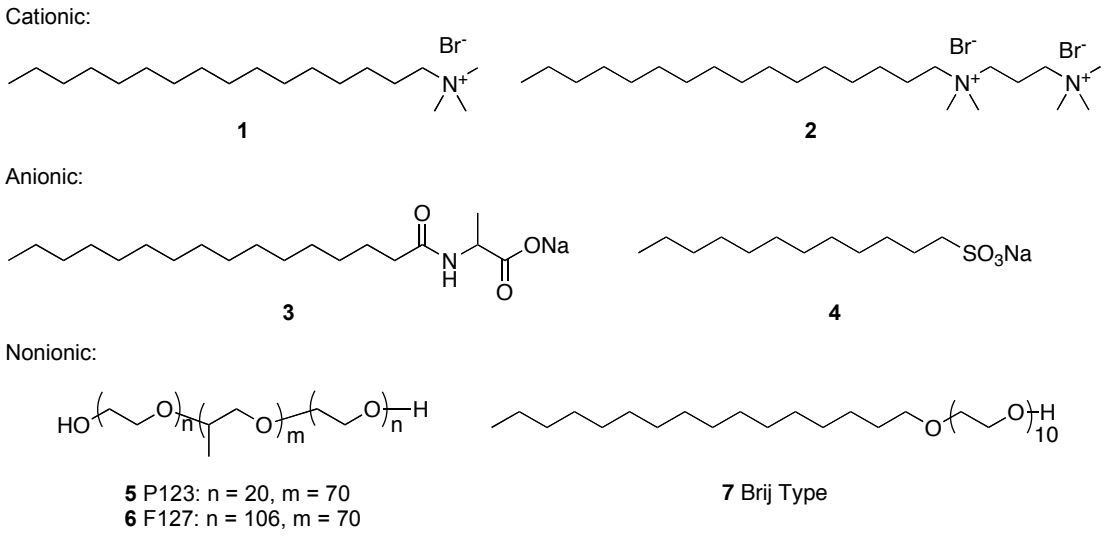

Figure 1.2: Representative surfactants utilized in mesoporous materials synthesis.

The most common mesoporous silica templated with a nonionic surfactant is SBA-15[32]. Similar to MCM-41, SBA-15 has a 2D hexagonally ordered pore system. However, SBA-15 has a larger pore size, thicker pore walls and higher hydrothermal stability than MCM-41. It is prepared using P123 (**5**) as a surfactant under acidic conditions with TEOS as the silica source. Pore size and wall thickness can be controlled by varying the hydrothermal treatment temperature and time, with higher temperatures and longer reaction times favouring larger pores and thinner walls[32]. Further increases in pore size can be achieved by addition of pore swelling agents like TMB[32]. Using this technique, ordered mesoporous silicas with pore sizes of up to 300 Å could be achieved using P123 and TMB while still maintaining the relatively thick walls[32]. One of the interesting features of materials

prepared by block co-polymers is the microporosity of the walls. The hydrophilic EO blocks are incorporated into the condensing silicate during synthesis, leading to microporosity that acts to interconnect the pores, potentially helping in diffusion of molecules in and out of the pores. This interconnection is evident from platinum castings of SBA-15, which maintain hexagonal order after removal of the silica (Figure 1.3)[35,36]. On the other hand, platinum castings of MCM-41 showed no such long range ordering, since there is no connection between the individual hexagonal channels[37]. The mesostructure of block copolymer-templated materials can be modified by increasing the ratio of the hydrophilic block (EO) relative to the hydrophobic block (PO); for example, F127 (**6**) yields a cubic material SBA-16[33]. Much like MCM-41, SBA-15 and SBA-16 are prepared by a cooperative self-assembly of surfactant and silica.

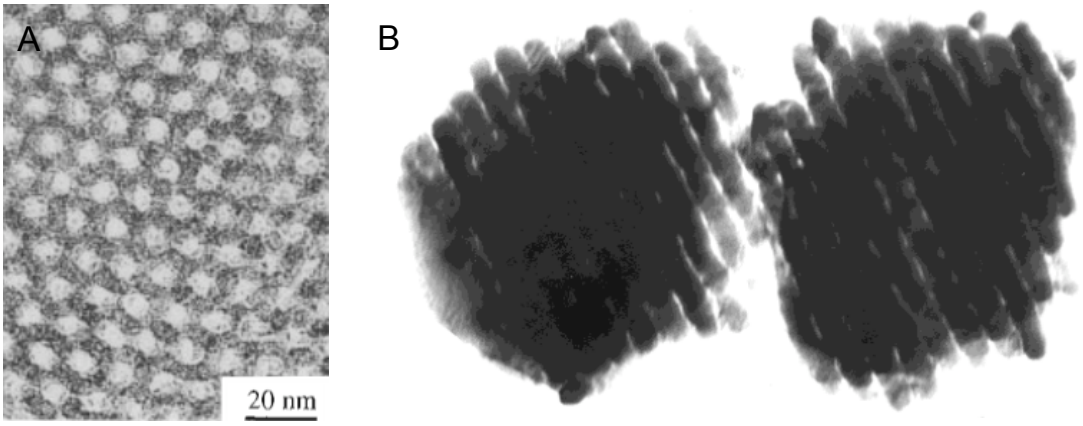

Figure 1.3: TEM image of SBA-15 (A) and a platinum replica of SBA-15 after removal of the silica (B). Reproduced from reference 32 (A) and 35 (B).

Co-operative self-assembly, as the name implies, requires the interaction of the silica species with the surfactant to generate the final

mesostructure. In the case of MCM-41, soluble anionic silicates interact with the positively charged head groups of the surfactant displacing the original counter ions (Figure 1.4). The charge density of the inorganic species initially determines the packing density of the surfactant-silica mix. The packing density in turn dictates the geometry of the surfactant species as a result of electrostatic interactions and van der Waals forces. As the silicate condenses, the changes in charge density induce further changes in the surfactant template. This dynamic process continues until the material has reached a structure of minimal energy for the given system[38].

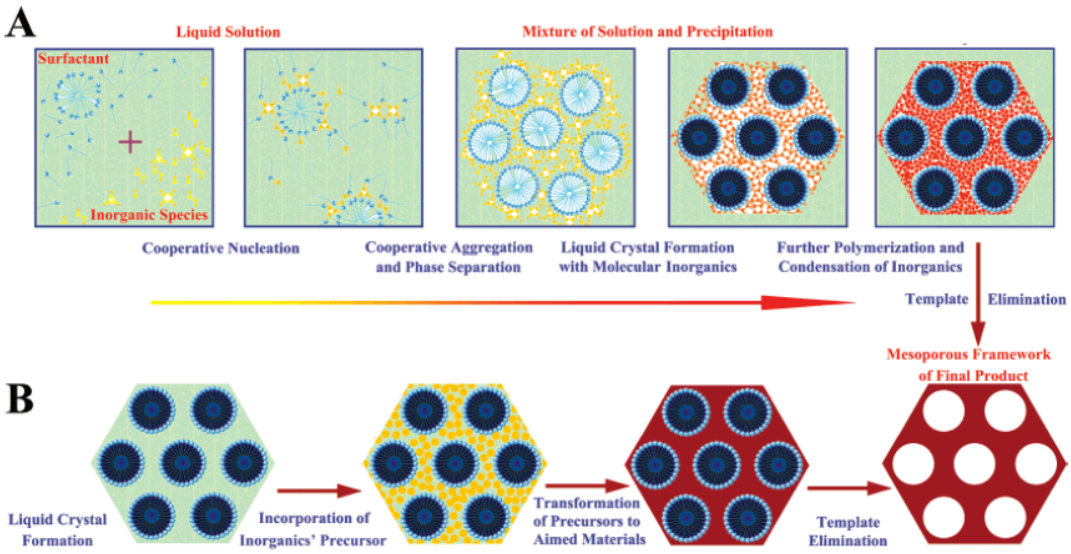

Figure 1.4: Comparison of co-operative self assembly (path A) and liquid crystal templating (path B) for formation of mesoporous materials. Reproduced from ref 2.

True liquid crystal templating can be achieved for mesoporous materials using higher concentrations of surfactants such that the surfactant has formed the mesostructure in the absence of the condensing silica source (Figure 1.4). The degree of condensation of silica species is higher for liquid

crystal templated materials relative to cooperatively assembled materials due to the growth of silica in the confined spaces around the preformed template yielding a more ceramic like material[34].

To obtain a well-ordered material, it is important to understand the ways in which the surfactant and silica species can interact. Initially, Stucky postulated four modes of interaction between the surfactant and silica: S^+I^-, S^-I^+, $S^+X^-I^+$ and $S^-X^+I^-$, where S represents a surfactant species, X is a counter ion and I represents the inorganic silica species[5]. MCM-41 operates through the S^+I^- interaction where the positively charged surfactant interacts with the silicate anions produced by hydrolysis of silica species in basic solution. The $S^+X^-I^+$ interaction has been used by Stucky for the formation of SBA-1[5]. In this material, cationic surfactants are used with acidic condensation of TEOS. It was found that the anion X^- can affect the structure, morphology and stability of the silica.

The use of non-ionic surfactants introduced two additional pathways S^0I^0 and $S^0H^+X^-I^+$. The first interaction was evoked to explain the formation of mesoporous silicas under neutral conditions[39,40]. SBA-15 is thought to result from association through a protonated neutral surfactant that interacts with the positively charged silica through an anion, usually that from the mineral acid catalyst[32]. Understanding of these interactions is vital for producing highly ordered materials as the choice of synthesis conditions will dictate how the surfactant and silica will interact (Figure 1.5).

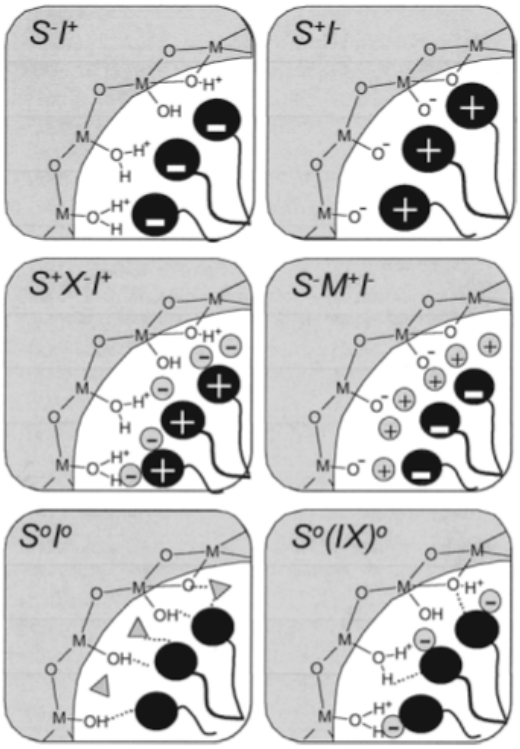

Figure 1.5: Schematic representation of the interactions between surfactants (S) and condensing silica species (I). Reproduced from reference 41.

In order to access the porous structure achieved in the synthesis of mesoporous materials, the surfactant must be removed from the pores. There are a number of methods currently employed to accomplish this. The most common method is via calcination, which involves heating the silicate in an atmosphere of air or oxygen to decompose and oxidize the surfactant. This method is advantageous in that removal of all the surfactant can be monitored by techniques such as TGA-MS and that surfactant removal can be accomplished in a relatively short time. However, in order to maintain a well ordered porous structure the rate of heating must be controlled to 1-2 °C/min and the final temperature must be held for several hours, usually 4-6 h. Increased calcination temperatures lead to lower surface areas, pore volumes

and reduced numbers of surface silanols through increased cross-linking of the silicon oxide network. This last point (loss of the surface silanols) can be a significant negative if post-synthesis functionalization is desired. Furthermore, destruction of the surfactant and calcination cannot be carried out with materials that are already functionalized with organic species, such as PMOs (*vide infra*)[42].

Extraction offers a milder alternative to calcination. A solvent such as ethanol or THF is generally effective at removing the surfactant[2]. A dilute acid can be added to improve the degree of cross-linking of the silica[37]. One of the advantages of using extraction is that the surfactant can be recovered and reused. Using super critical carbon dioxide as a solvent for extraction simplifies the process of surfactant recovery even further[43]. Furthermore, the pore sizes of extracted materials do not contract as much as calcined materials and more surface silanols are present in extracted materials. However, incomplete removal of the surfactant can be an issue with the extraction process[44].

Alternative methods for surfactant removal include irradiation with ultraviolet light to break the carbon-carbon bonds and decompose the material with the generated ozone and oxygen atoms, although this method is only applicable to cationic surfactants. UV irradiation produces materials with better ordering than calcination but is time consuming and not suitable for large scales[45]. Microwave irradiation can also be utilized remove the surfactant much quicker than with calcination, 10-30 min by microwaves

compared to 10 h for calcination. However, over-heating of the material can decrease the ordered structure so careful control over the microwave power needs to be applied[46]. Digestion of the surfactant with nitric acid and hydrogen peroxide has been achieved in a microwave reactor. This was found to rapidly remove all surfactant from the pores while maintaining the silanols and minimizing pore shrinkage[47].

Having formed the mesoporous material, the next step is to characterize its properties. Unlike small molecules, where a few techniques such as NMR and IR are generally sufficient for their characterization, solid mesoporous materials are generally characterized by multiple methods. Commonly employed are SEM, TEM, XRD, MAS NMR and nitrogen or argon porosimetry. SEM is employed to examine particle morphology: a variety of shapes can be prepared from spherical to rod-like. TEM, which typically has higher resolution than SEM, is utilized to examine the pore structure while pXRD indicates the long range order of the material. Solid state NMR can be used to probe silicon as well as other NMR active nuclei that may be incorporated into the material, commonly carbon and less frequently phosphorus. Solid state silicon NMR is also useful for determining the degree of condensation of the material. For purely silicaceous materials, resonances observed from -90 to -120 ppm can be attributed to Q_n sites, silicon attached to four oxygen with n being the number of Si-O-Si linkages[32]. In most mesoporous materials, Q_2, Q_3 and Q_4 sites are usually observed in varying ratios, dependent on the degree of condensation. However, when using cross

polarization NMR, Si nuclei in close proximity to protons (i.e. Q_2 and Q_3) sites are over represented. Thus to obtain an accurate degree of condensation it is imperative not to use cross polarization. For organically functionalized materials, the T_n sites are of importance. These resonances are attributed to silicon attached to three oxygen and usually one carbon and are observed in the -60 to -85 ppm range[48]. Other nuclei can be probed when functionalized silicas are prepared.

Gas porosimetry measurements are one of the more important techniques for characterization of mesoporous materials because they give information about the surface and pores[49]. Both nitrogen and argon are commonly used to characterize mesoporous solids. Nitrogen is more frequently used than argon owing to the availability of liquid nitrogen for cooling. However, argon is preferred for examination of the micropores. Additionally, organic molecules such as benzene or hexane are sometimes used to probe the surface[49]. Commonly observed isotherms with ordered silicas are classified as IUPAC type I and type IV (Figure 1.6)[50].

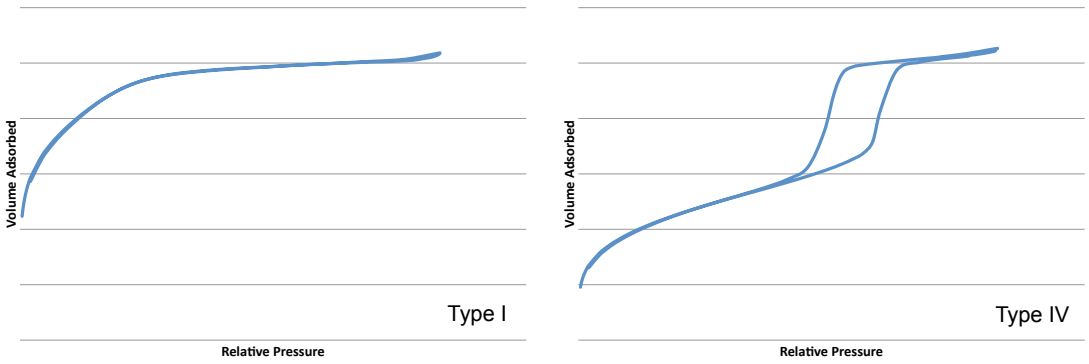

Figure 1.6: Examples of IUPAC type I and type IV isotherms.

Type I isotherms are characterized by prominent adsorption at low relative pressure and are usually indicative of microporous materials. However, type I isotherms have been observed for mesoporous materials with small pores or a broad pore size distribution. Type IV isotherms are characterized by steady adsorption at low relative pressures followed by a large capillary adsorption at intermediate relative pressures. Often this capillary condensation and capillary evaporation on desorption do not occur at the same relative pressure resulting in a hysteresis loop in the isotherm.

This hysteresis phenomenon is usually attributed to a combination of thermodynamic and network effects[51]. Thermodynamically, the metastability of the liquid nitrogen phase relative to the gas phase in the pore may be different for condensation or evaporation leading to a hysteresis between the adsorption and desorption curves. Alternatively, pore connectivity can also drive hysteresis behaviour and is expected to play a major role in the development of hysteresis. In what has often been termed the ink-bottle effect, if the entrance to a pore is narrow relative to a larger pore on the inside of the material, the larger pore cannot empty at the relative pressure expected for that pore size because the narrower pore is still occluded by liquid. Thus the pores empty at the relative pressure expected for the narrow pore opening[49].

The surface and pore properties can then be calculated from this experimentally obtained observation. The surface area of the materials is commonly estimated by the Brunauer-Emmett-Teller (BET) method[52]. The

BET method also gives an estimation of the strength of adsorbent-adsorbate interaction from the C parameter which can be linked to hydrophobicity or hydrophilicity of the surface[49]. Care must be taken in comparison of C parameters across materials with different functionalities as similar C parameters have been found for MCM-41 materials functionalized with a number of different groups[53]. Pore volume is calculated from the amount of nitrogen (or argon) adsorbed at high relative pressures. However for nitrogen, if the pore sizes are > 200-400 nm incomplete filling of pores can occur and the pore volume will be underestimated by this method[49].

The pore size distribution is calculated by the Barrett-Joyner-Halenda (BJH) method[54]. When there is a hysteresis loop in the isotherm, there is a the question of which branch to employ in the determination of pore size. As previously noted, the hysteresis arises from the difference in adsorption and desorption of nitrogen in the pore structure. For adsorption, condensation can occur anywhere in the pore network and the sorbent can be transported through either the liquid or vapour phase. Capillary condensation is therefore governed by the largest pores. Desorption on the other hand, only occurs through pores connected to the bulk vapour phase (i.e. the external pores). Once vaporization occurs in the pores near the surface, adjacent pores can begin to desorb. If the diameter of the pore entrance is smaller than the interior diameter of the pore than the critical desorption pressure is lower then the adsorption pressure of that pore and a hysteresis is observed in the isotherm[49]. Calculation of the pore size from the adsorption branch then gives

the size of the larger internal pores while the size of the pore openings can be determined by the desorption branch[49].

The presence of surface silanols imparts the ability to further functionalize the materials. Organosilanes of the formula $(R'O)_{4-n}SiR_n$ or $Cl_{4-n}SiR_n$ can be grafted onto the surface after extraction of the surfactant. Some common organic silanes utilized for functionalization of silicas are presented in Figure 1.7. The incorporation of organic functionalities increases the utility of these materials as scavengers for metals, supports for catalysis and other applications[48,55,56]. A number of excellent reviews about functionalizing silicas are available in the literature, selected examples are highlighted herein[55-58].

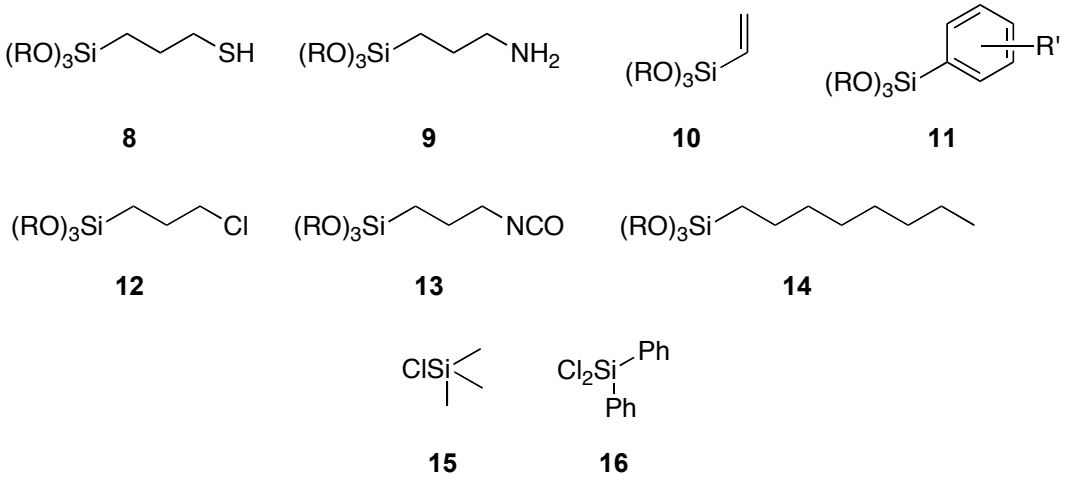

Figure 1.7: Representative organosilanes for functionalization of silica.

While grafting has become a standard technique for functionalization of silicas, one of the limitations is the poor and often irreproducible loading of organic groups. This can manifest itself in low overall loadings of organic species and batch-to-batch differences in loading. Brunel and co-workers

found that after calcining MCM-41, the material formed isolated hydrophilic and hydrophobic areas on the surface[59]. Grafting of organosilanes to these materials occurs preferentially in the hydrophobic zones leading to islands of functionality. Grafting methods to incorporate higher loadings of organosilanes have been developed for applications where more organic functionality is needed[60,61].

The introduction of simple organosilanes such as trimethylsilyl chloride and dichlorodiphenyl silane has been used to modify the surface properties of the material[56]. Inclusion of these types of organosilanes increases the hydrophobicity of the surface. Bulky groups like diphenyl silane can introduce a degree of steric hindrance towards adsorption of molecules on the surface. This strategy has been used by a number of groups to increase catalytic activity of mesoporous materials[62-66].

An alternative to grafting an organosilane after preparation of the mesoporous material is to co-condense the organosilane at the same time as the inorganic silica source. This method is considered to give a more homogeneous distribution of the organosilane in the material. However, there is a possibility that some of the organosilanes can be buried in the pore walls and therefore not available for further chemistry[67]. Lim and Stein demonstrated that functional groups were more likely to be on the external surfaces and around the pore openings with grafted materials while the co-condensed materials had a more even distribution[68]. Furthermore, as the co-condensed method does not rely on grafting to the surface silanols, materials

prepared by this method have surface silanols available for further functionalization.

When comparing the properties of mesoporous silicas and zeolites, researchers found that the strong acidity associated with zeolites was absent in mesoporous materials. Thus some of the first efforts in the application of functionalized mesoporous silicas to organic transformations centered around the preparation of strong acid catalysts by oxidation of the thiol group on silicas functionalized by ligand **8** resulting in sulfonic acid functionalized silicas. These materials show good activity in the esterification reaction with rates of reaction dependent on sulfur loading[69]. Furthermore, sulfonic acid functionalized silicas have been utilized in the addition of acetic acid to camphene (Figure 1.8)[70].

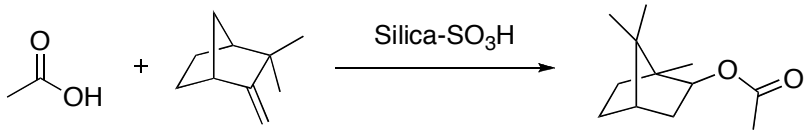

Figure 1.8: Sulfonic acid functionalized silica catalyzed addition of acetic acid to camphene.

In addition to acidic functionalized silicas, silicas functionalized with basic groups have been prepared for applications as solid base catalysis. These solid easily removable bases offer alternatives to soluble bases such as hydroxides, carbonates, amines and alkoxides. Corma's group prepared basic silica by grafting 3-(trimethoxysilyl)-propyl-trimethyl-ammonium chloride onto MCM-41 and then exchanging the anion by treatment with tetramethyl ammonium hydroxide. The silica was used to catalyze a Knoevanagel

condensation of aldehydes with a number of activated methylene compounds (Figure 1.9). Yields of 77 - 95 % were obtained, however, the solid base was much slower than the soluble tetramethyl ammonium hydroxide[71]. Macquarrie and coworkers formed a xerogel with APTES grafted to the surface for Knovenagel condensation. The catalyst gave high yields but suffered a loss of activity upon recycling[72]. The loss of activity was attributed to the formation of ammonium salts on the surface and some of the activity could be returned by treating the material with propyl amine in ethanol[56]. The Jacobs group has grafted 1,5,7-triazabicyclo[4.4.0]dec-5-ene (TBD) to MCM-41 and used the resulting material for both Knoevenagel and Michael reactions (Figure 1.10)[73].

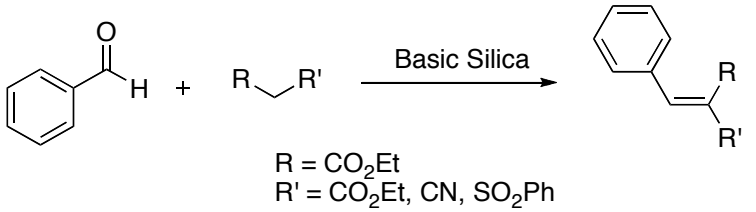

Figure 1.9: Base-catalyzed Knoevenagel condensation.

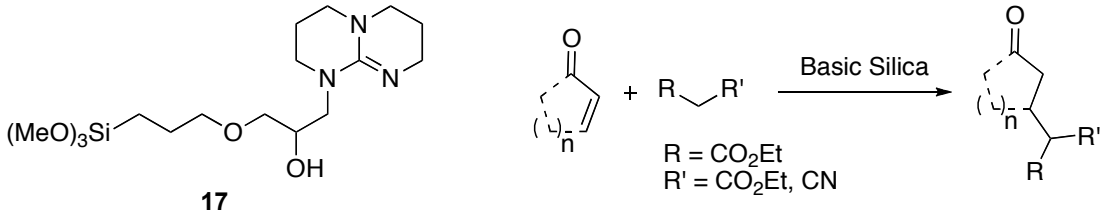

Figure 1.10: TBD-functionalized silane and base catalyzed Michael Addition.

An interesting bifunctional catalyst system was prepared by Sanchez *et al.* using SBA-15 as a host. APTES as well as rhodium complex **18** (Figure 1.11) were grafted onto SBA-15 and the resulting material used in a tandem

Knoevenagel/hydrogenation sequence (Figure 1.11). A mesoporous silica prepared with **18** in the absence of APTES was an active hydrogenation catalyst. Using ordered SBA-15-**18,** the recyclability and activity of the hydrogenation catalyst improved compared to amorphous silica gel[74].

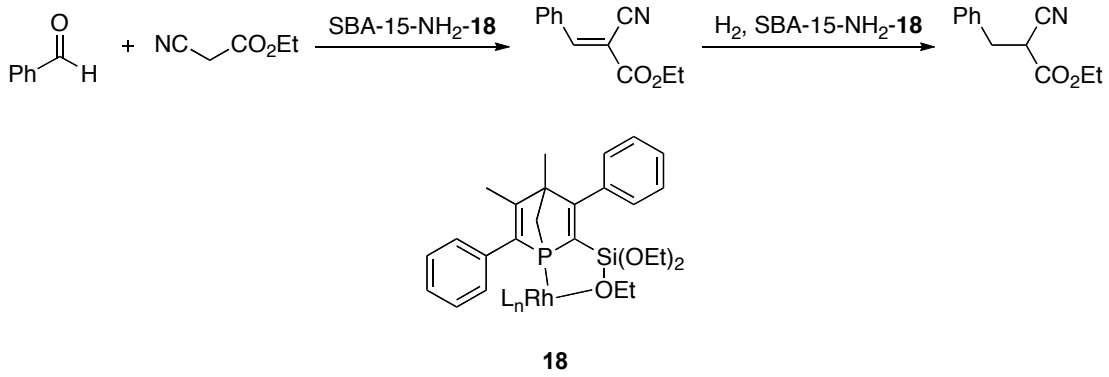

18

Figure 1.11: Silica-rhodium complex used for heterogeneous hydrogenations and bifunctional catalysis using SBA-15-NH_2-**18**.

Corma prepared a chiral basic silica using cinchonine and cinchonidine as chiral organic groups (Figure 1.12). These chiral bases were grafted onto MCM-41 and used in the asymmetric Michael reaction of methylvinyl ketone and ethyl 2-oxocyclopentanecarboxylate. The cinchonidine catalyst gave good yields of Michael products but the enantioselectivity was moderate peaking at 50 % ee. Cinchonine on the other hand was not as active as cinchonidine and also resulted in poor ee's[75]. One concern with the basic silica catalysis is the stability of the material, particularly hydrolysis of the anchored organic base. Fortunately, the amount hydrolysis can be lowered by grafting alkylsilanes to increase the hydrophobicity of the surface[76].

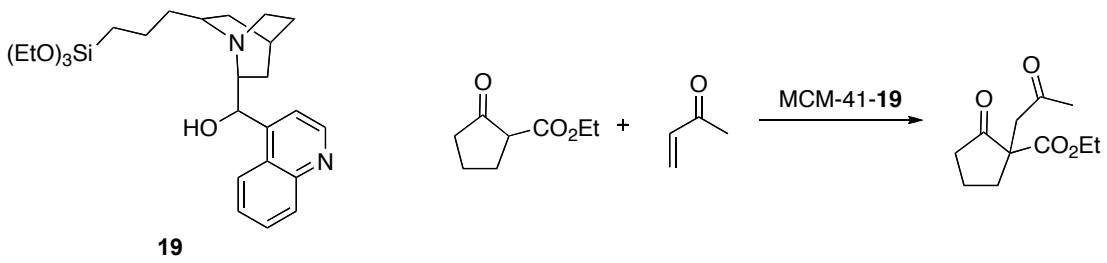

Figure 1.12: Silica functionalized cinchona alkaloid and asymmetric Michael reaction.

The Crudden group has also immobilized cinchona alkaloids as ligands for asymmetric dihydroxylation. We have prepared both ordered and amorphous materials functionalized with **20** (Figure 1.13) and employed them as catalysts for asymmetric dihydroxylation using an osmium oxide species for oxidation. Both materials were catalytically active for a number of disubstituted olefins and styrene derivatives, giving diols in high yield and enantioselectivities of >90 % ee[77]. In all cases, enantioselectivities matched those obtained in solution.

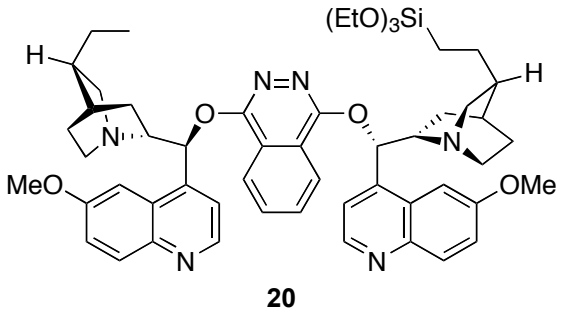

Figure 1.13: Supported cinchona alkaloid utilized by the Crudden group for asymmetric dihydroxylation.

Chiral silica incorporating ephedrine has been prepared by Lasperas and co-workers using MCM-41 as a support. The pristine material was grafted with 3-chloropropyl trimethoxysilane prior to functionalization with ephedrine

(Scheme 1.1). The chiral material was then used in the asymmetric alkylation of benzaldehyde with diethyl zinc. Enantioselectivities of up to 33 % with the solid supported ephedrine catalyst[78]. The rate of reaction and enantioselectivity were reduced compared to the homogeneous catalyst.

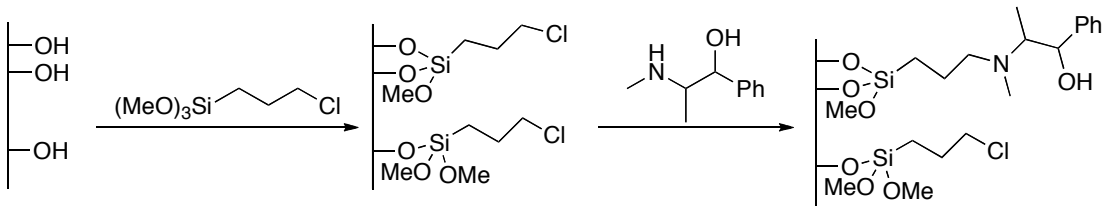

Scheme 1.1: Functionalization of MCM-41 with ephedrine.

The utility of functionalized silicas can be expanded by the addition of metals for catalysis. A number of groups have immobilized palladium on mesoporous silica to perform cross coupling reactions[79-83]. These materials will be discussed in detail in chapter 3. Clark *et al.* prepared a copper loaded HMS silica for the aziridation of styrene (Figure 1.14). The material gave higher conversions of styrene and higher TONs relative to the reaction catalyzed homogeneously by copper (II) acetylacetonate but activity decreased as the heterogeneous catalyst was recycled[84].

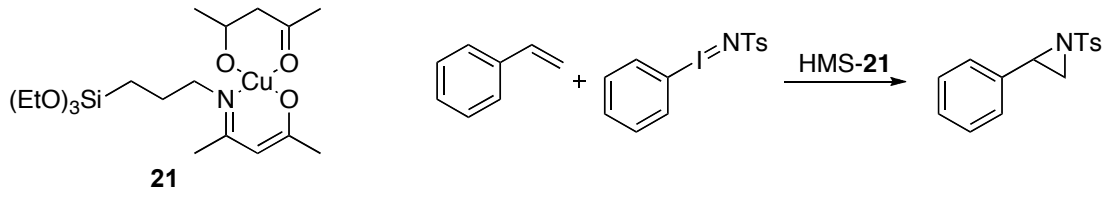

Figure 1.14: Silica immobilized copper catalyst for aziridation of styrene.

Our group prepared immobilized rhodium-phosphine complexes for the hydrogenation of olefins (Figure 1.15). These materials demonstrated higher activity on support than in solution, and furthermore, the highest TONs for the supported system were found with the lowest rhodium loadings, leading to the postulate that site isolation is preventing decomposition of the catalyst[85].

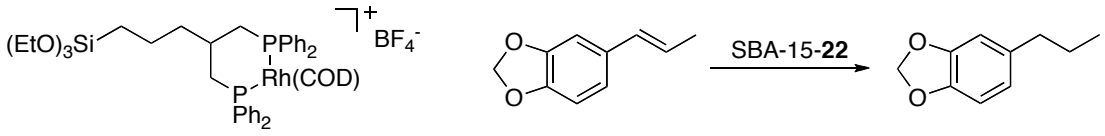

22

Figure 1.15: Immobilized rhodium hydrogenation catalyst produced in the Crudden group.

Corma *et al.* prepared MCM-41 and amorphous silica immobilized palladium and nickel salen complexes that were able to hydrogenate imines (Figure 1.16). They found that the ordered silica had higher initial reaction rates relative to amorphous silica. Despite their high catalytic activity, these catalysts suffer from a low enantioselectivity relative to homogeneous catalysis[86,87].

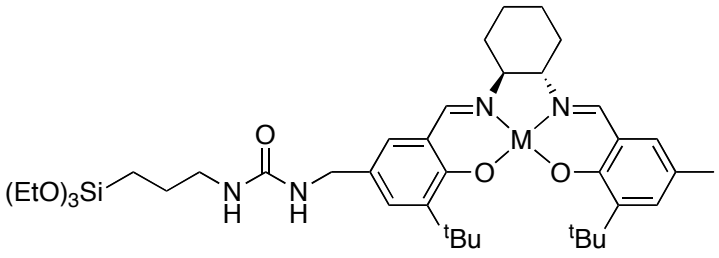

M = Pd, Ni

Figure 1.16: Immobilized metal salen complex for asymmetric hydrogenation of imines.

Kureshy's group has incorporated manganese salen ligand **23** into MCM-41 and SBA-15 for the asymmetric epoxidation of olefins (Figure 1.17). The supported catalyst showed greater ee (70 %) than its homogeneous counterpart (45 %) in the epoxidation of styrene. With bulkier alkenes the enantioselectivity increased to give epoxides in up to 92 % ee[88,89]. Li's group has also prepared siloxane-substituted manganese salen **24** and grafted it onto SBA-15 and MCM-41 (Figure 1.17). These silicas showed improved enantioselectivities over their homogeneous counterparts for a variety of substrates. Furthermore, in the epoxidation of cis-β-methyl styrene, the supported catalysts demonstrated an improved cis-trans ratio in the epoxide products over homogeneous catalysis[90].

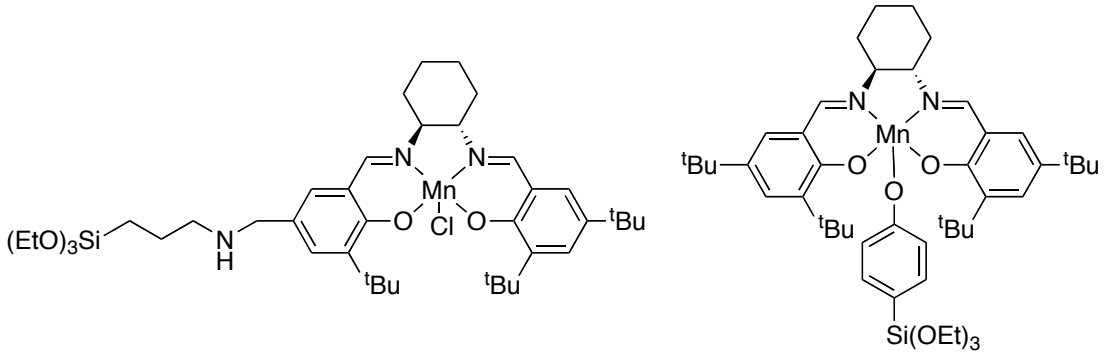

23 **24**

Figure 1.17: Immobilized Mn-salen complexes for asymmetric epoxidation.

The materials discussed so far have one point of attachment between the silica and organic functionality. It is possible to generate organosilanes with more than one silane group. The condensation of such a species would generate a material with organic groups incorporated into the pore walls. Due

to their bifunctional nature, these siloxanes can be used to prepare materials that do not require any silica additives. These materials have been prepared without the addition of surfactant since the 1980s[91], but when prepared in the presence of a surfactant to introduce order, Ozin, Stein and Inagaki termed these materials periodic mesoporous organosilicas (PMO)[22-24]. These materials will be discussed at length in chapter 5.

Silica-based materials have only begun to demonstrate their importance in a number of fields. New materials can be prepared using different surfactants and the properties of the materials can be tailored to its application. Mesoporous silicas will continue to be applied to new challenges making the future of these materials very exciting. However, due to the increased costs associated with their synthesis, comparison to regular non-templated materials needs to be carried out in every case.

1.2 References

(1) Kresge, C.T.; Leonowicz, M.E.; Roth, W.J.; Vartuli, J.C.; Beck, J.S. *Nature* **1992**, *359*, 710.
(2) Wan, Y.; Zhao, D. *Chem. Rev.* **2007**, *107*, 2821.
(3) Pinnavaia, T.J. *Science* **1983**, *220*, 365.
(4) Tindwa, T.M.; Ellis, D.K.; Peng, G.Z.; Clearfield, A. *J. Chem. Soc. Faraday Trans. 1* **1985**, *81*, 545.
(5) Huo, Q.; Margolese, D.I.; Ciesla, U.; Feng, P.; Gier, T.E.; Sleger, P.; Leon, R.; Petroff, P.M.; Schuth, F.; Stucky, G.D. *Nature* **1994**, *368*, 317.
(6) Sun, T.; Ying, J.Y. *Nature* **1997**, *389*, 704.
(7) Tian, Z.R.; Tong, W.; Wang, J.Y.; Duan, N.G.; Krishnan, V.; Suib, S.L. *Science* **1997**, *276*, 926.
(8) Yang, P.; Zhao, D.; Margolese, D.I.; Chmelka, B.F.; Stucky, G.D. *Nature* **1998**, *396*, 152.
(9) Zou, X.; Conradsson, T.; Klingstedt, M.; Dadachov, M.S.; O'Keeffe, M. *Nature* **2005**, *437*, 716.
(10) Tian, B.; Liu, X.; Tu, B.; Yu, C.; Fan, J.; Wang, L.; Xie, S.; Stucky, G.D.; Zhao, D. *Nat. Mater.* **2003**, *2*, 159.
(11) Grosso, D.; Boissere, C.; Smarsly, B.; Brezesinski, T.; Pinna, N.; Albouy, P.A.; Amenitsch, H.; Antonietti, M.; Sanchez, C. *Nat. Mater.* **2004**, *3*, 787.
(12) Corma, A.; Atienzar, P.; Garcia, H.; Channe-Ching, J.Y. *Nat. Mater.* **2004**, *3*, 394.
(13) MacLachlan, M.J.; Coombs, N.; Ozin, G.A. *Nature* **1999**, *397*, 681.
(14) Braun, P.V.; Osenar, P.; Stupp, S.I. *Nature* **1996**, *380*, 325.
(15) Trikalitis, P.N.; Rangan, K.K.; Bakas, T.; Kanatzidis, M.G. *Nature* **2001**, *410*, 671.
(16) Attard, G.S.; Bartlett, P.N.; Coleman, N.R.B.; Elliott, J.M.; Owen, J.R.; Wang, J.H. *Science* **1997**, *278*, 838.
(17) Armatas, G.S.; Kanatzidis, M.G. *Nature* **2006**, *441*, 1122.
(18) Sun, D.; Riley, A.E.; Cadby, A.J.; Richman, E.K.; Korlann, S.D.; Tolbert, S.H. *Nature* **2006**, *441*, 1126.
(19) Landskron, K.; Ozin, G.A. *Science* **2004**, *306*, 1529.
(20) Meng, Y.; Gu, D.; Zhang, F.; Shi, Y.; Yang, H.; Li, Z.; Yu, C.; To, B.; Zhao, D. *Angew. Chem. Int. Ed.* **2005**, *44*, 7053.
(21) Joo, S.H.; Choi, S.J.; Oh, I.; Kwak, J.; Liu, Z.; Terasaki, O.; Ryoo, R. *Nature* **2001**, *412*, 169.
(22) Inagaki, S.; Guan, S.; Fukushima, Y.; Ohsuna, T.; Terasaki, O. *J. Am. Chem. Soc.* **1999**, *121*, 9611.
(23) Melde, B.J.; Holland, B.T.; Blanford, C.F.; Stein, A. *Chem. Mater.* **1999**, *11*, 3302.
(24) Asefa, T.; MacLachlan, M.J.; Coombs, N.; Ozin, G.A. *Nature* **1999**, *402*, 867.
(25) Guan, S.; Inagaki, S.; Ohsuna, T.; Terasaki, O. *J. Am. Chem. Soc.* **2000**, *122*, 5660.

(26) Stein, A.; Melde, B.J.; Schroden, R.C. *Adv. Mater.* **2000**, *12*, 1403.
(27) Liu, S.; Cool, P.; Collart, O.; Van Der Voort, P.; Vansant, E.F.; Lebedev, O.I.; Van Tendeloo, G.; Jiang, M. *J. Phys. Chem. B* **2003**, *107*, 10405.
(28) Sakamoto, Y.; Kaenda, M.; Terasaki, O.; Zhao, D.; Kim, J.M.; Stucky, G.D.; Shin, H.J.; Ryoo, R. *Nature* **2000**, *408*, 449.
(29) Shen, S.; Garcia-Bennett, A.E.; Liu, Z.; Lu, Q.; Shi, Y.; Yan, Y.; Yu, C.; Liu, W.; Cai, Y.; Terasaki, O.; Zhao, D. *J. Am. Chem. Soc.* **2005**, *127*, 6780.
(30) Tan, B.; Dozier, A.; Lehmler, H.J.; Knutson, B.L.; Rankin, S.E. *Langmuir* **2004**, *20*, 6981.
(31) Che, S.; Liu, Z.; Ohsuna, T.; Sakamoto, K.; Terasaki, O.; Tatsumi, T. *Nature* **2004**, *429*, 281.
(32) Zhao, D.; Feng, J.; Huo, Q.; Melosh, N.; Fredrickson, G.H.; Chmelka, B.F.; Stucky, G.D. *Science* **1998**, *279*, 548.
(33) Zhao, D.; Huo, Q.; Feng, J.; Chmelka, B.F.; Stucky, G.D. *J. Am. Chem. Soc.* **1998**, *120*, 6024.
(34) Attard, G.S.; Glyde, J.C.; Goltner, C.G. *Nature* **1995**, *378*, 366.
(35) Ryoo, R.; Ko, C.H.; Kruk, M.; Antochshuk, V.; Jaroniec, M. *J. Phys. Chem. B* **2000**, *104*, 11465.
(36) Galarneau, A.; Cambon, H.; Di Renzo, F.; Ryoo, R.; Choi, M.; Fajula, F. *New. J. Chem.* **2003**, *27*, 73.
(37) Kruk, M.; Jaroniec, M.; Ko, C.H.; Ryoo, R. *Chem. Mater.* **2000**, *12*, 1961.
(38) Huo, Q.; Margolese, D.I.; Ciesla, U.; Demuth, D.G.; Feng, P.; Gier, T.E.; Sieger, P.; Firouzi, A.; Chmelka, B.F.; Schuth, F.; Stucky, G.D. *Chem. Mater.* **1994**, *6*, 1176.
(39) Tanev, P.T.; Pinnavaia, T.J. *Science* **1995**, *267*, 865.
(40) Bagshaw, S.A.; Prouzet, E.; Pinnavaia, T.J. *Science* **1995**, *269*, 1242.
(41) Soler-Illia, G.J.A.A.; Sanchez, C.; Lebeau, B.; Patarin, J. *Chem. Rev.* **2002**, *102*, 4093.
(42) Zhang, F.; Yan, Y.; Yang, H.; Meng, Y.; Meng, Y.; Yu, C.; To, B.; Zhao, D. *J. Phys. Chem. B* **2005**, *109*, 8723.
(43) Kawi, S.; Lai, M.W. *AIChE J.* **2002**, *48*, 1572.
(44) van Grieken, R.; Calleja, G.; Stucky, G.D.; Melero, J.A.; Garcia, R.A.; Iglesias, J. *Langmuir* **2003**, *19*, 3966.
(45) Hozumi, A.; Yokogawa, Y.; Kameyama, T.; Hiraku, K.; Sugimura, H.; Takai, O.; Okido, M. *Adv. Mater.* **2000**, *12*, 985.
(46) Gallis, K.W.; Landry, C.C. *Adv. Mater.* **2001**, *13*, 23.
(47) Tian, B.; Liu, X.; Yu, C.; Gao, F.; Luo, Q.; Xie, S.; Tu, B.; Zhao, D. *Chem. Commun.* **2002**, 1186.
(48) Sayari, A.; Hamoudi, S. *Chem. Mater.* **2001**, *13*, 3151.
(49) Kruk, M.; Jaroniec, M. *Chem. Mater.* **2001**, *13*, 3169.
(50) Sing, K.S.W. *Pure Appl. Chem.* **1985**, *54*, 603.
(51) Ball, P.C.; Evans, R. *Langmuir* **1989**, *5*, 714.
(52) Brunauer, S.; Emmett, P.H.; Teller, E. *J. Am. Chem. Soc.* **1938**, *60*, 309.
(53) Jaroniec, C.P.; Kruk, M.; Jaroniec, M. *J. Phys. Chem. B* **1998**, *102*, 5503.
(54) Barrett, E.P.; Joyner, L.G.; Halenda, P.P. *J. Am. Chem. Soc.* **1951**, *73*, 373.
(55) Li, C.; Zhang, H.; Jiang, D.; Yang, Q. *Chem. Commun.* **2007**, 547.

(56) Clark, J.H.; Macquarrie, D.; Tavener, S.J. *Dalton Trans.* **2006**, 4297.
(57) Corma, A.; Garcia, H. *Adv. Synth. Catal.* **2006**, *348*, 1391.
(58) Carrington, N.A.; Xue, Z.L. *Acc. Chem. Res.* **2007**, *40*, 343.
(59) Brunel, D.; Cauvel, A.; Di Renzo, F.; Fajula, F.; Fubini, B.; Onida, B.; Garrone, E. *New. J. Chem.* **2000**, *24*, 807.
(60) Abramson, S.; Lasperas, M.; Brunel, D. *Tetrahedron: Asymmetry* **2002**, *13*, 357.
(61) Feng, X.; Fryxell, G.E.; Wang, L.Q.; Kim, A.Y.; Liu, J.; Kemner, K.M. *Science* **1997**, *276*, 923.
(62) Macquarrie, D. *Green Chem.* **1999**, *1*, 195.
(63) Macquarrie, D.; Tavener, S.J.; Harmer, M.A. *Chem. Commun.* **2005**, 2363.
(64) Diaz, I.; Marquez-Alvarez, C.; Mohino, F.; Perez-Pariente, J.; Sastre, E. *J. Catal.* **2000**, *193*, 283.
(65) Diaz, I.; Marquez-Alvarez, C.; Mohino, F.; Perez-Pariente, J.; Sastre, E. *J. Catal.* **2000**, *192*, 295.
(66) Bhaumik, A.; Kapoor, M.P.; Inagaki, S. *Chem. Commun.* **2003**, 470.
(67) Yokoi, T.; Yoshitake, H.; Tatsumi, T. *J. Mater. Chem.* **2004**, *14*, 951.
(68) Lim, M.H.; Stein, A. *Chem. Mater.* **1999**, *11*, 3285.
(69) Wilson, K.; Lee, A.F.; Macquarrie, D.; Clark, J.H. *Appl. Catal. A* **2002**, *228*, 127.
(70) Dijs, I.J.; van Ochten, H.L.F.; van Walree, C.A.; J.W., G.; Jenneskens, L.W. *J. Mol. Catal. A: Chem.* **2002**, *188*, 209.
(71) Rodriguez, I.; Iborra, S.; Corma, A.; Rey, F.; Jorda, J.L. *Chem. Commun.* **1999**, 593.
(72) Sartori, G.; Bigi, F.; Maggi, R.; Sartorio, R.; Macquarrie, D.J.; Lenarda, M.; Storato , L.; Coluccia, S.; Martra, G. *J. Catal.* **2004**, *222*, 410.
(73) Rao, Y.V.S.; De Vos, D.; Jacobs, P. *Angew. Chem. Int. Ed.* **1997**, *36*, 2661.
(74) Goettmann, F.; Grosso, D.; Mercier, F.; Mathey, F.; Sanchez, C. *Chem. Commun.* **2004**, 1240.
(75) Corma, A.; Iborra, S.; Rodriguez, I.; Iglesias, M.; Sanchez, F. *Catal. Lett.* **2002**, *82*, 237.
(76) Brunel, D.; Blanc, A.C.; Galarneau, A.; Fajula, F. *Catal. Today* **2002**, *73*, 139.
(77) Motorina, I.; Crudden, C.M. *Org. Lett.* **2001**, *3*, 2325.
(78) Bellocq, N.; Abramson, S.; Lasperas, M.; Brunel, D.; Moreau, P. *Tetrahedron: Asymmetry* **1999**, *10*, 3229.
(79) Crudden, C.M.; Sateesh, M.; Lewis, R. *J. Am. Chem. Soc.* **2005**, *127*, 10045.
(80) Shimizu, K.I.; Koizumi, S.; Hatamachi, T.; Yoshida, H.; Komai, S.; Kodama, T.; Kitayama, Y. *J. Catal.* **2004**, *228*, 141.
(81) Ji, Y.; Jain, S.; Davis, R.J. *J. Phys. Chem. B* **2005**, *109*, 17232.
(82) Paul, S.; Clark, J.H. *J. Mol. Cat. A: Chem.* **2004**, *215*, 107.
(83) Corma, A.; Das, D.; Garcia, H.; Leyva, A. *J. Catal.* **2005**, *229*, 322.
(84) Silva, A.R.; Wilson, K.; Whitwood, A.C.; Clark, J.H.; Freire, C. *Eur. J. Inorg. Chem.* **2006**, *2006*, 1275.
(85) Crudden, C.M.; Allen, D.P.; Mikoluk, M.D.; Sun, J. *Chem. Commun.* **2001**, 1154.
(86) Gonzalez-Arellano, C.; Corma, A.; Iglesias, M.; Sanchez, F. *Adv. Synth. Catal.* **2004**, *349*, 1316.

(87) Ayala, V.; Corma, A.; Iglesias, M.; Rincon, J.A.; Sanchez, F. *J. Catal.* **2004**, *224*, 170.
(88) Kureshy, R.I.; Ahmad, I.; Kahn, N.H.; Abdi, S.H.R.; Pathak, K.; Jasra, R.V. *Tetrahedron: Asymmetry* **2005**, *16*, 3562.
(89) Kureshy, R.I.; Ahmad, I.; Kahn, N.H.; Abdi, S.H.R.; Pathak, K.; Jasra, R.V. *J. Catal.* **2006**, *238*, 134.
(90) Zhang, H.; Xiang, S.; Xiao, J.; Li, C. *J. Mol. Catal. A: Chem.* **2005**, *238*, 175.
(91) Loy, D.A.; Shea, K.J. *Chem. Rev.* **1995**, *95*, 1431.

Chapter 2: Removal of Ruthenium Residues Using Amino-Functionalized SBA-15

2.1 Introduction

Ruthenium catalysts have become some of the most important transition metal catalysts in organic synthesis. For example, asymmetric hydrogenation has revolutionized the field of asymmetric synthesis[1] while olefin metathesis has become one of the most reliable ways to form carbon-carbon double bonds[2]. The importance of both of these processes has been recognized by the awarding of two Nobel prizes this century: 2001 for asymmetric hydrogenation, 2005 for olefin metathesis. While these transformations are convenient and efficient, there are problems associated with contamination of the product with the ruthenium residues. Ruthenium byproducts present after the reaction are often not removed by chromatography[3]. In addition to regulatory concerns for pharmaceutical products prepared with ruthenium-based catalysts, ruthenium contaminants can present a range of problems during purification including olefin isomerization and product degradation[4].

Hydrogenation of unsaturated functional groups in a molecule is an important process for the synthesis of many value added chemicals. Of the transition metals that catalyze hydrogenation reactions, the platinum group metals: palladium, rhodium, ruthenium and platinum have been employed in both homogeneous and heterogeneous fashions with notable success[1]. In the absence of asymmetric ligands, the hydrogenations catalyzed by these

metals will produce racemic products. Knowles developed one of the first practical asymmetric hydrogenation reactions for alkenes using rhodium with chiral bidentate phosphines[5]. However, despite the success of these rhodium-based catalysts, the substrate scope remained limited mainly to olefins[1]. A switch of metal to ruthenium and the introduction of BINAP as a chiral ligand widened the substrate scope[6]. Further modification of the catalyst permitted the asymmetric hydrogenation of ketones revolutionizing the way chiral secondary alcohols are synthesized[7,8]. BINAP-ruthenium dihydride catalysts facilitated the reduction of ketones bearing a pendant Lewis base (Scheme 2.1) with high enantioselectivites[9]. However, the selective reduction of simple ketones still relied on metal hydride reagents, for example sodium borohydride[10]. Enantioselective reduction could be afforded with chiral hydride sources, such as alpine-borane, unfortunately stoichiometric amounts of the chiral reducing agents were required to perform this transformation[11]. The enantioselective hydrogenation of simple ketones was finally accomplished in 1995 when Noyori's group discovered that a BINAP-ruthenium chiral diamine complex in the presence of an alkaline base could be used to hydrogenate simple ketones enantioselectively[12]. Additionally, this system was selective for C=O bonds in the presence of C=C bonds[13,14]. This Ru-BINAP-diamine catalyst system is one of the most active ever described, with turnover numbers in the millions and turnover frequencies of 63 s^{-1} [15]. The high rate of reactivity is attributed to a non-classical ligand-assisted process.

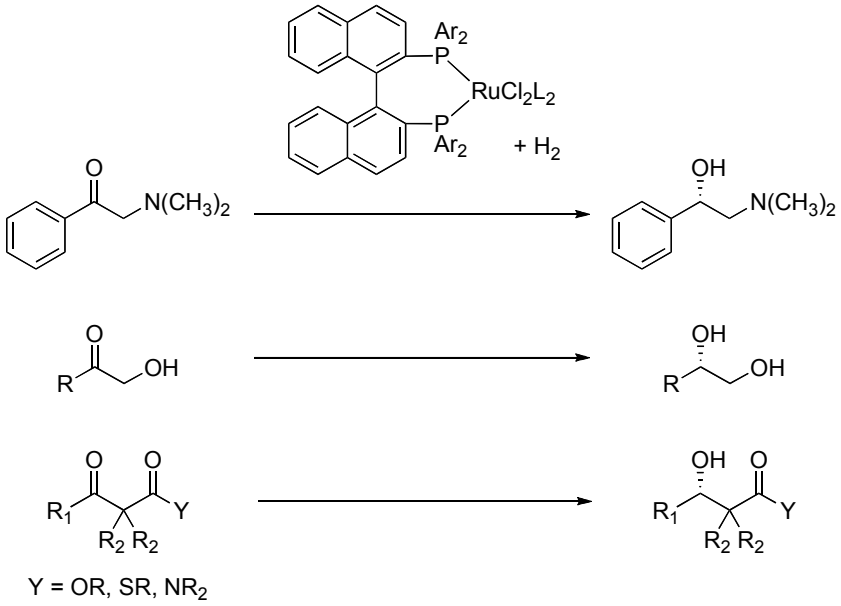

Scheme 2.1: Asymmetric hydrogenation of functionalized ketones catalyzed by Ru-BINAP complexes.

In a traditional hydrogenation, the ketone species co-ordinates to the metal and a hydride is transferred to the electrophilic carbon of the ketone forming a metal alkoxide bond that is later protonated. In Noyori's system, a six-membered transition state, involving the ketone, ruthenium hydride and a protic N-H from one of the diamines, is formed (Figure 2.1) without co-ordination of the ketone to ruthenium.

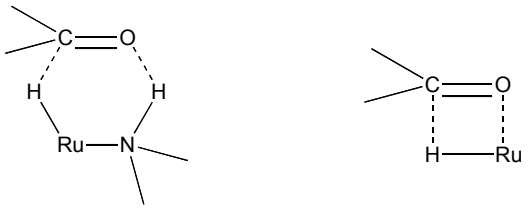

Figure 2.1: Comparison of non-classical bifunctional mechanism reported for Noyori's system (left) with classical [2+2] mechanism of metal hydrides (right).

Noyori's methodology has allowed the synthesis of a variety of secondary alcohols that are important for pharmaceutical processes (Figure 2.2)[1]. Little has been done to remove ruthenium from these systems likely due to the low catalyst loadings. However, the possibility for ruthenium contamination in the product is present and even the low amounts of ruthenium catalyst used can result in significant concentrations of ruthenium in the final product[16]. This is particularly important when the hydrogenation is used in the synthesis of pharmaceutically important products, such as those shown in Figure 2.2

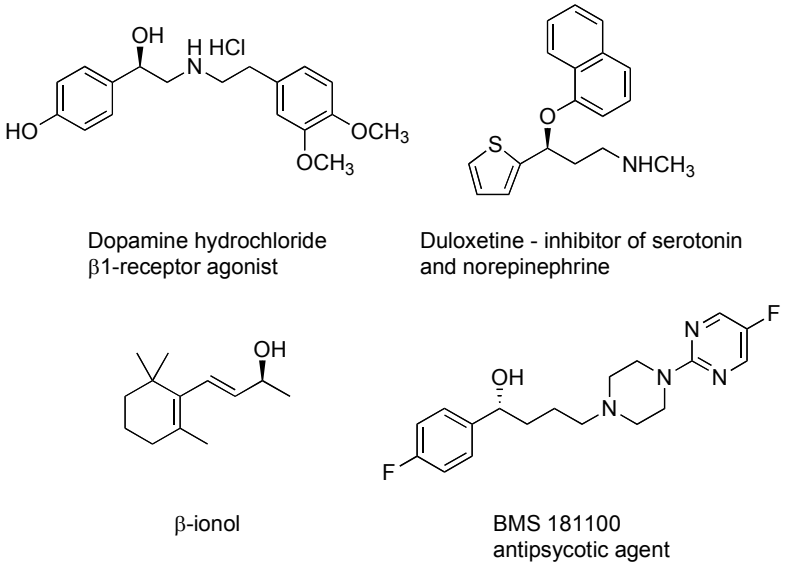

Dopamine hydrochloride
β1-receptor agonist

Duloxetine - inhibitor of serotonin and norepinephrine

β-ionol

BMS 181100
antipsycotic agent

Figure 2.2: Application of asymmetric hydrogenation to pharmaceutically interesting molecules.

Olefin metathesis is one of the easiest and most readily utilized methods for manipulating carbon-carbon double bonds. Early olefin metathesis research stemmed from polymer chemistry where ring-opening polymerization was utilized to form unsaturated polymers[17]. The catalysts were poorly defined utilizing early transition metals with alkylating agents or

grafted on silica, such as WCl_6/Bu_4Sn or MoO_3/SiO_2[18]. These catalysts suffered from long initiation times and forcing reaction conditions, likely due to the poor generation of the requisite metal alkylidenes. Additionally, these reactions were hampered by a lack of air and moisture stability and were characterized by low functional group compatibility. Eventually, tuning of the ligand environment around molybdenum led to the development of well-defined molecular catalysts such as the Schrock metathesis catalyst **1** (Figure 2.3)[19,20]. This well-defined catalyst improved functional group tolerance over the ill-defined supported metals and over early catalysts from the same group.

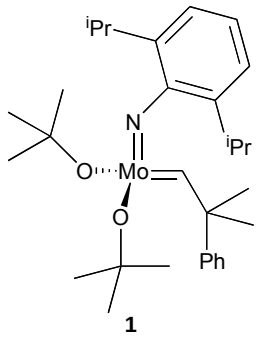

1

Figure 2.3: Schrock molybdenum based metathesis catalyst.

During the late 1980s, ruthenium species were found to catalyze ring opening metathesis polymerization (ROMP)[21-23]. After preparation of a stable ruthenium carbene (Figure 2.4, **2**), ruthenium catalyzed processes were expanded to ring closing metathesis (RCM)[24]. Furthermore, these ruthenium catalysts increased functional group tolerance over the molybdenum system and were significantly more stable to air and moisture[2]. Continued studies

have led to the development of several ruthenium-based catalysts with improved stabilities, reactivities or functional group tolerances (Figure 2.4)[2,25].

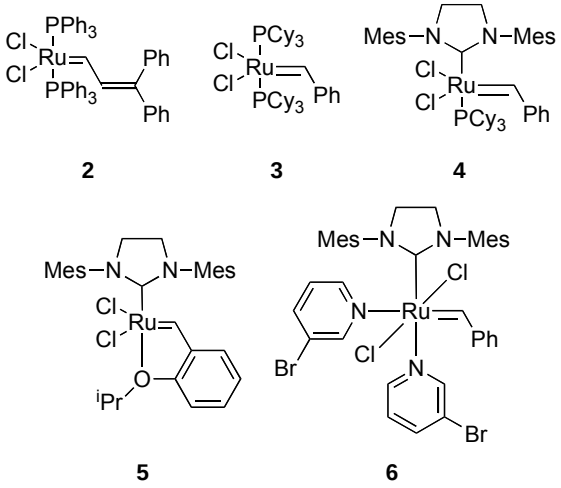

Figure 2.4: Ruthenium based olefin metathesis catalysts. Grubbs first generation catalyst **3**, Grubbs second generation catalyst **4**, Grubbs third generation catalyst **6**, Grubbs-Hoveyda catalyst **5**.

These catalysts have been utilized in a variety of synthetic methods for construction of carbon frameworks about a double bond. In particular, RCM is useful to synthesize medium and large macrocycles in natural products that would be difficult to form using other techniques (Figure 2.5). Compound **7**, a precursor to an HCV protease inhibitor, has even been scaled up to production scale by Boeringher Ingleheim[26].

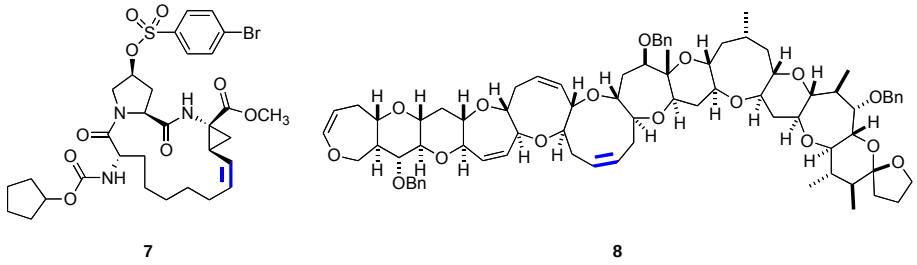

Figure 2.5: Complex macrocycles formed by ring closing metathesis (blue bonds)[26,27].

Despite the utility of ruthenium catalyzed asymmetric hydrogenation and olefin metathesis reactions, contamination of the product with highly coloured ruthenium by-products is a serious problem. This residual ruthenium can cause olefin isomerization during purification and product degradation over time[4]. There are also concerns about toxicity since ruthenium metal is easily oxidized to ruthenium tetroxide, a compound with similar toxicity to osmium tetroxide[28].

Since ruthenium contamination is problematic for the purification of fine chemicals, a number of groups have developed methods to remove ruthenium after reaction[3,16,29-31]. Almost exclusively, ruthenium remediation has focused on olefin metathesis reactions. This is likely due to the problems of olefin isomerization during purification of these products that are not present with other ruthenium catalyzed reactions[4]. Additionally, olefin metathesis catalysts are generally employed in greater amounts. Up to 20 mol % is not uncommon for a difficult metathesis, at least on bench-scale[27,29].

Attempts to reduce ruthenium contamination in the products can be divided into two categories, preparation of supported ruthenium catalysts and scavenging ruthenium after the reaction. Preparation of supported ruthenium catalysts involves modifying the catalysts to facilitate separation; this can be accomplished by using soluble or insoluble organic polymers, inorganic supports such as silica, ionic liquid or fluorous tags. The catalyst can be attached through the alkylidene, through an anionic ligand, replacing one or both of the chlorides, or through the NHC[25]. Scavenging techniques include

complexation by ligands, oxidation of the metal, adsorption on activated carbon or silica[16,29]. The residual ruthenium levels have been reported in two different units in the literature. Common with the scavenging reagents ruthenium will be reported as μg/5 mg of product, while the supported ruthenium is reported as ppm. To convert between the units, it should be noted that 200 ppm = 1 μg/5 mg for diethyl cyclopent-3-ene-1,1-dicarboxylate studied here.

One of the first ruthenium remediation methods proposed was oxidation of the residual ruthenium with lead tetraacetate[32]. Oxidation of ruthenium itself is not sufficient to remove the contaminants from the product and oxidation of ruthenium may convert it into a more toxic form, such as ruthenium tetroxide. However, oxidation facilitates the separation of ruthenium from the desired product on a silica column. This method was successful at reducing ruthenium levels in the product to 1.5 μg/5 mg of product but suffers from the introduction of another toxic metal, lead[32]. Although the silica column does help to remove most of the lead, it seems counterintuitive to remove a mildly toxic metal with a more highly toxic metal. Furthermore, silica chromatography is not feasible on an industrial scale and any method relying on silica to remove ruthenium will not be applicable to large-scale remediation.

Milder oxidizing agents such as triphenylphosphine oxide (TPPO) or dimethylsulfoxide (DMSO) were utilized by Georg's group, again aiding in separation of ruthenium by-products using chromatography[33]. Exposure of the

olefin metathesis products to 50 equivalents of either TPPO or DMSO for 12 h followed by chromatography reduced ruthenium levels from 59.7 μg/5 mg for product in the untreated case to 1.20 μg/5 mg for TPPO and 1.81 μg/5 mg for DMSO. Unfortunately, long oxidation times were required and the ruthenium content rapidly increases with exposure times of less than 12 h. Georg later immobilized the phosphine oxide on a polymer to improve the removal of ruthenium and the large number of equivalents of phosphine oxide that result[30]. To remove the need for chromatography, silica was added to the scavenging solution and the silica filtered off with the polymeric phosphine oxide. Fifty equivalents of the phosphine oxide and 50 equivalents of DMSO were required. Additional scavenging improvements were made by switching the solvent from dichloromethane to toluene and heating to reflux for 6 h. This afforded residual ruthenium levels to as low as 0.04 μg/5 mg of product[30]. While heating the spent reaction did decrease the scavenging time, there is no mention to any olefin isomerization that is likely to occur while refluxing the product in the presence of ruthenium.

A number of groups have removed ruthenium by-products with a variety of specially designed ligands to improve separation of ruthenium from the product[3,4,34]. Grubbs and coworkers have used water soluble tris(hydroxymethyl) phosphine (THMP, **9**, Figure 2.6) to bind ruthenium and remove it by aqueous extraction[4]. Binding of ruthenium was achieved using 86 equivalents of THMP to displace the tricyclohexyl phosphines already coordinated to the catalyst. The removal of chelated ruthenium could then be

performed by aqueous extraction leading to ruthenium levels of 3.35 µg/5 mg of product[4]. However, the best removal of ruthenium was after adsorption of the mixture of product and bound ruthenium on silica. Elution of the product from the silica afforded residual ruthenium concentrations of 1.03 µg/5 mg.

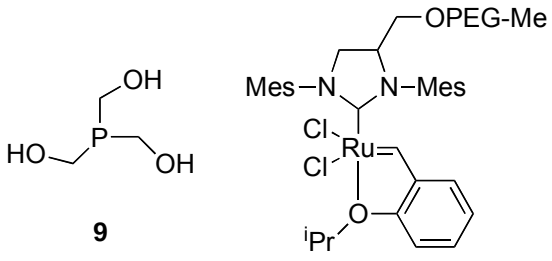

9 **10**

Figure 2.6: Water soluble phosphine scavenger and the polyethylene glycol modified Ru catalyst utilized by Grubbs.

Grubbs later improved on this method by modifying the catalyst, introducing a poly (ethylene glycol) group to increase the hydrophilicity of the ruthenium species (**10**, Figure 2.6)[35]. Treatment of this catalyst with 50 equivalents of THMP followed by aqueous extraction resulted in ruthenium levels of 0.01 µg/5 mg [3]. However, these methods suffer from the requirement of a large excess of THMP at $ 74/g (Strem). Additionally, modification of the catalyst is time consuming and dramatically increases the cost of the synthesis.

Breinbauer's group utilized a polystyrene-based chelating phosphine (**11**, Figure 2.7) to separate ruthenium from olefin metathesis products. After a metathesis reaction, treatment of the solution with 20 equivalents of **11** for 17 h followed by filtration reduced ruthenium levels from 108 µg/5 mg of product to 12 µg/5 mg[34].

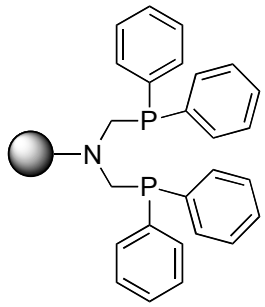

11

Figure 2.7: Polymer bound phosphine scavenging resin.

The scavenging efficiency of this reagent could be improved by filtration through a plug of silica or adsorption on activated carbon prior to filtration. Additionally, the amount of scavenging resin could be reduced to five equivalents using either of these filtration aids. This reduced the ruthenium levels to 8.3 μg/5 mg or 5.6 μg/5 mg for silica or activated carbon, respectively[34]. The long remediation times are a drawback of this method and losses in yield are observed when silica or activated carbon are used.

While trying to develop a method to stop olefin metathesis for kinetic purposes, Driver's group found that addition of carbon monoxide inhibited the metathesis activity of Grubbs' second-generation catalyst[36]. Upon isolating the organometallic complex, they discovered that the carbene had been incorporated into one of the mesityl rings of the NHC ligand through a cyclopropanation-6-π electrocyclic ring opening to give a cycloheptatriene (**12**, Figure 2.8). Isocyanates were also capable of affecting this rearrangement and also caused a loss of metathesis activity. The use of a polar isocyanate (**13**, Figure 2.8) was found to halt metathesis catalysis and,

by increasing the polarity of the ruthenium species, ease its separation from the product by chromatography.

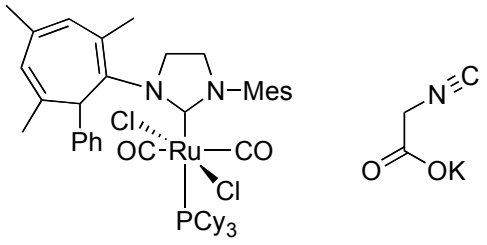

12 **13**

Figure 2.8: Carbon Monoxide poisoned metathesis inactive ruthenium complex and polar isocyanate utilized for ruthenium removal.

Indeed this method was able to halt catalysis and reduce ruthenium levels to 4.61 µg/5 mg of product for Grubbs second generation catalyst **4** (Figure 2.4) and 4.87 µg/5 mg for Grubbs first generation catalyst **3** (Figure 2.4)[31]. Driver also demonstrated the ability of this isocyanate to remediate a variety of other ruthenium-based metathesis catalysts.

An alternative approach to coordination is removal by adsorption. Cho and Kim adsorbed the ruthenium by-products on activated carbon then utilized column chromatography to remove the adsorbed ruthenium[37]. With 100 equivalents of activated carbon and a 12 h treatment, they were able to reduce ruthenium levels to 1.52 µg/5 mg of product. This could be further diminished to 0.30 µg/5 mg by adsorption of the crude reaction mixture on silica gel and filtration through a silica pad prior to treatment with activated carbon and chromatography[37]. However, this increased handling of the product resulted in a loss of overall yield as some material will be adsorbed with the ruthenium on the silica and activated carbon.

Activated carbon was also used in the first production scale ring closing metathesis reported by Nicola at Boehringer Ingleheim[26]. Using the Hoveyda-Grubbs catalyst **5**, they were able to form a 15-membered macrocycle to form **7** using RCM. The product was purified by an aqueous work up followed by treatment with activated carbon and distillation to remove most of the toluene reaction solvent. The product was then precipitated and isolated using centrifugation. Overall residual ruthenium levels varied between 2.5 µg/5 mg of product and 5 µg/5 mg[26].

Scavenging methods to remove ruthenium from organics show promise in that any ruthenium that is lost during the reaction can be recovered. Although the overall residual ruthenium levels are still somewhat high for scavenging reagents, a number have shown promise for minimizing the ruthenium contamination. The largest difficulty with the methods reported above is the reliance on chromatography, which is not a preferred method of purification on an industrial scale.

As mentioned previously, an alternative to scavenging after the reaction is to modify the catalyst to make it easier to separate from the product. One of the first attempts to generate a solid supported catalyst was performed by Grubbs[38]. They synthesized a chelating phosphine supported by polystyrene to form three ruthenium complexes of similar structure to **14** (Figure 2.9). Catalysts bound to these immobilized phosphines suffered from very low turnover numbers with rates about 150 times slower than their homogeneous analogues.

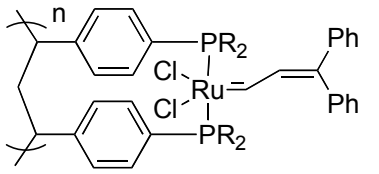

14 R = Ph, Cy

Figure 2.9: Supported olefin metathesis catalysts.

The slow rate of reaction was attributed to incomplete substitution of the non-chelating phosphine, mass transport issues with the catalyst being immobilized inside the polystyrene and a phosphine chelation effect that prevented the formation of the catalytically-active 14 electron ruthenium species[38]. There is no mention of ruthenium contamination in the paper but the catalyst was recycled three times with a loss of activity of about 20 % each cycle suggesting that ruthenium is being leached out of the polymer[38]. Similarly, Verpoort's group attached the catalyst to MCM-41 through grafted phosphine ligands. They report that the catalyst acts through a release and capture mechanism and that 1.2 – 3.2 % of the ruthenium is leaching into the product after each recycle[39].

With the advent of Grubbs second generation metathesis catalyst, modification through the NHC is a logical choice for supporting the catalyst. For instance, the modification of Grubbs second generation metathesis catalyst **4** with polyethylene glycol to serve as an aqueous soluble handle has already been discussed[3]. Blechert's group prepared two catalysts attached to Merrifield resin through the NHC (**15**, **16**, Figure 2.10)[40,41]. While they are both recyclable for RCM reactions, the later cycles require longer reaction times.

No leaching data are available. Buchmeiser and co-workers developed a monolithic support for Grubbs second generation catalyst **4** that could be used in a continuous flow system (**17**, Figure 2.10). These catalysts were active for ROMP and RCM reactions with ruthenium leaching of less than 70 ppm after the reaction[42,43]. Subner and Plenio utilized a novel technique for removing ruthenium. Employing a novel metathesis catalyst containing ferrocene groups (**18**, Figure 2.10) permitted catalyst precipitation by oxidation. The catalyst was recyclable three times for RCM but no leaching data were reported[44].

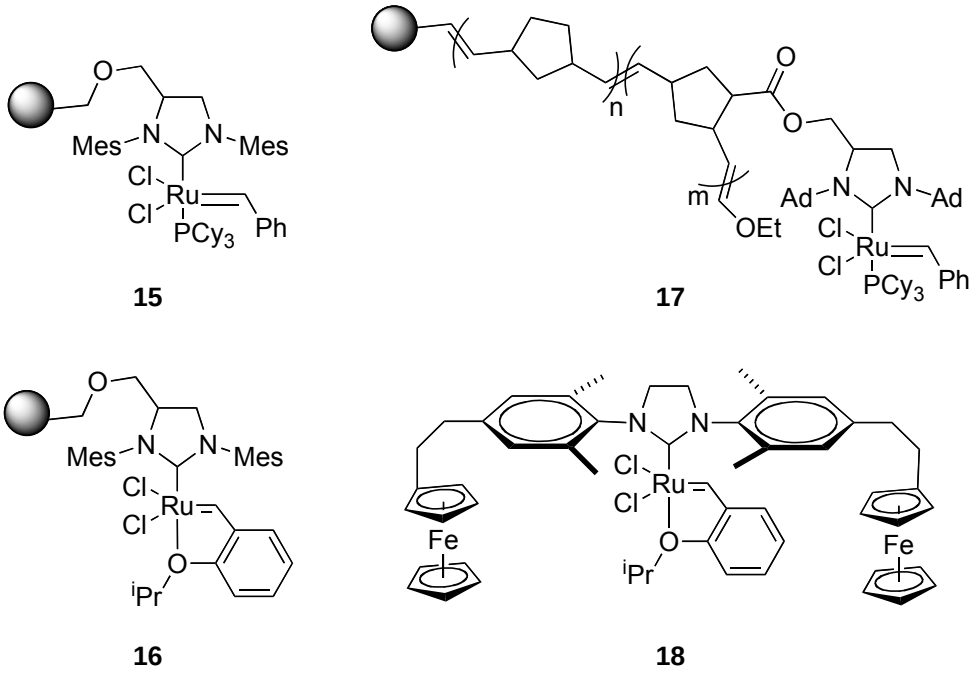

Figure 2.10: NHC immobilized catalysts.

Immobilization can also be affected through the anionic ligands, however, the metathesis activity of the catalyst has been shown to be very sensitive to the anionic ligand with chloride being optimum in most cases[25].

Mol's group introduced a fluorous polystyrene carboxylate, replacing one of the chlorides on Grubbs first generation catalyst (**19**, Figure 2.11)[45]. For RCM, residual ruthenium levels were 4.0 μg/5 mg of product and for CM 0.78 μg/5 mg with just simple filtration of the reaction. The catalyst suffered substantial decreases in activity upon recycling attributed to a 19 % loss of ruthenium from the resin after the first cycle, although this loss decreased to about 3 % for subsequent cycles[45]. Blechert utilized a similar strategy employing silica as a support instead of polystyrene (**20**, **21**, Figure 2.11). No recycling studies were preformed and the catalysts displayed similar or poorer reactivity to the homogeneous variant. Ruthenium contamination was measured to be 10-186 ppm[46].

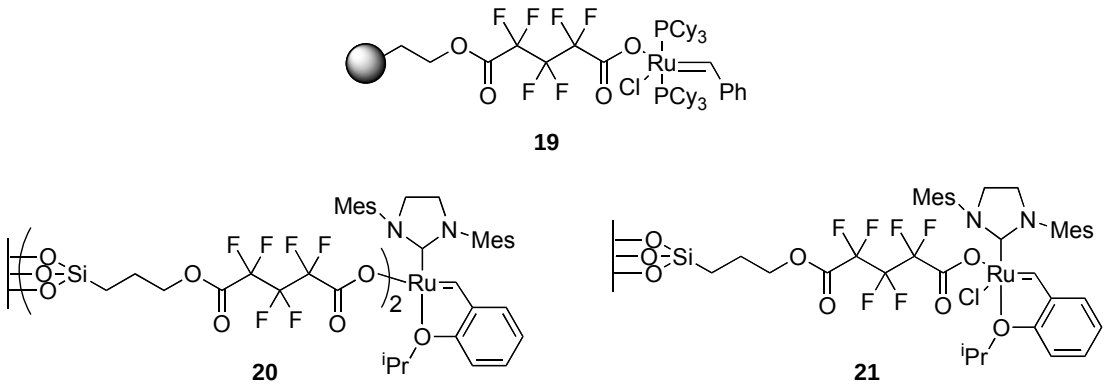

Figure 2.11: Supported metathesis catalysts through anionic ligands.

Buchmeiser's group has performed extensive modifications through the anionic ligands, mainly as carboxylate salts. Utilizing a polymer linked carboxylic acid to form immobilized catalysts similar to **19** based on second generation catalysts with an NHC instead of one of the phosphines. After catalysis with these supported ruthenium species, the residual Ru content

was 15-85 ppb[47,48]. Similarly to his NHC monoliths, Buchmeiser has also prepared monolith or silica-supported ruthenium catalysts attached through a carboxylate (Figure 2.12)[49,50]. Again these catalysts were active for metathesis reactions with low residual ruthenium contamination of 0.14 ppm.

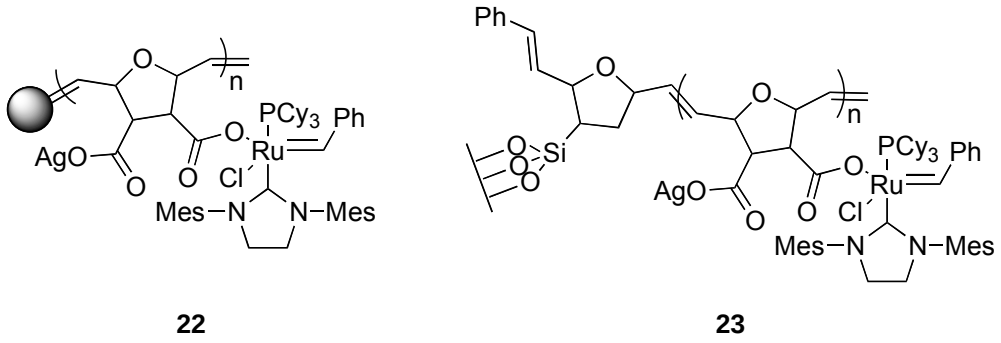

22 **23**

Figure 2.12: Monolith and silica supported ruthenium complexes for olefin metathesis.

Fogg and coworkers modified Grubbs second generation catalyst **4** replacing the chlorides with pseudohalides such as pentafluoro phenol (Figure 2.13). They were able to maintain the activity of the catalyst while facilitating its separation from the product by chromatography. While they do not report detailed numbers for ruthenium levels after chromatography, they report that all reactions were below the 100 ppm detection limit of the ICP-AES method used[51].

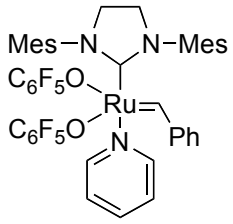

24

Figure 2.13: Alkoxyphenyl substituted metathesis catalyst utilized by Fogg's group.

The last site for immobilization is through the alkylidene ligand itself. This may seem counterintuitive, as the alkylidene ligand is lost after the first cycle of catalysis. However, Hoveyda has elegantly shown that using the bidentate alkylidene as in catalyst **5**, at least some of the ruthenium species can be recaptured and reused[52]. This offers the advantage of having solution phase catalysis after the first metathesis with the ease of removal of a heterogeneous catalyst. Hoveyda immobilized a ruthenium catalyst to a sol gel bead to give catalyst **25** (Figure 2.14). This catalyst was recyclable up to 20 cycles with good activity but high ruthenium contamination was observed in the product (300-600 ppm)[53]. Matsugi and Curran prepared a fluorous-tagged alkylidene that formed an active catalyst that was recyclable up to seven times (**26**, Figure 2.14). However, purification by fluorous phase extraction or filtration through fluorous silica gel could only lower ruthenium levels to 500 ppm[54].

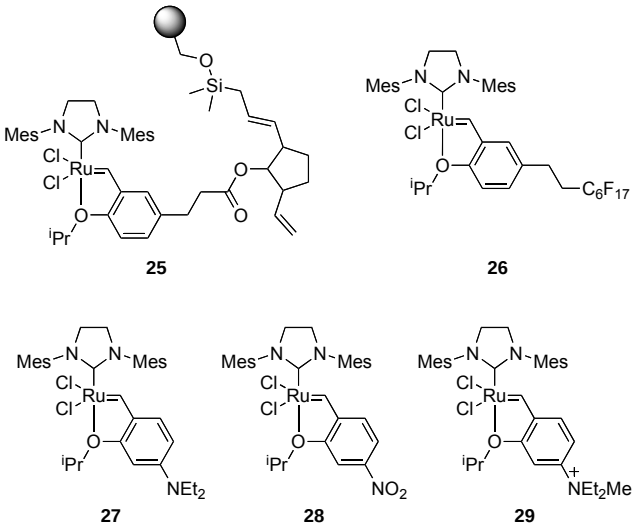

Figure 2.14: Metathesis catalysts modified through the alkylidene group.

Grela and co-workers have modified both the Hoveyda-Grubbs catalyst **5** and Grubbs third generation catalyst **6**[55-57]. In the first case, they synthesized a catalyst with an amine on the aromatic ring of the benzylidene **27** (Figure 2.14)[56]. Interestingly, with a nitro group on this aromatic ring (**28**) the catalyst is more active than the parent Grubbs-Hoveyda catalyst **5**[55]. However, with the electron donating amine, the catalyst was effectively inactive for metathesis. Quaternization of the amine to the ammonium salt (**29**) returned the catalytic activity and led to low levels of ruthenium in the product after chromatography (37 ppm)[56]. For the Grubbs third generation catalyst, one of the coordinated bromo pyridines was replaced with poly (vinyl pyridine) to generate a supported catalyst (**30**, Figure 2.15)[57]. The supported catalyst is mildly recyclable with activity being lost after 4 runs. The support can be reactivated by loading fresh **6** after washing to remove any residual metals. Unfortunately, residual ruthenium levels are not reported in the products and there is no attempt to determine the cause of the loss of activity in the supported material[57].

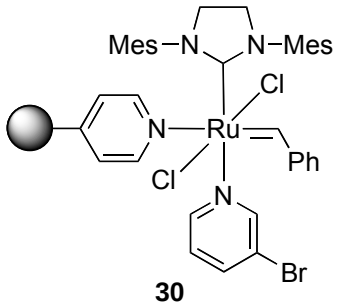

30

Figure 2.15: Polyvinylpyridine supported Grubbs third generation catalyst.

In spite of the fact that supported ruthenium systems appear to be recyclable, most suffer from appreciable leaching during each recycle and often a loss of activity. Even if the ruthenium is removed during purification the loss of ruthenium from these supported catalysis makes large scale application impractical.

As previously mentioned, the majority of current scavenging methods rely on chromatography as the ultimate means of removing ruthenium. However, for industrial purposes chromatography is not an option. Additionally, long remediation times plague many of the methods and there are toxicity issues with some of the scavengers. Other methods for ruthenium remediation rely on modifications to the catalyst which can be time consuming and costly to synthesize. Therefore we set out to develop a new method to remove ruthenium without the need for chromatography with short remediation times. Few methods utilize nitrogen–based ligands for ruthenium which is surprising given that ruthenium and nitrogen form strong bonds.

2.2 Results and Discussion

The success of our lab's thiol modified silicate-based palladium scavengers led us to examine other metals as remediation targets using mesoporous silicates[58]. Previous demonstrations that porous silicates remove ruthenium more efficiently than regular silica[59] and the use of zeolites to remove ruthenium from nuclear waste[60] suggested that ruthenium would be amenable to remediation by our silicates.

Suspecting that ruthenium, being harder than palladium, would require a different ligand for scavenging, we compared the ruthenium scavenging ability of commercially available thiol- and amino- modified amorphous silica. A 4.6 ppm solution of ruthenium trichloride trihydrate was prepared in water and the functionalized silicas were added to this solution. After one hour of scavenging, the silica was removed by simple filtration. Visual inspection of the solutions showed the amino modified silica to be a better scavenger, as indicated by the colour of the solution (Figure 2.16). ICPMS analysis showed that the thiol-functionalized silica was a relatively poor scavenger of ruthenium lowering the concentration of ruthenium to only 1.7 ppm (Table 2.1). Thus only 62 % of the ruthenium was removed from solution. However, the amino functionalized silica was a very efficient scavenger of ruthenium with a residual ruthenium concentration of 0.16 ppm after scavenging.

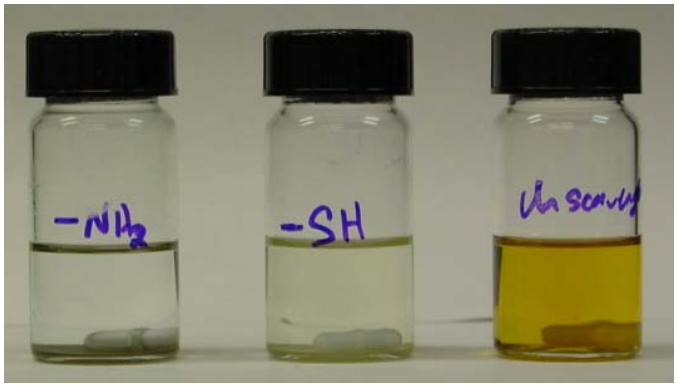

Figure 2.16: Scavenging of $RuCl_3 \bullet (H_2O)_3$ from aqueous solutions by amorphous silica functionalized with mercaptopropyl silane (middle) or aminopropyl silane (left).

Table 2.1: Scavenging of $RuCl_3 \cdot (H_2O)_3$ from aqueous solutions by amorphous silica functionalized with mercaptopropyl silane or aminopropyl silane.

Entry	Treatment	Ru conc. (ppm)	% Ru removed
1	Untreated	4.55	-
2	SiO_2-SH	1.74	62
3	SiO_2-NH_2	0.16	96

Additional scavengers were prepared by grafting various nitrogen-containing ligands onto either SBA-15 or amorphous silica (Figure 2.17). The grafting of amino ligands did not markedly change the mesostructure of SBA-15. The nitrogen sorption isotherms still show a rapid initial uptake of nitrogen indicative of a high surface area material and a sharp capillary condensation step consistent with a narrow pore size distribution (Figure 2.18). The nitrogen sorption data and elemental analysis for the modified SBA-15 silicates are summarized in Table 2.2.

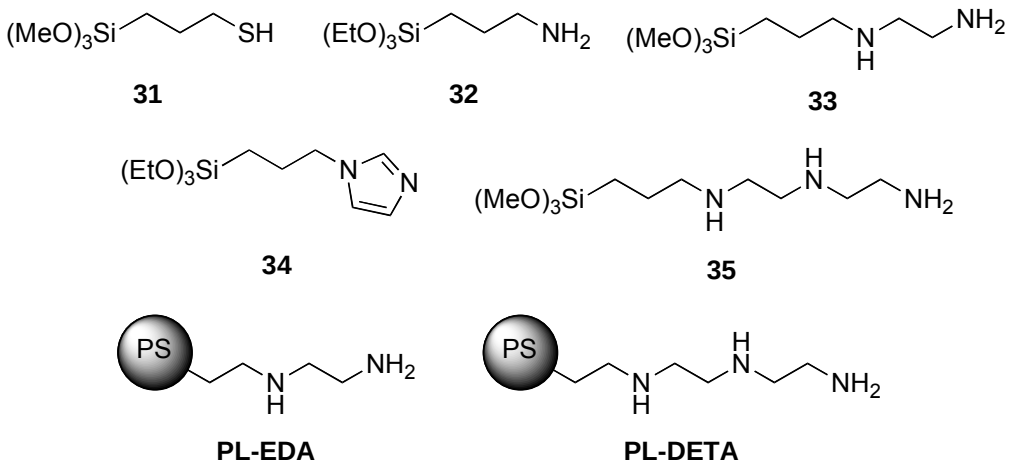

Figure 2.17: Ligands employed for the removal of ruthenium.

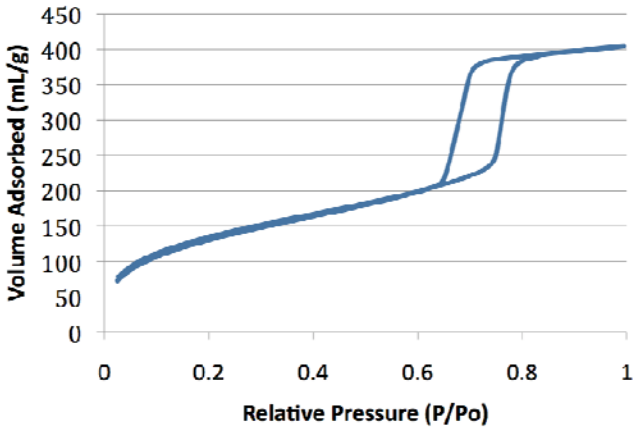

Figure 2.18: Nitrogen porosimitry of aminopropyl functionalized SBA-15 scavenger.

Aminopropyl-modified silicate (SBA-15-**32**) exhibits a large pore diameter of 52.5 Å and a high surface area of 500 m^2/g. Addition of an ethylamino group (SBA-15-**33**) to the ligand decreases the surface area but the pore size is maintained (50.1 Å). Further addition of another ethylamino group (SBA-15-**35**) again decreases the surface area but no change in pore size is observed. The nitrogen content of SBA-15-**32** was consistently around 2 mmol N/g. Consistent with this, the elemental analysis of SBA-15-**33** showed an increase of nitrogen content to 4.18 mmol N/g which corresponds to a ligand loading of 2.1 mmol/g.

Table 2.2: Characterization of ordered silicates used for ruthenium scavenging by nitrogen sorption and elemental analysis.

Entry	Silicate	Surface Area (m^2/g)	Pore Dia. (Å)	Pore Vol. (mL/g)	Nitrogen Content (mmol/g)	Ligand Loading (mmol/g)
1	SBA-15-**32**	497	52.5	0.552	1.97	1.97
2	SBA-15-**33**	307	50.1	0.440	4.18	2.09
3	SBA-15-**35**	232	53.3	0.334	5.06	1.69

A further increase in nitrogen content was observed for SBA-15-**35** but a lower ligand loading of 1.7 mmol/g was observed possibly due to congestion in the openings of the pores during grafting. Additionally, two commercially available polymer-based ruthenium scavengers (PL-EDA and PL-DETA) were purchased from Polymer Laboratories for comparison.

With a host of amine-based scavengers at hand, we examined the capability of these scavengers to remove $RuCl_3 \bullet (H_2O)_3$ from aqueous solutions (Table 2.3 and 2.4). An ordered thiol modified silicate (SBA-15-**31**) was also ineffective at removing ruthenium from solution, removing only 25 % of the ruthenium. All of the amine-based scavengers proved to be extremely effective at removing ruthenium, reducing the levels by a minimum of 98% at low initial metal concentrations (Table 2.3). Although the differences in scavengers were marginal, the aminopropyl modified SBA-15-**32** and SiO_2-**32** removed 99.95 % of the ruthenium corresponding to a drop from 38.3 ppm to less than 20 ppb. While the amorphous SiO_2-**32** scavenger performed as well as the ordered silicate at low concentrations, at higher concentrations of ruthenium the difference between the two scavengers became apparent (Table 2.4). SBA-15-**32** maintained its high scavenging ability, removing 99.98 % of the 234 ppm ruthenium to yield a solution of 32 ppb ruthenium. SiO_2-**32**, on the other hand, was a poorer scavenger removing only 90 % of the initial ruthenium (21.5 ppm). The coordinating triamine ligand (SiO_2-**35**) was more effective bringing ruthenium levels down to 4.36 ppm. The imidazole ligand

that was particularly effective at low ruthenium concentration became a poor scavenger at high concentrations, removing only 75 % of the ruthenium.

Table 2.3: Comparison of amine based scavengers for low initial concentrations of Ru.

Entry	Scavenger	Initial [Ru] (ppm)	Ligand:Ru ratio	Residual Ru in solution	
				[Ru] (ppm)	% Removed
1	SBA-15-**31**	42.3	17.3:1	31.5	25.5
2	SBA-15-**32**	38.3	52.5:1	0.017	99.95
3	SiO_2-**32**	38.3	26.6:1	0.016	99.95
4	SBA-15-**33**	38.7	55.4:1	0.139	99.64
5	SiO_2-**34**	34.0	30.8:1	0.420	99.83
6	SBA-**35**	38.7	45.0:1	0.227	99.28
7	SiO_2-**35**	34.0	40.5:1	0.056	98.76
8	PL-EDA	38.7	85.9:1	0.130	99.66
9	PL-DETA	38.7	75.2:1	0.255	99.34

Table 2.4: Comparison of amine based scavengers at a Ru concentration of 234 ppm.

Entry	Scavenger	Ligand:Ru ratio	Residual Ru in solution	
			[Ru] (ppm)	% removed
1	SBA-15-**32**	8.66:1	0.032	99.98
2	SiO_2-**32**	4.53:1	21.5	90.8
3	SiO_2-**34**	4.39:1	57.9	75.3
4	SiO_2-**35**	5.76:1	4.36	98.1

Having shown that the amino-functionalized silicates were effective scavengers in aqueous solutions, we next examined the ability of the scavengers to remove ruthenium from organic solvents, closer to actual reaction conditions. Both SiO_2-**32** and SBA-**32** were very effective at removing $RuCl_3 \bullet (H_2O)_3$ from THF, likely due to the hydrophilicity of the ruthenium complex. Even at high loadings of 613 ppm, both scavengers were able to remove >99 % of the ruthenium (Table 2.5).

Our next challenge was to show that our scavengers could remove ruthenium from solution when it was complexed with ligands, such as phosphines. We selected Grubbs first generation catalyst **3** as a representative ruthenium complex since most remediation work in the literature has focused on cleaning up Grubbs catalyzed metathesis reactions[4,16,29,31-34,37]. Both SBA-15-**32** and SiO_2-**32** were successful at removing Grubbs first generation catalyst from solution. As expected, Grubbs catalyst was more difficult to remove from THF than the inorganic ruthenium complex, and highly coloured solutions were obtained at concentrations higher than 200 ppm (Figure 2.19). Even at ruthenium concentrations near 100 ppm, slight colour still exists in solution. High levels of scavenging (>90 %) were obtained for initial concentrations of Grubbs first generation catalyst less than 100 ppm (Table 2.5). At low concentrations of ruthenium, both scavengers are able to remove 99 % of Ru with SBA-15-**32** remediating the solution to 30 ppb levels.

Table 2.5: Scavenging of ruthenium complexes from THF solutions with amine based scavengers.

Entry	Ru Source	Initial [Ru] (ppm)	Residual Ru in solution	
			[Ru] (ppm)	% removed
		Scavenger: SBA-**32**		
1	$RuCl_3•(H_2O)_3$	419	0.0085	99.998
2		613	3.64	99.4
3	Grubbs' Gen I	13.7	0.031	99.5
4		40.2	0.241	99.4
5		105	1.73	97.6
6		242	35.3	82.9
		Scavenger: SiO_2-**32**		
7	$RuCl_3•(H_2O)_3$	419	0.0043	99.999
8		613	0.0124	99.998
9	Grubbs' Gen I	13.7	0.139	99.0
10		40.2	1.51	96.2
11		105	3.33	96.8
12		242	48.6	79.9

The final challenge was to remediate ruthenium from actual reaction mixtures. Many groups have attempted ruthenium removal from Grubbs metathesis reactions, as described in the introduction. The precise details of scavenging with different materials are given in Table 2.6.

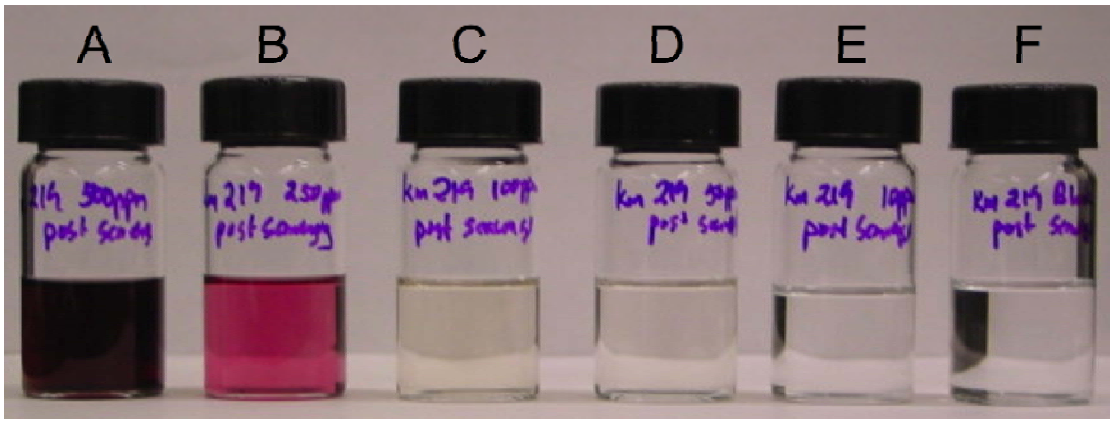

Figure 2.19: Scavenging of Grubbs' generation I catalyst from THF solution by SBA-15-**32.** All vials are shown after scavenging and filtration of the scavenging reagent. Initial ruthenium concentrations: A = 533, B = 242, C = 105, D = 40, E = 14, F = 0.

Grubbs' group used water soluble phosphine **9**, followed by an aqueous work up[4]. Without the use of silica, 86 equivalents of the phosphine and three aqueous washes were able to reduce the ruthenium content from 74.6 µg/5 mg to 3.35 µg/5 mg. The use of a silica plug was able to further reduce these levels to 1.03 µg/5 mg[4]. Breinbauer and co-workers used polymer bound chelating phosphine **11**[34]. After treatment 12 µg/5 mg of ruthenium remain, this value could be improved to 8.3 µg/5 mg by passing the crude mixture through a silica plug or treatment with activated carbon improved the scavenging to 5.6 µg/5 mg[34]. Unfortunately, treatment with silica or activated carbon reduced the recovered yield by up to 20 %.

Georg *et al.* utilized triphenylphosphine oxide (TPPO) and dimethylsulfoxide (DMSO) for the removal on silica. Their method was able to successfully reduce ruthenium levels from 59.7 µg/5 mg to 1.91 µg/5 mg with 100 equivalents of TPPO and 1.34 µg/5 mg with 100 equivalents of DMSO[33].

Table 2.6: Scavenging of olefin metathesis reactions from literature sources.

Entry	Ref	Treatment	[Ru] (μg/5 mg)
1	[4]	Untreated	74.6
2		86 eq ($P(CH_2OH)_3$ + 3 H_2O washes	3.35
3		86 eq $P(CH_2OH)_3$ + silica	1.03
4	[34]	Untreated	108
5		20 eq **11**	12
6		5 eq **11** then silica	8.3
7		5 eq **11** then activated carbon	5.6
8	[33]	Untreated	59.7
9		100 eq TPPO then silica	1.91
10		100 eq DMSO then silica	1.34
11	[32]	Untreated	84.5
12		1.25 eq $Pb(OAc)_4$ then silica	1.50
13	[31]	Untreated	97
14		4.4 eq **13** then silica	4.87
15	[37]	Untreated	71.58
16		100 eq activated carbon then silica	1.52
17		Adsorb in silica then as entry 16	0.30
19	[51]	Catalyst **24** then silica	< 0.5
20	[3]	Untreated	22
21		5 H_2O washes then activated carbon	< 0.0002

Lead tetracetate was utilized by Paquette's group to oxidize ruthenium to improve remediation. Under their conditions an initial concentration of 84.5

μg/ 5 mg was reduced to 1.50 μg/5 mg using 1.25 equivalents of lead tetraacetate[32]. After purification there was still trace amounts of lead present in the product, 0.025 μg/5 mg.

Driver and co-workers utilized polar isocyanate **13** for ruthenium removal. Using 4.4 equivalents of the isocyanide they were able to reduce ruthenium levels from 97 μg/5 mg to 4.87 μg/5 mg after silica chromatography[31]. Cho and Kim remediated the Grubbs' metathesis reaction using only activated carbon and silica gel[37]. Treatment with 100 equivalents of activated carbon followed by a silica column was able to reduce the ruthenium levels from 71.6 μg/5 mg to 1.52 μg/5 mg. This number was reduced further (0.30 μg/5 mg) by first adsorbing the crude product onto a silica pad and eluting prior to treatment with activated carbon and a silica column.

Fogg's catalyst **24**, after chromatography gives less that 0.5 μg of Ru/5 mg of product[51]. Other modifications have been more complex, Hong and Grubbs have modified a Grubbs-Hoveyda catalyst by attaching polyethylene glycol (PEG) to the carbene forming **10**. Ruthenium levels as low as 0.0002 μg/5 mg could be achieved by aqueous extraction and treatment with activated carbon[3]. While both these methods produce essentially ruthenium free metathesis products they suffer from the need to derivatize the catalysts prior to the reaction, which can be time consuming and costly.

As in previous cases, diallyl-diethylmalonate was chosen as a substrate for Grubbs' ring closing metathesis, performed with Grubbs' first generation catalyst in a dilute dichloromethane solution (Equation 2.1).

36 **37** (eq. 2.1)

After 2 hrs of stirring at room temperature the reaction had gone to completion and only the cyclopentene product was observed by ^{1}H NMR (Figure 2.20).

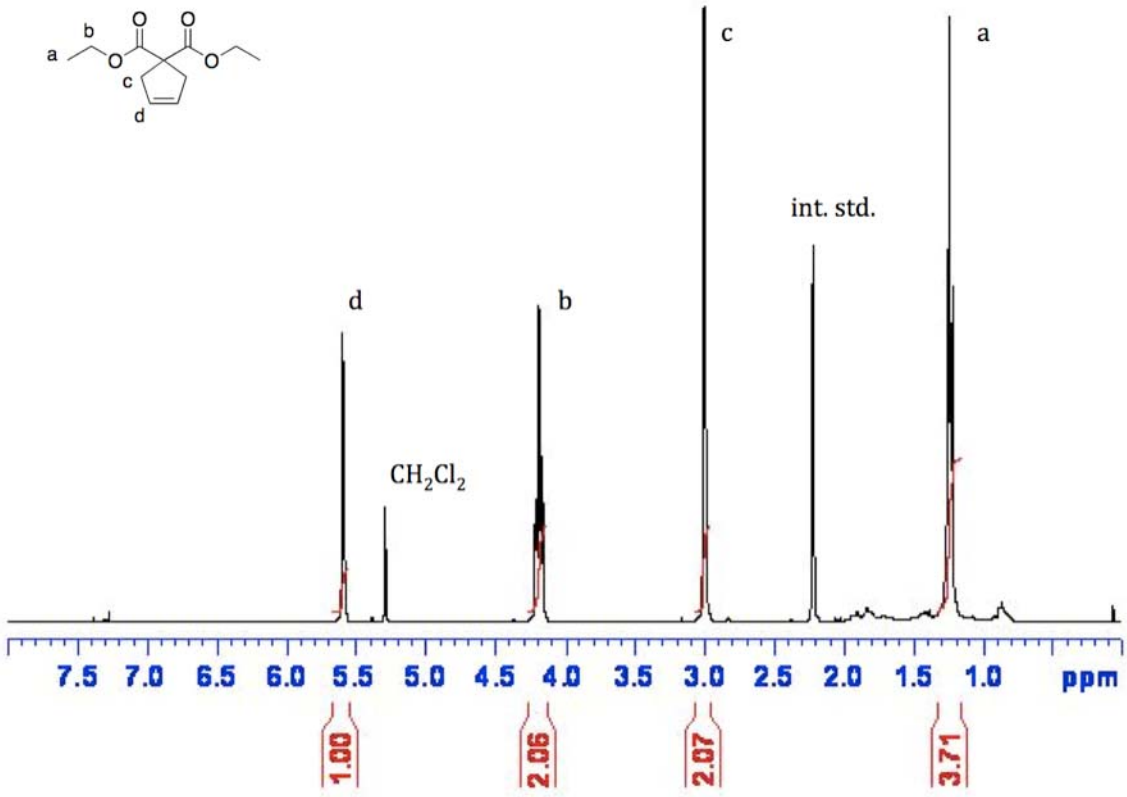

Figure 2.20: NMR of crude metathesis product.

The solution was treated with one or two portions of SBA-**32** or SiO_2-**32** for 1 hr to remove the catalyst. ICPMS analysis of the resulting solutions showed reduced levels of ruthenium compared to the unscavenged reaction (Table

2.7). Ruthenium remediation of 88 % was achieved with scavenging in either one large batch (entry 2 Table 2.7) or two smaller batches (entry 4). While our values are comparable to those found in the literature our method offers the significant advantages of no requirement to modify the catalyst, little handling of the material after the reaction, simple filtration to remove the ruthenium bound silicate, short remediation time (1 hr), easily attainable scavenging reagents and most importantly, no need for chromatography.

Table 2.7: Scavenging of metathesis reactions with amine-functionalized scavengers.

Entry	Scavenger	Initial [Ru] (ppm)[a]	Residual [Ru]		
			[Ru] (ppm)	[Ru] (μg/5 mg)	% removed
1	SBA-15-**32**	237 (126)	35.0	18.7	85.23
2		197 (105)	23.0	12.2	88.32
3		74.0 (34.9)	17.7	8.36	76.08
4[b]		74.0 (34.9)	8.23	3.88	88.88
5	SiO_2-**32**	66.8 (31.5)	18.3	8.64	72.60
6[b]		66.8 (31.5)	11.6	5.49	82.63

[a] The number in parenthesis is the concentration of ruthenium as μg/5 mg of product. [b] The sample from the previous entry was treated with another portion of silicate.

Our second test reaction was the hydrogenation of acetophenone with Noyori's catalyst **40** (Equation 2.2). The hydrogenation was carried out at 150 psi for 6 hrs. The crude solution was treated with 250 mg of SBA-15-**32** and after filtration, the solution analyzed by ICPMS. The residual ruthenium

content was 0.17 ppm, corresponding to a removal of 99.2 % of the initial ruthenium added. To the best of our knowledge, this is the first reported ruthenium remediation of Noyori's catalyst.

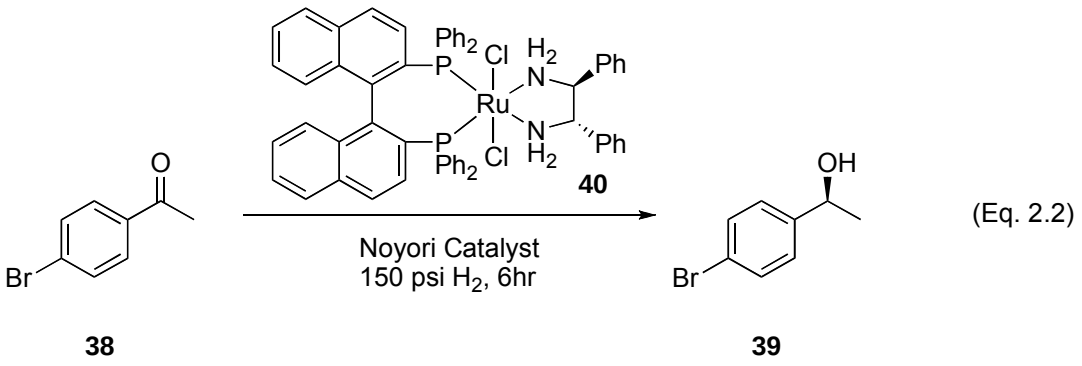

38 **39** (Eq. 2.2)

2.3 Conclusions

We have successfully prepared and characterized by nitrogen sorption and elemental analysis a variety of amino functionalized SBA-15 materials. The ordered materials as well as commercially available amino-functionalized silica and polymers were successfully employed to scavenge ruthenium from aqueous and organic solutions of ruthenium complexes. The aminopropyl ordered and amorphous silicates proved to be most efficient at removing ruthenium from solution. These were then both used to remove ruthenium from metathesis reactions. Our scavengers were able to remove residual ruthenium in the metathesis product to levels comparable to other scavenging methods previously reported, offering the advantage of using low toxicity reagents, simple removal of the scavenging reagent and abolishing the need for silica chromatography to remove ruthenium. Furthermore, we applied our amino functionalized SBA-15 scavenger to Noyori's asymmetric

hydrogenation reaction. Our scavenger was successful at reducing the ruthenium contamination after the hydrogenation. To the best of our knowledge this is the first reported remediation of a ruthenium catalyzed hydrogenation. Given the ubiquity of these reactions and the importance of removing ruthenium by products this method promises to increase the utility of ruthenium catalyzed reactions.

2.4 References

(1) Noyori, R. *Angew. Chem. Int. Ed.* **2002**, *41*, 2008.
(2) Trnka, T.M.; Grubbs, R.H. *Acc. Chem. Res.* **2001**, *34*, 18.
(3) Hong, S.H.; Grubbs, R.H. *Org. Lett.* **2007**, *9*, 1955.
(4) Maynard, H.D.; Grubbs, R.H. *Tetrahedron Lett.* **1999**, *40*, 4137.
(5) Knowles, W.S.; Sabacky, M.J. *Chem. Commum.* **1968**, 1445.
(6) Noyori, R.; Takaya, H. *Acc. Chem. Res.* **1990**, *23*, 345.
(7) Kitamura, M.; Tokunaga, M.; Ohkuma, T.; Noyori, R. *Tetrahedron Lett.* **1991**, *32*, 4163.
(8) Mashima, K.; Kusano, K.; Sato, N.; Matsumura, Y.; Nozaki, K.; Kumobayashi, H.; Sayo, N.; Hori, Y.; Ishizaki, T.; Akutagawa, S.; Takaya, H. *J. Org. Chem.* **1994**, *59*, 3064.
(9) Kitamura, M.; Ohkuma, T.; Inoue, S.; Sayo, N.; Kumobayashi, H.; Akutagawa, S.; Ohta, T.; Takaya, H.; Noyori, R. *J. Am. Chem. Soc.* **1988**, *110*, 629.
(10) Brown, H.C.; Krishnamurthy, S. *Tetrahedron* **1979**, *35*, 567.
(11) Midland, M.M. *Chem. Rev.* **1989**, *89*, 1553.
(12) Ohkuma, T.; Ooka, H.; Hashiguchi, S.; Ikariya, T.; Noyori, R. *J. Am. Chem. Soc.* **1995**, *117*, 2675.
(13) Ohkuma, T.; Ooka, H.; Ikariya, T.; Noyori, R. *J. Am. Chem. Soc.* **1995**, *117*, 10417.
(14) Ohkuma, T.; Ikehira, H.; Ikariya, T.; Noyori, R. *Synlett* **1997**, 467.
(15) Doucet, H.; Ohkuma, T.; Murata, K.; Yokozawa, T.; Kozawa, M.; Katayama, E.; England, A.F.; Ikariya, T.; Noyori, R. *Angew. Chem. Int. Ed.* **1998**, *37*, 1703.
(16) McEleney, K.; Allen, D.P.; Holliday, A.E.; Crudden, C.M. *Org. Lett.* **2006**, *8*, 2663.
(17) Calderon, N.; Chen, H.Y.; Scott, K.W. *Tetrahedron Lett.* **1967**, *8*, 3327.
(18) *Handbook of Metathesis*; Grubbs, R.H., Ed.; Wiley-VCH: Weinheim, Germany, 2003; Vol. 1.
(19) Schrock, R.R.; Murdzek, J.S.; Bazan, G.C.; Robbins, J.; DiMare, M.; O'Regan, M. *J. Am. Chem. Soc.* **1990**, *112*, 3875.
(20) Oskam, J.H.; Fox, H.H.; Yap, K.B.; McConville, D.H.; O'Dell, R.; Lichtenstein, B.J.; Schrock, R.R. *J. Organomet. Chem.* **1993**, *459*, 185.
(21) Novak, B.M.; Grubbs, R.H. *J. Am. Chem. Soc.* **1988**, *110*, 960.
(22) Zenkl, E.; Stelzer, F. *J. Mol. Catal.* **1992**, *75*, 1.
(23) Lu, S.Y.; Quayle, P.; Heatley, F.; Booth, C.; Yeates, S.G.; Padget, J.C. *Macromolecules* **1992**, *25*, 2692.
(24) Nguyen, S.T.; Johnson, L.K.; Grubbs, R.H.; Ziller, J.W. *J. Am. Chem. Soc.* **1992**, *114*, 3974.
(25) Deshmukh, P.H.; Blechert, S. *Dalton Trans.* **2007**, 2479.
(26) Nicola, T.; Brenner, M.; Donsbach, K.; Kreye, P. *Org. Proc. Res. Dev.* **2005**, *9*, 513.
(27) Hirama, M.; Oishi, T.; Uehara, H.; Inoue, M.; Maruyama, M.; Oguri, H.; Satake, M. *Science* **2001**, *294*, 1904.

(28) Tojo, G.; Fernandez, M. In *Oxidation of Primary Alcohols to Carboxylic Acids*; Tojo, G., Ed.; Springer: New York, 2007, p 61.
(29) Conrad, J.C.; Fogg, D.E. *Curr. Org. Chem.* **2006**, *10*, 185.
(30) Haack, K.L.; Ahn, Y.M.; Georg, G.I. *Molecular Diversity* **2005**, *9*, 301.
(31) Galan, B.R.; Kalbarczyk, K.P.; Szczepankiewicz, S.; Keister, J.B.; Driver, S.T. *Org. Lett.* **2007**, *9*, 1203.
(32) Paquette, L.A.; Schloss, J.D.; Efremov, I.; Fabris, F.; Gallou, F.; Mendez-Andino, J.; Yang, J. *Org. Lett.* **2000**, *2*, 1259.
(33) Ahn, Y.M.; Yang, K.L.; Georg, G.I. *Org. Lett.* **2001**, *3*, 1411.
(34) Westhus, M.; Gonthier, E.; Brohm, D.; Breinbauer, R. *Tetrahedron Lett.* **2004**, *45*, 3141.
(35) Hong, S.H.; Grubbs, R.H. *J. Am. Chem. Soc.* **2006**, *128*, 3508.
(36) Galan, B.R.; Gembicky, M.; Dominiak, P.M.; Keister, J.B.; Driver, S.T. *J. Am. Chem. Soc.* **2005**, *127*, 15702.
(37) Cho, J.H.; Kim, B.M. *Org. Lett.* **2003**, *5*, 531.
(38) Nguyen, S.T.; Grubbs, R.H. *J. Organomet. Chem.* **1995**, *497*, 195.
(39) Melis, K.; De Vos, D.; Jacobs, P.; F., V. *J. Mol. Catal. A: Chem.* **2001**, *169*, 47.
(40) Schurer, S.C.; Gessler, S.; Buschmann, N.; Blechert, S. *Angew. Chem. Int. Ed.* **2000**, *39*, 3898.
(41) Randl, S.; Buschmann, N.; Connon, S.J.; Blechert, S. *Synlett* **2001**, *10*, 1547.
(42) Mayr, M.; Mayr, B.; Buchmeiser, M.R. *Angew. Chem. Int. Ed.* **2001**, *40*, 3839.
(43) Buchmeiser, M.R. *New J. Chem.* **2004**, *28*, 549.
(44) Subner, M.; Plenio, H. *Angew. Chem. Int. Ed.* **2005**, *45*, 6885.
(45) Nieczypor, P.; Buchowicz, W.; Meester, W.J.N.; Rutjes, F.P.J.T.; Mol, J.C. *Tetrahedron Lett.* **2001**, *42*, 7103.
(46) Vehlow, K.; Maechling, S.; Kohler, K.; Blechert, S. *J. Organomet. Chem.* **2006**, *691*, 5267.
(47) Krause, J.O.; Nuyken, O.; Wurst, K.; Buchmeiser, M.R. *Chem. Eur. J.* **2004**, *10*, 777.
(48) Halback, T.S.; Mix, S.; Fischer, D.; Maechling, S.; Krause, J.O.; Sievers, C.; Blechert, S.; Nuyken, O.; Buchmeiser, M.R. *J. Org. Chem.* **2005**, *70*, 4687.
(49) Krause, J.O.; Lubbad, S.; Nuyken, O.; Buchmeiser, M.R. *Adv. Synth. Catal.* **2003**, *345*, 996.
(50) Yang, L.; Mayr, M.; Wurst, K.; Buchmeiser, M.R. *Chem. Eur. J.* **2004**, *10*, 5761.
(51) Conrad, J.C.; Parnas, H.H.; Snelgrove, J.L.; Fogg, D.E. *J. Am. Chem. Soc.* **2005**, *127*, 11882.
(52) Kingsbury, J.S.; Hoveyda, A.H. *J. Am. Chem. Soc.* **2005**, *127*, 4510.
(53) Kingsbury, J.S.; Garber, S.B.; Giftos, J.M.; Gray, B.L.; Okamoto, M.M.; Farrer, R.A.; Fourkas, J.T.; Hoveyda, A.H. *Angew. Chem. Int. Ed.* **2001**, *40*, 4251.
(54) Matsugi, M.; Curran, D.P. *J. Org. Chem.* **2005**, *70*, 1636.

(55) Grela, K.; Harutyunyan, S.; Michrowska, A. *Angew. Chem. Int. Ed.* **2002**, *41*, 4038.
(56) Michrowska, A.; Gulajski, L.; Kaczmarska, Z.; Mennecke, K.; Kirschning, A.; Grela, K. *Green Chem.* **2006**, *8*, 658.
(57) Mennecke, K.; Grela, K.; Kunz, U.; Kirschning, A. *Synlett* **2005**, *19*, 2948.
(58) Crudden, C.M.; Sateesh, M.; Lewis, R. *J. Am. Chem. Soc.* **2005**, *127*, 10045.
(59) Krompiec, S.; Pigulla, M.; Krompiec, M.; Baj, S.; Mrowiec-Bialon, J.; Kasperczyk, J. *Tetrahedron Lett.* **2004**, *45*, 5257.
(60) Granados, F.; Bertin, V.; Bulbulian, S. *J. Radioanal. Nucl. Chem.* **2004**, *260*, 379.

Chapter 3: Palladium Loaded Thiol-Functionalized SBA-15. Catalyst Activity, Reusability, and Stability.

3.1 Introduction

Palladium catalyzed cross-coupling reactions to form C-C and C-X bonds have become commonplace in the field of organic chemistry (Figure 3.1)[1,2]. These cross-coupling reactions offer mild conditions and good functional group tolerance relative to conventional methods for forming these bonds. A number of halide and pseudohalide electrophiles can be used with virtually any main-group organometallic nucleophile (Figure 3.1).

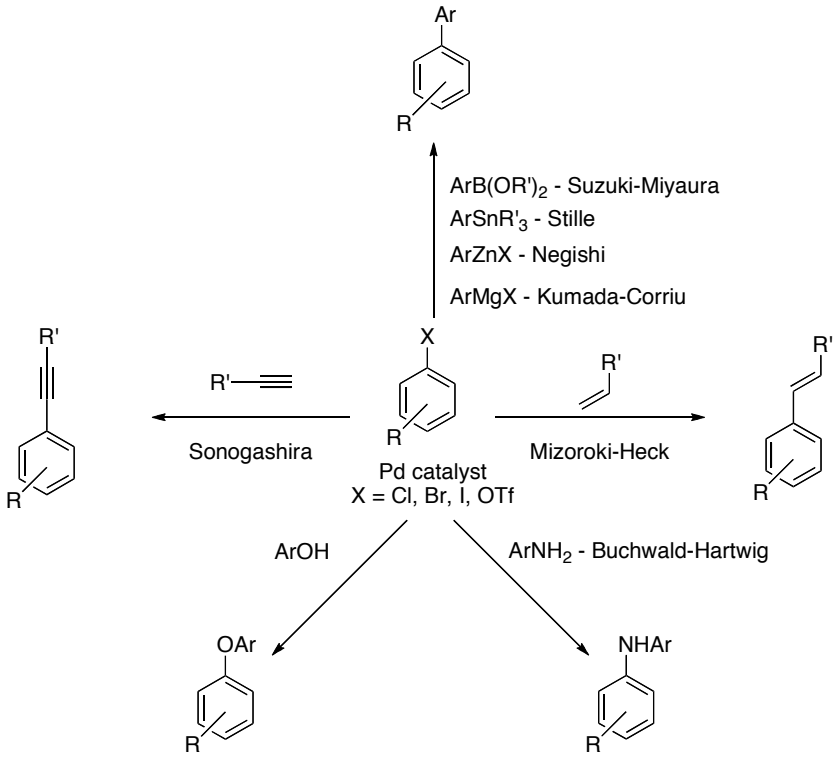

Figure 3.1: Palladium catalyzed coupling reactions.

In particular, the use of organoboron compounds through the Suzuki-Miyaura reaction has become widespread due to the ease of handling and low toxicity of organoboron compounds[3,4]. The biaryl motif is common amongst natural products and biologically active molecules. For example Losartan **1**, an AT II antagonist produced by Merck, and Boscalid **2**, a fungicide from BASF, are both prepared by a Suzuki-Imamura coupling to form the core biaryl unit (Figure 3.2)[5].

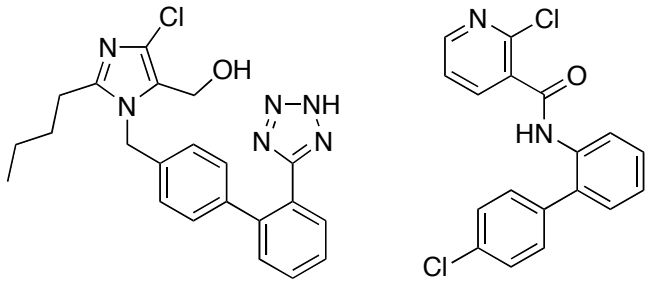

1, Losartan **2**, Boscalid

Figure 3.2: Active pharmaceutical ingredients synthesized using a Suzuki-Miyaura reaction to form the birayl motif.

These structures would be difficult to synthesize without cross coupling chemistry. A good example of the reduction in synthetic complexity that results from the application of a cross coupling reaction is the construction of the biphenyl core of Valsartan **3** (Figure 3.3). Using conventional reactions it took five steps from methoxybenzoic acid, whereas this same group could be prepared in one step using a Suzuki Coupling[5].

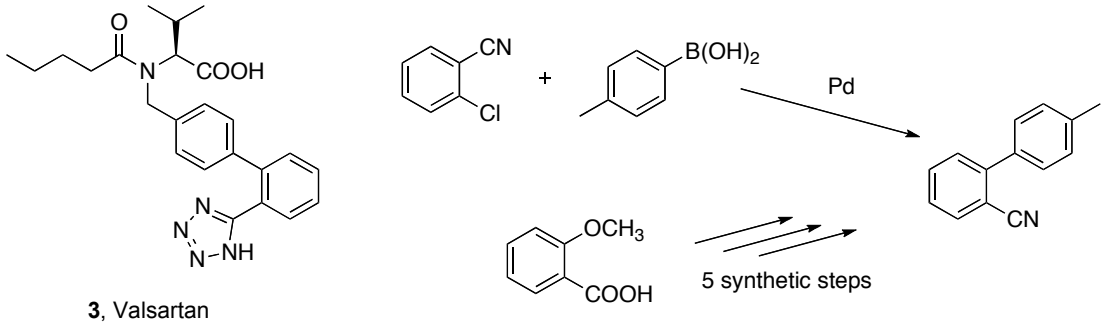

3, Valsartan

Figure 3.3: Synthetic improvement by using Suzuki-Miyaura coupling.

The Sonogashira reaction is also of significant industrial utility for the synthesis of Csp^2-Csp bonds in a number of bioactive molecules such as Tazarotene from Allergan and Terbinafine produced by Sandoz (Figure 3.4)[5,6].

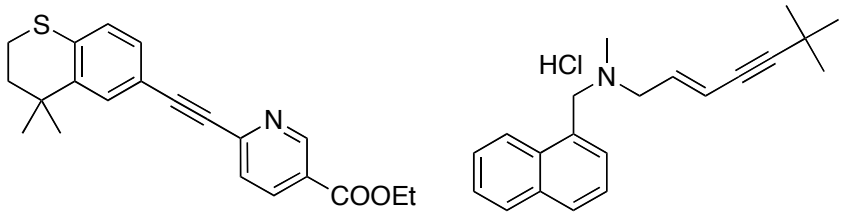

4, Tazarotene **5**, Terbinafine

Figure 3.4: Sonogashira coupling applied to pharmaceutically active molecules.

Soluble palladium complexes are commonly utilized as catalysts for these reactions. However, their use presents a challenge in that palladium is often retained in the product as an unwanted contaminant, even after attempted purification[6,7]. Thus removing palladium from organic compounds is important in order to meet FDA guidelines due to unknown toxicological effects and also due to cost. Palladium is not a cheap metal and even using

fractions of percentage loadings of catalysts on industrial scale this amounts to a considerable loss of palladium. A number of purification methods have been developed to remove palladium from pharmaceutical ingredients[6]. As palladium is not volatile, distillation of the product away from the palladium is one possibility. However, isomerization and degradation of the product is a significant possibility during heating in the presence of a transition metal, especially as many pharmaceutical compounds are not highly volatile. Another technique is to adsorb the palladium onto a solid with subsequent filtration to remove the bound palladium. A variety of functionalized solids from polymers to silicas have been utilized for Pd removal with good results[6]. Activated carbon has also been used as an absorbent however, adsorption of the desired product often occurs along with the palladium[6]. Often palladium can be removed by crystallization of the product while keeping palladium in solution[6].

Instead of removing palladium after catalysis, another alternative is to utilize a heterogeneous catalyst. Converting a homogeneous complex to a heterogeneous one offers several advantages, including easier recovery of the catalyst, recyclability and the capability to be used in continuous flow or batch reactors[8-10]. A variety of strategies have been used to convert homogeneous catalysts to heterogeneous materials, the most straightforward of these being adsorption of the metal onto a solid support, such as the ubiquitous palladium on carbon[11]. However, this method relies on weak physisorptive interactions to keep the metal bound to the solid and often

results in a large amount of leached metal contaminating the product. In addition, detailed studies have shown that such catalysts generally operate by a homogeneous mechanism, via dissolved Pd[11-21].

Other, more complex supports have also been investigated. Ying's group has incorporated palladium into mesoporous silicas by impregnation or vapour deposition[22,23]. These materials are active catalysts for the Mizoroki-Heck reaction but they have been demonstrated to act by leaching of the catalyst into solution[22-24]. Pd can also be immobilized by weak interactions with organic supports. For example, Kobayashi's group microencapsulated palladium in polymer capsules. After encapsulation in a polystyrene-based functionalized polymer, the polymer is then cross linked to trap palladium in the microcapsule. The catalyst was active for the hydrogenation of a variety of alkenes and alkynes and was recyclable up to five times[25]. Allylic alkylation, Mizoroki-Heck and Suzuki-Miyaura reactions were also performed with their catalyst with low levels of leaching. However, addition of a phosphine ligand induced significant leaching of palladium[26]. It appears that this catalyst, like many other heterogeneous palladium catalysts, is acting through a release and return mechanism and addition of phosphines is stabilizing the released palladium so that it does not redeposit on the support after the reaction. Kirschning's group prepared polymer supported ionic gel **6** for the immobilization of palladium (Figure 3.5). After loading of $Pd(PPh_3)_4$, the gel was an active catalyst for Suzuki-Miyaura reactions of aryl bromides and iodides. The polymer could be prepared for flow-through reactions allowing a

continuous flow approach and reuse of the catalyst up to 20 times[27]. Mioskowski and co workers have prepared a similar ionic gel **7** to immobilize palladium (Figure 3.5). The catalyst was active for Suzuki-Miyaura coupling with a variety of aryl bromides including those containing heteroatoms[28].

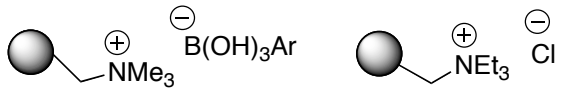

6 **7**

Figure 3.5: Ionic gels for immobilization of palladium.

Tang's group encapsulated palladium in a zeolite cage[29]. This material was catalytically active for the Mizoroki-Heck reaction and could be used for ten consecutive catalytic reactions. However, degradation of the cages were observed and small amounts of leaching of palladium occurred in the first cycle[29]. Ley and co-workers utilized palladium-containing perovskites as catalysts for the Suzuki-Miyaura reaction. They postulated that the catalysts would have high activity and improved recyclability due to suppression of Pd nanoparticle growth[30]. Extensive studies on these catalysts demonstrated that the activity was due to soluble leached palladium that is redeposited after the reaction is complete[31]. Ley's group has also developed a catalyst based on palladium encapsulated in polyurea, which he termed PdEnCat. This material proved to be an effective catalyst for the Suzuki-Miyaura reaction. The material was highly recyclable however, again detailed studies showed that PdEnCat was acting as a reservoir of homogeneous palladium with efficient

recapture of the soluble catalyst after the reaction[32,33]. The Ley group was also able to load PdEnCat into a capillary for flow through reactions and using microwave assisted synthesis were able to rapidly generate a library of biaryl structures[34]. Despite the success of these methods to increase the affinity of the support for palladium these catalysts still act as reservoirs of soluble palladium and still provide the possibility of contamination of the organic component.

Another strategy is to covalently attach a well-defined ligand to the surface and then bind a metal to it[35,36]. In this vein, typical ligands for transition metal catalysis including phosphines, carbenes, amines, sulfides, thiols and pyridines have been immobilized on inorganic supports[37,38]. While investigating the mechanism of catalysis with SCS pincer complex **8** and related NCN, PCP and CNC palladacycles developed by Bergbreiter[39], Jones and Weck immobilized the palladacycles on SBA-15 (Figure 3.6). The SCS complex was catalytically active for the Mizoroki-Heck reaction but induction kinetics suggested that leaching of palladium from the pre-catalyst was occurring. Despite the leaching of palladium the catalyst could be reused up to 3 times with increased induction times in the third cycle[36,40].

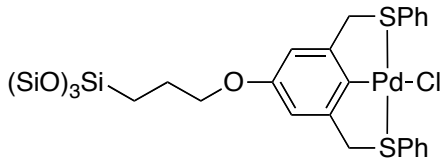

8

Figure 3.6: Immobilized SCS pincer catalyst for Mizoroki-Heck coupling.

Clark and co workers prepared a pyridylimine based chelating ligand **9** for palladium, immobilizing it on silica or dodecylamine-templated mesoporous silica (Figure 3.7). The catalyst was recyclable up to eight times with decreasing activity after the sixth cycle[41].

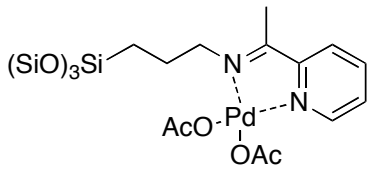

9

Figure 3.7: Palladium catalyst for Suzuki-Miyaura coupling.

Corma's group grafted palladacycle **10** onto MCM-41 to prepare a catalyst for Suzuki-Miyaura reactions (Figure 3.8). Their catalyst was recyclable however, activity dropped after the second cycle despite no measurable loss of palladium in the silicate[42]. However, in the homogeneous case the complex demonstrated a long induction time for the first cycle with no induction period for subsequent cycles. Thus the complex is breaking down, likely to a Pd(0) species that is leached to perform catalysis[43].

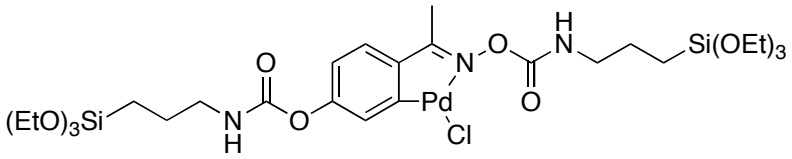

10

Figure 3.8: Palladacycle catalyst for Suzuki-Miyaura reaction.

Although potentially more effective than simple adsorption, this type of immobilization requires the preparation of a bifunctional ligand with remote

functionality for attachment to the inorganic support, greatly increasing the cost and difficulty of preparing the supported catalyst. Considering the fact that most of these catalysts seem to act by a homogeneous mechanism regardless of the method of ligation, the design of complex ligands seems excessive, especially when simple commercially available ligands can be used to immobilize palladium.

To overcome this issue, we and others have used simple commercially available organosilanes, such as mercaptopropyl-trimethoxysilane, in place of traditional transition metal ligands. The groups of Shimizu[44], Davis[45], and Crudden[46-48] have described thiol-functionalized mesoporous silicates as supports for Pd catalysts. These materials have been shown to be catalytically active for the Suzuki-Miyaura and Mizoroki-Heck reactions demonstrating low levels of leached palladium following use. Davis[45] and Crudden[46-48] showed that, similar to the previous methods of immobilization, these materials leach Pd species that are catalytically active, although high levels of recapture after reaction renders these species potentially interesting catalysts for industrial purposes where minimizing Pd contamination is more critical than the exact mode of action[6,7].

Despite this fact, whether a supported catalyst is acting as a homogeneous or heterogeneous catalyst is an important basic question. Ideally, a material that truly functioned as a heterogeneous catalyst would be preferable to prevent contamination, and also maintain catalyst activity since leaching and redeposition leads to catalyst death due to losses into solution

and agglomeration during redeposition. Often researchers will cite an extensive number of reuses without loss of activity as proof that the catalyst is acting in a heterogeneous fashion. However, Sheldon *et al.* have demonstrated that continued activity over a number of recycles does not mean that a catalyst is truly heterogeneous and other means for demonstrating heterogeneity are needed[49]. Indeed proving that a catalyst is truly heterogeneous proves to be quite difficult as ppt levels of palladium have been shown to be highly active catalysts for the Mizoroki-Heck reaction[50,51].

A number of heterogeneity tests have been developed to determine whether a heterogeneous catalyst is performing through a homogeneous route. One of the first methods for assessing heterogeneity is through a so-called hot-filtration test[49]. This involves initiating a reaction, and then filtering a portion of the solution before allowing it to cool (Figure 3.9). Both the unfiltered solution and the filtrate are then allowed to continue reacting.

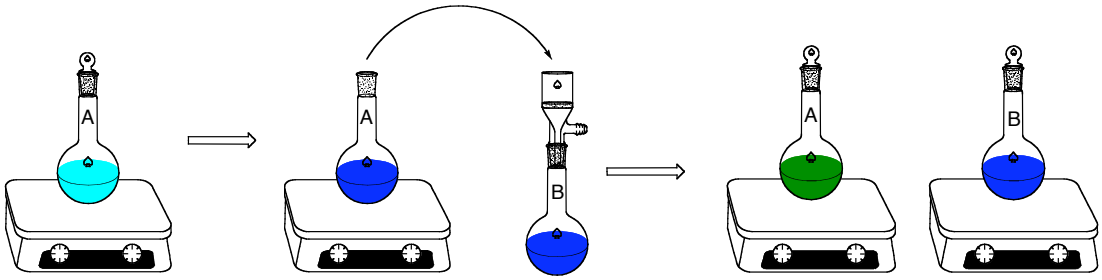

Figure 3.9: Representation of a hot filtration test.

With a truly heterogeneous catalyst, no activity would be observed in the filtrate (B, Figure 3.9). However, the absence of catalytic activity in the filtrate cannot be taken as proof that the catalyst is performing through a

heterogeneous pathway. If the solution cools prior to filtration, the catalyst can redeposit onto the support thus leading to a false negative. Even if the temperature of the solution is maintained, catalyst redeposition can occur during filtration and the catalyst may deactivate in the absence of stabilizers leading to false readings from the hot filtration test[12,21]. While a positive result indicates homogeneous catalysis a negative result must be confirmed by other tests.

When looking for homogeneous catalysis, researchers usually examine the solution at the end of reaction. As has been discussed above, the catalyst can rapidly redeposit at the end of the reaction and if this is the only point at which the solution is examined, valuable information may be missed. In determining the leaching of palladium from Pd/C Arai and Kohler both demonstrated that the reaction rate correlated closely with the amount of palladium dissolved in solution. Also the amount of palladium varied with the extent of reaction completion, with a low level at the beginning prior to initiation of activity, high levels during reaction, and low levels after the reaction was complete and the catalyst had redepositied (Figure 3.10)[12-15,17-19]. Additionally, the amount of catalyst recovered is often used as an assessment of leaching. However, recovering a quantitative amount of catalyst, while important from a practical standpoint does not indicate a heterogeneous reaction since undetectable amounts of leached species can be responsible for all of the solution activity observed[21].

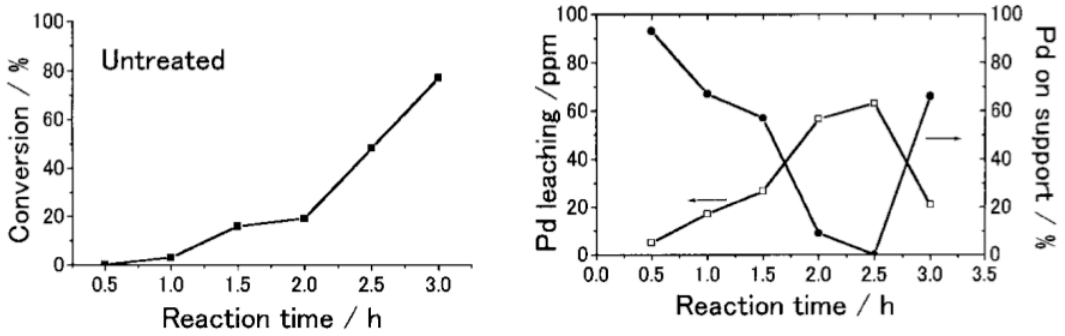

Figure 3.10: Mizoroki-Heck reaction conversion and leaching as a function of time. Reproduced from ref 13.

An alternative method of assessing heterogeneity is through a catalyst poisoning test. In this test, a poison for homogeneous metals is added to the catalyst. Any metal leached from the heterogeneous catalyst will be bound by the insoluble poison and removed from catalysis. Jones' group has utilized poly (vinyl pyridine) (PVPy) as a poison for soluble palladium in the Mizoroki-Heck reaction[40,52,53]. Treatment of a reaction with 300 equivalents of PVPy relative to palladium stopped all catalytic activity of their SBA-15-Pd pincer catalysts. PVPy is too large to enter the pores of SBA-15 so the conclusion is that palladium must be leaching to interact with the poison[53]. However, the addition of PVPy changes the viscosity of the solution and can attach itself to the surface preventing interaction of surface species with reactants and reagents. Thus it is important to also examine the effect of non-scavenging polymers such as polystyrene. In the case of the supported pincer catalyst described above, the addition of polystyrene was shown to decrease the reaction rate however, some catalytic activity is still observed.

Mercury(0) is another common poison used for testing of heterogeneity. Addition of Hg(0) can halt catalytic activity in the case of catalysis by metal nanoparticles or metal surfaces by the formation of an amalgam. Initially it was used to study hydrogenation reactions to prove catalysis from a molecular complex rather than metal nanoparticles. Catalysts with protective ligands and metals in high oxidation states are not affected by mercury[54,55]. Utilizing heterogeneous palladium catalysts for coupling chemistry, leached Pd(0) would be affected by the presence of Hg(0) and a decrease in catalytic activity in the presence of mercury should occur. However, once again, highly-ligated catalysts, or catalysts that are in equilibrium with nanoparticles can give erroneous negative results upon treatment with mercury.

Given the issues with mercury toxicity and increased viscosity of PVPy based poisoning, and the uncertainties that they introduce, other immobilized poisons for soluble palladium have been developed, for example, Quadrapure TU, which is thiourea-based. The commercially available polymer has a high capacity for palladium meaning far less polymer is needed than with PVPy, alleviating any viscosity issues. Examining the PdEnCat catalysts described earlier in the Mizoroki-Heck reaction, Jones was able to demonstrate complete cessation of catalytic activity upon addition of Quadrapure TU even if the reaction was already underway[56]. Furthermore, Richardson and Jones found that SBA-15-SH or SiO_2-SH could act as poisons for homogeneous catalysis[57]. This is not entirely surprising given our results which demonstrate

that increasing the S:Pd ratio of the catalysts leads to a decrease and eventual cessation of activity. It is noteworthy to point out that the catalyst poison tests only indicate that soluble metals are present they give no indication as to the catalytic capability of the soluble metals.

The three phase test is perhaps the most indicative test for soluble catalytically active species. First proposed by Rebek[58-60] in the seventies, the test involves chemically tethering one of the two reactants to a solid support. The reaction can then be performed in the solution phase and the solid catalyst is in the third phase. If there is no background reaction in the absence of the catalyst, the reagent on the support should only show reaction when the catalyst is leaching. Like all of the tests described below, the manner in which this test is carried out is critical. This is elegantly demonstrated in the methoxy carbonylation of **11** catalyzed by Pd/C, which results in large amounts of palladium in the product (Figure 3.11)[61].

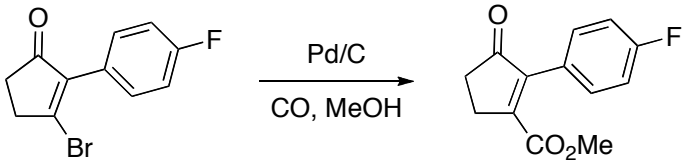

11 **12**

Figure 3.11: Methoxy carbonylation of a vinyl halide catalyzed by Pd/C.

A three phase test was carried out to assess the potential catalytic activity of the soluble palladium. Using supported aryl iodide **13**, no reaction on the support was observed suggesting that the reaction was truly heterogeneous. However, when soluble aryl bromide **11** was added at the same time,

complete conversion of the supported aryl iodide was observed (Figure 3.12). As described below, this is likely because it is the aryl iodide that is responsible for leaching of the Pd from the surface[62]. Thus it is important to ensure that the reagents responsible for leaching of the catalyst are incorporated into the three phase test in order for the results to be meaningful.

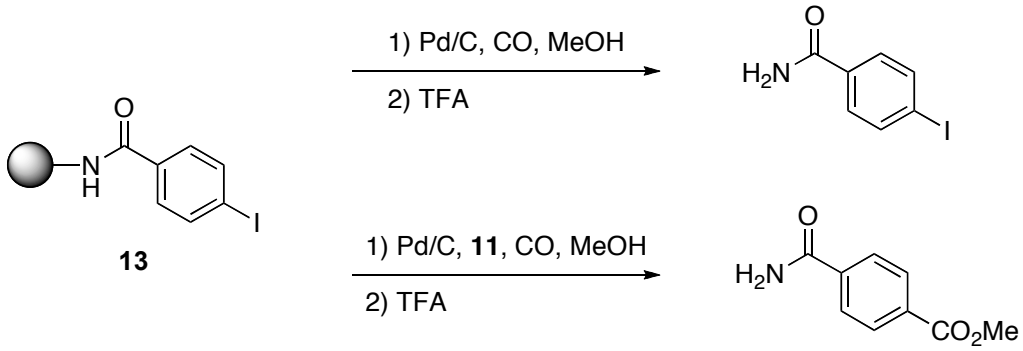

Figure 3.12: Three phase test used by Davies *et al.*

Arai and Kohler postulated that exposure to the aryl halide initiates dissolution of Pd from the activated carbon by oxidative addition[12-15,17-19]. Reetz's group has also demonstrated that Pd nanoparticles could be dissolved by treatment with aryl iodides[63]. Furthermore, our group has studied the redeposition of aryl halide solubilized palladium on palladium foils, and showed conclusively that it was the aryl iodide component that led to dissolution of the Pd[62]. Thus, for a three phase test for the Suzuki-Miyaura reaction it is important to have either the boronic acid immobilized or to utilize a soluble aryl halide in addition to the immobilized aryl halide. Utilizing a soluble aryl halide also offers the ability to confirm that an active catalyst is actually generated by observing coupling in the liquid phase.

Another issue with the three phase test that needs to be considered is the reactivity of the soluble aryl halide vs. the immobilized aryl halide. If the soluble aryl halide is much faster at reacting than the immobilized one the soluble aryl halide may be used up before any reaction can take place on the surface[21]. Additionally, if a limiting amount of the coupling partner is present the extent of reaction on the surface may be attenuated. If these concerns are met by proper experiment design, the three phase test proves to be the most powerful tool for assessing heterogeneity of a catalyst.

Finally, the results of these heterogeneity tests need to be considered carefully and the tests must be validated using known homogeneous catalysts. While no one heterogeneity test is sufficient to declare a catalyst truly heterogeneous, combining a number of heterogeneity tests can be useful for elucidating the heterogeneity of a catalyst system.

3.2 Results and Discussion

We have previously shown that thiol modified SBA-15 materials are efficient scavengers for palladium and, after palladium loading, they are active catalysts for Mizoroki-Heck and Suzuki-Miyaura reactions[46]. However, within these two reactions, only a limited scope of substrates was examined. Thus we set out to further characterize these palladium loaded materials as catalysts for coupling reactions (Suzuki-Miyaura, Sonogashira) and catalysts for other palladium catalyzed processes (hydrogenation). We were also

interested in studying the long term stability and reusability of the catalysts. Finally, we wanted to determine if our catalysts were performing in a truly heterogeneous fashion. This was assessed by a variety of heterogeneity tests.

3.2.1 Catalyst preparation

SBA-15 was chosen as our silica support since it has higher hydrothermal stability and larger pores than MCM-41. Thiols were incorporated by co-condensation of MPTMS and TEOS with a 6:94 ratio of the silica species to afford SBA-15-SH. After removal of the surfactant by extraction, the resulting materials have highly ordered, hexagonally arrayed pores as evidenced by nitrogen porosimetry (Figure 3.13) and TEM (Figure 3.14). Sulfur incorporation was assessed by elemental analysis with loadings between 0.4 to 1.1 mmol/g of material. Palladium could be incorporated by treatment of the materials with a solution of palladium acetate in THF with no loss of order in the material (Figure 3.13). The amount of palladium to be loaded was calculated based on the sulfur content of the material to give a S:Pd ratio of 2:1. ICPMS of the THF solution after palladium loading indicated that less than 0.3 % of the initially added palladium remained in solution.

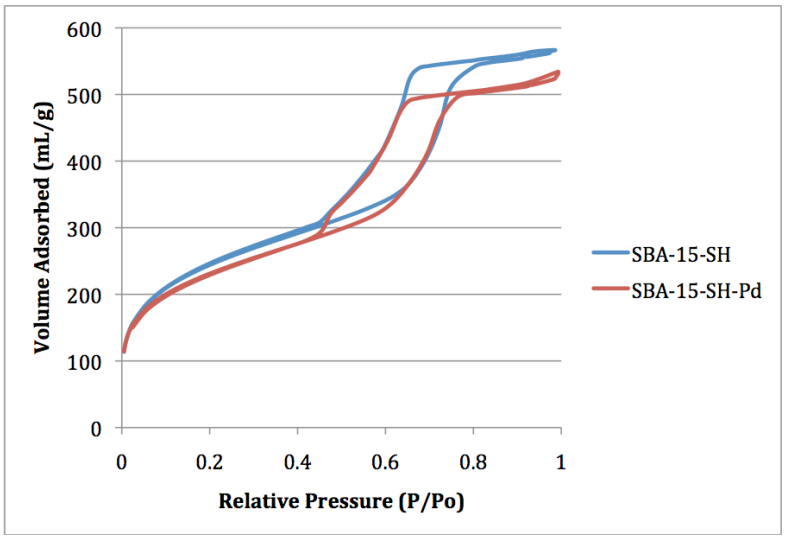

Figure 3.13: Nitrogen porosimetry isotherms for SBA-15-SH and SBA-15-SH-Pd.

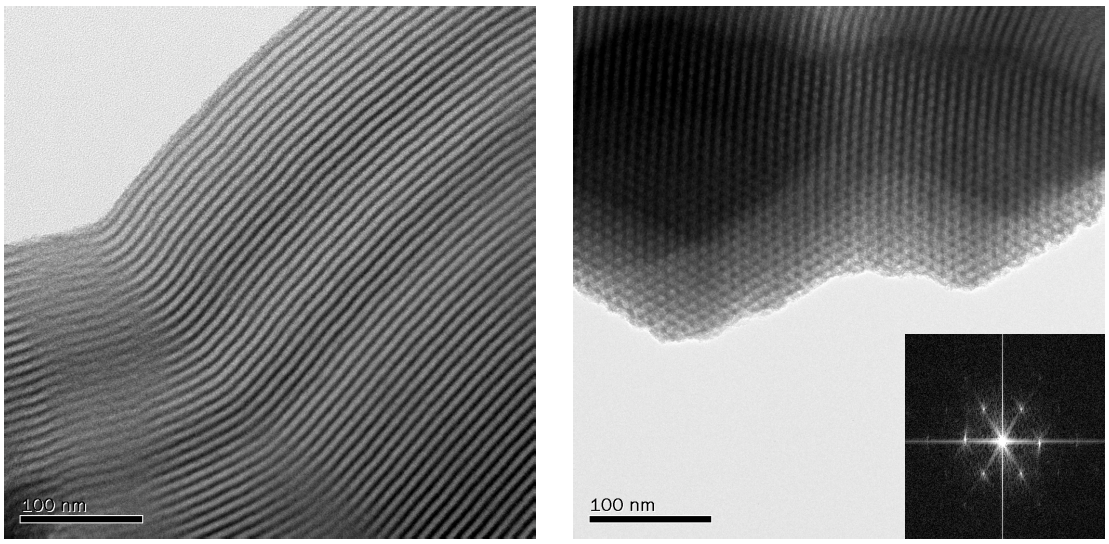

Figure 3.14: TEM images of SBA-15-SH showing different views of the 2-d hexagonal pores.

Having incorporated palladium into the SBA-15-SH material, we examined the ability of this material to catalyze the Suzuki-Miyaura reaction of bromoacetophenone and the pinacol ester of phenyl boronic acid (Equation 3.1). The reaction proceeds with high yields under both inert atmosphere and

in air (Table 3.1). Atmosphere does have an effect on the reaction, since turnover frequency (TOF) and turnover number (TON) were higher for the catalyst in an inert atmosphere relative to air (Table 3.1). Under argon, the materials seemed to maintain more order than in air. However, in both systems, significant destruction of the pores was observed by TEM (Figure 3.15 and 3.16). Furthermore, palladium nanoparticles were observed in both materials particularly in the disordered regions, although more nanoparticles are observed in the materials reacted under an inert atmosphere than that in air. Finally, after completion of the reaction and filtration of the silica catalyst, ICPMS analysis of the product indicates low levels of Pd contamination (Table 3.1).

Table 3.1: Suzuki-Miyaura coupling with SBA-15-SH-Pd

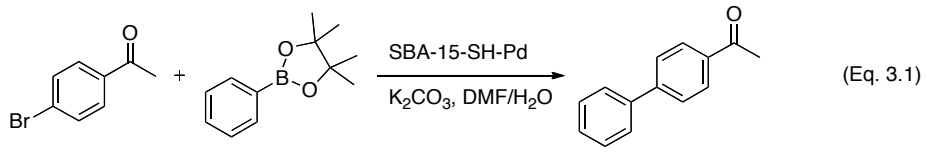

14 15 16 (Eq. 3.1)

Entry	Conditions	Yield (%)	TON	TOF (h^{-1})	Pd Leaching (%)
1	Air, 18 h	90-98	2760	590	0.17 ± 0.09
2	Argon 4 h	90-95	3450	900	0.22 ± 0.09

To further characterize the catalyst, we examined the effect of the S:Pd ratio on catalytic activity of the resulting materials. Catalysts prepared from co-condensed SBA-15-SH showed comparable activities at S:Pd ratios between 1.2:1 and 4.6:1. However, when this ratio was increased beyond 6.8:1, the material was catalytically inactive (Table 3.2). Our group found similar results

with amorphous silica[48] and, as previously noted, Richardson and Jones[57] found that addition of palladium-free SBA-15-SH to a reaction catalyzed by SBA-15-SH-Pd caused the reaction to halt. Thus an excess of sulfur relative to palladium on the materials causes poisoning of the catalyst.

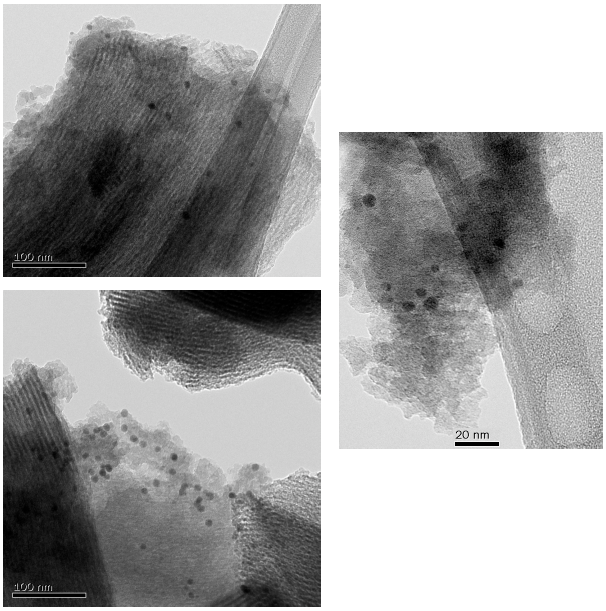

Figure 3.15: TEM images of SBA-15-SH-Pd after a Suzuki-Miyaura reaction in an air atmosphere.

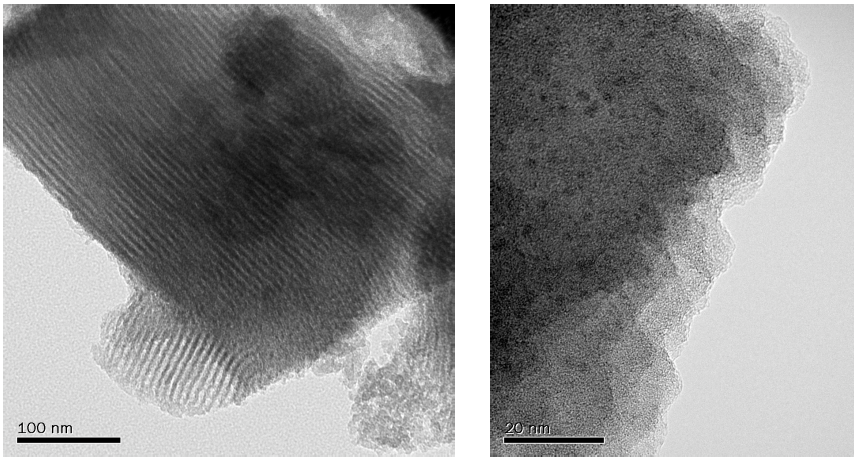

Figure 3.16: TEM images of SBA-15-SH-Pd after a Suzuki-Miyaura reaction in an argon atmosphere.

Table 3.2: Effect of S:Pd ratio on Suzuki-Miyaura Coupling

Entry	S:Pd Ratio	Yield (%)
1	1.2:1	63
2	2.2:1	66
3	4.6:1	62
4	6.8:1	0
5	9.2:1	0
6	11.8:1	0

3.2.2 Application to Various Coupling Reactions

In addition to the important Mizoroki-Heck and Suzuki-Miyaura reactions,[46] we were interested in exploring the use of our material for other palladium catalyzed coupling reactions. The Sonogashira reaction is another palladium catalyzed process for the coupling of terminal alkynes with aryl halides which is widely used in industry (Equation 3.2)[64]. The Sonogashira reaction typically utilizes a copper co-catalyst for activation of the alkyne and assistance in transmetallation. However, copper salts can induce Glaser-type homocoupling of the alkyne and copper acetylides are potentially explosive[65]. Thus a number of groups have prepared copper free Sonogashira protocols[66-68]. We chose to employ this type of copper-free protocol since application of our method for industrial synthesis would have to address the removal of copper as well. Unlike typical Suzuki-Miyaura conditions, the Sonogashira reaction required increasing the temperature to 100 °C for efficient catalysis. We performed a simple solvent and base screen to determine optimal conditions (Table 3.3). Similar to the Suzuki-Miyaura reaction, DMF:water mixtures proved to be the best solvent system. A number of amine bases

were tested at 80 °C but did not show any activity, however, sodium acetate proved effective giving the desired product in 87% yield.

Table 3.3: Sonogashira coupling with SBA-15-SH-Pd

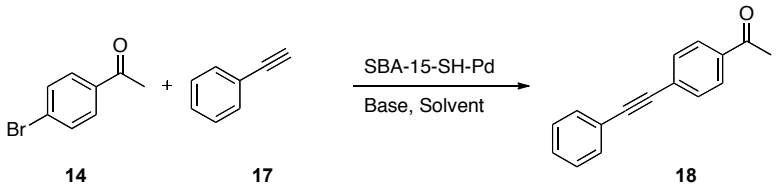

14 17 18 (Eq. 3.2)

Entry	Solvent	Base	Yield (%)
1	DMF/H_2O	NaOAc	87
2	DMF	NaOAc	40
3	H_2O	NaOAc	0
4	Toluene	NaOAc	0
5	Dioxane	NaOAc	0
6	DMF/H_2O	K_2CO_3	25
7	DMF/H_2O	Cs_2CO_3	31
8	DMF/H_2O	KOH	0

ICPMS analysis of the product after removal of the catalyst showed increased leaching relative to the Suzuki-Miyaura reaction. After reaction, ca. 1-5 ppm palladium was detected in the solution. This is possibly due to the strong coordination of palladium by alkynes that serves to retain palladium in the product. However, the level of Pd was still significantly less than would have been expected using a homogeneous catalyst. Thus we moved to more complex substrates that would yield industrially relevant molecules. The examples chosen involve more complex functional groups and heteroatoms that are likely to induce higher levels of palladium leaching than the simple substrates employed thus far (Figure 3.17). These substrates were chosen

because they have been reported to be problematic in terms of Pd retention[5,6].

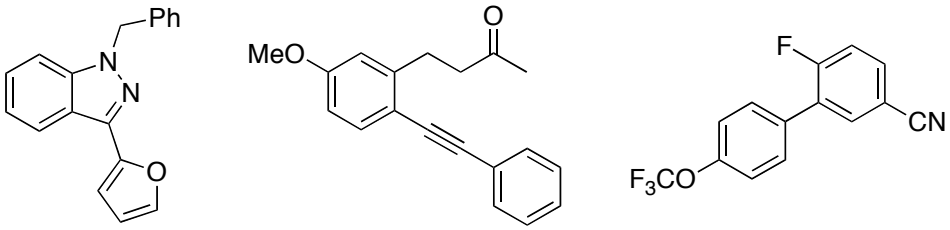

19 **20** **21**

Figure 3.17: Pharmaceutical intermediates utilizing palladium catalyzed coupling reactions.

The first substrate we examined was **19**, which is a precursor to the blood platelet inhibitor YC-1 from Yung Shin Pharmaceutical. One of the key steps in the synthesis of this pharmaceutical compound is a palladium catalyzed Suzuki coupling of N-benzyl-3-iodoindazole and 2-furyl boronic acid. The synthesis of the YC-1 precursor **19** is outlined in Scheme 3.1. We synthesized the pinacol ester of 2-furyl boronic acid to increase the organic solubility of the boronic acid for purification purposes. This was achieved by the condensation of 2-furyl boronic acid and pinacol in benzene. 3-Iodoindazole was prepared in high yield from indazole and iodine in basic DMF. The resulting product was quantitatively N-benzylated with benzyl bromide in the presence of potassium *tert*-butoxide to yield N-benzyl-3-iodoindazole. The Suzuki-Miyaura coupling of the two reagents was successfully carried out with our SBA-15-SH-Pd catalyst to yield N-benzyl-3-(2-furyl)-indazole in a moderate isolated yield of 58 %. ICPMS analysis of the residual palladium level was 1.04 ppm. Considering that the reaction was

performed with an aryl iodide and it is known that aryl iodides promote greater leaching in cross coupling reactions, this level is quite reasonable[12].

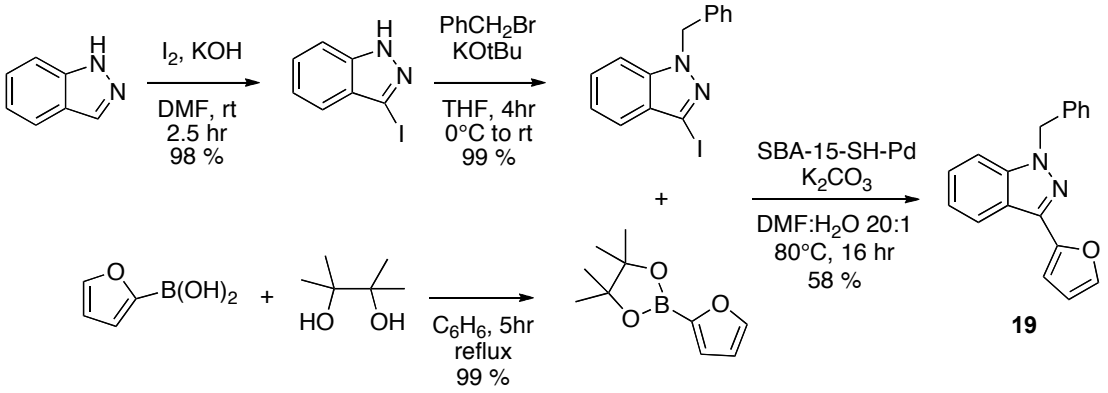

Scheme 3.1: Synthesis of YC-1 precursor **19**.

The second active pharmaceutical ingredient synthesized was compound **20**, which is a precursor to a calcium channel blocker. The route is described in Scheme 3.2. The synthesis begins with an aldol condensation between *m*-anisaldehyde and acetone in an acetone/water solvent system. Hydrogenation of the resulting alkene over palladium on carbon afforded the reduced butane in a moderate yield. Electrophilic iodination of the phenyl ring with silver acetate, to assist in the generation of I^+ from iodine, afforded the desired 4-(2-iodo-5-methoxyphenyl)-2-butanone coupling partner. A Sonogashira coupling between **20** and phenyl acetylene utilizing the SBA-15-SH-Pd catalyst afforded the coupled product in 75 % yield. Industrially this product was contaminated with 100-900 ppm of palladium due to a good chelation site for palladium (Figure 3.18)[6]. However, using our catalyst, we were able to reduce the palladium content in this product to 2.25 ppm. As with YC-1, one of the coupling products is an aryl iodide and this may have

increased the leaching relative to our aryl bromide examples (typically 0.04 – 0.06 ppm).

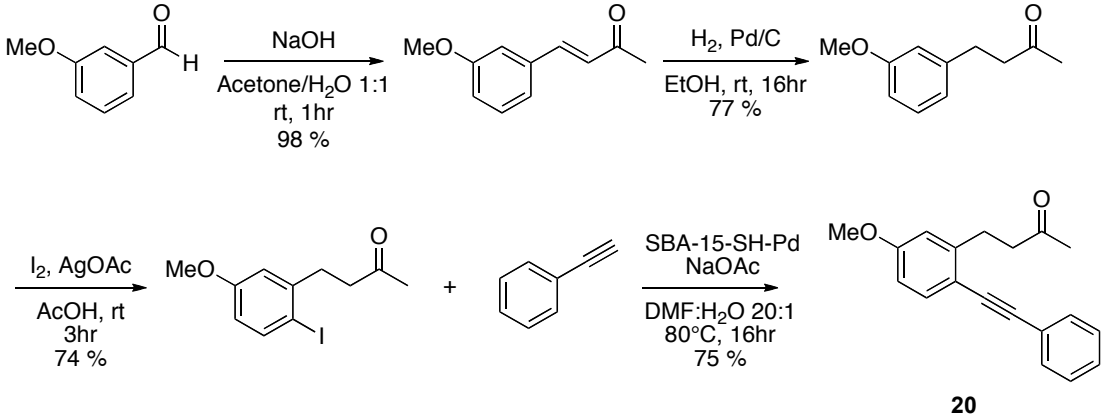

Scheme 3.2: Synthesis of calcium channel blocker precursor **20**.

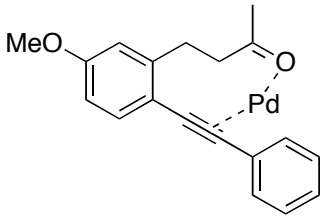

Figure 3.18: Potential chelation site for palladium in pharmaceutical precursor **20.**

Finally, a precursor of ABT-100, a farnesyl transferase inhibitor from Abbot Pharmaceutical was also selected as a target. In the key palladium-catalyzed coupling step, a commercially available aryl bromide is coupled with a simple boronic acid (Scheme 3.3). Again we prepared the pinacol ester of the boronic acid for purification purposes. The Suzuki coupling reaction catalyzed by SBA-15-SH-Pd provided the coupled biaryl in 81 % yield after 16 hr at 80 °C.

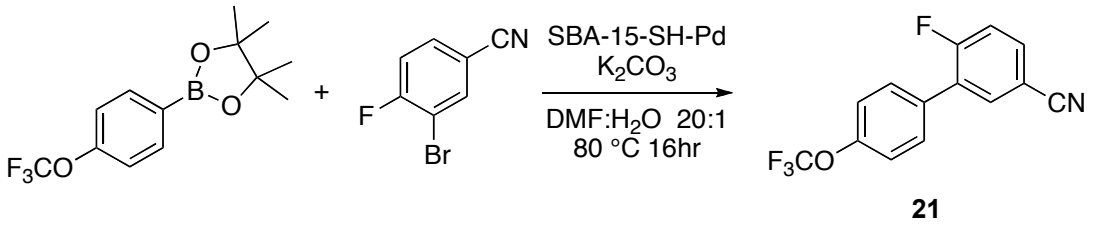

21

Scheme 3.3: Synthesis of ABT-100 precursor **21**.

ICPMS analysis of the solution after reaction found residual palladium levels of 0.37 ppm. In this case using an aryl bromide shows lower levels of leaching than in the two cases with aryl iodides. Preparation of the bromide coupling partners for YC-1 and the calcium channel blocker would be useful to confirm this hypothesis, however the levels of Pd obtained using our supported Pd catalyst are still significantly lower than that observed in the literature.

3.2.3 SBA-15-SH-Pd in Semi-Hydrogenation Reactions

In addition to coupling reactions, palladium catalysts are widely employed for hydrogenation and hydrogenolysis reactions. Lindlar's catalyst is perhaps one of the best known supported palladium catalysts for the hydrogenation of alkynes to alkenes. In order to prevent over reduction to the alkane, catalysts are often poisoned with quinoline to obtain the alkene products. Other supported palladium reagents have been utilized as catalysts for heterogeneous hydrogenations, for example Pd/C, Pd/SiO_2 and $Pd/BaSO_4$. Since our SBA-15-SH-Pd catalysts are a form of supported palladium, with the thiol potentially attenuating reactivity, we investigated their use in hydrogenation reactions.

As a model system, we performed the hydrogenation of diphenylacetylene (Equation 3.3). The results are presented in table 3.4. Hydrogenation under one atmosphere of hydrogen was insufficient to cause any reduction of the triple bond. Increasing the pressure to 15 psig afforded small amounts of all three possible hydrogenation products but mainly unreacted alkyne was observed. A further increase to 20 psig resulted in an increase in the amount of hydrogenation (Table 3.4, entry 3) with cis-diphenylethylene being the major product.

Table 3.4: Hydrogenation of diphenylacetylene with supported palladium catalysts.

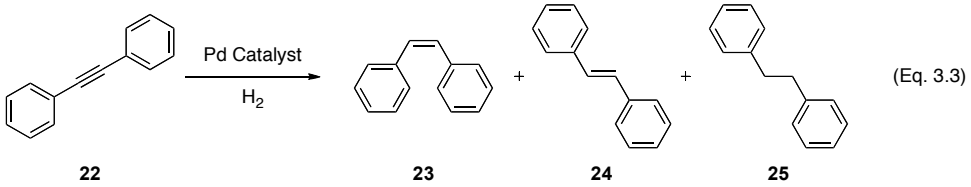

Entry	Catalyst	Time (h)	H_2 pres.	Yield **23** (%)	Yield **24** (%)	Yield **25** (%)	Yield **22** (%)
1	SBA-15-SH-Pd	48	1 atm	0	0	0	100
2	SBA-15-SH-Pd	5	15 psig	4.7	2.7	7.8	83
3	SBA-15-SH-Pd	5	20 psig	62	15	7.2	15
4	SBA-15-SH-Pd/ Quinoline	5	20 psig	2.4	13	0	84
5	SBA-15-SH-Pd	18	20 psig	0	48	48	0
6	SiO_2-SH-Pd	5	20 psig	13	10	3.4	73
7	SiO_2-SH-Pd	6	20 psig	27	8.4	1.3	62
8	SiO_2-SH-Pd	7	20 psig	69	9.3	4.6	10
9	SiO_2-SH-Pd	8	20 psig	44	32	25	10
10	SiO_2-SH-Pd	18	125 psi	0	0	100	0
11	Pd/C	5	20 psig	0	0	100	0
12	$Pd/BaSO_4$	5	20 psig	56	4.8	22	14
13	$Pd/BaSO_4$/ Quinoline	5	20 psig	42	3.8	4.6	42
14	Lindlar's Cat.	5	20 psig	36	4.7	50	8
15	Lindlar's Cat./ Quinoline	5	20 psig	4.4	12	0	80

This reactivity of our catalyst is similar to that observed with $Pd/BaSO_4$ (Table 3.4, entry 12) with the exception that more reduction to diphenylethane is observed with $Pd/BaSO_4$. Lindlar's catalyst also demonstrated a similar reactivity with almost complete conversion in 5 hr. However, with Lindlar's catalyst, complete hydrogenation to the alkane was observed (Table 3.4, entry 14). Palladium on carbon afforded 1,2-diphenylethane exclusively with no alkene products present. Increasing the reaction time from 5 hr to 18 hr for the SBA-15-SH-Pd catalyst results in increased isomerization to trans-diphenylethylene and over reduction to diphenylethane (Table 3.4, entry 5).

Poisoning the SBA-15-SH-Pd catalyst with quinoline significantly reduces catalytic activity, but only alkene products are observed (Table 3.4, entry 4). In the case of quinoline poisoned $Pd/BaSO_4$ (Table 3.4, entry 13), the activity is reduced but the selectivity for the cis-alkene isomer is improved. Lindlar's catalyst, when poisoned with quinoline performs similarly to quinoline-poisoned SBA-15-SH-Pd catalyst: very little hydrogenation takes place and no alkane product is observed (Table 3.4, entry 15).

We also prepared an amorphous version of the catalyst (SiO_2-SH-Pd). This catalyst was far less reactive over 5 hr than the ordered material; compare Table 3.4 entry 6 and entry 3, although alkenes were still the predominant products. Increasing the reaction time led to increased amounts of cis-diphenylethylene until the alkyne was almost completely consumed (Table 3.4, entries 6 - 9). After consumption of the alkyne, the amount of isomerization to trans-diphenylethylene and hydrogenation to 1,2-

diphenylethane increased. Finally, increasing the pressure to 125 psi resulted in the complete hydrogenation to 1,2-diphenylethane.

These results suggest that SBA-15-SH•Pd catalysts are potential replacements for semi-hydrogenation catalysts such as Lindlar's catalyst. The reaction appears to follow a normal hydrogenation mechanism whereby a syn addition of hydrogen generates the cis alkene. At longer reaction times, isomerization can occur to give the trans alkene and eventually complete hydrogenation to the alkane is observed. The preference for cis product at short time periods indicates that the thiols of our support may act as inhibitors for palladium preventing complete hydrogenation as seen with Pd/C. Our catalysts compare favourably with the commonly employed supported palladium catalysts in terms of selectivity for the cis alkene even without rigorous optimization of the hydrogenation conditions. Further work in improving the conditions for cis alkene production is underway in our lab.

3.2.4 Mechanism of Action

Despite the strong palladium scavenging ability and low residual Pd contamination observed with our SBA-15-SH based catalysts, most heterogeneous palladium catalysts have been shown to operate through leaching of palladium into solution to perform catalysis. Previous work in our lab in determining the heterogeneity of our SBA-15 catalysts involved the hot filtration test and the three phase test[46,47]. Both tests indicated only a small amount of catalysis was occurring in the solution. However, as discussed

previously, the absence of catalytic activity in the filtrate is not a definitive indicator of heterogeneous catalysis. Thus we were interested in exploring our SBA-15-SH-Pd catalysts with more rigorous methods to determine if the catalysts are truly heterogeneous.

A common test for heterogeneous catalysts is to challenge the system with a soluble species capable of binding the metal. A variety of poisons have been reported in the literature[36]. The effect of several key poisons on our SBA-15-SH-based catalysts can be found in figure 3.19. Poly (vinyl pyridine) (PVPy) is a soluble poison that can bind and sequester palladium through the pyridyl nitrogens. The ratio of nitrogen to palladium for our poisoning with PVPy was 300:1. Comparison of the reaction profile for an unpoisoned reaction (Figure 3.19 blue diamonds) with the reaction profile for a PVPy poisoned reaction (Figure 3.19 red squares) shows that the reaction is retarded by the presence of the soluble poison although catalytic activity is not quenched completely. As noted previously, the large amount of PVPy that has to be employed leads to a significant increase in the viscosity of the solution. To assess the effect of the increased viscosity, another poisoning experiment was carried out by adding an equivalent amount of polystyrene. Since it doesn't have any heteroatoms, polystyrene is a poor binder of palladium but it does increase the viscosity of the solution and may agglomerate on the surface in the same way that PVPy can. The reaction profile for the polystyrene poisoned reaction (Figure 3.19 green triangles) shows a decrease in activity compared to the free reaction, but there is

considerably more activity than the PVPy poisoned reaction. This suggests that while the increased viscosity does contribute to the decrease in activity with PVPy, coordination of leached palladium by the PVPy nitrogen is likely playing a role as well.

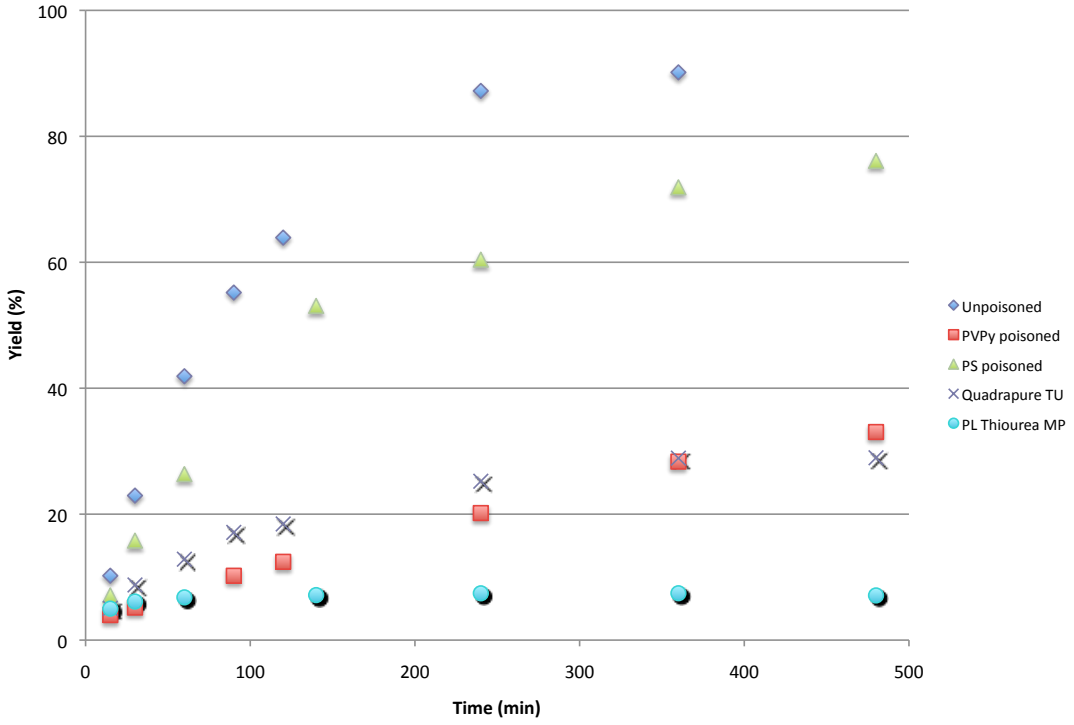

Figure 3.19: Effect of various catalysts poisons on the Suzuki-Miyaura coupling of 4-bromoacetophenone and phenylboronic acid pinacol ester with SBA-15-SH-Pd as the catalyst.

We then examined the thiourea-based poisons. In the case of PL-Thiourea MP, the palladium binding capacity was not known so an excess of thiourea was added to ensure enough scavenger was present to slow the reaction. With this poison, catalytic activity is almost completely halted (Figure 3.19 pale blue circles). Quadrapure TU does have a known palladium capacity[56] and so we added two equivalents per palladium atom on support.

In previous studies, the addition of Quadrapure resulted in complete cessation of activity, even if it was added after the reaction had started[56]. In our system, addition of Quadrapure resulted in a decrease but not cessation of activity (Figure 3.19 X-marks). In fact, the catalytic activity is similar to that observed for PVPy as a poison. This begs the question why is there a difference between our work and previous work. One possible explanation is that the observed decrease in activity is due to a redistribution of palladium rather than scavenging of soluble active palladium. We have shown that increasing the sulfur to palladium ratio of the catalysts results in a decrease of catalytic activity[48]. This suggests that there is some mobility of palladium on the thiol surface and in solution. Thus it is possible that active Pd on the surface is in equilibrium with inactive or active Pd in solution, and when the scavenger is added, Pd is redistributed between the surface and the scavenger. The fact that we see a slower rate of catalysis would mean that this redistribution occurs at a rate comparable to that of coupling. While the homogeneous poison test does tell us that palladium from our catalysts is accessible to the solution it does not tell us if catalytically competent homogeneous palladium is present (Figure 3.20).

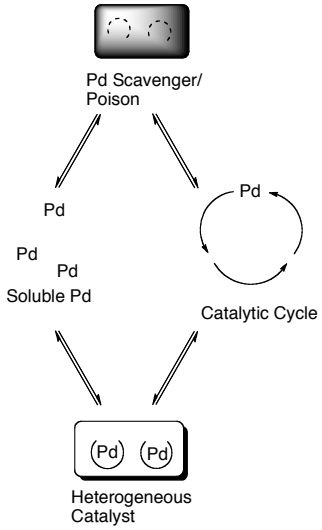

Figure 3.20: Illustration of leaching and recovery by heterogeneous catalysts and scavengers.

In order to determine whether the Pd in solution was catalytically active, we carried out a detailed analysis of the three phase test (Scheme 3.4). As previously discussed, it is important to incorporate a soluble aryl halide **14** to properly mimic solution conditions. Furthermore, the presence of a soluble aryl halide permits one to determine if a catalytically competent system was achieved. This is critical, since the lack of reaction on the supported reagent can also mean that for some reason an active catalyst was not produced. After isolation and hydrolysis of the solids, the ratio of 4-bromo benzoic acid **27** and 4-phenyl benzoic acid **28** illustrates the amount of reaction that occurred on the immobilized phase.

As shown in Table 3.5, our catalyst was able to successfully couple bromoacetophenone and phenyl boronic acid in the presence of the supported aryl halide. At times similar to the normal Suzuki coupling, however, lower yields of the soluble product were obtained with about 10 %

coupling on support. As the reaction time was extended the amount of reaction on the immobilized phase increased. If the soluble aryl halide is removed, reaction with the immobilized aryl halide is still observed (Table 3.5, entry 5). This shows that the soluble aryl halide is not required to generate soluble palladium in this system.

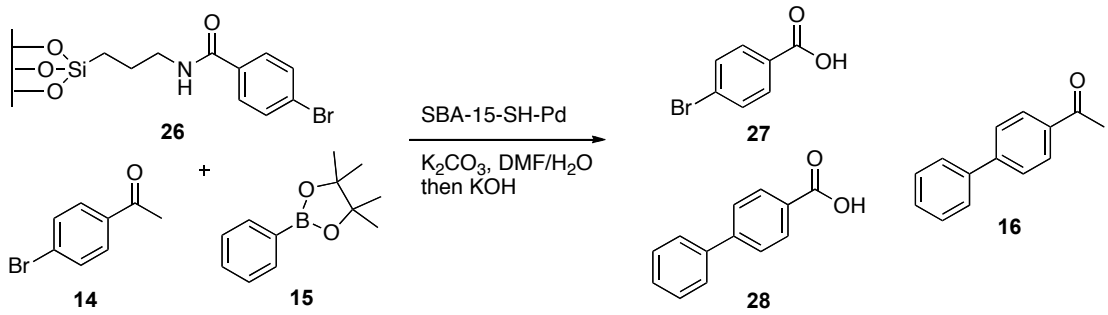

Scheme 3.4: Three phase test for SBA-15-SH-Pd catalyzed Suzuki-Miyaura reaction.

Increasing the amount of boronic acid in the system also led to increased formation of the coupled benzoic acid from reaction with the supported reagent. This suggests that solution phase coupling occurs more readily than reaction on support, which is expected. Unfortunately, the three phase tests with Pd/C or PdEnCat were unsuccessful, only 1% of the solution phase biphenyl was found. This is likely due to the aqueous conditions employed. Both of these catalysts are known to operate as reservoirs of soluble palladium in Suzuki reactions, and thus would have been good indicators of the effectiveness of our three-phase test. With the non-existent catalytic activity, the amount of coupling on the immobilized phase could not be determined. Thus the results of our three phase test qualitatively tell us that

there is catalytically competent palladium in solution but do not allow us to quantify the amount or to determine whether catalysis also occurs on support.

Table 3.5: Summary of three-phase test results.

Entry	Catalyst	Solvent	Time (h)	Atm.	Yield **16** (%)	Ratio **27**:**28**
1	SBA-15-SH-Pd	H_2O	5	Air	51	94:6
2	SBA-15-SH-Pd	H_2O	5	$Ar_{(g)}$	42	85:15
3	SBA-15-SH-Pd	H_2O	20	Air	48	85:15
4	SBA-15-SH-Pd	H_2O	20	$Ar_{(g)}$	56	58:42
5[a]	SBA-15-SH-Pd	H_2O	5	Air	0	84:16
6[b]	SBA-15-SH-Pd	H_2O	5	Air	69	73:27
7	Pd/C	H_2O	5	Air	1	95:5
8	PdEnCat	H_2O	5	Air	1	97:3
9[c]	SBA-15-SH-Pd	H_2O	5	$Ar_{(g)}$	63	94:6
10[c]	SBA-15-SH-Pd	DMF/H_2O	5	$Ar_{(g)}$	48	90:10

[a]No **14** added to the reaction. [b]Three equivalents of the boronic ester coupling partner were added. [c]Using supported halide **32**.

While we were able to perform the three phase test in aqueous solutions, as shown in Table 3.5, our initial attempts in organic solvents were unsuccessful. It was not clear why there was no reaction in organic solvents until we examined the immobilized aryl halide. The amide was formed by the reaction of amino propyl modified silica with an acid chloride (Scheme 3.5).

29 **30** **26**

Scheme 3.5: Synthesis of the immobilized aryl halide for the three phase test.

Elemental analysis of the resulting solid (**26**) showed that the coupling reaction was incomplete and about 0.3 mmol/g of free NH_2 groups were

present on the support. This amounted to a ratio of 35:1 amine to palladium. As demonstrated in the homogeneous poisoning tests, the presence of excess ligands for palladium will inhibit the reaction. To avoid this problem, we prepared a supported aryl halide with no free amines on the surface (Scheme 3.6). This was achieved by synthesizing the amide prior to its introduction onto a silica surface.

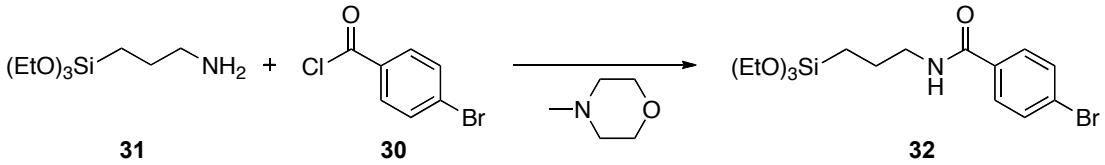

31 **30** **32**

Scheme 3.6: Synthesis of immobilized aryl halide with no free amines.

This new reagent displayed the expected activity in the aqueous three phase test as before (Table 3.5, entry 9). More importantly, we were able to use this material in DMF/water mixtures identical to the conditions normally employed in our Suzuki reactions. The results in the DMF/water system are similar to those observed in pure water with only slightly increased levels of reaction of the immobilized aryl halide (compare entries 10 and 1). Although we could not rule out the possibility that the Pd on the surface is active, it is clear that active Pd exists in solution. Most importantly, the observation of 27% reaction on support when excess boronic acid is employed, is a strong indication that the reaction with the supported reagent suffers from a decreased rate relative to the solution-phase experiment. This, taken along with the cessation or decrease in activity observed upon the addition of scavengers, leads to the

most likely conclusion that the catalyst is likely functioning by a release and catch mechanism[46,47].

3.2.5 Material Stability and Reusability

For heterogeneous catalysts, in addition to total leaching and catalytic activity, recyclability is a critical feature. Interestingly, we found that the recyclability and stability of the catalyst depended strongly on how the thiol was introduced. If co-condensed SBA-15-SH-Pd was employed as the catalyst, activity was lost after two cycles of catalysis (Figure 3.21). Interestingly, this drop in activity coincided with an increase in palladium leaching from the catalyst (Figure 3.22). Switching from air to argon atmosphere did not improve the recyclability of these catalysts. Other materials prepared in our group by grafting of MPTMS onto SBA-15 showed better recyclability compared to the co-condensed materials, and, for example, could be used 5 times before their activity was lost[48].

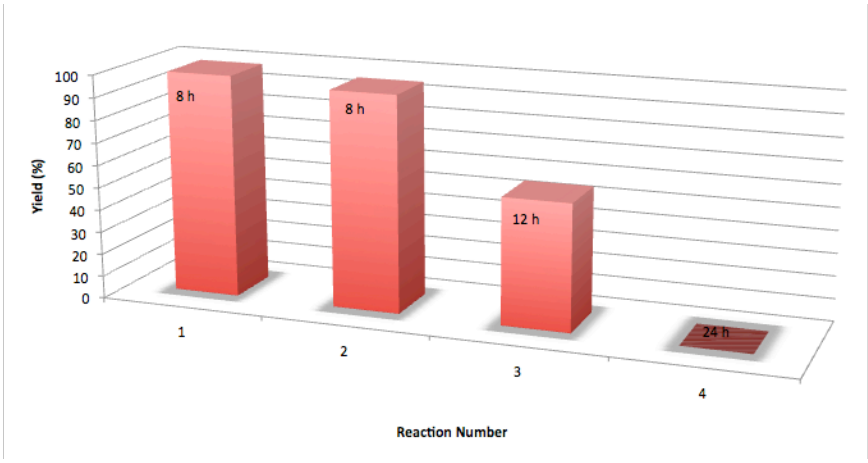

Figure 3.21: Effect of recycling on Suzuki-Miyaura reaction run in air. Time for each cycle is given on the graph.

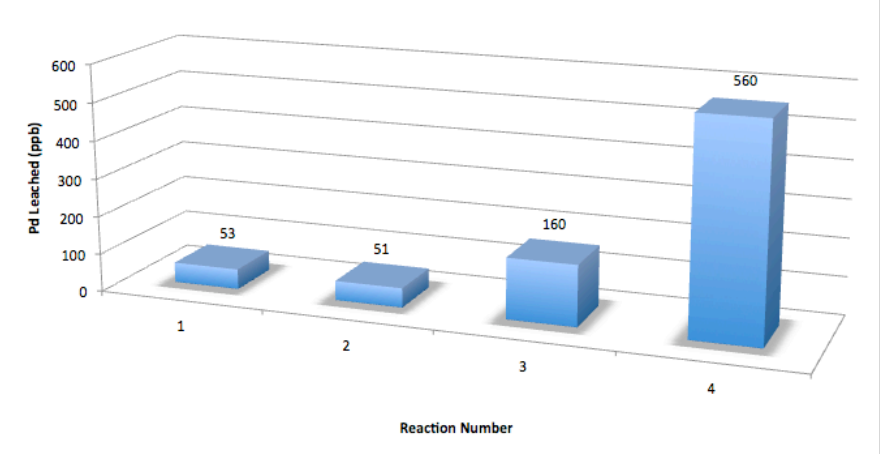

Figure 3.22: Effect of recycling on Pd leaching from SBA-15-SH-Pd in the Suzuki-Miyaura reaction.

Analysis of the materials by TEM after use demonstrated that the materials were losing order during use. However, TEM is not a bulk analysis, and therefore, we employed nitrogen porosimetry to asses the loss of order after reuse of these catalysts. From this study, it is clear that the materials are undergoing serious degradation under the reaction conditions (Figure 3.23).

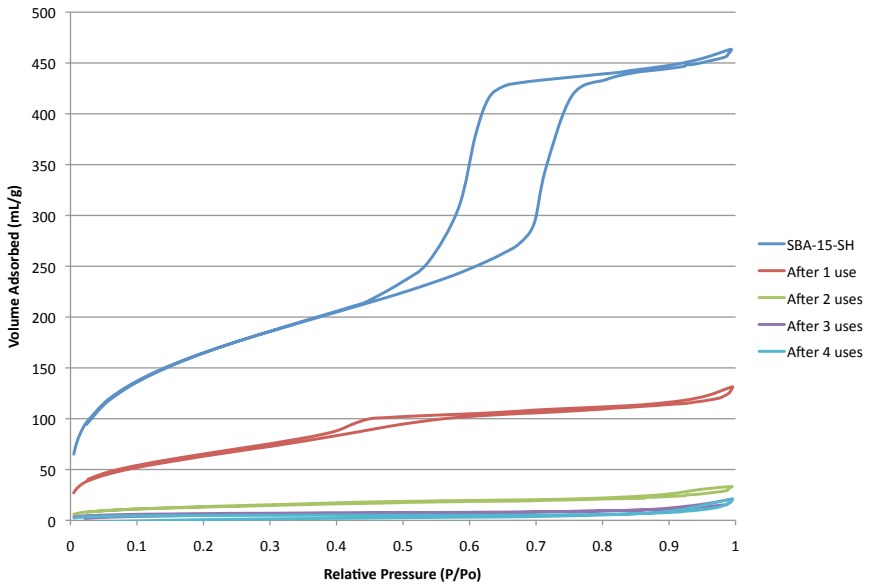

Figure 3.23: Effect of recycling on pore structure measured by nitrogen porosimetry.

While hydrothermal stability is often assessed for mesoporous silicas[69-73], there have been very few studies of the stability of these materials to other reaction conditions[74]. It is well known that the silica framework can be restructured under basic conditions and, without a structure directing agent, this will lead to collapse of the pores[74,75]. In fact, treatment of our SBA-15-SH-Pd catalyst with potassium carbonate in water at 80 °C for 2 h completely degrades the material such that no silica based solids can be recovered by filtration. Interestingly, the grafted SBA-15-SH(g) catalyst was recycled five times and maintained order for more cycles of Suzuki-Miyaura reactions than the co-condensed SBA-15-SH(cc) catalyst (Figure 3.24)[48].

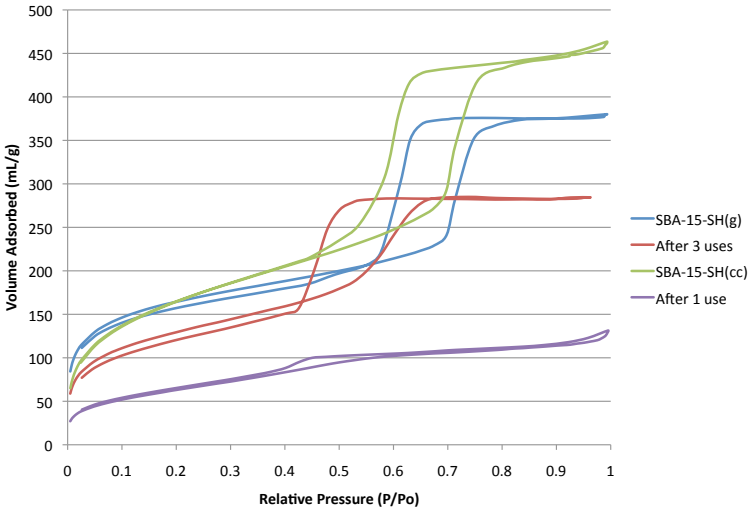

Figure 3.24: Comparison of grafted [SBA-15-SH(g)] and co-condensed [SBA-15-SH(cc)] catalysts. Effect of recycling on the porosity of the materials.

We postulated that grafting of MPTMS onto the surface might protect the surface by blocking the surface silanols or by creating a more hydrophobic surface. In an attempt to improve the recyclability of the co-condensed materials, the surfaces were end-capped with hydrophobic dimethylsilyl

(DMS-SBA-15-SH-Pd) and diphenylsilyl (DPS-SBA-15-SH-Pd) groups after removal of the surfactant. The recycling results are presented in Table 3.6.

Table 3.6: Recycling studies with silylated SBA-15-SH-Pd catalysts under inert atmosphere.

Entry	Catalyst	Yield (%)				
		1	2	3	4	5
1	SBA-15-SH-Pd	87	72	26	-	-
2	DMS-SBA-15-SH-Pd	96	96	93	89	82
3	DPS-SBA-15-SH-Pd	94	54	14	-	-

For DPS-SBA-15-SH-Pd, catalytic activity dropped rapidly after the first catalytic cycle. This was accompanied by a collapse of the mesopore structure, although micropores were clearly still present (Figure 3.25).

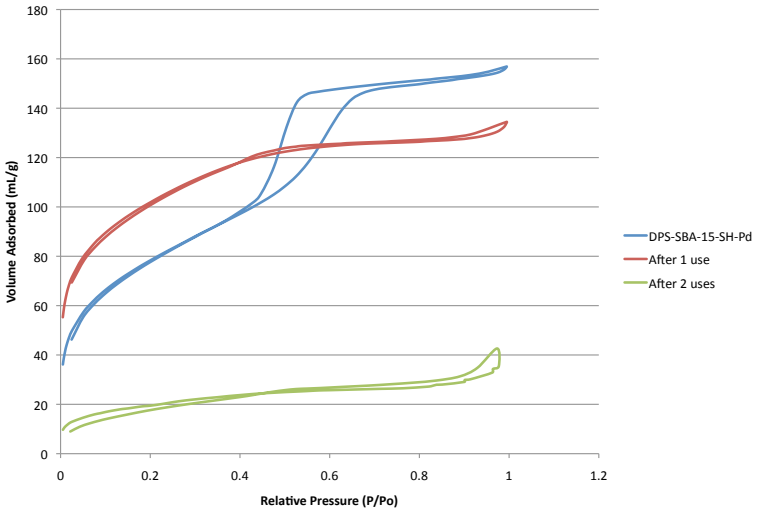

Figure 3.25: Effect of recycling on the pore structure of DPS-SBA-15-SH-Pd as measured by nitrogen porosimetry.

However, for DMS-SBA-15-SH-Pd the recyclability over unprotected silica was greatly improved and, similar to the grafted SBA-15-SH-Pd, five cycles of catalysis were achieved (Figure 3.26), although a continued degradation of

the material is obvious. It appears that capping of the surface silanols protects the material from degradation and allows continued use in the Suzuki-Miyaura reaction. Further investigation into new protecting agents for the surface may increase the stability of mesoporous silicas to basic conditions. In the case of grafted materials, the incorporation of aluminum into the material has been shown to dramatically enhance its stability, and therefore this approach should also be examined with the co-condensed materials.

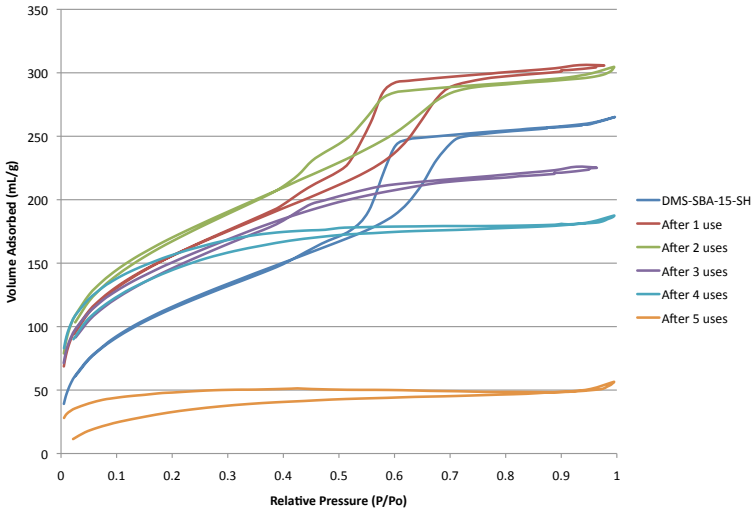

Figure 3.26: Effect of recycling on the pore structure of DMS-SBA-15-SH-Pd as measured by nitrogen porosimetry.

3.3 Conclusions

We have prepared thiol-functionalized mesoporous silica-based palladium catalysts and demonstrated their utility in the Suzuki-Miyaura, copper-free Sonogashira and hydrogenation reactions. Even in the case of heteroatom-containing complex substrates, low levels of Pd leaching are

observed. In general, higher leaching is observed with aryl iodide substrates, however there is still less than 5 ppm Pd in the solution after reaction. The synthesis of the aryl bromide equivalents of these coupling partners may reduce the level of leaching during the coupling reaction. We have demonstrated through a variety of heterogeneity tests that the catalyst likely operates by a release and return mechanism with homogeneous palladium being catalytically active. Furthermore, we have shown that the results of heterogeneity tests must be examined carefully. Initially the co condensed materials were not stable to prolonged recycling experiments, with a loss in catalytic activity accompanied by a degradation of the pore structure. We have shown that recyclability can be improved by protecting surface silanols with hydrophobic silanes presumably hampering the base promoted degradation of the materials.

3.4 References

(1) *Handbook of Organopalladium Chemistry for Organic Synthesis*; Negishi, E.I.; de Meijere, A., Eds.; Wile-VCH: New York, 2002.
(2) *Metal-Catalyzed Cross Coupling Reactions*; Diederich, F.; Stang, P.J., Eds.; Wiley-VCH: New York, 1998.
(3) Miyaura, N.; Suzuki, A. *Chem. Rev.* **1995**, *95*, 2457.
(4) Suzuki, A. *J. Organomet. Chem.* **2002**, *653*, 83.
(5) *Organometallics in Process Chemistry*; Larsen, R.D., Ed.; Springer-Verlag: New York, 2004; Vol. 6.
(6) Garrett, C.E.; Prasad, K. *Adv. Synth. Catal.* **2004**, *346*, 889.
(7) Konisberger, K.; Chen, G.P.; Wu, R.R.; Girgis, M.J.; Prasad, K.; Repic, O.; Blacklock, T.J. *Org. Proc. Res. Dev.* **2003**, *7*, 733.
(8) Jas, G.; Kirschning, A. *Chem. Eur. J.* **2003**, *9*, 5708.
(9) Shore, G.; Morin, S.; Organ, M.G. *Angew. Chem. Int. Ed.* **2006**, *45*, 2761.
(10) Nikbin, N.; Ladlow, M.; Ley, S.V. *Org. Proc. Res. Dev.* **2007**, *11*, 458.
(11) Yin, L.; Liebscher, J. *Chem. Rev.* **2007**, *107*, 133.
(12) Zhao, F.; Shirai, M.; Ikushima, Y.; Arai, M. *J. Mol. Catal. A: Chem.* **2002**, *180*, 211.
(13) Zhao, F.; Bhanage, B.M.; Shirai, M.; Arai, M. *Chem. Eur. J.* **2000**, *6*, 843.
(14) Zhao, F.; Murakami, K.; Shirai, M.; Arai, M. *J. Catal.* **2000**, *194*, 479.
(15) Zhao, F.; Shirai, M.; Arai, M. *J. Mol. Catal. A: Chem.* **2000**, *154*, 39.
(16) Kohler, K.; Kleist, W.; Prockl, S.S. *Inorg. Chem.* **2007**, *46*, 1876.
(17) Prockl, S.S.; Kleist, W.; Gruber, M.A.; Kohler, K. *Angew. Chem. Int. Ed.* **2004**, *43*, 1881.
(18) Kohler, K.; Heindenreich, R.G.; Krauter, J.G.E.; Pietsch, J. *Chem. Eur. J.* **2002**, *8*, 622.
(19) Heindenreich, R.G.; Krauter, J.G.E.; Pietsch, J.; Kohler, K. *J. Mol. Catal. A: Chem.* **2002**, *182-183*, 499.
(20) Dams, M.; Drijkoningen, L.; Pauwels, B.; Tendeloo, G.V.; de Vos, D.E.; Jacobs, P. *J. Catal.* **2002**, *209*, 225.
(21) Phan, N.T.S.; Van Der Sluys, M.; Jones, C.W. *Adv. Synth. Catal.* **2006**, *348*, 609.
(22) Mehnert, C.P.; Weaver, D.W.; Ying, J.Y. *J. Am. Chem. Soc.* **1998**, *120*, 12289.
(23) Mehnert, C.P.; Ying, J.Y. *Chem. Commun.* **1997**, 2215.
(24) Ying, J.Y.; Mehnert, C.P.; Wong, M.S. *Angew. Chem. Int. Ed.* **1999**, *38*, 56.
(25) Akiyama, R.; Kobayashi, S. *J. Am. Chem. Soc.* **2003**, *125*, 3412.
(26) Hagio, H.; Sugiura, M.; Kobayashi, S. *Org. Lett.* **2006**, *8*, 375.
(27) Solodenko, W.; Wen, H.; Leue, S.; Stuhlmann, F.; Sourkouni-Argirusi, G.; Jas, G.; Schonfeld, H.; Kunz, U.; Kirschning, A. *Eur. J. Org. Chem.* **2004**, *2004*, 3601.
(28) Thiot, C.; Schmutz, M.; Wagner, A.; Mioskowski, C. *Angew. Chem. Int. Ed.* **2006**, *45*, 2868.
(29) Ren, N.; Yang, Y.H.; Zhang, Y.H.; Wang, Q.R.; Tang, Y. *J. Catal.* **2007**, *246*, 215.

(30) Smith, M.D.; Stepan, A.F.; Ramarao, C.; Brennan, P.E.; Ley, S.V. *Chem. Commun.* **2003**, 2652.
(31) Andrews, S.O.; Stepan, A.F.; Tanaka, H.; Ley, S.V.; Smith, M.D. *Adv. Synth. Catal.* **2005**, *347*, 647.
(32) Lee, C.K.Y.; Holmes, A.B.; Ley, S.V.; McConvey, I.F.; Al-Duri, B.; Leeke, G.A.; Santos, R.C.D.; Seville, J.P.K. *Chem. Commun.* **2005**, 2175.
(33) Ramarao, C.; Ley, S.V.; Smith, S.C.; Shirley, I.M.; DeAlmeida, N. *Chem. Commun.* **2002**, 1132.
(34) Baxendale, I.R.; Griffiths-Jones, C.M.; Ley, S.V.; Tranmer, G.K. *Chem. Eur. J.* **2006**, *12*, 4407.
(35) de Vos, D.E.; Dams, M.; Sels, B.F.; Jacobs, P.A. *Chem. Rev.* **2002**, *102*, 3615.
(36) Weck, M.; Jones, C.W. *Inorg. Chem.* **2007**, *46*, 1865.
(37) Fan, Q.H.; Li, Y.M.; Chan, A.S.C. *Chem. Rev.* **2002**, *102*, 3385.
(38) Leadbeater, N.E.; Marco, M. *Chem. Rev.* **2002**, *102*, 3217.
(39) Bergbreiter, D.E.; Osburn, P.L.; Wilson, A.; Sink, E.M. *J. Am. Chem. Soc.* **2000**, *122*, 9058.
(40) Yu, K.; Sommer, W.; Weck, M.; Jones, C.W. *J. Catal.* **2004**, *226*, 101.
(41) Mubofu, E.B.; Clark, J.H.; Macquarrie, D. *Green. Chem.* **2001**, *3*, 23.
(42) Corma, A.; Das, D.; Garcia, H.; Leyva, A. *J. Catal.* **2005**, *229*, 322.
(43) Alonso, D.A.; Najera, C.; Pacheco, M.C. *Adv. Synth. Catal.* **2002**, *344*, 172.
(44) Shimizu, K.I.; Koizumi, S.; Hatamachi, T.; Yoshida, H.; Komai, S.; Kodama, T.; Kitayama, Y. *J. Catal.* **2004**, *228*, 141.
(45) Ji, Y.; Jain, S.; Davis, R.J. *J. Phys. Chem. B* **2005**, *109*, 17232.
(46) Crudden, C.M.; Sateesh, M.; Lewis, R. *J. Am. Chem. Soc.* **2005**, *127*, 10045.
(47) Crudden, C.M.; McEleney, K.; MacQuarrie, S.; Blanc, A.; Sateesh, M.; Webb, J.D. *Pure Appl. Chem.* **2007**, *79*, 247.
(48) Webb, J.D.; MacQuarrie, S.; McEleney, K.; Crudden, C.M. *J. Catal.* **2007**, *252*, 97.
(49) Sheldon, R.A.; Wallau, M.; Arends, I.W.C.E.; Schuchardt, U. *Acc. Chem. Res.* **1998**, *31*, 489.
(50) Arvela, R.K.; Leadbeater, N.E.; Sangi, M.S.; Williams, V.A.; Granados, P.; Singer, R.D. *J. Org. Chem.* **2005**, *70*, 161.
(51) Alimardanov, A.; Schmieder-van de Vondervoort, L.; de Vries, A.H.M.; de Vries, J.G. *Adv. Synth. Catal.* **2004**, *346*, 1812.
(52) Sommer, W.J.; Yu, K.; Sears, J.S.; Ji, Y.; Zheng, X.; Davis, R.J.; Sherrill, C.D.; Jones, C.W.; Weck, M. *Organometallics* **2005**, *24*, 4351.
(53) Yu, K.; Sommer, W.; Richardson, J.M.; Weck, M.; Jones, C.W. *Adv. Synth. Catal.* **2005**, *347*, 161.
(54) Foley, P.; DiCosimo, R.; Whitesides, G.M. *J. Am. Chem. Soc.* **1980**, *102*, 6713.
(55) Anton, D.R.; Crabtree, R.H. *Organometallics* **1983**, *2*, 855.
(56) Richardson, J.M.; Jones, C.W. *Adv. Synth. Catal.* **2006**, *348*, 1207.
(57) Richardson, J.M.; Jones, C.W. *J. Catal.* **2007**, *251*, 80.
(58) Rebek, J.; Gavina, F. *J. Am. Chem. Soc.* **1974**, *96*, 7112.
(59) Rebek, J.; Brown, D.; Zimmerman, S. *J. Am. Chem. Soc.* **1975**, *97*, 454.
(60) Rebek, J. *Tetrahedron* **1979**, *35*, 723.

(61) Davies, I.W.; Matty, L.; Hughes, D.L.; Reider, P.J. *J. Am. Chem. Soc.* **2001**, *123*, 10139.
(62) MacQuarrie, S.; Horton, J.H.; Barnes, J.; McEleney, K.; Loock, H.P.; Crudden, C.M. *Angew. Chem. Int. Ed.* **2008**, *47*, 3279.
(63) Reetz, M.T.; Westermann, E. *Angew. Chem. Int. Ed.* **2000**, *39*, 165.
(64) Negishi, E.I.; Anastasia, L. *Chem. Rev.* **2003**, *103*, 1979.
(65) Zhang, L.Y.; Wang, L. *Chinese J. Chem.* **2008**, *26*, 1601.
(66) Soheili, A.; Albaneze-Walker, J.; Murray, J.A.; Dormer, P.G.; Hughes, D.L. *Org. Lett.* **2003**, *5*, 4191.
(67) Yi, C.; Hua, R. *J. Org. Chem.* **2006**, *71*, 2535.
(68) Gholap, A.R.; Venkatesan, K.; Pasricha, R.; Daniel, T.; Lahoti, R.J.; Srinivasan, K.V. *J. Org. Chem.* **2005**, *70*, 4869.
(69) Han, Y.; Li, N.; Zhao, L.; Li, D.; Xu, X.; Wu, S.; Di, Y.; Li, C.; Zou, Y.; Yu, Y.; Xiao, F.S. *J. Phys. Chem. B* **2003**, *107*, 7551.
(70) Lim, M.H.; Stein, A. *Chem. Mater.* **1999**, *11*, 3285.
(71) Mokaya, R. *J. Phys. Chem. B* **1999**, *103*, 10204.
(72) Zhang, F.; Yan, Y.; Yang, H.; Meng, Y.; Meng, Y.; Yu, C.; To, B.; Zhao, D. *J. Phys. Chem. B* **2005**, *109*, 8723.
(73) Ryoo, R.; Jun, S. *J. Phys. Chem. B* **1997**, *101*, 317.
(74) Bass, J.D.; Grosso, D.; Boissere, C.; Belamie, E.; Coradin, T.; Sanchez, C. *Chem. Mater.* **2007**, *19*, 4349.
(75) Wan, Y.; Zhao, D. *Chem. Rev.* **2007**, *107*, 2821.

Chapter 4: X-Ray Photoelectron Spectroscopy Studies of SBA-15-SH-Pd

4.1 Introduction

As previously discussed, heterogeneous catalysts are difficult to characterize owing to a lack of analytical techniques comparable to those developed for liquids. Thus, the role of surface science in characterizing and developing heterogeneous catalysts is important[1]. Of the surface science techniques, X-ray photoelectron spectroscopy (XPS) is a useful tool for examining the chemical state of elements, with the position of an XP peak for a given element being sensitive to its chemical state[2]. However, this information can be limited due to the narrow range of binding energies observed for some elements. Additionally, while XPS offers information about the metal sites, it can be used to study the support material as well.

X-ray induced Auger emission spectroscopy (XAES) is another powerful surface science tool for inspection of heterogeneous catalysts. Strong chemical effects are observed in the shape, intensity and location of Auger peaks[3]. In many cases the kinetic energy shift of XAE peaks with changes in chemical state is larger than for XP peaks. However, these shifts are harder to interpret and the use of Auger analysis for determining chemical states has been under utilized[3]. Wagner first recognized the utility of Auger transitions in XPS[4]. He noted that comparison of the difference in the kinetic energy of the Auger and photoelectron was more accurate than direct comparison of binding energies, since static charging corrections for the two

peaks cancel out[4]. Combining the XPS and XAES data into a two-dimensional chemical state plot (Wagner plot) yields more information about the chemical environment in which an element resides than is gleaned from either technique alone[2]. Experimentally, it is more practical to sum the XPS binding energy (*BE*) and XAES kinetic energies (*KE*) together rather than examine the difference in the kinetic energies, as the value is no longer dependent on the photon energy of the spectrometer. This provides one with the Auger parameter, α'[5]:

$$\alpha' = KE_{(Auger)} + BE_{(photoelectron)} \quad \text{(Eq 4.1)}$$

The Auger parameter has been shown to be a measure of the extra-atomic relaxation or screening effect of the surrounding medium on the final ion state[3]. When the Auger transition involves only core levels, the change in Auger parameter is equal to twice the change in extra-atomic relaxation, R_{ea}[3]:

$$\Delta\alpha' = 2\Delta R_{ea} \quad \text{(Eq. 4.2)}$$

This is particularly helpful in interpreting binding energy shifts between samples because binding energy shifts between two species, ΔBE, depends not only on the difference in ground state energy between two species, $\Delta\varepsilon$, but also on the extra-atomic relaxation[6]:

$$\Delta BE = \Delta\varepsilon - \Delta R_{ea} \quad \text{(Eq 4.3)}$$

Differences in oxidation state control the value of $\Delta\varepsilon$ and often result in "diagnostic" binding energy ranges associated with a particular oxidation state of a given element. Nonetheless, the extra-atomic relaxation term can be significant and thus the polarizability of the surrounding chemical species can

have a strong, and sometimes counterintuitive, effect on the observed binding energy shift if only oxidation state is considered. Equation 4.2 is not strictly applicable in systems where the Auger transition involves the valence band, such as here with Pd. Nonetheless, the Auger parameter is still a useful qualitative measure of the polarizability of the medium in which the core hole is located and an indicator of the extent to which the true oxidation state of Pd differs between samples.

Despite extensive studies detailing catalytic activity and mode of action for supported palladium catalysts[7], the oxidation state of the catalyst before and after use, and the nature of the palladium-sulfur interaction within the catalyst are not fully understood. EXAFS spectroscopy has been employed to obtain information about changes in oxidation state after catalysis for a closely related catalyst to the one we employ in this study[8]. In their detailed analysis, Shimizu *et al.* saw evidence of a Pd-S bond in an FSM-SH-Pd catalyst and demonstrated varying amounts of reduction of palladium (II) to palladium nanoparticles in the used catalysts[8,9]. Palladium-based coupling catalysts have also been studied using X-ray photoelectron spectroscopy (XPS)[10-14]. A general trend from these studies is that catalysts that have Pd $3d_{5/2}$ spectra of lower binding energy, and hence presumably lower Pd oxidation state, tend to have higher activity. For example, Paul and Clark studied a series of eight different N-N, N-O and N-S chelating pyridine-type ligands (Figure 4.1) in homogeneous catalysts and found binding energies ranging from 333.45 eV to 336.35 eV for the catalysts before use[11].

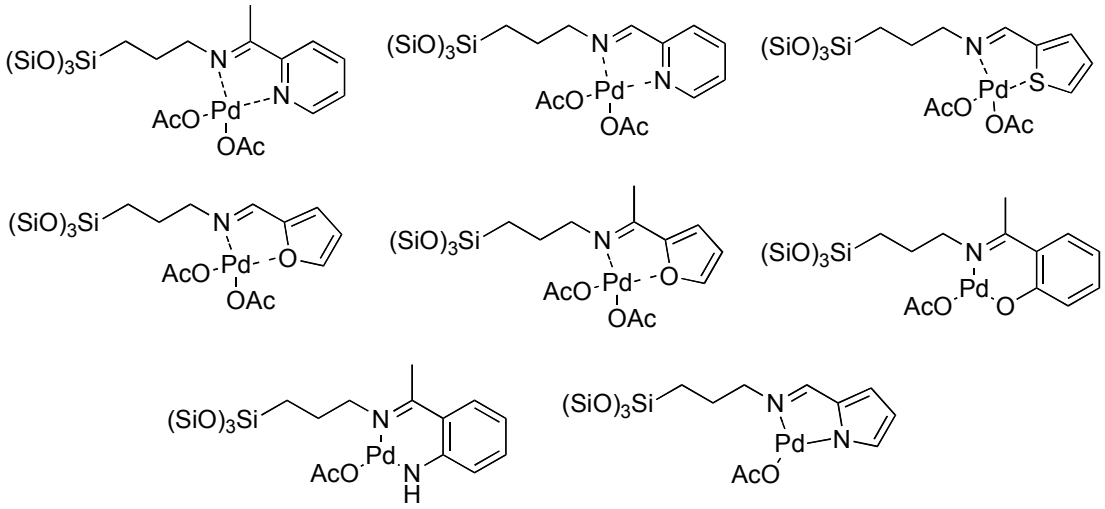

Figure 4.1: Chelated palladium (II) catalysts studied by Paul and Clark[11].

They ascribed the increased activity of the low binding energy Pd species (most of which also tended to have higher co-ordination numbers around the Pd centre) to a larger electron density about the Pd, facilitating oxidative addition. Pd nanoparticle catalysts on polyaniline supports[10,13] and thiol Pd catalysts supported on mesoporous silicate MCM–41[12] were both found to be more active in the reduced form, as expected based on the mechanism. However, based on XANES studies, Shimizu et al. proposed that the oxidation state of Pd is primarily +2 in thiol-modified FSM-based Pd catalysts, with small amounts Pd(0) observed[8]. Larger amounts of Pd(0) were observed on thiol-modified silica compared with the mesoporous analog, and significant deposits of Pd(0) nanoparticles were observed by TEM when Pd was supported on unfunctionalized supports[8].

While XPS of the Pd $3d_{5/2}$ state alone may provide valuable information on the oxidation state of the reactive Pd centre, there is much less information

in the literature on the characterization of the support and ligand portions of the catalysts using photoelectron spectroscopy. The binding energy of any XPS line alone is also not a definitive indication of the oxidation state of an element. For example, Pd foils are often studied as they are used as catalysts for methane oxidation[15]. Prins *et al.* reported XPS data on foils, films and nanostructured palladium on silicon oxide and found that as the nanodots or nanopits of palladium became smaller the binding energy of Pd increased relative to that of the foil[16]. They attributed this not to a change in oxidation state but to a valence electronic effect due to the isolation of Pd nanoparticles on an insulating surface.

We performed comprehensive XPS and XAES study of our silicate-supported palladium catalysts used in Suzuki-Miyaura cross-coupling reactions. The electronic structure of both the reactive Pd centre and the S portion of the thiol ligand which tethers it to the silica support are examined. Using Wagner plots of binding energy vs. Auger kinetic energy, we compared our measured data to those from a series of standard compounds containing both Pd and S, as well as a number of XPS and Auger parameter data on these elements previously published in the literature. We show that combined XAES and XPS data, especially when compared to values from a wide range of Pd and S compounds, are effective in ascertaining the electronic structure of both the Pd and S sites in the catalyst as a function of Pd loading and catalyst activity.

4.2 Results and Discussion

Typical XP and XAE spectra for palladium, sulfur, silicon and carbon from a pristine sample of SBA-15-SH are shown in figure 4.2. The two Pd $3d_{3/2,5/2}$ spin states are well resolved and the binding energy of the more intense $3d_{5/2}$ peak was used for our measurements. For sulfur and silicon, the $2p_{1/2,3/2}$ spin states are not well resolved, so the binding energy of the overall peak envelope is reported. The Pd XAES peak is the MNN transition while the S XAES peak is the KLL transition. Carbon 1s was used as an internal standard such that binding energies of the other elements were referenced to the C 1s binding energy of 285.0 eV.

Figures 4.3 to 4.6 show Wagner plots in which the kinetic energy of the XAES peak is plotted as a function of the XPS binding energy peak. The diagonal elements in these figures correspond to lines of equal Auger parameter (α'). These data may be also found in tabular format in Appendix A. Generally, open symbols in the figures refer to data collected here, while filled symbols are taken from the literature. We examined both ordered SBA-15 and amorphous thiol-functionalized silica loaded with palladium, in the form of $Pd(OAc)_2$. Catalysts were examined prior to use, and after one use. All the catalysts from our study were found to have binding energies in the range of 337.3 eV to 338.1 eV and Auger parameters between 661 eV and 664 eV, as shown in figure 4.3. An expansion of the central region of figure

4.3, focusing on the catalysts prepared in this study (binding energy 337 eV to 339 eV), is given in figure 4.4.

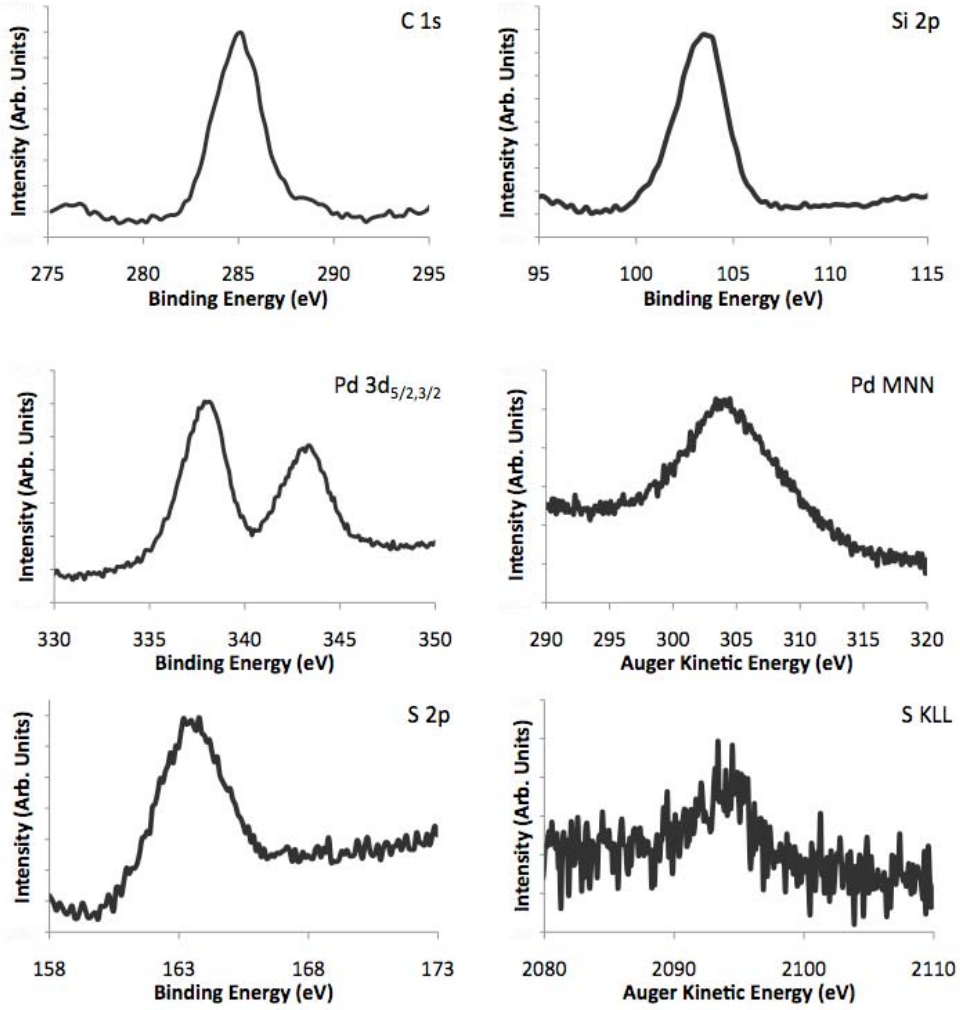

Figure 4.2: Representative XPS and Auger specra for C, Pd, S and Si collected from an SBA-15-SH(g)-Pd sample before use. (a) C 1s; (b) Si 2p; (c) Pd 3d; (d) Pd MNN; (e) S 2p; (f) S KLL.

From this figure, it is obvious that there is a change in the nature of Pd after the catalyst is subjected to the Suzuki-Miyaura reaction conditions. Before use, all of the Pd complexes employed herein have Pd $3d_{5/2}$ binding energies above 337.6 eV in a region considered to be palladium II species.

These values are clearly different from that for palladium acetate (338.8 eV) indicating that the palladium species is not merely adsorbed on the silica, but rather they are interacting with the thiol on the surface. Furthermore, the Auger energy and binding energy of palladium sulfide lies in between the values of the catalysts before and after use. This suggests that there is some degree of palladium sulfur bonding in these materials.

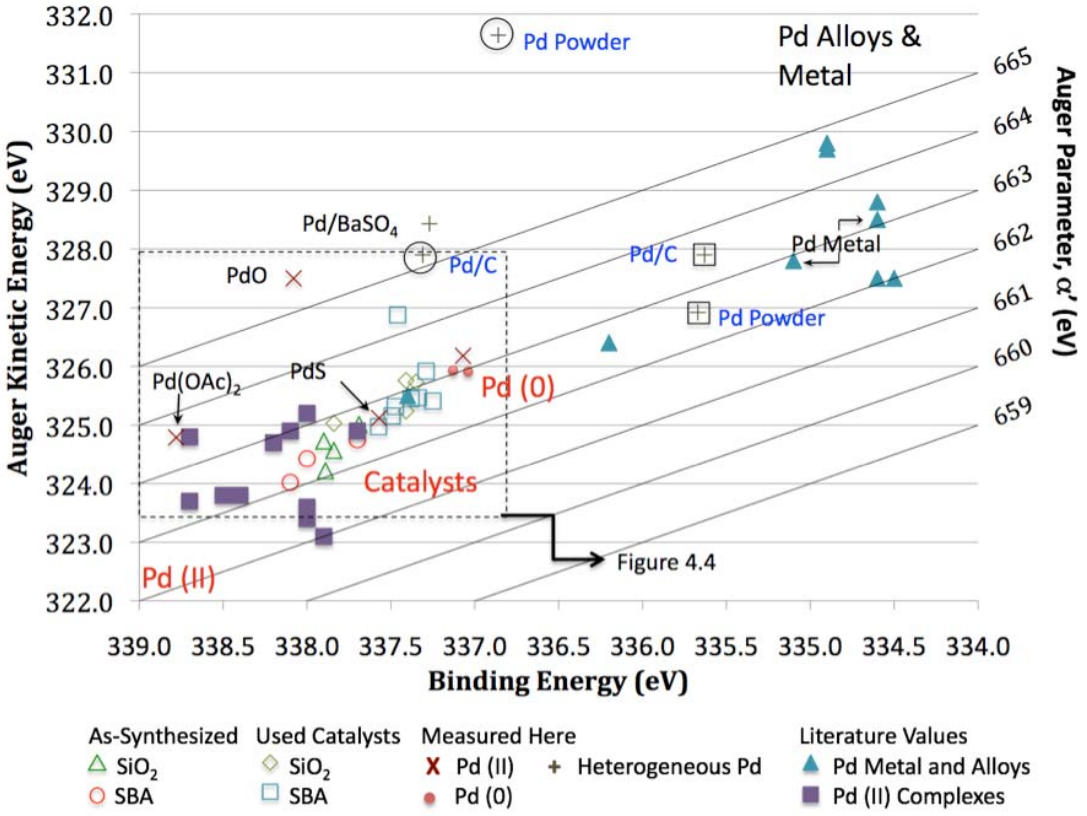

Figure 4.3: Wagner chemical state plot for Pd $3d_{5/2}$ XPS and Pd MNN XAES data. The region denoted in the dashed lines is expanded in figure 4.4.

The lack of a systematic pattern in the binding energy or Auger parameter upon changing the silica support indicated that the support has little effect on the electronic structure of palladium, consistent with the idea that binding of the thiol ligand controls the adsorption of palladium onto the silica.

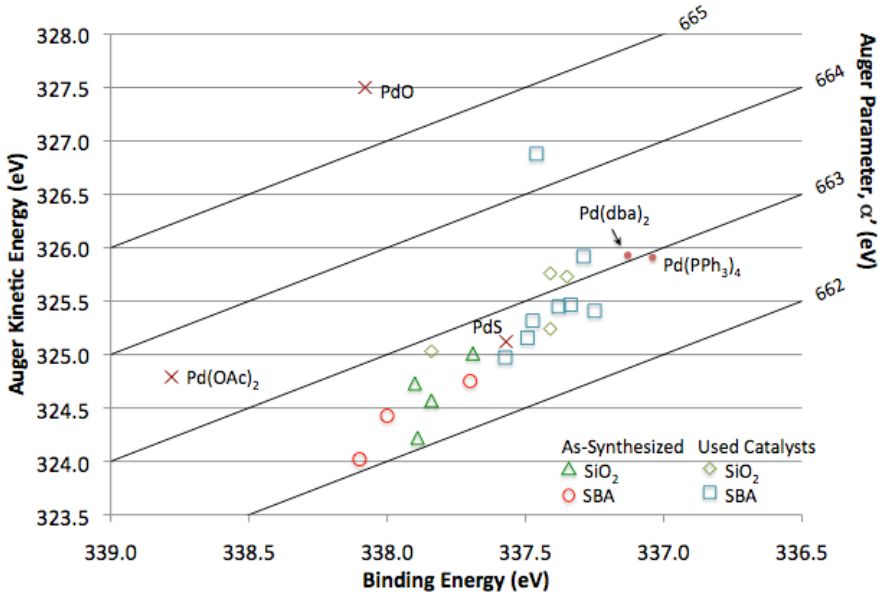

Figure 4.4: Expansion of the Wagner Chemical State plot for Pd in the binding energy region of our catalysts.

After the catalysts have been used in the Suzuki-Miyaura reaction, the palladium binding energies have shifted to lower binding energy values, less than 337.6 eV. As with the unused catalysts, there is no systematic difference observable in the Pd binding energies for Pd supported on amorphous silica and that supported on SBA-15. We postulated that the reduction of Pd binding energy was due to a reduction of the palladium species to Pd(0) based on the proposed mechanism of the Suzuki-Miyaura reaction as well as the observation of small nanoparticles in the catalysts after reaction[17-20]. However, metallic palladium, presumably in the 0 oxidation state has binding energies between 334.5 eV and 335.5 eV. This may be a bit ambiguous as catalysts prepared by Paul and Clark containing palladium (II) species had binding energies between 333.45 eV and 336.35 eV, typically considered to be Pd(0) binding energies[11]. To determine the cause of this apparent

discrepancy we measured XP and XAE spectra of a number of other palladium-containing molecules. Palladium oxide (PdO) has a high binding energy of 338.1 eV and an Auger parameter of 665.6 eV, which is much higher than those measured for other species observed so far. Two common Pd(0) catalysts, palladium tetrakistriphenylphosphine $Pd(PPh_3)_4$ and bis-(dibenzylideneacetone) palladium $Pd(dba)_2$ were found to have very similar binding energies of 337.0 eV and 337.1 eV respectively (Figure 4.4). Their Auger parameters were similar as well, 663.0 eV for $Pd(PPh_3)_4$ and 663.1 eV for $Pd(dba)_2$. These values are generally lower than those found for the used catalysts, but some of these catalysts are clearly close to the values of the Pd(0) complexes. Since palladium (0) complexes are sensitive to air, care was taken to minimize oxidation during transfer to the XP spectrometer. Solid state ^{31}P NMR was performed on $Pd(PPh_3)_4$ with a single ^{31}P chemical shift of 14.1 ppm observed consistent with palladium coordinated phosphine. Importantly, no peak around 30 ppm for oxidized phosphine was observed suggesting that the palladium complex was intact and that palladium was in the 0 oxidation state.

This difference in binding energy between metallic palladium and mono-atomic palladium can be explained by extra-atomic relaxation effects. The relatively diffuse electronic structure of a metal allows the charge generated by the core-electron loss to be shared over a large number of atoms. This extra-atomic relaxation lowers the binding energy of the metal species[16]. If we look at a mono-atomic metal complex, this relaxation energy

is absent and the binding energy is increased relative to bulk metal. Nanoparticles are an intermediate case where a compact environment around the metal atoms lowers the extra-atomic relaxation effect with consequent increase in binding energy. Increases of up to 1.6 eV have been reported for small metal clusters relative to bulk metal[21]. Since there is no effort to control exposure of the used catalysts to air, it is possible that they may have partially oxidized to Pd (II). However, given the very different binding energy of palladium oxide and lack of observable oxidation of sulfur it is unlikely that we are observing oxidized palladium.

Furthermore, measurement of two typical supported palladium catalysts, palladium on carbon and palladium on barium sulfate, along with palladium powder revealed a chemical state intermediate to mono-atomic Pd and bulk Pd. All of these materials gave two distinct signals, the first lying at a binding energy midway between the Pd(0) species and that of metallic Pd (squares in Figure 4.3) and the other in the same region as PdO (circled in Figure 4.3). The higher binding energy species have similar XP and XAE energies to palladium oxide indicating oxidation of the surface palladium in these samples. This is a commonly observed contaminant on commercial Pd/C and other commercial palladium sources, and can be a major species in some cases[8,22]. The lower binding energy species lies in between mono-atomic palladium and bulk palladium. Previous TEM data on the silica supported used catalysts demonstrated the presence of nanoparticles on the order of 5 to 7 nm in diameter, about the size of the pores. Palladium on

carbon and palladium powder are known to contain nanoparticles of 10 to 20 nm diameter. These larger nanoparticles presumably have a larger extra-atomic relaxation effect which serves to lower the binding energy of these particles. These observations are consistent with the reduction of palladium (II) in the unused catalyst to palladium (0) species after use. The palladium (0) is likely in the form of small nanoparticles (<6 nm) constrained by the mesoporous silica support coordinated to the sulfur sites in the material. These small nanoparticles are too small to behave as bulk palladium.

In addition to palladium, the sulfur 2p signal was also monitored. Figure 4.5 shows a Wagner plot for S 2p/S KLL data. Published values for the S Auger parameter range from 2275 eV to 2280 eV. Sulfur species in various oxidation states show clearly differentiated S 2p binding energies, starting with S^{2-} below 160 eV, S^{0} between 160 eV and 162 eV, S^{4+} between 165 eV and 166 eV and S^{6+} >166.5 eV[23]. However, it should be noted that there is some disparity in the literature on the placement of the sulfur oxidation states along the binding energy axis. Unlike Yu *et al.*[23], Bensebaa *et al*.[24] place alkyl thiols (S^{0}) between 163.5 eV and 163.8 eV. They also define thiolates chemisorbed on metals (S^{-}) at 161.8 eV to 162.6 eV and oxidized sulfur at binding energies >167 eV. No corresponding Auger data were given for these groupings, so these ranges are noted as black bars along the binding energy axis on figure 4.5. An expansion of the Wagner plot in figure 4.5 for the binding energy region corresponding to our catalysts is shown in figure 4.6.

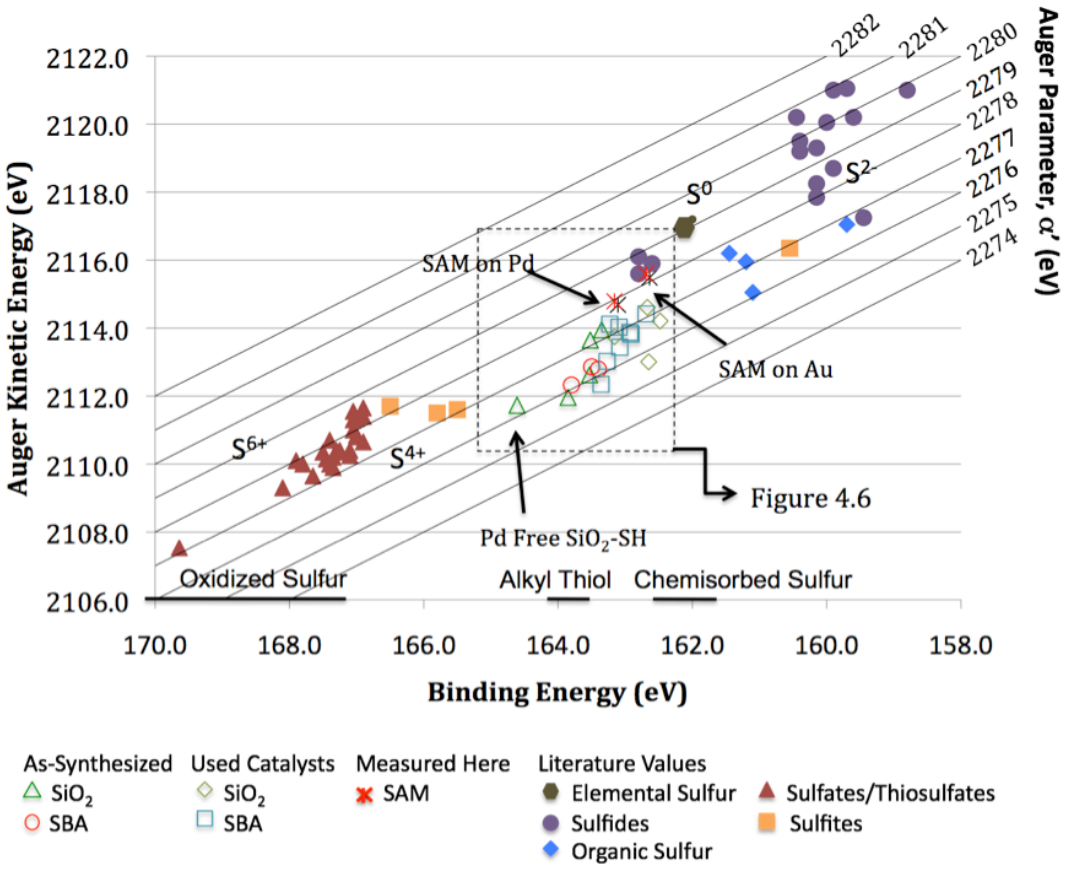

Figure 4.5: Wagner chemical state plot for S 2p XPS and S KLL XAES data. The region denoted in the dashed lines is expanded in Figure 3. The binding energy ranges for various sulfur chemical states given in ref [24] are shown as lines above the x-axis.

As with the Pd data, this plot shows that there is a clear differentiation of the sulfur 2p binding energy data between the catalysts before and after use with pristine catalysts having binding energies above 163.5 eV and used catalysts below this value. Functionalized amorphous SiO_2 in which no Pd was present has a sulfur binding energy of 164.6 eV, which is significantly higher than materials containing Pd but similar to alkane thiols reported by Bensbaa[24]. Addition of palladium to the functionalized silica lowered the S 2p binding energy to between 163.4 eV and 163.9 eV. These are similar to values we

have measured for dodecanethiol SAM on Au (162.7 eV) or Pd (163.2) and slightly higher than C14 alkanethiol SAM on Au or Ag nanoparticles[24]. The binding energies are thus consistent with a Pd-thiolate bond with increased electron density at sulfur in these materials.

Cai et al. immobilized palladium on MCM-41 through coordination of a thioether. As coordination occurred through one of the lone pairs of the thioether generating a three coordinate sulfur with reduced electron density the S 2p binding energy increased upon coordination to palladium[12]. Given that our S 2p binding energy is decreasing presumably due to an increase at electron density at sulfur, the palladium-sulfur bond is formed with loss of the thiolate hydrogen to generate a two-fold coordinate sulfur (C and Pd).

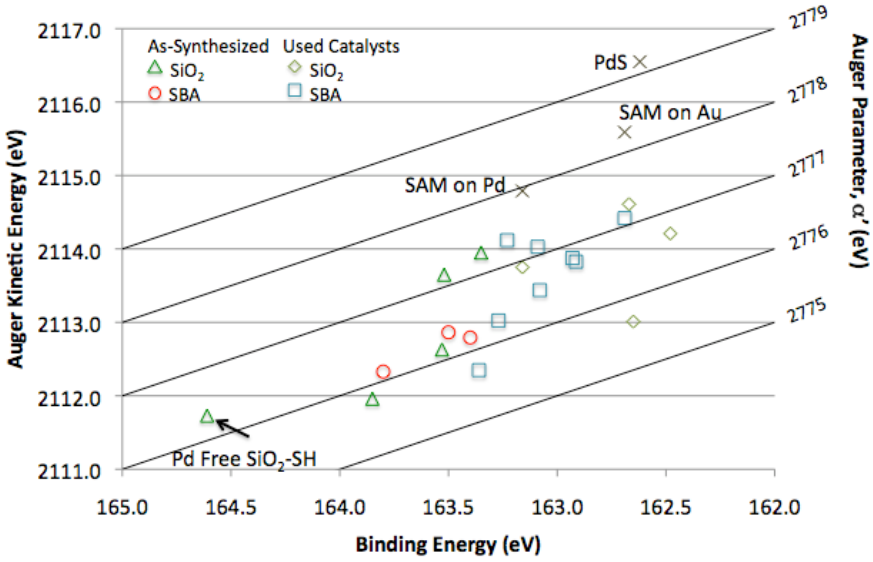

Figure 4.6: Expansion of the Wagner chemical state plot for S in the binding energy region of our catalysts.

The Auger parameters for both pristine and used catalysts lie between 2275.7 eV and 2277.4 eV and did not show a clear differentiation between the

two types. There do not appear to be any previously published Auger parameters for alkanethiol SAMs in the literature. Therefore, we measured Auger parameters for dodecanethiol on Au 2278.3 eV and on Pd 2278.0 eV. Both Auger parameters are considerable higher than those observed for the catalysts, which is consistent with the SAMs having a more polarizable S species. This is due to the SAM sulfur being adjacent to a bulk metal whereas in the catalyst it is at best adjacent to a Pd nanoparticle.

With the amorphous silica catalysts, the S:Pd ratio had an affect on the S 2p binding energy. Increasing the S:Pd ratio from 1:1 to 4:1 resulted in an increase in the S 2p binding energy from 163.4 eV for 1:1 to 163.9 eV for 4:1 (Figure 4.6). As the amount of palladium in the material decreases, the sulfur binding energy becomes closer to that of pure silica thiol (164.6 eV). Considering that Pd is unlikely to bind 4 sulfur ligands on the surface in such a constrained framework (2-2.5 ligands per Pd are likely)[8], this change reflects the presence of more than one sulfur environment with the reported values representing an average of bound and unbound sulfur.

Figure 4.6 indicates that upon use, the sulfur environment of the materials changes with a slightly lower S 2p binding energy (162.5 – 163.4 eV). A decrease in binding energy and the smaller magnitude of the change relative to that of palladium is consistent with an increased electron density at the sulfur site due to the reduction of neighbouring palladium atoms. The Auger parameter for the used catalysts was similar to that of the as-

synthesized catalysts. No oxidation of sulfur was observed in the used catalysts, as no high binding energy peaks (>167 eV) were observed.

We also recorded the Si 2p XP peak for the silicate materials studied expecting that this peak would remain unchanged over our catalytic manipulations (see Appendix A for Si 2p XPS table). The as-synthesized catalysts had binding energies between 103.6 eV and 103.8 eV with the exception of an SBA-15-SH catalyst prepared by co-condensation of the thiol and silicate precursor $Si(OEt)_4$, which had a lower binding energy of 103.1 eV. These values are similar to those in the literature for SiO_2 (103.2 eV to 103.9 eV)[6,25]. After use, the catalysts demonstrated lower Si 2p binding energies of 103.1 eV to 103.3 eV. This difference may be attributed to the effect of the potassium carbonate base on the silica. As our Suzuki-Miyaura reactions are performed in 20:1 DMF:H_2O, it is reasonable to assume that potassium hydroxide is formed under the reaction conditions. Potassium hydroxide is known to restructure silicas by converting bridging oxygen Si-O-Si bonds to non-bridging species Si-O-X (X = K or H)[26]. This has the effect of lowering the binding energy of silicon by increasing the electron density at that atom. The relatively minor shift in Si 2p binding energy is likely due to the low potassium incorporation. It should be noted that potassium was only observed in the materials after catalysis. The K 1s peak was observed near the C 1s spectral window at 293.5 eV.

4.3 Conclusions

We have applied XPS and XAES for the characterization of heterogeneous Suzuki-Miyaura catalysts both before and after use. By using both XPS and XAES, Auger parameters can be determined for the various elements in the catalyst. This allows us to determine information not only on the oxidation state of the catalytic metal centre and the ligands coordinated to the metal but also the polarizability of the environment in which these species are located. This information would be lost if XPS binding energies were taken by themselves. The differentiation in oxidation state by binding energy alone is shown to be potentially misleading as to the true electronic nature of the catalysts species. Effects such as extra-atomic relaxation, core-hole screening and polarization need to be considered. This can lead to very different behaviours between bulk metal and mono-atomic species of the same oxidation state.

We have also shown that change in the chemical environment for both palladium and sulfur occurs upon addition of palladium to the thiol-modified silicas. Furthermore, the chemical environment undergoes changes after the catalyst has been employed in the Suzuki-Miyaura reaction, with a reduction of the palladium species and an increase in the electron density of the sulfur ligand.

4.4 References

(1) Bhasin, M.M. *Catal. Lett.* **1999**, *59*, 1.
(2) Wagner, C.D.; Gale, L.H.; Raymond, R.H. *Anal. Chem.* **1979**, *51*, 466.
(3) Moretti, G. *J. Elec. Spec. Relat. Phenom.* **1998**, *95*, 95.
(4) Wagner, C.D. *Anal. Chem.* **1972**, *44*, 967.
(5) Wagner, C.D.; Passoja, D.E.; Hillery, H.F.; Kinisky, T.G.; Six, H.A.; Jansen, W.T. *J. Vac. Sci. Technol.* **1982**, *21*, 933.
(6) Wagner, C.D. *Faraday Disscuss. Chem. Soc.* **1975**, *60*, 291.
(7) Yin, L.; Liebscher, J. *Chem. Rev.* **2007**, *107*, 133.
(8) Shimizu, K.I.; Koizumi, S.; Hatamachi, T.; Yoshida, H.; Komai, S.; Kodama, T.; Kitayama, Y. *J. Catal.* **2004**, *228*, 141.
(9) FSM is a mesoporous silica prepared from kanemite silica with an alkylammonium surfactant under basic conditions
(10) Houdayer, A.; Schneider, R.; Billaud, D.; Ghanbaja, J.; Lambert, J. *Appl. Organomet. Chem.* **2005**, *19*, 1239.
(11) Paul, S.; Clark, J.H. *J. Mol. Cat. A: Chem.* **2004**, *215*, 107.
(12) Cai, M.; Xu, Q.; Huang, Y. *J. Mol. Catal. A: Chem.* **2007**, *271*, 93.
(13) Kantam, M.L.; Roy, M.; Roy, S.; Sreedhar, B.; Madhavendra, S.S.; Choudary, B.M.; Lal De, R. *Tetrahedron* **2007**, *63*, 8002.
(14) Hasik, M.; Bernasik, A.; Drelinkiewicz, A.; Kowalski, K.; Wenda, E.; Camra, J. *Surf. Sci.* **2002**, *507-510*, 916.
(15) Gabasch, H.; Hayek, K.; Klotzer, B.; Unterberger, W.; Kleimenov, E.; Teschner, D.; Zafeiratos, S.; Havecker, M.; Kopp-Gericke, A.; Schlogl, R.; Aszalos-Kiss, B.; Zemlyanov, D. *J. Phys. Chem. C* **2007**, *111*, 7957.
(16) Schildenberger, M.; Prins, R.; Bonetti, Y.C. *J. Phys. Chem. B* **2000**, *104*, 3250.
(17) Miyaura, N.; Suzuki, A. *Chem. Rev.* **1995**, *95*, 2457.
(18) Crudden, C.M.; Sateesh, M.; Lewis, R. *J. Am. Chem. Soc.* **2005**, *127*, 10045.
(19) Crudden, C.M.; McEleney, K.; MacQuarrie, S.; Blanc, A.; Sateesh, M.; Webb, J.D. *Pure Appl. Chem.* **2007**, *79*, 247.
(20) Webb, J.D.; MacQuarrie, S.; McEleney, K.; Crudden, C.M. *J. Catal.* **2007**, *252*, 97.
(21) Fleisch, T.H.; Hicks, R.F.; Bell, A.T. *J. Catal.* **1984**, *87*, 398.
(22) MacQuarrie, S.; Horton, J.H.; Barnes, J.; McEleney, K.; Loock, H.P.; Crudden, C.M. *Angew. Chem. Int. Ed.* **2008**, *47*, 3279.
(23) Yu, X.R.; Liu, F.; Wang, Z.Y.; Chen, Y. *J. Elec. Spec. Relat. Phenom.* **1990**, *50*, 159.
(24) Bensebaa, F.; Zhou, Y.; Deslandes, Y.; Kruus, E.; Ellis, T.H. *Surf. Sci.* **1998**, *405*, L472.
(25) Guittet, M.J.; Crocombette, J.P.; Gautier-Soyer, M. *Phys. Rev. B* **2001**, *63*, 125117.
(26) Zemek, J.; Jiricek, P.; Gedeon, O.; Lesiak, B.; Jozwik, A. *J. Non-Cryst. Solids* **2005**, *351*, 1665.

Chapter 5: Preparation and Characterization of BINAP Functionalized Periodic Mesoporous Organosilica

5.1 Introduction

Thus far, all of the materials discussed have had the organic group attached to the silica wall either by co-condensation or by post-synthetic grafting. While these routes incorporate organic groups into the materials, they have disadvantages. With post-synthetic grafting, inhomogeneous distribution and low overall loadings of the organic functionality are observed[1]. Additionally, as the organosilane is grafted to the surface of the material, the pore size is decreased and there is a possibility of blocking entry to the pore system. For co-condensed materials, loadings can be higher than with grafting, but increasing the organosilane component beyond 25 % of the silica content decreases long range order and can even lead to collapse of the pore structure yielding amorphous materials[1,2]. There is also a possibility of the organic functionality becoming buried in the pore wall and no longer being accessible to the exterior of the material. Moreover, due to differing rates of hydrolysis and condensation of organosilanes and inorganic silica sources or phase segregation of the different silica sources, islands of organic functionality can appear in a co-condensed material[3,4]. Alternatively, the organic group can be incorporated directly into the pore wall by preparing bridged silsesquioxanes, where the organic functionality is connected to two or more condensable silanes[5]. This was first demonstrated by the synthesis of

xerogels and aerogels of bridged polysilsesquioxanes. A number of organic bridging groups have been incorporated into these gels from rigid arylene spacers **5-8** to alkylene spacers of varying length (Figure 5.1)[6]. This molecular variety offers a range of chemical and physical properties[6]. One of the advantages of using bridged monomers over co-condensation of an organotrialkoxysilane and TEOS is that bridged monomers form gels at significantly lower concentrations[5].

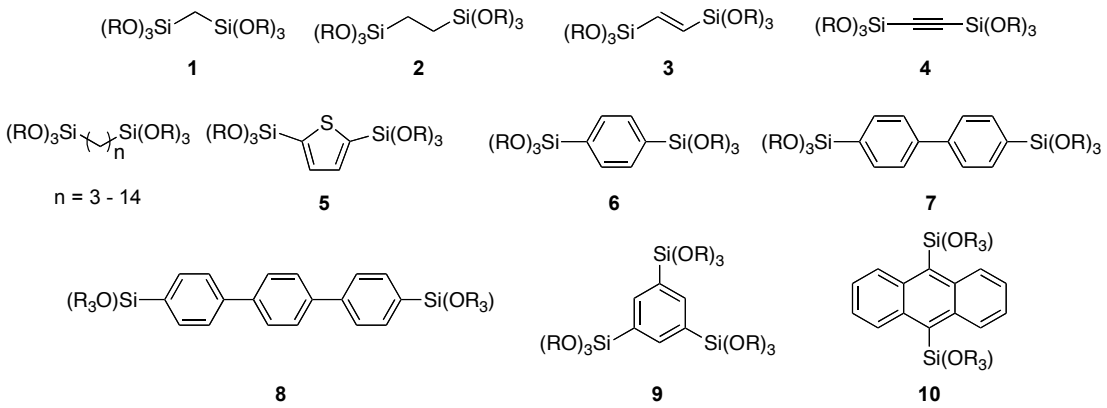

Figure 5.1: Bridged silsesquioxanes monomers for materials synthesis.

With arylene-bridged silsesquioxanes such as phenylene **6** or biphenylene **7,** the resultant materials have high surface areas with pores ranging from 10 to 50 Å[7]. For the alkylene bridged materials the gelation time and porosity were strongly dependent on the length of the alkylene bridge[6,8,9]. Under basic conditions porous gels could be obtained with alkyl lengths up to 10 carbons. However, materials prepared with longer alkyl spacers showed a collapse of porosity. Acid catalyzed condensation showed a much narrower scope in terms of monomer. In this case, the rigidity of the linker was critical to the

maintenance of porosity as the arylene bridged materials were always porous[5,8]. Furthermore, the time to obtain a gel was dependent on the length of the alkyl spacer. For the longer spacers, fast gelation times were observed. Monomers with one or two carbons had gelation times that were somewhat longer. However, three to four carbon linkers were found to have extremely long gelation times or would not gel at all. This decrease in gelation rate was attributed to the formation of five to eight membered cyclic intermediates that are slow to continue further condensation[9,10].

The porosity in these materials can be further tuned by incorporation of an organic linker that can be cleaved thermally, photochemically or chemically. For instance monomers **11** and **12** can be cleaved thermally after the formation of the polysilsesquioxane (Figure 5.2)[11]. The resulting material offers new functionality that could not be formed by direct condensation[11].

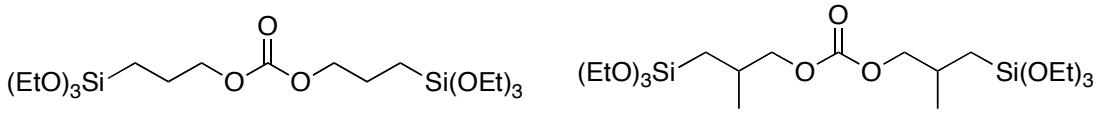

11 **12**

Figure 5.2: Cleavable bridging groups for polysilsesquioxane synthesis.

Other strategies such as using plasma to remove the organic linker can be used to create pores of different sizes[12]. Organometallic bridged polysilsesquioxanes can be generated using preformed metal complexes bearing ligands with condensable siloxanes such as those in Figure 5.3[12]. Thus, bridged silsesquioxanes are a versatile class of materials whose properties can be manipulated by changing the organic linker.

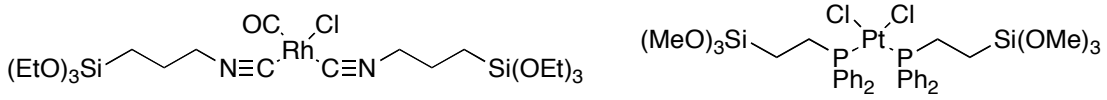

13 **14**

Figure 5.3: Organometallic bridged silsesquioxane precursors.

If monomers of this type are condensed in the presence of a surfactant template, ordered materials with narrow pore size distributions can be obtained. These materials have been named periodic mesoporous organosilicas (PMO). Unlike grafted or co-condensed mesoporous silicas, PMOs contain homogeneously distributed organic functionality in the pore wall with loadings of up to 100 % of the organic species possible. Incorporating the organic functionality into the pore wall also allows the chemical properties of the material, for instance hydrophobicity, to be tuned by modifying the organic bridge. Furthermore, the physical and mechanical properties of the material are more significantly affected by chemically changing the organic group. Finally, since they are incorporated into the walls, the organic groups do not hinder the space inside the pores.

A number of PMOs have been synthesized using the organosilane bridges illustrated in Figure 5.1. The diversity of these organic bridges allows for the modification of the material properties such as optical clarity, porosity, stability, chemical resistance, hydrophobicity, and dielectric constant[2]. The precursors can be condensed by themselves or with an inorganic silica species such as tetraethylorthosilicate (TEOS) to form PMOs with varying properties based on the amount of organic bridge used. Using this technique,

PMOs can be prepared with narrow pore size distributions depending on the organic spacer[13].

The simplest PMO is methylenesilica **1**[14]. Despite its simple structure, the material presents unique chemistry. The methylene bridge is an isoelectronic substitution for oxygen in an SiO_2 framework. However, unlike Si-O-Si which has a flexible angle that can vary from 90 to 180 °, the methylene bridge has a much more restricted angle limited to that of a tetrahedral group around 109.5 °[14]. This conformational rigidity may affect the structure-reactivity relationships in this PMO. Furthermore, the chemistry of the walls can be further altered by heat treatment. The bridging methylene unit can be converted to a terminal methyl group between 350 and 600 °C without loss of the mesostructure. This transformation increases the hydrophobicity of the material (Scheme 5.1)[15]. Utilization of this decomposition pathway may lead to materials with homogeneous distribution and high population of terminal organic groups (Si-R) in the pores while maintaining mesostructural order.

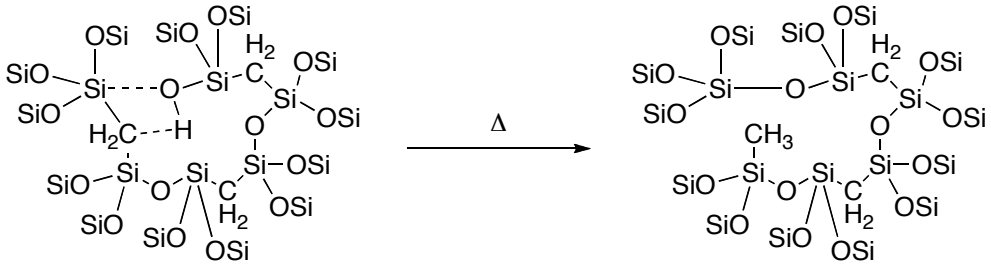

Scheme 5.1: Decomposition of a bridging methylene to give a terminal methyl group.

Both Stein and Ozin described PMOs containing ethylene bridges templated with ammonium surfactants[13,16]. Stein prepared a PMO with a worm-like pore structure while Ozin formed a two-dimensional hexagonally ordered PMO. To demonstrate that the organic groups were available for further chemistry, both groups attempted bromination of the alkene. A gas phase bromination of the material prepared by Stein's group showed that many of the ethylene bridges were accessible for functionalization and that bromination did not markedly change the porosity of the material as assessed by XRD and TEM[16]. However, solid state ^{13}C NMR demonstrated the presence of both ethylene groups as well as brominated ethyl groups, suggesting that either 18 h was not sufficiently long to brominate the alkene or that some of the alkenes were not available for functionalization[16]. Given that the bromination of MCM-41 surface-modified with grafted vinyl groups was complete in 40 min under the same conditions, the latter explanation is more likely. Ozin's group attempted bromination of their material in refluxing dichloromethane. After eight days of treatment, CP MAS ^{13}C NMR demonstrated that all of the alkene groups had been consumed without structural changes in the adsorption analysis. However, chemical analysis indicated that only 10 % bromine incorporation occurred with the rest of the ethylene groups postulated to have reacted with the solvent to form ethyl bridges[13]. Both of these studies indicate that further modification of the organic moiety is possible after incorporation into a PMO suggesting that

these materials are amenable to be used as heterogeneous supports for further chemistry.

Phenyl and biphenyl linkers (**6** and **7**) are of interest due to the ability to functionalize the walls using aromatic chemistry and the possibility of π-π stacking between the aromatic groups leading to crystallinity in the pore walls. Molecular order in the wall enhances the materials applications in electronic, optical and sensing fields[2]. Ozin *et al.* first reported a PMO prepared from phenylene disiloxane (**6**). Significant carbon silicon bond cleavage was observed under basic conditions and even in acidic conditions some carbon silicon bond cleavage was observed. An optimized procedure under mildly acidic conditions with a pyridinium-based surfactant minimized the amount of Si-C bond cleavage[17]. However, XRD showed only 2D hexagonal mesoscopic ordering with no orientational order of the phenyl groups in the wall. Sayari was also able to generate a phenyl bridged PMO using Brij surfactants in acidic media[18]. From TEM images he infers that partial ordering is present in the walls although there were no peaks observed in the XRD for order in the walls[18]. Inagaki's group published the first report of a PMO with crystal-like pore walls. Utilizing phenyl bridged monomer **6** with alkyl ammonium surfactants under basic conditions, the Inagaki group was able to prepare materials with crystallinity in the wall observed via powder XRD, which showed sharp peaks with a periodicity of 7.6 Å in addition to the peaks attributed to the 2D hexagonal mesoscopic order (Figure 5.4).

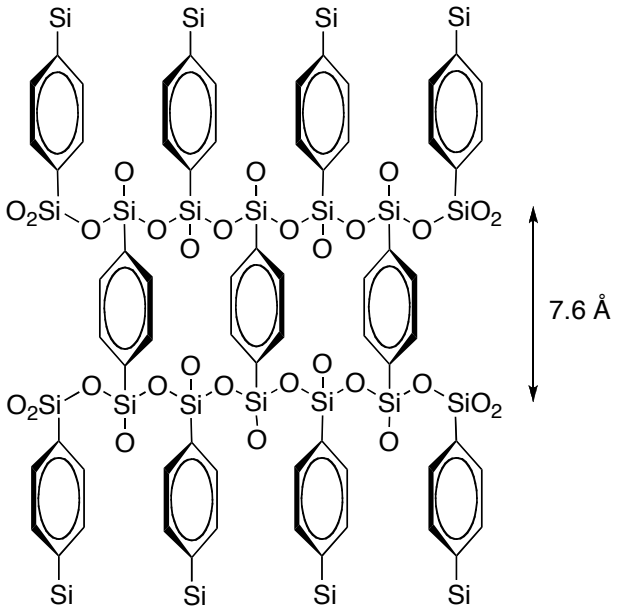

Figure 5.4: Diagrammatic representation of phenylene PMO with crystallinity in the pore wall.

The observed order was attributed to a lamellar wall structure alternating between silicon oxide and phenyl layers. A π-π stacking interaction between adjacent benzene units was invoked to explain the lamellar structure of the wall, although sharp peaks demonstrating order within the organic groups were not observed[19]. Furthermore, Inagaki was able to functionalize the benzene walls by electrophilic aromatic substitution incorporating a sulfonic acid group resulting in a solid phase acid catalyst[19]. In the acid catalyzed esterification of acetic acid with ethanol, the sulfonic acid-functionalized PMO performed better than the commercially available solid phase acid Nafion-H[20].

The Inagaki group later published the synthesis of a PMO based on **7**. Again XRD peaks with a periodicity of 11.6 Å were observed in addition to the peaks attributed to mesoscopic order (Figure 5.5).

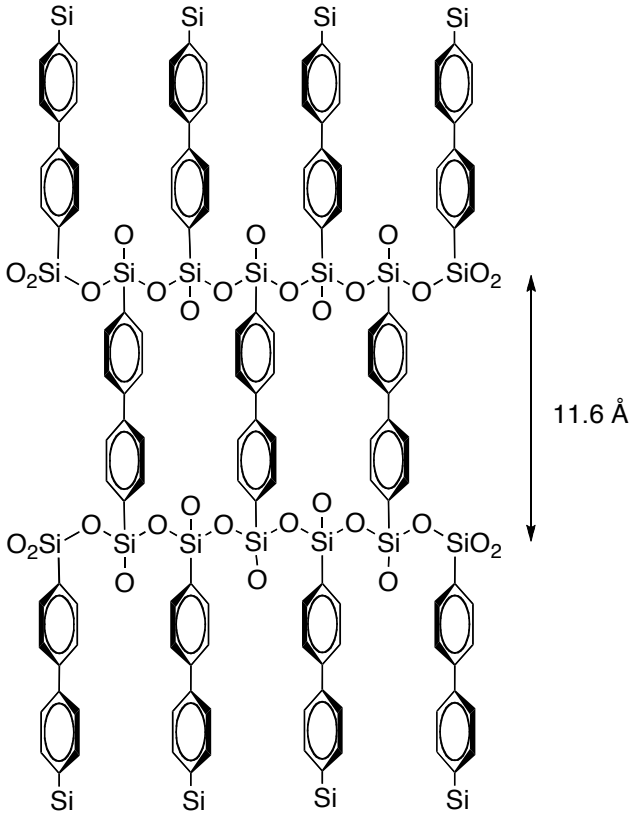

Figure 5.5: Diagrammatic representation of biphenylene PMO with crystallinity in the pore wall.

This increase in spacing relative to the phenyl bridged PMO arises from the longer biphenyl bridge[21]. Additionally, sulfonic acid groups could be incorporated into these PMOs by co-condensation of MPTMS with **7**. Upon oxidation of the thiols, this material provides a highly hydrophobic mesoporous solid with crystalline walls and acid functionalities inside the pore voids[22].

The organic linkers already discussed and shown in Figure 5.1 are all fairly rigid structures. PMOs with larger and more flexible linkers have been prepared, for instance the linkers illustrated in Figure 5.6. Unfortunately, these linkers do not self assemble into well ordered structures and a co-silica

source, often TEOS, is required to generate highly ordered materials. A similar phenomenon has been observed with xerogels composed of alkylene polysilsesquioxanes[5]. As the chain length of the alkylene bridge increases a collapse of porosity is observed. This collapse is possibly due to the larger distance between cross-linking silicon groups or the organic bridges forming microstructural domains in the gel as previously noted[5]. Dilution with TEOS is problematic in that it lowers the concentration of functional sites, it also introduces the possibility of phase segregation between the organosilica and co-silica source with potential inaccessibility of the organic functionality.

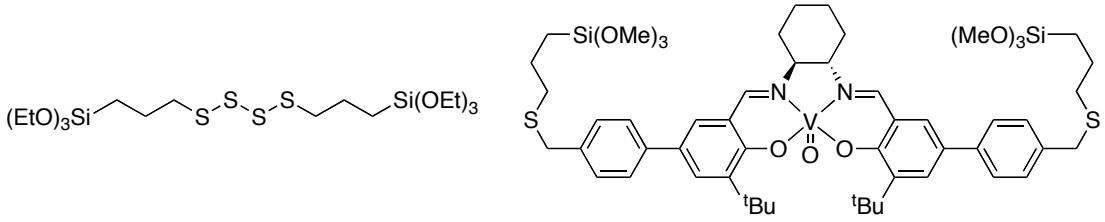

15 **16**

Figure 5.6: Non-rigid PMO precursors.

Despite these drawbacks PMOs from these linkers have been utilized for practical applications. A PMO with 15 % of the tetrasulfide **15** was shown to be highly effective and selective for removal of Hg^{2+} ions in the presence of other divalent cations (Pb^{2+}, Cd^{2+}, Zn^{2+} and Cu^{2+}). This PMO has a mercury capacity of close to 3 g of mercury per gram of PMO[23]. Additionally, the vanadium oxide PMO was capable of catalyzing the enantioselective cyanosilation of benzaldehyde with enantiomeric excess of 30 %[24]. However, the ee rises to 63 % when catalyst **16** is grafted onto the pore walls. This loss

of enantioselectivity likely arises from detrimental steric interactions when the catalyst is in the pore wall.

Materials prepared from **16** are also of interest because they are the first examples of chiral PMOs. Subsequently, other chiral monomers have been prepared and used to form chiral PMOs (Figure 5.7). Garcia's group prepared PMOs from monomers **17**, **18** and **19** as mixtures with TEOS in a maximum organosilane loading of 15 %. Increasing the loading beyond 15 % led to decreases in order.

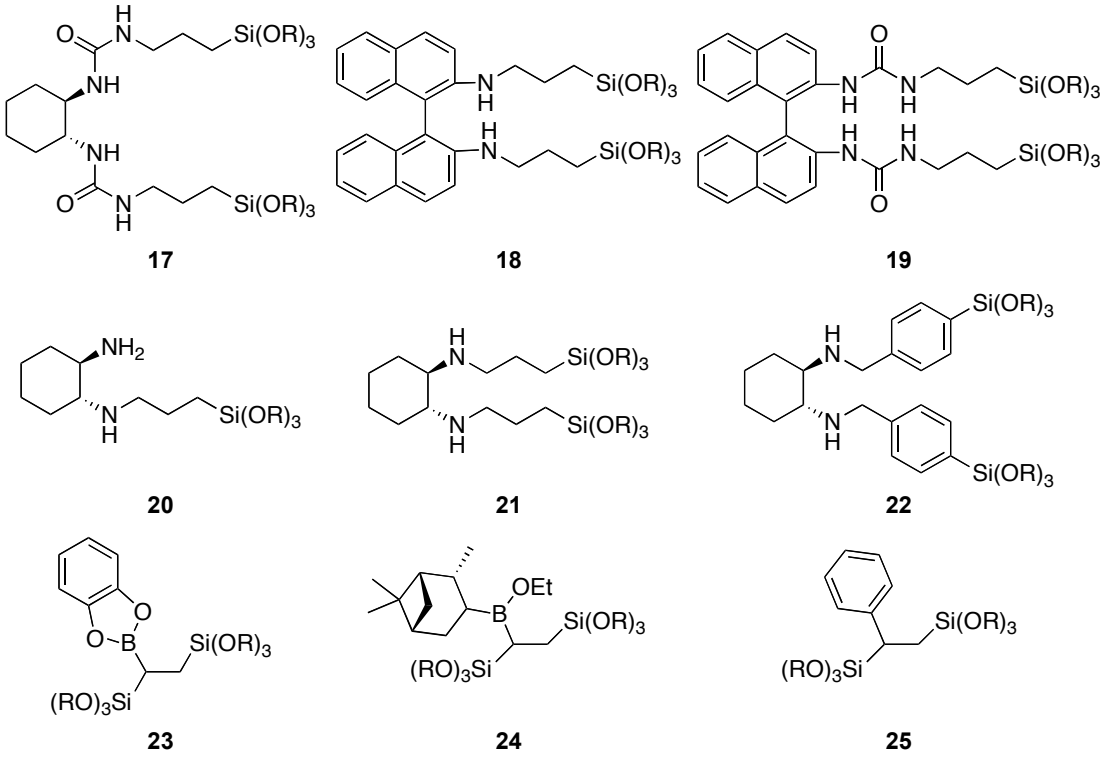

Figure 5.7: Chiral PMO precursors.

Garcia's group was examined the chirality of their materials using suspension optical rotation and enantioselective fluorescence[25]. They later demonstrated that the material incorporating **17** could be used as a host for the

photochemical rearrangement of **26** (Scheme 5.2). The reaction gave 11 % conversion with 24 % ee, these values were higher than the other zeolites/entrapped chiral molecule combinations tested[26].

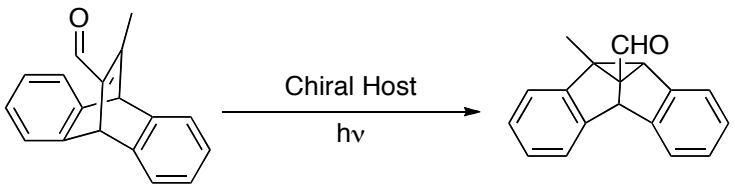

26 **27**

Scheme 5.2: Photocatalyzed di-π-methane isomerization.

Li and coworkers utilized the chiral diamine moiety (**20**, **21** and **22**) as the basis of their PMOs. The monomers were co-condensed with either **2** or tetramethylorthosilicate (TMOS) at up to 30 % loading of the chiral monomer. After the surfactant was removed, the materials could be loaded with $[Rh(cod)Cl]_2$ and were catalytically active for the asymmetric transfer hydrogenation of acetophenone with conversions of up to 97 % and up to 30 % ee[27,28].

In a similar system, Moreau's group employed **20** and **21**, again loaded with rhodium for transfer hydrogenation. In their system, they were able to achieve ee's of up to 98 %[29]. However, co-condensation with five equivalents of TEOS was required to obtain highly ordered materials. Recently, Polarz's and Ozin's groups have published the synthesis of chiral PMOs based on hydroborated versions of ethylene silica **3**. Polarz's work utilized a rhodium catalyzed asymmetric hydroboration with catecolborane to prepare monomer **23**. Subsequent condensation under basic conditions with an alkyl ammonium

surfactant led to a chiral PMO without the need for a co-silica source. Chirality in the resulting material was detected by solid state circular dichroism[30]. However, the asymmetric hydroboration of non-styrenic olefins generally occurs with low enantioselectivity, and since no method was employed to determine the magnitude of the chirality transfer in the initial hydroboration reaction, it is likely that the level of enantiopurity of the monomer was low.

Ozin employed a chiral borane to affect an asymmetric hydroboration of **3**. Treatment of the resulting borane with ethanol led to monomer **24**. Incorporation into a PMO using an acid promoted hydrolysis route afforded a chiral material. However, doping TEOS into the material was required to generate ordered, mesoporous materials since materials synthesized without any TEOS were mostly microporous and had low surface area**.** Boron could be removed from the material by aminolysis leading to chiral amino functionalized materials. ^{11}B solid state NMR shows some residual boron even after aminolysis indicating that some of the functional groups are buried in the pore walls[31].

Inagaki's group prepared PMOs with chiral monomer **25**. Under acidic conditions with a cationic surfactant, a microporous material with high surface area was obtained. Digestion of the silica network with HF and recovery of the organic linker demonstrated that no racemization occurred during synthesis. However, the only conditions employed that led to mesoporous materials, namely basic conditions and 60-80% of **6**, resulted in complete racemization of **25**[32].

All of the chiral monomers used thus far to synthesize PMOs have long alkyl chains and there is some evidence that the chiral organic group sits inside the pore void and is not incorporated into the walls[27,28]. In many ways these chiral PMOs function like co-condensed silicaceous materials in that the organic loading is limited[2].

Besides using a chiral monomer, other routes, such as grafting of chiral species to pre-formed ordered silicas or using chiral surfactant templates, have been utilized to generate chiral ordered silicas[33-38]. Perhaps the simplest way to prepare a chiral silica is to start with a chiral template (Figure 5.8).

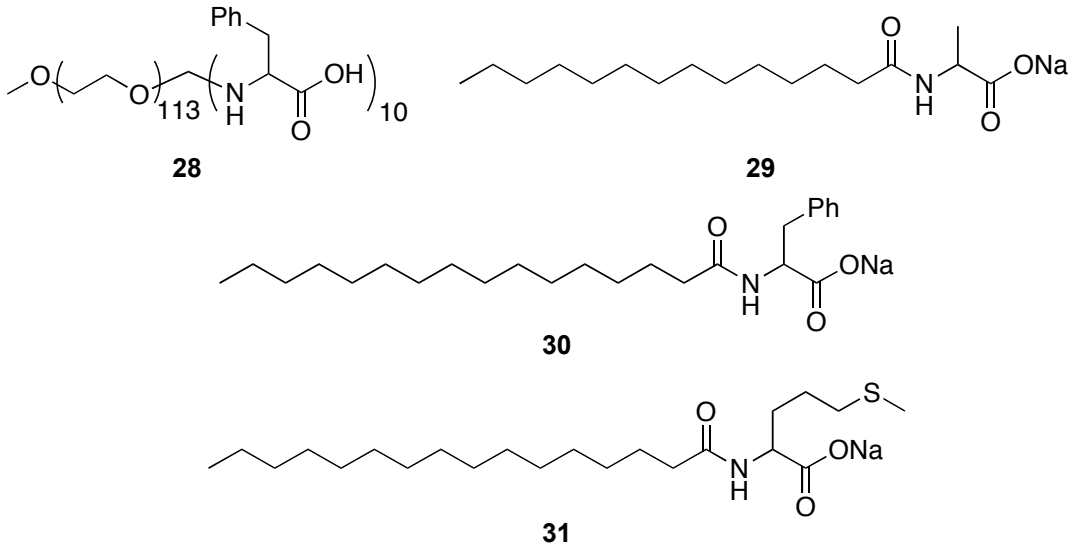

Figure 5.8: Chiral surfactants used in the synthesis of chiral silicas.

Mastai's group prepared a chiral silica-based material utilizing chiral block co-polymer surfactant **28** under acidic conditions[33]. This afforded 2D hexagonally ordered mesoporous materials with pore sizes of 50 Å. After extraction, the chiral silica was then used to selectively adsorb one

enantiomer of amino acids, valine and alanine[33]. Using D-phenylalanine as the amino acid block of the surfactant, the D enantiomer of the amino acid was preferentially adsorbed relative to the L enantiomer, although absorption of the L enantiomer also occurred to some extent. The authors attributed the adsorption of the L enantiomer to surface interactions with non-chiral sites. Using racemic amino acids as the adsorbents, solutions with enantiomeric excesses of up to 40 % could be obtained. However, in order to achieve this level of enantiopurity, 16 h of exposure to the material was required, which is too slow to be considered viable for chiral separations[33].

Che's group has also studied materials with chiral pores using amino acid based surfactants[34]. However, instead of block co-polymer surfactants, they employed N-acyl amino acid surfactant **29** in the presence of a co-structure directing agent, APTES or N-trimethoxysilylpropyl-N,N,N-trimethyl ammonium chloride (TMAPS). In the presence of TEOS under slightly acidic conditions, the group was able to prepare materials with 2D hexagonally ordered helically twisted pores (Figure 5.9).

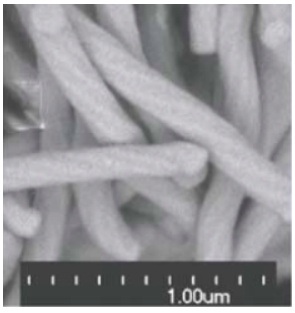

Figure 5.9: SEM image of material prepared with surfactant **29**. Reproduced from reference 34.

The co-structure directing agent, a positively charged ammonium group, was essential in order to interact with the negatively charged surfactant. The helical twist could be observed by SEM or TEM and a pitch length of ~1.5 μm could be calculated by measuring the distances between fringes on the TEM[34]. The enantiomeric purity of the material was determined by counting the number of particles with helical twists occurring in the same direction in SEM images. This procedure gives 30 – 50 % ee in favour of left handed helices using L-alanine and the opposite with D-alanine[35]. By screening different amino acid-containing surfactants, it was found that enantiomeric purity of greater than 90 % could be obtained employing surfactants **30** and **31**, with lower ee's being obtained with other amino acid headgroups[36]. Conformational analysis of the surfactant demonstrated that the helical twist was introduced from a propeller like packing of the surfactant. The lack of complete enantioselectivity was attributed to diasteromeric rotamers about the N-C_α bond with the less favoured rotamer leading to erosion of the enantioselectivity (Figure 5.10)[36].

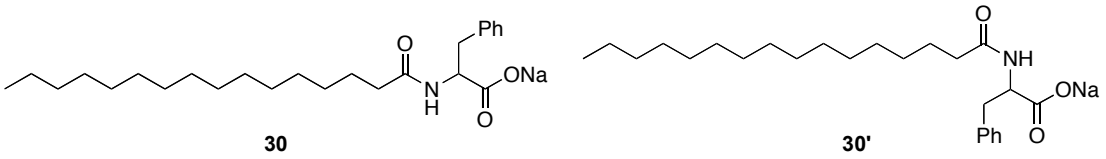

30 **30'**

Figure 5.10: Diastereomeric rotamers of anionic amino acid based surfactants.

Interestingly, it was found that when the synthesis temperature was decreased to 0 °C, a helical ribbon containing a disordered pore structure was obtained instead of helically twisted rods. At this temperature, the helix of the

ribbon was dependent on the chirality of the surfactant with D-amino acid head groups giving rise to ribbons with left twists and L-amino acids gave right handed twisted ribbons[37].

Fascinatingly, Tatsumi's group was able to prepare helical silicas without employing any chiral precursors[38]. Utilizing a mixed surfactant system of a fluorinated surfactant FC-4911 [$CF_3(CF_2)_3SO_2NH(CH_2)_3N^+(CH_3)_3I^-$] and CTAB with **3** or **6** as silica sources, they were able to produce silica-based materials with helical or spiral morphologies. Because no chirality was introduced into the system, an equal number left handed and right handed forms were observed (Figure 5.11).

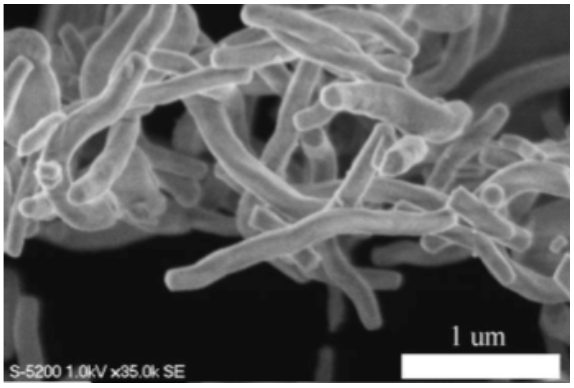

Figure 5.11: SEM image of material prepared by Tatsumi *et al.* Reproduced from reference 38.

The formation of the helices is postulated to arise from a reduction of surface free energy in the surfactant micelles, which results in a twisted structure. Unfortunately, this system is limited to PMO monomers, when TEOS was used as a silica source only amorphous materials were formed[38]. However, this work illustrates the important point that helical structures can be formed

without the presence of any chiral additives, although the resulting material is racemic.

Research in the Crudden group has focused on biphenyl-type PMOs[39]. Although biphenyl is chiral in the ground state due to breaking of the symmetry in the most stable conformer, this chirality is not "useful" since achiral conformations are easily accessed, and the two enantiomeric forms interconvert readily[40]. However, if biphenyl is substituted in the 2,2' and 6,6' positions with groups that are large enough to prevent racemization by rotation around the central bond, the two enantiomers can be separated (Figure 5.12).

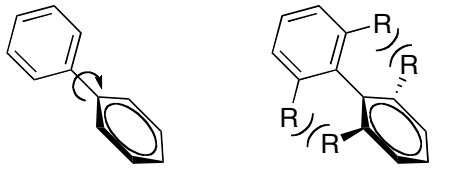

Free Rotation Restricted Rotation

Figure 5.12: Restricted rotation with a 2,2'-6,6' substituted biphenyl

In the first study, chiral biphenyl monomer **32** was employed for chiral PMO synthesis (Figure 5.13)[41]. In this substrate, relatively small groups are employed on the axis of chirality in order to minimize the lateral bulk of the monomer. Chiral PMO materials were then prepared using chiral monomer **32** as a dopant in varying amounts with **7** as the main constituent. The best materials were obtained using Brij 76 surfactant in the presence of acid catalyst, which afforded 2D hexagonally ordered materials with no evidence of carbon silicon bond cleavage[30].

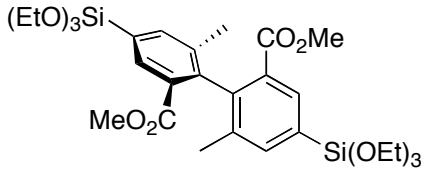

32

Figure 5.13: Chiral biphenyl monomer for PMO synthesis.

Chirality in these materials was assessed using solid state circular dichroism. Mirror image CD spectra were obtained using opposite enantiomers of **32**, as expected. Interestingly, the λ_{max} of the CD spectrum appeared at 315 nm in materials prepared with biphenyl **7** as the bulk constituent (Figure 5.14), and at 260 nm when the PMO was prepared with TEOS in place of **7**. Additionally, in PMOs prepared with 100 % **32**, the peak at 315 nm was again absent. This suggests that the signal at 315 nm results from interactions between **32** and **7** in the material which lead to new chiral aggregate species in the material, a proposal that was confirmed using DFT calculations[39].

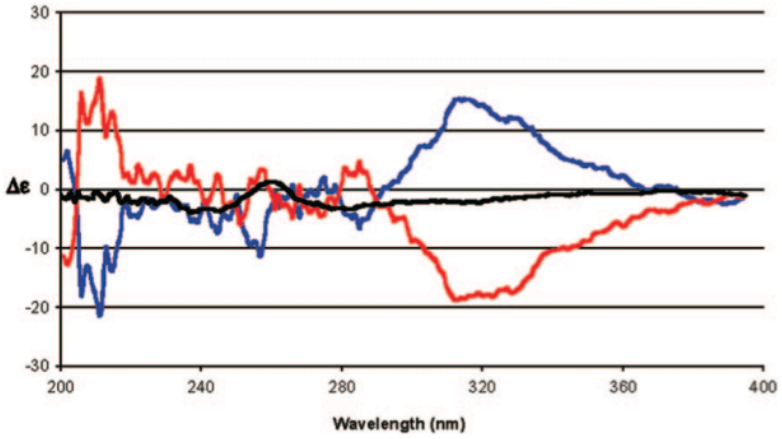

Figure 5.14: Circular dichroism spectra of PMOs prepared with P or M **26** (blue and red) with biphenyl as a co-silica source and SiO_2 (black). Reproduced from reference 39.

After demonstrating the effectiveness of this strategy at preparing chiral PMO materials, the next step was to prepare a *functional* chiral PMO. Chiral ligands are an obvious choice since heterogenization of a metal catalyst offers advantages in separation of the metal species after the reaction. Additionally, we can easily assess the effect of the chiral environment (organic or inorganic, grafted or co-condensed) on the chiral ligand. Two commonly employed chiral ligands are 1,1'-binaphthyl-2,2'-diol (BINOL) and 2,2'-bis(diphenylphosphino)-1,1'-binaphthyl (BINAP)[42,43]. Therefore, we set forth to prepare siloxy functionalized versions of these monomers.

Chan and coworkers have prepared a number of polymeric BINOL materials for catalysis[44]. A polystyrene supported variant **33** (Figure 5.15) was loaded with $Ti(O^iPr)_4$ and utilized as a catalyst for the asymmetric addition of diethyl zinc to aldehydes. At loadings of 20 mol %, the catalyst gives high ee's (>90 %) for a number of aldehydes[44,45]. However, when the catalyst loading is decreased the ee declines rapidly with only 15 % ee attained at 5 mol % loading[44]. Further materials were prepared by forming imine bridged polymers of BINOL and p-functionalized benzene **34** or BINAP **35** (Figure 5.15)[46,47]. In both cases, the BINOL ligand was functionalized with titanium with similar results to the polystyrene supported BINOL for asymmetric addition of diethyl zinc to aldehydes. However, in the bifunctional material the BINAP could be coordinated to ruthenium. The resulting material was utilized for the

asymmetric hydrogenation of alkenes. Activity and enantioselectivity of the polymeric catalyst were similar to the homogeneous catalyst[47].

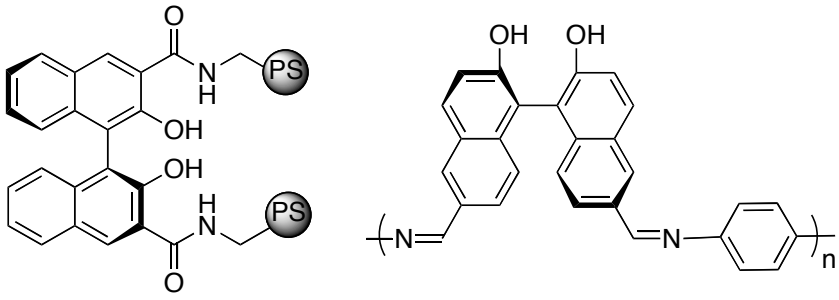

33

34

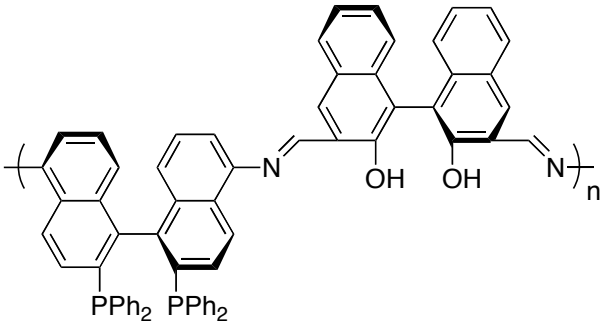

35

Figure 5.15: Polymeric BINOL and BINAP ligands developed by Chan *et al.*

Pu's group has also developed polymeric BINOL materials (Figure 5.16)[48-50]. The polymeric BINOL could be loaded with lanthanum or ytterbium and used as catalysts for asymmetric epoxidation of α,β-unsaturated ketones. While the catalysts were highly active, the enantioselectivity was moderate with a maximum of 73 % ee. The complex could be isolated and reused. However, enantioselectivity decreased upon reuse[49].

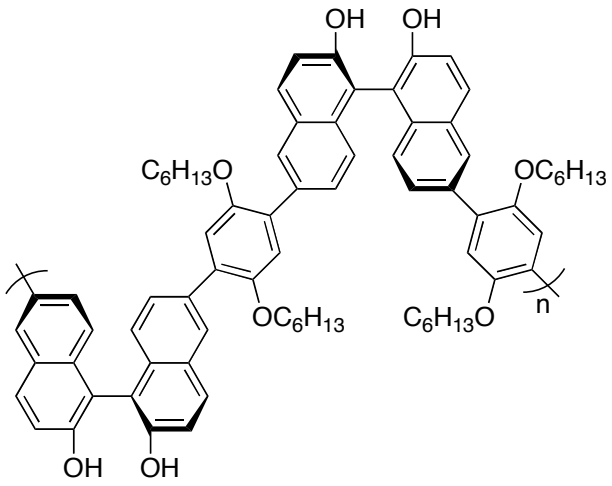

36

Figure 5.16: Polymeric BINOL ligand for asymmetric epoxidation of α,β-unsaturated ketones.

Additionally, Pu's group prepared a BINOL-BINAP copolymer for tandem asymmetric catalysis[50]. The BINAP was functionalized with a ruthenium diamine (Figure 5.17).

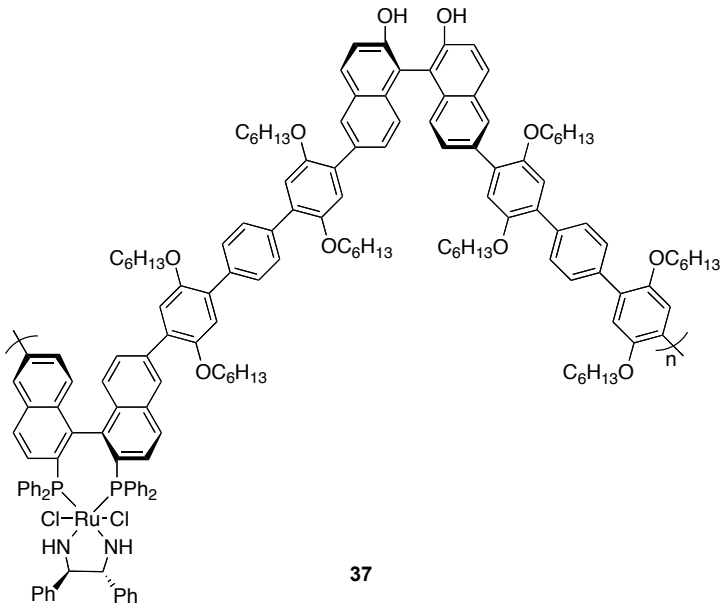

37

Figure 5.17: Bifunctional BINOL-BINAP polymer.

The catalyst was then used for the asymmetric addition of diethyl zinc to aldehydes and transfer hydrogenation of ketones with molecule **38** (Figure 5.18). Both enantioselectivity and diastereoselectivity were high in this system, although considerable optimization of the spacer between the BINOL and BINAP units was required[50].

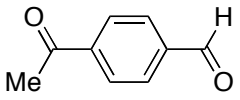

38

Figure 5.18: Substrate for tandem diethyl zinc addition/transfer hydrogenation.

In addition to the previous examples, there are a number of reports where BINOL and BINAP have been immobilized on polymers[51-55]. However, there are relatively few reports of these ligands immobilized on silica. Moreau's group prepared a non-surfactant templated BINOL-containing silica using monomers **39** and **40** (Figure 5.19) co-condensed with TMOS. They did not perform any asymmetric reactions but report that some of the silicas prepared displayed interesting optical properties for applications as fluorescent chemosensors[56]. Later Hesemann and Moreau immobilized BINOL by converting the free alcohols into polymerizable groups as shown in **41** (Figure 5.19). They then prepared xerogels by co-condensing **41** with TEOS and loaded the resulting materials with rhodium. When used for the asymmetric hydrogenation of acetophenone, the xerogels gave 32 % ee with 94 % conversion. This was a marked improvement from the homogeneous

version which gave 13 % conversion and 7 % ee under the same conditions[57].

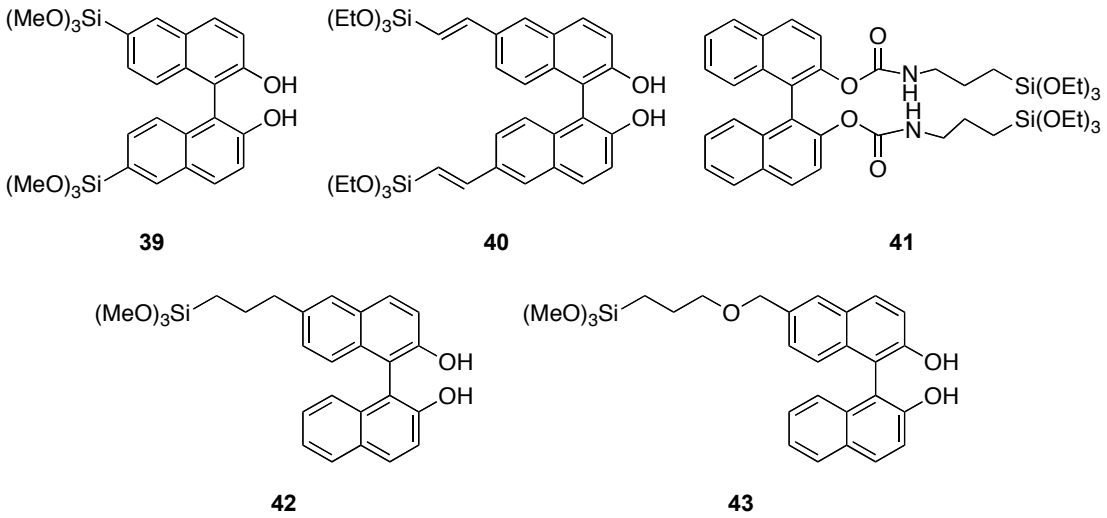

Figure 5.19: Silica immobilized BINOL ligands.

Abdi's group loaded BINOL onto amorphous silica and MCM-41 using monomer **42** (Figure 5.19), which still retained its free hydroxyl groups. The BINOL was loaded with lanthanum and used as a chiral catalyst for the asymmetric Henry reaction of aldehydes and nitroalkanes. The catalyst proved to be fairly active with yields between 56 and 84 % and ee's of 75 to 86 %, comparable to the homogeneous reaction. However, the immobilized catalysts did take almost twice as long to promote the reaction. The MCM-41 based catalyst was recyclable up to four times but the activity decreased with each recycle[58]. Liu and Li's groups prepared a SBA-15-based BINOL material using monomer **43** (Figure 5.19). The BINOL was functionalized with titanium for the asymmetric allylation of aldehydes. Yields of up to 99 % and ee's

between 93 and 99 % were obtained and the catalyst was recyclable up to five times with slight losses in yield and enantioselectivity[59].

The first attempts to immobilize BINAP on silica was through non-covalent attachment and entrapment[60,61]. Dickson and co workers immobilized ruthenium-BINAP complexes on mesoporous silicas through simple adsorption. The catalysts were active for the hydrogenation of dehydroamino acids but had poor enantioselectivities (highest was 51 % ee) and rapidly lost activity upon recycling[60]. Avnir's group entrapped ruthenium-BINAP complexes in silica xerogels by condensing TMOS around the complex. Similar to Dickson's work the catalysts afforded moderate enantioselectivities and lost catalytic activity upon recycling[61]. These catalysts suffered from rapid loss of activity as the metal complex was able to leave the silica[60]. Bianchini and co workers utilized hydrogen bonding and ion pairing to immobilize a rhodium BINAP complex on amorphous silica (Figure 5.20)[62].

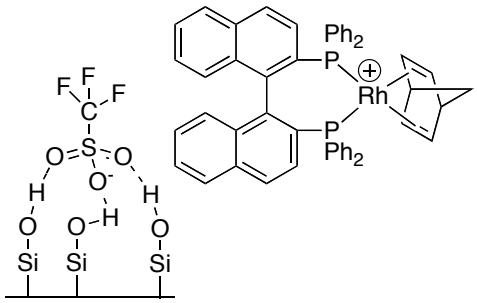

Figure 5.20: Immobilized BINAP-rhodium complex employed by Bianchini *et al.*

The immobilized catalyst demonstrated comparable activity and enantioselectivity to the homogeneous analog in asymmetric hydrogenation of dehydroamino acids. Furthermore, no loss of activity, enantioselectivity or

leaching (detection limit 1 ppm) was observed over three reuses of the catalyst[62]. Kesanli and Lin reported the first covalent immobilization of BINAP on silica using monomer **44** (Figure 5.21). Using SBA-15 as a support, they grafted ligand **44** onto the surface prior to loading of ruthenium. Hydrogenation of various β-ketoesters with the solid catalyst yielded quantitative conversions with ee's between 72 and 95 %. The catalyst was recyclable, however the conversion and ee were eroded after the second cycle. The authors attribute the loss of activity to air sensitivity of the ruthenium hydride[63]. In a further study, van Koten's group prepared a bis-silylated BINAP monomer **45** (Figure 5.21). This was grafted on amorphous silica and loaded with ruthenium or rhodium.

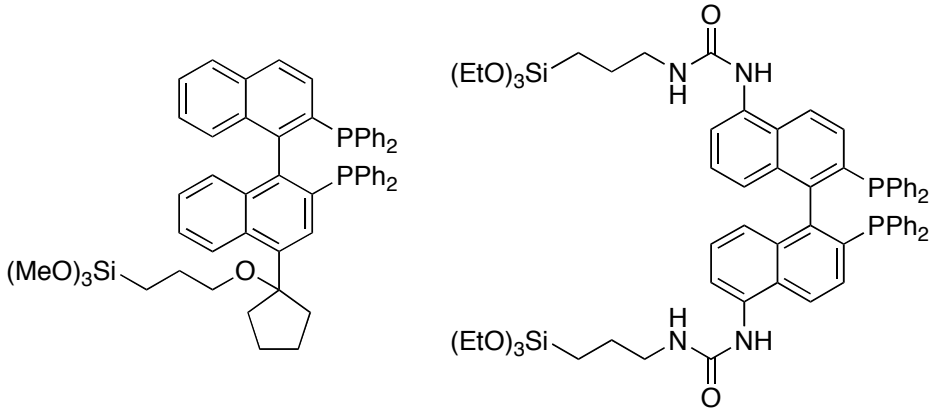

44 **45**

Figure 5.7: Silica immobilized BINAP ligands.

Using **45** with rhodium, the asymmetric hydrogenation of dehydroamino acids was performed with quantitative conversion and up to 85 % ee. Two ruthenium variants were prepared, one for the asymmetric hydrogenation of

β-ketoesters yielding quantitative conversion with > 99 % ee. The other ruthenium catalyst, with a chiral diamine ligand, was used for the asymmetric hydrogenation of prochiral ketones. This system was able to achieve 95 % ee for naphthylacetophenone. The ruthenium material was recyclable up to 5 cycles without loss of activity or ee but the rhodium system decomposed after the first reaction[64].

BINOL and BINAP have been incorporated into silica based materials and after loading with metals the complexes have comparable activities and enantioselectivities to the homogeneous analogues. However, using non-covalent interactions for immobilization, the catalysts suffer from leaching of the metal complexes into the solution. Furthermore, incorporation by grafting can cause reduced pore diameters due to the size of these complexes, which can inhibit diffusion of reactants and products into and away from the catalyst. Incorporating the ligand directly into the wall should limit the leaching as well as maintain good pore sizes.

5.2 Results and Discussion

We began by looking at the synthesis of a PMO precursor based on BINOL. The proposed synthesis of the silicate is shown in scheme 5.3. Starting with 1-amino naphthalene **46**, bromination in acetic acid was performed to install bromine at the 2 and 4 positions. The bromonaphthylamine was diazotized with sodium nitrite and the 2-bromo

substituent replaced with oxygen in the second reaction to give oxadiazole **48**. The diazonium group was reduced with sodium borohydride to produce 4-bromonaphthol **49**, which was then homocoupled in a copper catalyzed oxidative coupling to afford 4,4'-dibromobinaphthol **50**. Any protection of the alcohol prior to the coupling step resulted in no coupling and recovery of starting material. Thus the protecting groups were installed after the binaphthol coupling but prior to installation of the silicon moiety. Both the methoxymethyl (MOM) and methoxy groups were utilized as protecting groups for the alcohol.

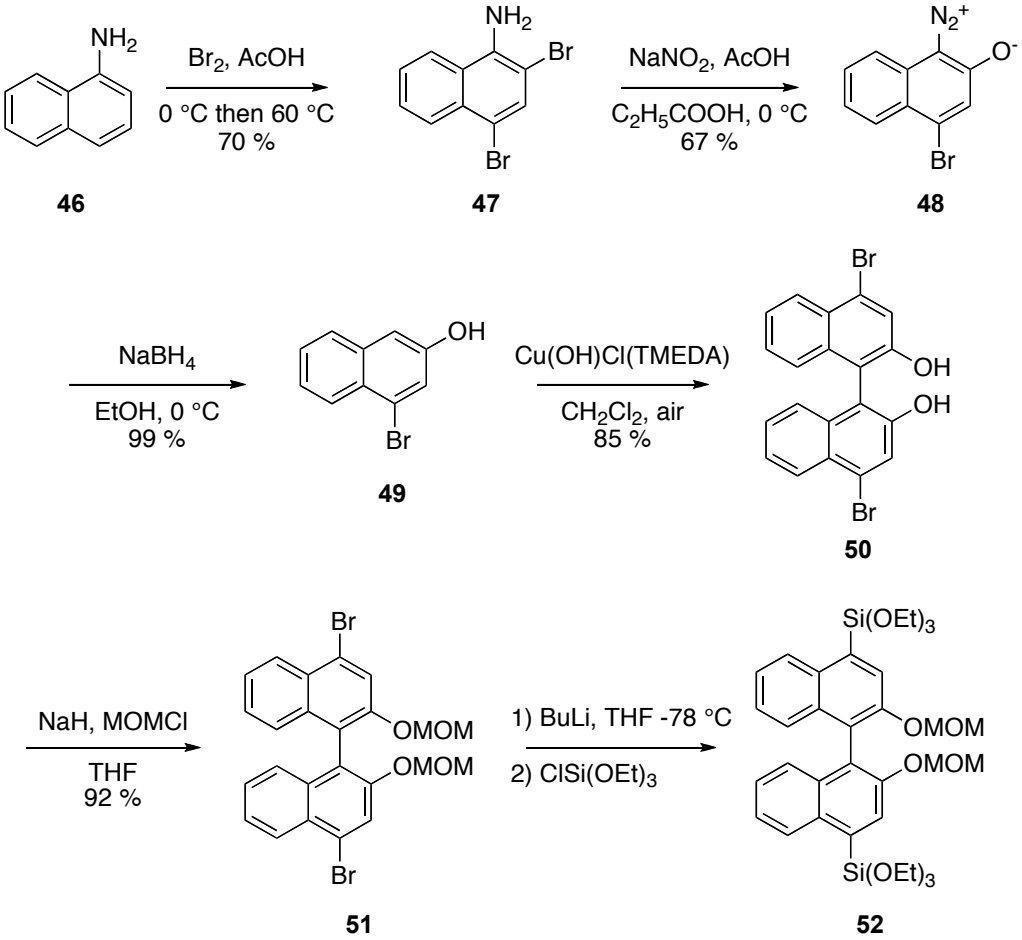

Scheme 5.3: A proposed synthesis of BINOL based bis-silyl monomer.

Starting with the methoxymethyl protected dibromo BINOL, the first attempt at installation of silicon was to perform a nucleophilic substitution on 3-iodopropyl trimethoxysilane, (Equation 5.1) which would place a tether between the rigid BINOL bridge and the silicon dioxide network.

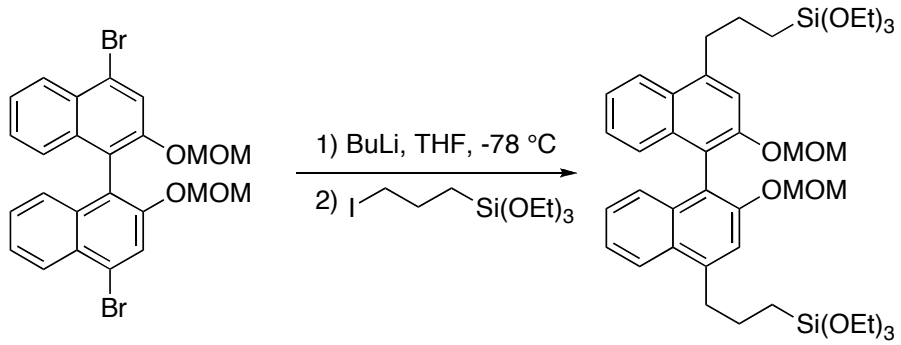

51 **53** (Eq. 5.1)

Lithium-halogen exchange of the dibromo BINOL with n-butyl lithium at -78 °C should generate a dilithio aryl species, followed by addition of the silane electrophile. The substitution did not occur successfully; it appears there may have been some difficulty generating the dianion in this case. However, rigidity of the organic monomer is thought to impart greater order upon the final mesoporous silicate so we decided to remove the alkyl linker between the silicon and BINOL. Chloro triethoxysilane was selected as a suitable electrophile to install the requisite alkoxy silicon groups in the monomer. Our first approach was to generate the lithiated anion by lithium halogen exchange at low temperature followed by a quench with the chlorosilane and warming to room temperature. The NMR spectra of the crude product resulting from this sequence contained seven different methyl peaks from the methoxymethyl protecting group as well as increased multiplicity at the methylene signal of

the methoxymethyl group with no less than five spots by thin layer chromatography. Since the methoxymethyl group is a weak directing group for metallation chemistry, it is possible that deprotonation is occurring at the 3 position of the BINOL or at the methylene group of the MOM unit. To avoid organolithium species, we decided to try forming a bis-Grignard-reagent as shown in Equation 5.2. This also failed to install the silicon moiety and loss of the methoxymethyl group was observed in the crude NMR.

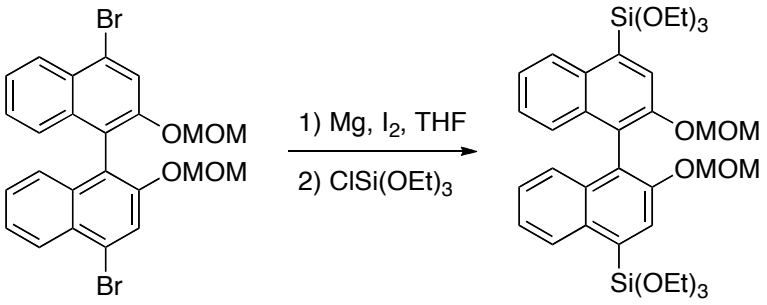

51 **52** (Eq. 5.2)

Taking advantage of the potential ability of methoxymethyl to direct ortho metalation, an attempt was made to functionalize 2,2'-bis(methoxymethyloxy)binaphthyl directly using butyl lithium and chloro triethoxysilane (Equation 5.3).

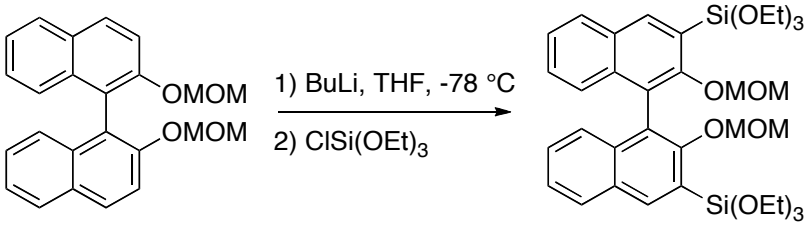

53 **54** (Eq. 5.3)

Ultimately the conversion was unsuccessful, with multiple ethoxy, and methoxymethyl species appearing in the crude NMR and an unresolvable streak by TLC. This reaction most likely resulted a combination of partially

deprotected and mono- and bis- silylated products accounting for all of the extra species in the NMR.

Since the methoxymethyl group appeared to cause more problems than it solved, the protecting group was changed to methyl. Introduction of the methyl group was facile involving refluxing the binaphthol in acetone with potassium carbonate and methyl iodide (Equation 5.4). This resulted in high yields of the methyl protected binaphthol (83 %). To install the alkoxy silicon group the dianion was generated by lithium halogen exchange using n-butyl lithium at -88 °C.

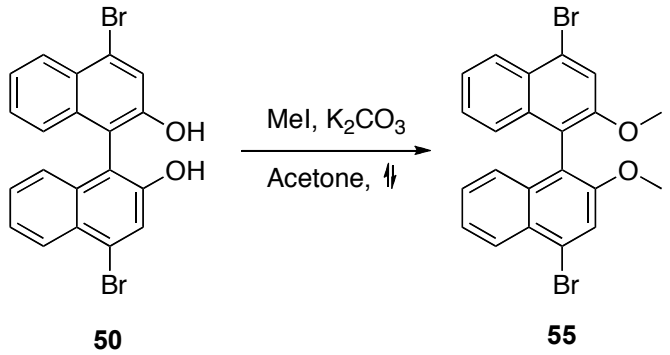

50 **55** (Eq. 5.4)

The dilithiated species was then quenched with chloro triethoxysilane while cold (Equation 5.5). A poor yield of 13 % of the bis-silylated product was obtained in one reaction however, this proved difficult to reproduce. Even after column purification, the ^{1}H NMR often contained multiple ethoxy-containing species. These contaminants likely result from derivatives of the chloro triethoxysilane and monosilylation products co-eluting with the bis-silylated product **45**. Increasing the amount of butyl lithium from 2.2 eq to 3 eq

or increasing the chloro triethoxysilane from 2.2 eq to 4 eq did not improve the yield of the reaction.

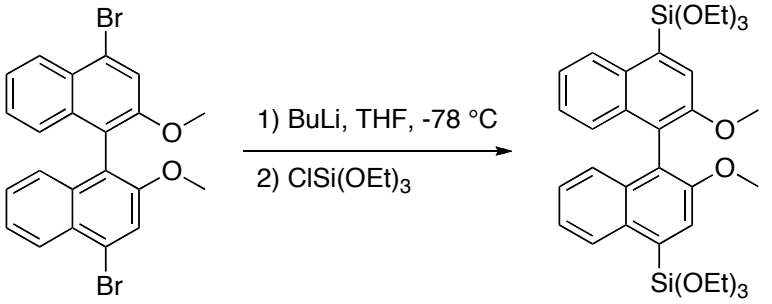

55 **56** (Eq. 5.5)

As we were seeing reproducibility problems with the anion generation and quench chemistry we investigated silylation chemistry using p-bromoanisole **57** as a model for our BINOL material (Equation 5.6). In this case, we generated the anion with n-butyl lithium varying the amount from 1.15 eq to 3 eq. The electrophile was again chloro triethoxysilane varying the amounts from 1.15 eq to 4 eq.

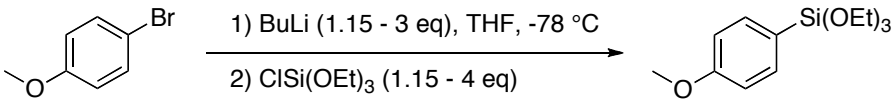

57 **58** (Eq. 5.6)

Using lower amounts of base and electrophile, the silylated anisole **58** could be generated relatively cleanly, only the remnants of the excess chloro triethoxysilane were observed in the crude ^{1}H NMR. However, in the mass spectrum, higher mass products are observed suggesting that some oligomerization is occurring during the reaction. Increasing the amount of

base or electrophile leads to increased generation of side products as the NMR in both the aromatic region and the ethoxy region increases in complexity.

Since it was particularly difficult to reproducibly carry out the lithium halogen exchange/silicon quench with bifunctional monomers, we turned our attention to other methods of attaching silicon to aromatic groups. For instance, hydrosilylation can be used to incorporate siloxy functionality. Shea *et al.* describe platinum catalyzed hydrosilylation of alkenes to generate bis-siloxy alkane monomers for polysilsesquioxane synthesis (Figure 5.22)[8]. Furthermore, vinyl siloxanes have been introduced through Mizoroki-Heck chemistry (Figure 5.22).

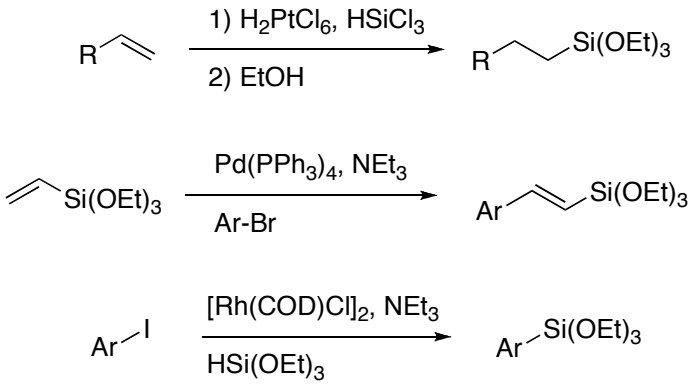

Figure 5.22: Methods for the introduction of siloxy functionality.

Sayari and Wang incorporated this functionalization in the synthesis of a bis-vinylsilylbenzene monomer for a PMO[65]. Masuda and co workers have developed a direct coupling of trialkoxysilanes with aryl halides catalyzed by a rhodium source (Figure 5.22)[66,67]. As this method installs the siloxy group directly onto the aromatic ring, we examined it first.

We also turned our attention to generating a material containing BINAP, since this would obviate the need to introduce phosphine groups after preparation of the material. Furthermore, a BINAP-based material would offer the possibility to employ a variety of different metals in catalytic processes that would not be sensitive to the presence of silanols. Given the availability of both enantiomers of BINAP, both enantiomers of a chiral PMO would be readily accessible. In our previous work, we incorporated the polymerizable silicon group along the axis of chirality, so that the bite angle of the ligand would not be dictated by the polymerization points[39]. As such we set forth to synthesize 4,4'-halo substituted BINAP molecules (Figure 5.23).

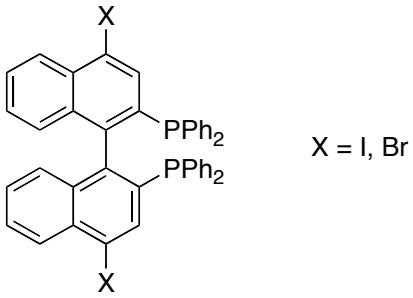

Figure 5.23: Proposed 4,4'-disubstituted BINAP monomer.

The synthetic route to the 4,4'-bis-functionalized BINAPOs is shown in scheme 5.4. Protection of the phosphines as phosphine oxides was easily performed by oxidation with hydrogen peroxide in quantitative yield for the racemic as well as the enantiopure compounds.

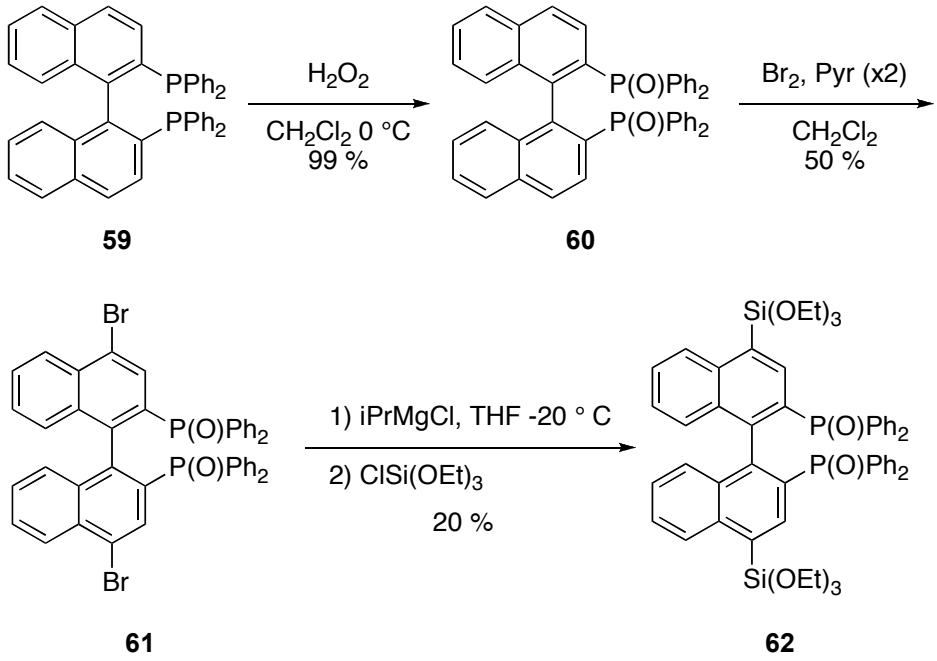

Scheme 5.4: Proposed synthesis of 4,4'-bis(triethoxysilyl) BINAPO.

Regioselective bromination can be achieved by careful control of the conditions. Berthod *et al.* developed methods for adding bromine to either the 4,4' or 5,5' positions of BINAPO[68]. Installing bromine at the 4 position utilizes pyridine and bromine, while iron catalysis will brominate the 5 position of the naphthyl ring (Scheme 5.5)[68]. We could attain a 50 % yield of the dibrominated product after two treatments of BINAPO with bromine and pyridine. The main by-products were monobrominated BINAPO and unreacted BINAPO. Fortunately, these can be separated from the dibrominated BINAPO and recycled to generate more dibromo BINAPO. Additionally, we were able to increase the yield of the dibromo BINAPO to 76 % by a third treatment with bromine and pyridine.

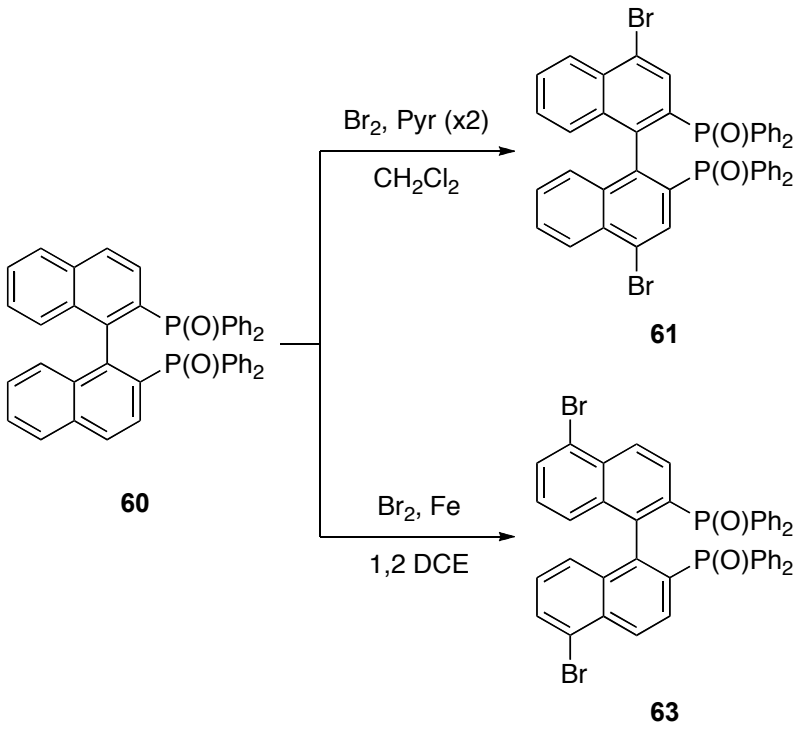

Scheme 5.5: Regioselective bromination of BINAPO utilizing two different EAS systems.

The first attempt to install silicon was to generate the Grignard reagent from dibromo BINAPO (Scheme 5.6). Treatment of **61** with isopropyl magnesium chloride for 1 hr at -5 °C followed by dropwise introduction of the electrophile [$ClSi(OEt)_3$] into a cold solution led to the recovery of mainly starting material with a small amount of reduction to mono-bromo BINAPO. No silyl species were observed in this reaction. To ensure that Grignard formation was complete, the same sequence was carried out, except that iodine was used to quench the Grignard (Scheme 5.6). Despite using excesses of both isopropyl magnesium chloride and iodine, very little of diiodo BINAPO **66** was formed. Furthermore, using deuterated methanol as a quenching agent, no deuterium incorporation was observed by deuterium

NMR and the proton NMR shows recovered dibromo BINAPO **61** (Scheme 5.6). This indicates that the aryl Grignard reagent is not forming and an alternate method for installation of silicon is needed.

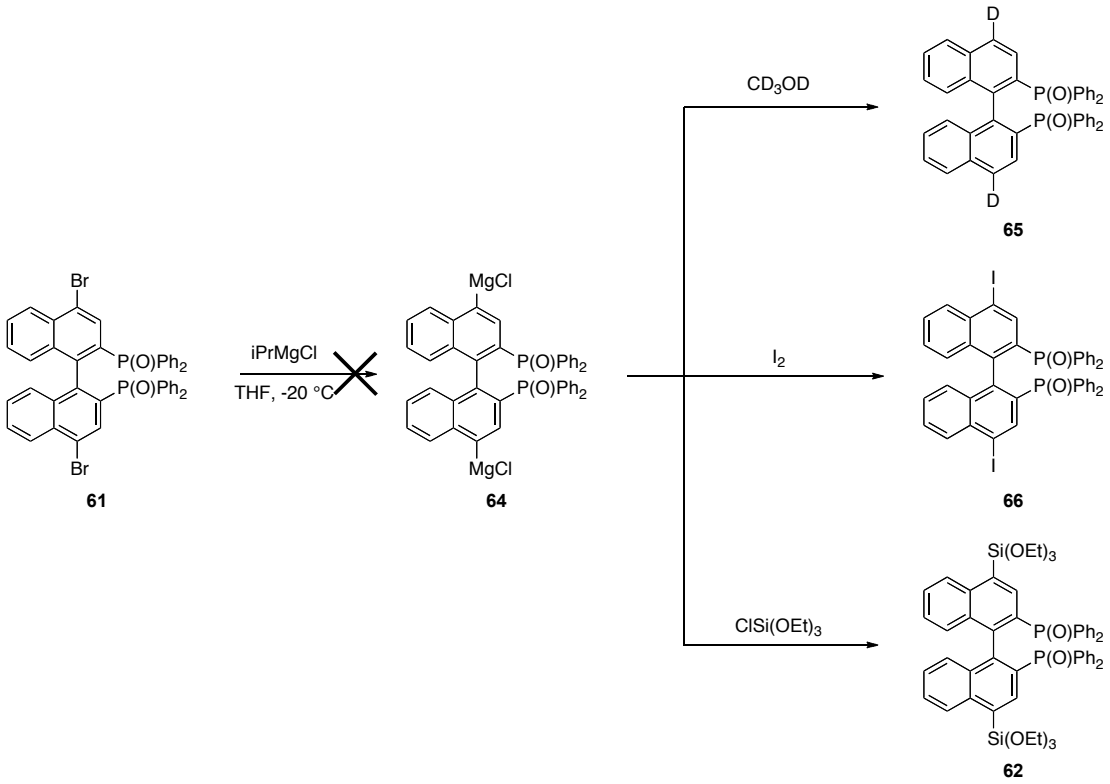

Scheme 5.6: Attempted Grignard synthesis from 4,4'-Dibromo BINAPO.

Given our lab's previous success with the Masuda reaction for installing silicon we investigated using the Masuda coupling for the BINAPO system[39,41]. However, since the Masuda reaction works far better with iodides than bromides,[66,67,69] we set out to convert 4,4'-dibromo BINAPO **61** to 4,4'-diiodo BINAPO **66**. Our first strategy employed an aromatic Finkelstein reaction[70]. To test this reaction, we prepared (3-bromophenyl)diphenyl phosphine oxide **67** and converted it to (3-iodophenyl)diphenyl phosphine

oxide **68** (Equation 5.7). The bromo triphenylphosphine molecule was prepared in a 95 % yield over two steps. Conversion to the iodide was achieved using catalytic copper (I) iodide in the presence of a diamine ligand and sodium iodide[70], this easily afforded (3-iodophenyl)diphenyl phosphine oxide **68** in 97 % yield.

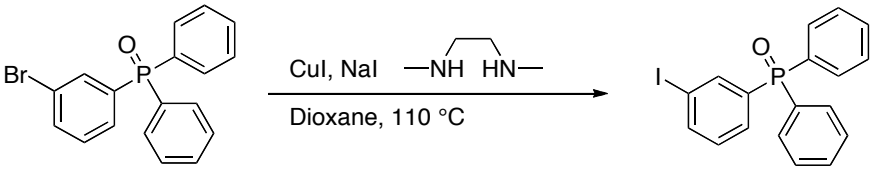

67 **68** (Eq. 5.7)

Having successfully employed the Finkelstein reaction on model compound **56**, we attempted the reaction with dibromo BINAPO **61** (Equation 5.8). Unfortunately, using the same conditions as for **67**, very little reaction was observed and dibromo BINAPO **61** was recovered in a 91 % yield .

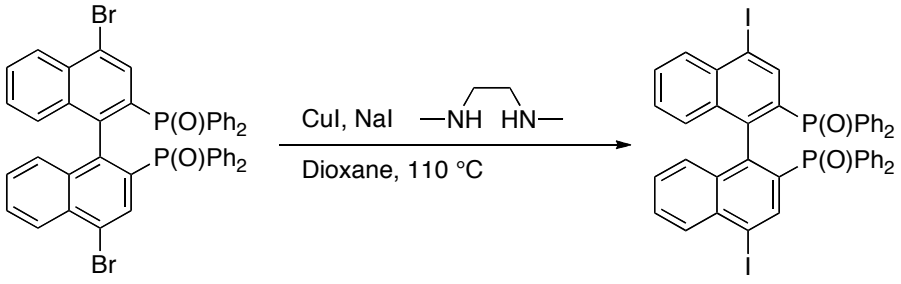

61 **66** (Eq. 5.8)

Increasing the reaction time led to reduction of the aryl bromide and recovery of BINAPO **60**. Increasing the amount of copper (I) iodide and dimethylethylene diamine to one and two equivalents respectively, was successful, increasing product formation. However, the dibromo and diiodo

BINAPOs have similar R_fs and cannot be separated by chromatography. Thus any product recovered contained starting material as well. Taking this recovered product and re-subjecting it to the Finkelstein conditions allowed the recovery of clean diiodo BINAPO **66** in a 20 % yield over the two steps. The remaining material was recovered as mono halogenated BINAPOs or reduced BINAPO. The difficulty of the double substitution on this molecule made this pathway unfeasible for the synthesis of PMO monomers. The small amount of 4,4'-diiodo BINAPO was subjected to the Masuda conditions (Equation 5.9). None of the desired product was obtained and largely reduction of the aryl iodide bond occurred.

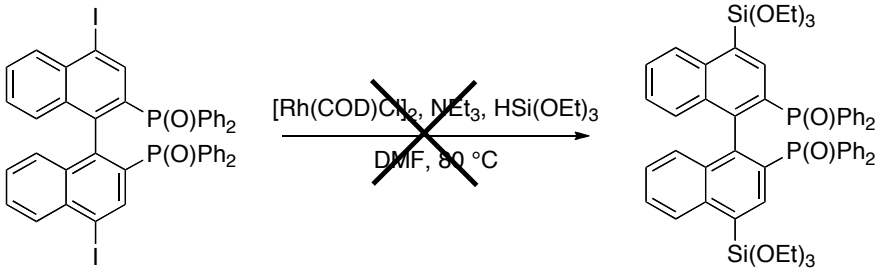

66 **62** (Eq. 5.9)

Considering the difficulties we encountered converting an aryl bromide into an aryl iodide, we decided to install the iodide directly (Scheme 5.7). Using with the procedure we employed to install bromine in the 4 position, we replaced Br_2 with iodine monochloride as an I^+ source. However, only starting material was recovered at room temperature in dichloromethane. Switching the solvent to toluene and increasing the temperature to reflux did not afford the desired iodide either. Following a report by Olah *et al.,* we attempted

aromatic iodination with NIS and triflic acid[71]. This combination generates a very electrophilic iodine for aromatic substitution. We were successful at installing iodine onto the naphthyl rings in an 88 % yield, however, NMR and X-ray crystal structure demonstrated that the iodine was in the 5,5' positions not the 4,4' positions (Figure 5.24).

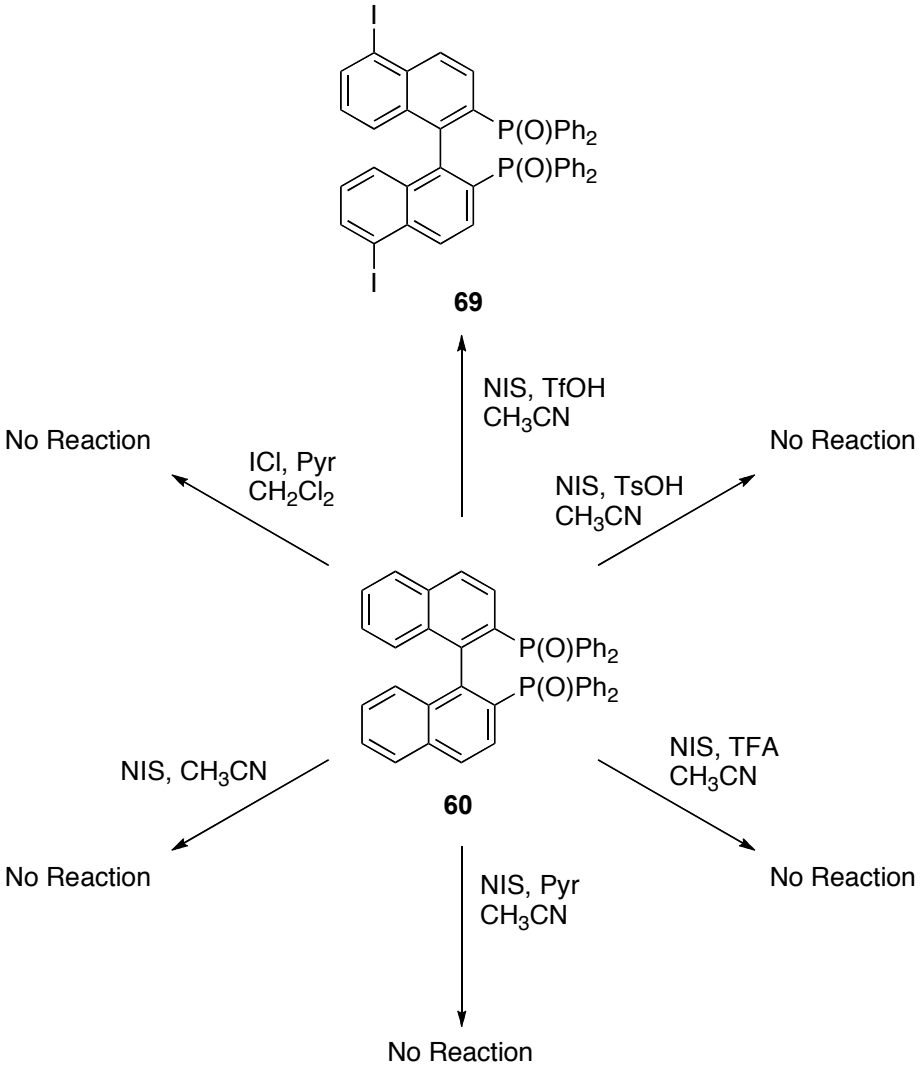

Scheme 5.7: Direct synthesis of bis-iodinated BINAPO compounds.

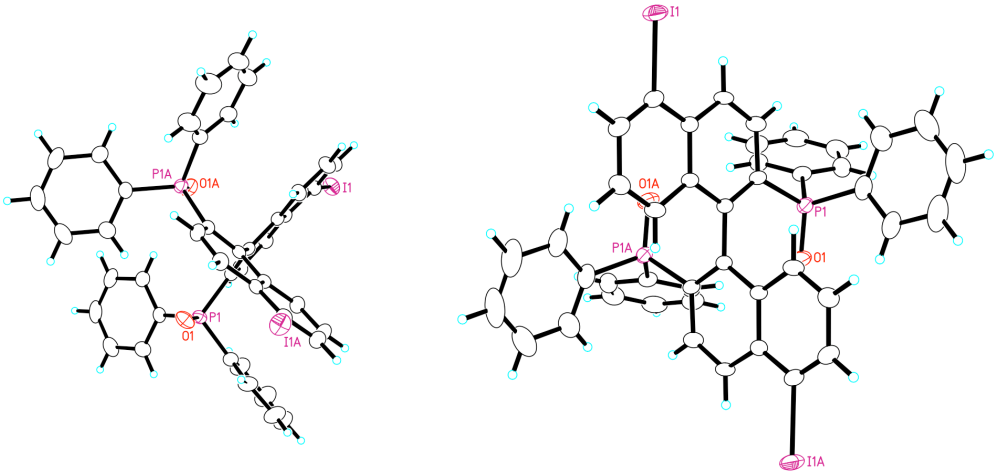

Figure 5.24: Crystallographic Representations of 5,5'-Diiodo BINAPO.

We further attempted to synthesize the 4,4' diiodo BINAP by varying the strength of the acid or removing it altogether (Scheme 5.7). Unfortunately, only with triflic acid were any iodinated products found: starting material was recovered in all other cases. We then decided to move ahead with the iodide in the 5,5' positions for the Masuda reaction.

Initial attempts at the Masuda coupling[39,66,67] with triethoxysilane as the silicon source resulted in reduction of the carbon iodine bond to give **60**. As triethoxysilane is a reducing agent, the Masuda reaction was attempted with hexaethoxydisilane, which lacks the reducing silicon hydrogen bond. However, this was unsuccessful leading to recovery of the starting material. The rate of addition of the silane was found to play a role in the amount of reduction. A fast addition of the silane gave complete reduction of the carbon iodine bond to BINAPO **60**. Alternatively, a slow, dropwise addition of triethoxysilane over a period of 10 to 20 minutes gave a 20 % yield of 5,5'-

bis(triethoxysilyl) BINAPO **70** after purification. It was important to fully consume the starting diiodide, as it and the product co-eluted during chromatography and they could not be separated. The remaining 80 % of material was recovered as various mono-silyl **71**, mono-iodo **72** and non-iodinated BINAPO **60**. While this was a poor yield for a synthetic procedure, it afforded enough material to carry forward with the materials synthesis, which was the critical part of the project.

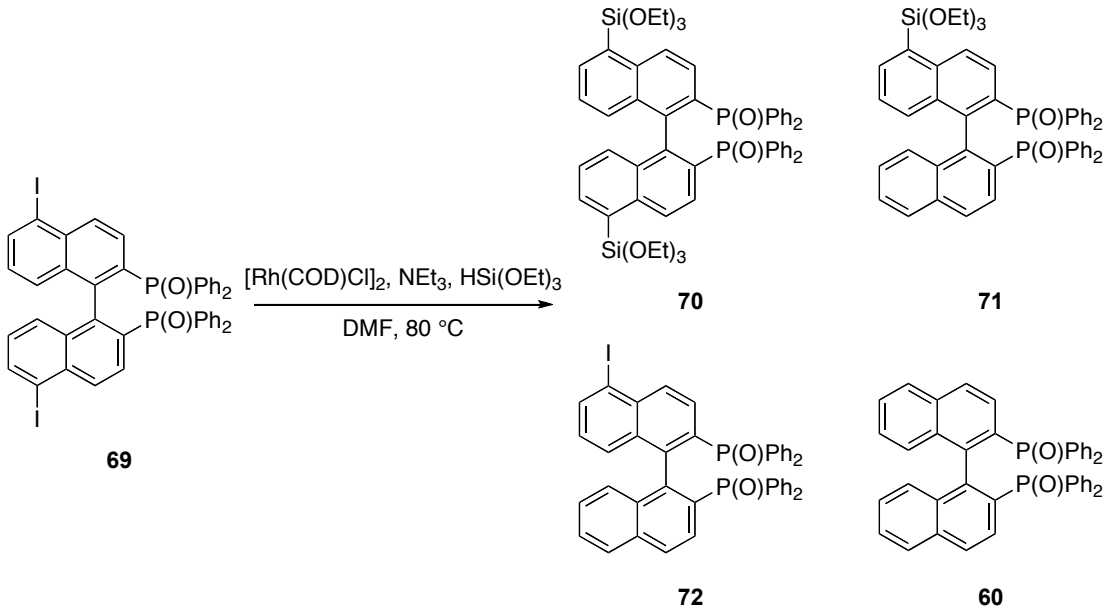

Scheme 5.8: Masuda reaction and products for 5,5'-diiodo BINAPO.

With the silylated monomers in hand, we turned our attention to the synthesis of chiral, enantiomerically pure PMOs. Thus PMOs were prepared using monomer **70** as a dopant at 15% loading along with 4,4'-bis(triethoxysilyl) biphenyl **7** or TEOS as the bulk material using Brij 76 as the surfactant. The resulting materials prepared with racemic or enantiomerically pure BINAPO were all mesoporous with pore sizes of about 25 Å (Figure

5.25, Table 5.1). TEM images show the materials to be well ordered with what looks like a bending of the channels (Figure 5.26).

Table 5.1: Physical Characteristics of BINAPO/Biphenyl Chiral PMOs.

Entry	PMO	Surface Area (m^2/g)	Pore Size (Å)	Pore Volume (mL/g)
1	S	626	26.4	0.461
2	R	481	24.2	0.339
3	Rac	785	25.1	0.549

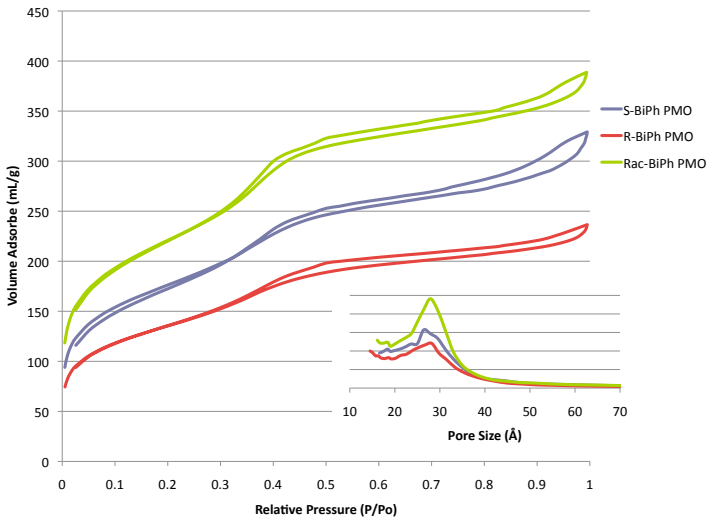

Figure 5.25: Nitrogen adsorption isotherms and pore size distribution plot (inset) for BINAPO/Biphenyl Chiral PMOs.

It is unclear at this time if the axial chirality of the BINAPO is responsible for the bend in the channels. However, there is precedent for this in the literature. Che *et al.,* using a chiral surfactant or a chiral dopant in the surfactant, observed a helical twist to their hexagonally ordered channels[34]. Chen *et al.*

not only saw helical channels but the rods themselves formed helical shapes. In this case no chiral molecule was added and the synthesis conditions were responsible for the formation of helical structures, with equal amounts of right and left-handed helices[72].

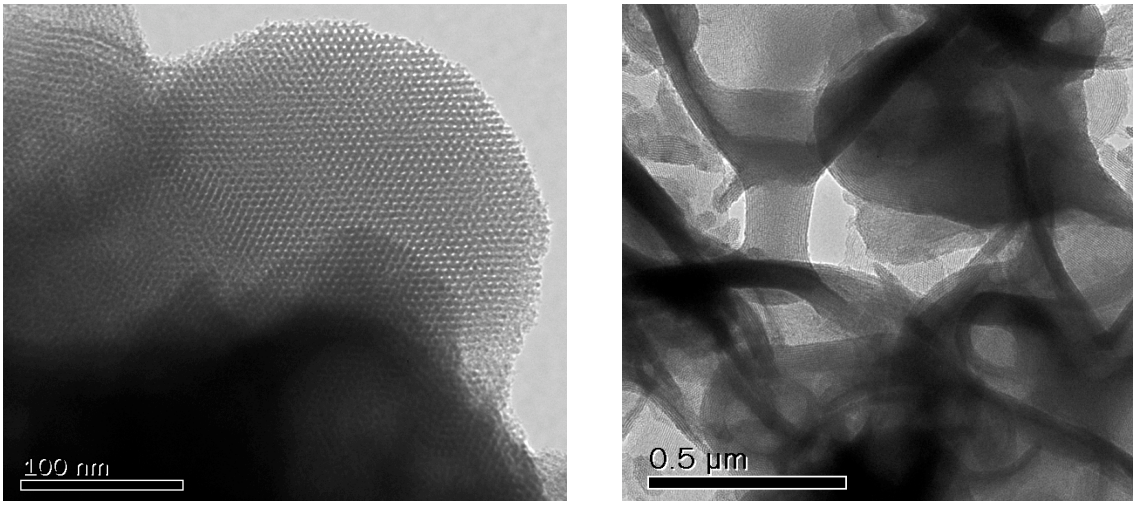

Figure 5.26: TEM images of BINAPO/Biphenyl Chiral PMOs.

To demonstrate that the chirality from the monomer was incorporated into the materials, solid state circular dichroism was employed. We started by examining the spectra of the diiodo BINAP monomers. The racemic molecule showed no CD as expected, while both enantiomers showed opposite spectra (Figure 5.27). After material synthesis the racemic material showed no CD signals (Figure 5.28). Examining the enantiomerically pure materials, rotation of circular polarized light was observed with opposite enantiomers resulting in opposite rotations with the exception of a shoulder at 360 nm in the S material. This is in a similar area to where we previously had observed a transfer of chirality from our chiral monomer to the biphenyl host[39]. To

determine if such an effect was occurring with the BINAPO monomer we prepared a PMO with and inorganic silica source that is incapable of transfer of chirality.

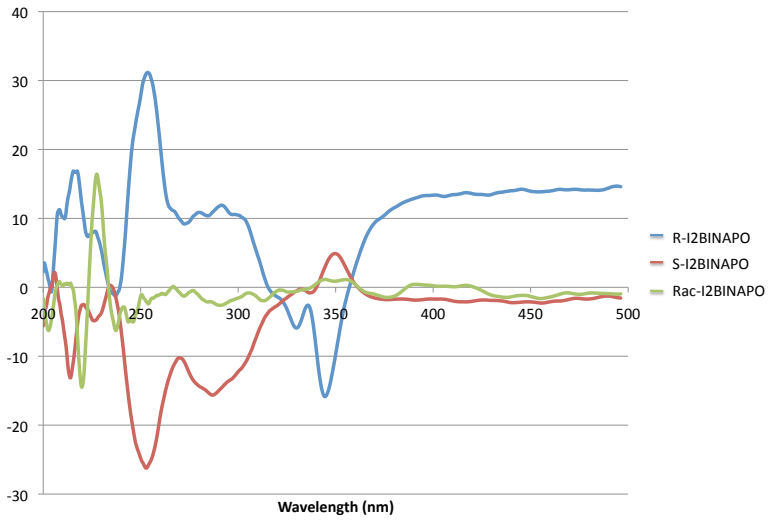

Figure 5.27: Circular dichroism spectra of iodinated BINAPO molecules

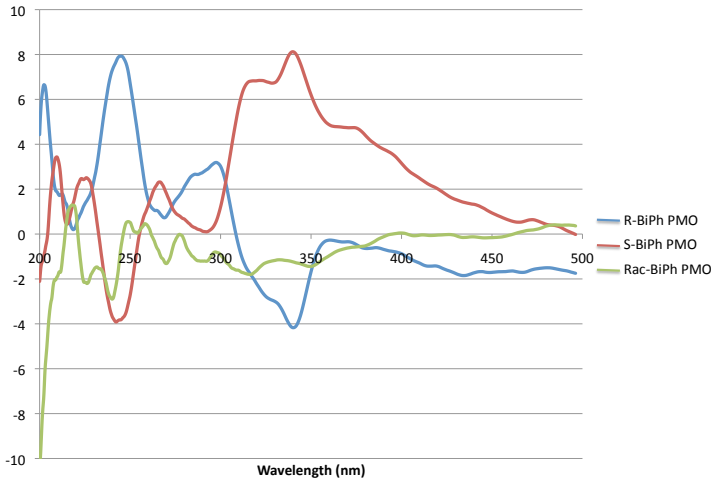

Figure 5.28: Circular dichroism spectrum of BINAPO/Biphenyl PMOs.

The BINAPO/TEOS materials were successfully prepared, replacing the biphenyl monomer with 2 equivalents of TEOS in the synthesis procedure.

These PMOs were microporous yielding Type 1 isotherms from nitrogen sorption (Figure 5.29) but the PMOs still have high surface areas and good pore volumes (Table 5.2). Examining chirality by solid state CD the materials prepared with TEOS show the same CD as those prepared with biphenyl (Figure 5.30). This shows that in these materials there is little or no transfer of chirality from the BINAPO monomer to biphenyl.

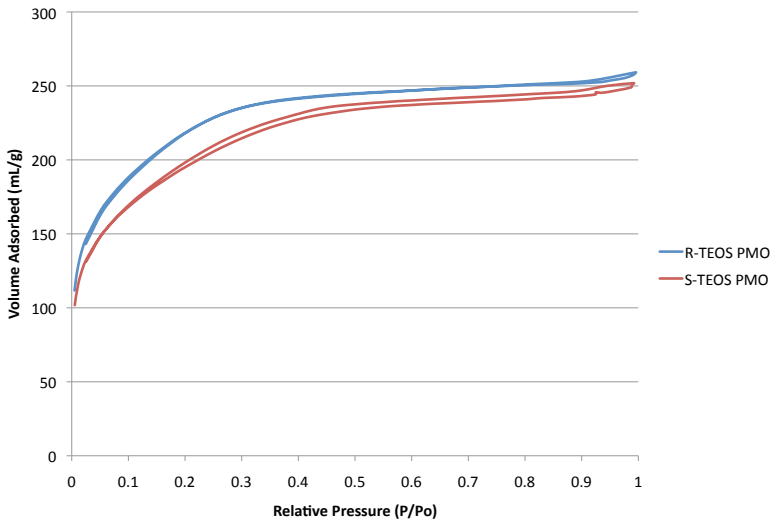

Figure 5.29: Nitrogen sorption isotherms for BINAPO/TEOS PMOs.

Table 5.2: Physical Characteristics of BINAPO/TEOS Chiral PMOs.

Entry	PMO	Surface Area (m2/g)	Pore Size (Å)	Pore Volume (mL/g)
1	R	786	16.5	0.347
2	S	701	18.1	0.345

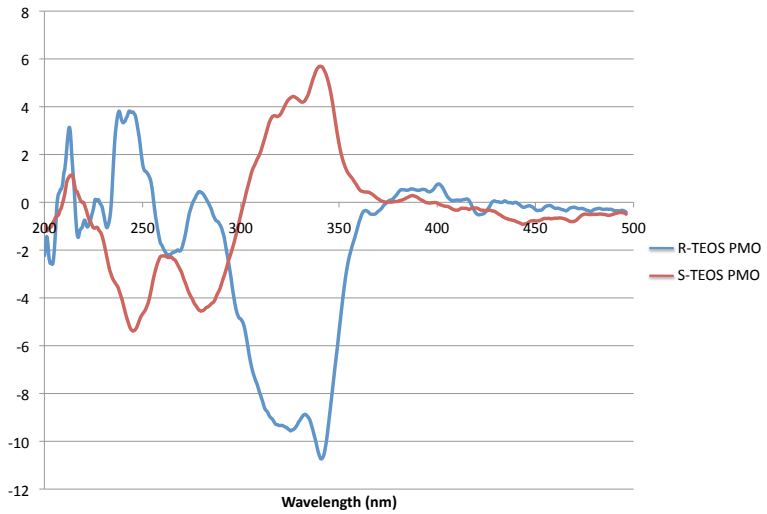

Figure 5.30: Circular dichroism spectrum of BINAPO/TEOS PMOs.

Ultimately, this PMO material is envisioned as a ligand for asymmetric catalysis but prior to metal loading, the phosphine oxides need to be reduced to phosphines. Using triphenylphosphine oxide as a model system, trichlorosilane and phenylsilane were good reductants to produce the phosphine while other reducing agents such as lithium aluminum hydride, tributylstannane, borane and di-isobutylaluminum hydride were ineffective. When the condensed PMO was treated with either trichlorosilane or phenyl silane, however, no reduction was observed by IR or solid state ^{31}P NMR. Interestingly, Si-H vibrations were observed in the IR (2254 cm^{-1} for $HSiCl_3$ and 2172 cm^{-1} for $PhSiH_3$) and the OH vibration at 3420 cm^{-1} was reduced in intensity after treatment of the PMO with either of the reducing agents. This suggests that the reducing agents were being incorporated into the material instead of reducing the phosphine. We postulated that free silanols on the surface were reacting with the silane reducing agent as a competing pathway

that was preventing reduction. Furthermore, McDonald *et al.* had shown that TMS capping of free silanols was required in their amorphous silica system for the reduction of BINAPO to BINAP[64]. After capping of the silanols with TMSCl, the PMO was then treated with phenyl silane and trichlorosilane together as described by McDonald *et al.*[64] This reduced but did not eliminate the fraction of the phosphine oxides as evidenced by solid state ^{31}P NMR and IR suggesting that some of the BINAPO monomers are buried in the pore walls and not accessible to the solvent. At this time only the racemic BINAPO PMO has been reduced but we anticipate similar reactivity in reducing the enantiomerically pure materials.

5.3 Conclusion

In the process of developing novel hybrid organic-inorganic periodic mesoporous organosilicates, we have explored methods for introducing alkoxy silyl groups to aromatic rings in order to facilitate preparation of new PMO monomers with different organic functionalities. While it is fairly easy to introduce the alkyl silyl substituent on an aromatic system, the chemistry is considerably more difficult with alkoxy silyl groups. This leaves room for improvement of the current methodologies to expand on the range of organic functionalities that can be incorporated into PMOs. Unfortunately, we were not successful in preparing a bis-silylated BINOL based monomer but we were able to generate a BINAP based PMO. The BINAPO monomer co-condensed with bis-silyl biphenyl or TEOS formed ordered materials with racemic or

either enantiomerically pure form of BINAP. TEM analysis of the materials demonstrated interesting spiral morphologies of the bulk particles. Whether this is due to the chirality of the monomers or the synthesis conditions remains to be determined. Retention of the BINAP chirality was established by solid state circular dichroism. Unlike the previous chiral material developed in our labs, there was no evidence of transfer of chirality from the chiral monomer to the achiral biphenyl monomer. Finally, reduction of the phosphine oxide on the silicate was successful and with the reduced phosphines, co-ordination of metals and asymmetric catalysis can commence.

5.4 References:

(1) Kickelbick, G. *Angew. Chem. Int. Ed.* **2004**, *43*, 3102.
(2) Fujita, S.; Inagaki, S. *Chem. Mater.* **2008**, *20*, 891.
(3) Hatton, B.; Landskron, K.; Whitnall, W.; Perovic, D.; Ozin, G.A. *Acc. Chem. Res.* **2005**, *38*, 305.
(4) Yang, Y.; Sayari, A. *Chem. Mater.* **2008**, *20*, 2980.
(5) Loy, D.A.; Shea, K.J. *Chem. Rev.* **1995**, *95*, 1431.
(6) Shea, K.J.; Loy, D.A. *Acc. Chem. Res.* **2001**, *34*, 707.
(7) Shea, K.J.; Loy, D.A.; Webster, O. *J. Am. Chem. Soc.* **1992**, *114*, 6700.
(8) Oviatt, H.W.; Shea, K.J.; Small, J.H. *Chem. Mater.* **1993**, *5*, 943.
(9) Loy, D.A.; Carpenter, J.P.; Alam, T.M.; Shaltout, R.; Dorhout, P.K.; Greaves, J.; Small, J.H.; Shea, K.J. *J. Am. Chem. Soc.* **1999**, *121*, 5413.
(10) Loy, D.A.; Carpenter, J.P.; Myers, S.A.; Assink, R.A.; Small, J.H.; Greaves, J.; Shea, K.J. *J. Am. Chem. Soc.* **1996**, *118*, 8501.
(11) Loy, D.A.; Beach, J.V.; Baugher, B.M.; Assink, R.A.; Shea, K.J.; Tran, J.; Small, J.H. *Chem. Mater.* **1999**, *11*, 3333.
(12) Shea, K.J.; Loy, D.A. *Chem. Mater.* **2001**, *13*, 3306.
(13) Asefa, T.; MacLachlan, M.J.; Coombs, N.; Ozin, G.A. *Nature* **1999**, *402*, 867.
(14) MacLachlan, M.J.; Asefa, T.; Ozin, G.A. *Chem. Eur. J.* **2000**, *6*, 2507.
(15) Asefa, T.; MacLachlan, M.J.; Grondey, H.; Coombs, N.; Ozin, G.A. *Angew. Chem. Int. Ed.* **2000**, *39*, 1808.
(16) Melde, B.J.; Holland, B.T.; Blanford, C.F.; Stein, A. *Chem. Mater.* **1999**, *11*, 3302.
(17) Yoshina-Ishii, C.; Asefa, T.; Coombs, N.; MacLachlan, M.J.; Ozin, G.A. *Chem. Commun.* **1999**, 2539.
(18) Wang, W.; Zhou, W.; Sayari, A. *Chem. Mater.* **2003**, *15*, 4886.
(19) Inagaki, S.; Guan, S.; Ohsuna, T.; Terasaki, O. *Nature* **2002**, *416*, 304.
(20) Yang, Q.; Kapoor, M.P.; Inagaki, S.; Shirokura, N.; Kondo, J.H.; Domen, K. *J. Mol. Catal. A* **2005**, *230*, 85.
(21) Kapoor, M.P.; Yang, Q.; Inagaki, S. *J. Am. Chem. Soc.* **2002**, *124*, 15176.
(22) Kapoor, M.P.; Yang, Q.; Goto, Y.; Inagaki, S. *Chem. Lett.* **2003**, *32*, 914.
(23) Zhang, L.; Zhang, W.; Shi, J.; Hua, Z.; Li, Y.; Yan, J. *Chem. Commun.* **2003**, 210.
(24) Baleizao, C.; Gigante, B.; Das, D.; Alvaro, M.; Garcia, H.; Corma, A. *Chem. Commun.* **2003**, 1860.
(25) Alvaro, M.; Benitez, M.; Das, D.; Ferrer, B.; Garcia, H. *Chem. Mater.* **2004**, *16*, 2222.
(26) Benitez, M.; Bringman, G.; Dreyer, M.; Garcia, H.; Ihmels, H.; Waidelich, M.; Wissel, K. *J. Org. Chem.* **2005**, *70*, 2315.
(27) Jiang, D.; Yang, Q.; Yang, J.; Zhang, L.; Zhu, G.; Su, W.; Li, C. *Chem. Mater.* **2005**, *17*, 6154.
(28) Jiang, D.; Yang, Q.; Wang, H.; Zhu, G.; Yang, J.; Li, C. *J. Catal.* **2006**, *239*, 65.
(29) Adima, A.; Moreau, J.J.; Man, M.W.C. *Chirality* **2000**, *12*, 411.
(30) Polarz, S.; Kuschel, A. *Adv. Mater.* **2006**, *18*, 1206.

(31) Ide, A.; Voss, R.; Sholz, G.; Ozin, G.A.; Antonietti, M.; Thomas, A. *Chem. Mater.* **2007**, *19*, 2649.
(32) Inagaki, S.; Guan, S.; Yang, Q.; Kapoor, M.P.; Shimada, T. *Chem. Commun.* **2008**, 202.
(33) Gabashvili, A.; Medina, D.D.; Gedanken, A.; Mastai, Y. *J. Phys. Chem. B* **2007**, *111*, 11105.
(34) Che, S.; Liu, Z.; Ohsuna, T.; Sakamoto, K.; Terasaki, O.; Tatsumi, T. *Nature* **2004**, *429*, 281.
(35) Yokoi, T.; Yamataka, Y.; Ara, Y.; Sato, S.; Kubota, Y.; Tatsumi, T. *Microporous and Mesoporous Mater.* **2007**, *103*, 20.
(36) Qiu, H.; Wang, S.; Zhang, W.; Sakamoto, K.; Terasaki, O.; Inoue, Y.; Che, S. *J. Phys. Chem. C* **2008**, *112*, 1871.
(37) Jin, H.; Qiu, H.; Sakamoto, Y.; Shu, P.; Terasaki, O.; Che, S. *Chem. Eur. J.* **2008**, *14*, 6413.
(38) Meng, X.; Yokoi, T.; Lu, D.; Tatsumi, T. *Angew. Chem. Int. Ed.* **2007**, *46*, 7796.
(39) MacQuarrie, S.; Thompson, M.P.; Blanc, A.; Mosey, N.J.; Lemieux, R.P.; Crudden, C.M. *J. Am. Chem. Soc.* **2008**, *130*, 14099.
(40) Almenningen, A.; Bastiansen, O.; Fernholt, L.; Cyvin, B.N.; Cyvin, S.J.; Samdal, S. *J. Mol. Struct.* **1985**, *128*, 56.
(41) Montoya-Pelaez, P.J.; Uh, Y.S.; Lata, C.J.; Thompson, M.P.; Lemieux, R.P.; Crudden, C.M. *J. Org. Chem.* **2006**, *71*, 5921.
(42) Marchand, A.P.; Chong, H.S.; Ganguly, B. *Tetrahedron: Asymmetry* **1999**, *10*, 4695.
(43) Noyori, R. *Angew. Chem. Int. Ed.* **2002**, *41*, 2008.
(44) Yang, X.; Su, W.; Liu, D.; Wang, H.; Shen, J.; Da, C.S.; Wang, R.; Chan, A.S.C. *Tetrahedron* **2000**, *56*, 3511.
(45) Yang, X.W.; Sheng, J.H.; Da, C.S.; Wang, H.S.; Su, W.; Wang, R.; Chan, A.S.C. *J. Org. Chem.* **2000**, *65*, 295.
(46) Dong, C.; Zhang, J.; Zheng, W.; Zhang, L.; Yu, Z.; Choi, M.C.K.; Chan, A.S.C. *Tetrahedron: Asymmetry* **2000**, *11*, 2449.
(47) Fan, Q.H.; Liu, G.H.; Deng, G.J.; Chen, X.M.; Chan, A.S.C. *Tetrahedron Lett.* **2001**, *42*, 9047.
(48) Hu, Q.S.; Vitharana, D.; Zheng, X.F.; Wu, C.; Kwan, C.M.S.; Pu, L. *J. Org. Chem.* **1996**, *61*, 8370.
(49) Jayaprakash, D.; Kobayashi, Y.; Arai, T.; Hu, Q.S.; Zheng, X.F.; Pu, L.; Sasai, H. *J. Mol. Catal. A: Chem.* **2003**, *196*, 145.
(50) Yu, H.B.; Hu, Q.S.; Pu, L. *J. Am. Chem. Soc.* **2000**, *122*, 6500.
(51) Jayaprakash, D.; Sasai, H. *Tetrahedron: Asymmetry* **2001**, *12*, 2589.
(52) Jayaprakash, D.; Kobayashi, Y.; Watanabe, S.; Arai, T.; Sasai, H. *Tetrahedron: Asymmetry* **2003**, *14*, 1587.
(53) Matsunaga, S.; Ohshima, T.; Shibasaki, M. *Tetrahedron Lett.* **2000**, *41*, 8473.
(54) Ohkuma, T.; Takeno, H.; Honda, Y.; Noyori, R. *Adv. Synth. Catal.* **2001**, *343*, 369.
(55) Bayston, D.J.; Fraser, J.L.; Ashton, M.R.; Baxter, A.D.; Polywka, M.E.C.; Moses, E. *J. Org. Chem.* **1998**, *63*, 3137.

(56) Brethon, A.; Hesemann, P.; Rejaud, L.; Moreau, J.J.; Man, M.W.C. *J. Organomet. Chem.* **2001**, *627*, 239.
(57) Hesemann, P.; Moreau, J.J. *C.R. Chemie* **2003**, *6*, 199.
(58) Bhatt, A.P.; Pathak, K.; Jasra, R.V.; Kureshy, R.I.; Khan, N.H.; Abdi, S.H.R. *J. Mol. Catal. A Chem.* **2006**, *244*, 110.
(59) Liu, G.; Gao, Y.; Lu, X.; Liu, M.; Zhang, F.; Li, H. *Chem. Commun.* **2008**, 3184.
(60) Jamis, J.; Anderson, J.R.; Dickson, R.S.; Campi, E.M.; Jackson, W.R. *J. Organomet. Chem.* **2001**, *627*, 37.
(61) Gelman, F.; Avnir, D.; Schumann, H.; Blum, J. *J. Mol. Catal. A: Chem.* **1999**, *146*, 123.
(62) Bianchini, C.; Barbaro, P.; Dal Santo, V.; Gobetto, R.; Meli, A.; Oberhauser, W.; Psaro, R.; Vizza, F. *Adv. Synth. Catal.* **2001**, *343*, 41.
(63) Kesanli, B.; Lin, W. *Chem. Commun.* **2004**, 2284.
(64) McDonald, A.R.; Muller, C.; Vogt, D.; van Klink, G.P.M.; van Koten, G. *Green Chem.* **2008**, *10*, 424.
(65) Sayari, A.; Wang, W. *J. Am. Chem. Soc.* **2005**, *127*, 12194.
(66) Murata, M.; Ishikura, M.; Nagata, M.; Watanabe, S.; Masuda, Y. *Org. Lett.* **2002**, *4*, 1843.
(67) Murata, M.; Yamasaki, H.; Ueta, T.; Nagata, M.; Ishikura, M.; Watanabe, S.; Masuda, Y. *Tetrahedron* **2007**, *63*, 4087.
(68) Berthod, M.; Saluzzo, C.; Mignani, G.; Lemaire, M. *Tetrahedron: Asymmetry* **2004**, *15*, 639.
(69) Murata, M.; Suzuki, K.; Watanabe, S.; Masuda, Y. *J. Org. Chem.* **1997**, *62*, 8569.
(70) Klapars, A.; Buchwald, S.L. *J. Am. Chem. Soc.* **2002**, *124*, 14844.
(71) Olah, G.A.; Wang, Q.; Sandford, G.; Prakash, G.K.S. *J. Org. Chem.* **1993**, *58*, 3194.
(72) Wang, J.; Wang, W.; Sun, P.; Yuan, Z.; Li, B.; Jin, Q.; Ding, D.; Chen, T. *J. Mater. Chem.* **2006**, *16*, 4117.

Chapter 6: Experimental Procedures

6.1 General Procedures

All reagents were purchased from Aldrich or Fisher with the following exceptions: P123 was donated by BASF. Sodium borohydride was purchased from BDH. Deuterated solvents were purchased from Cambridge Isotope Labs. Phenyl boronic acid, 2-furyl boronic acid and p-trifluoromethylphenyl boronic acid were purchased from Frontier Scientific. Sodium acetate and sodium nitrite were purchased from JT Baker Chemical. PL EDA (1 % crosslinked polystyrene resin, 3.21 mmol ligand/g), PL DETA (1 % crosslinked polystyrene resin, 2.71 mmol ligand/g) and PL thiourea MP (highly crosslinked polystyrene resin, 1.05 mmol ligand/g) were purchased from Polymer Labs. Quadrapure TU was purchased from Aldrich. Palladium acetate and rhodium cyclooctadiene chloride dimmer were purchased from Pressure Chemical Company. Dichloro[(S)-(-)-2,2'-bis(diphenylphosphine)-1,1'-binaphthyl][(1S, 2S)-diphenylethylene diamine] ruthenium (II), R, S and racemic BINAP were purchased from Strem. Triflic anhydride was purchased from TCI.

NMR analysis was performed on Brucker (300, 400, 500 and 600 MHz) spectrometers. Automated flash chromatography was performed on a Biotage Horizon chromatography system. Nitrogen porosimetry measurements were taken on a Micromeretics ASAP 2010 system. Gas chromatography was performed on an Agilent 6850 GC with flame ionization detection. Infrared spectroscopy was performed on a BOMEM MB-series machine. Circular

dichroism spectra were obtained on a Jasco J-715 spectropolarimeter. Samples for ICPMS were sent to Worsfold Water Quality Centre at Trent University for analysis.

6.2 Experimental Procedures from Chapter 2

Synthesis of SBA-15

The sol-gel procedure was adapted from Stucky *et al.*[1] In a typical synthesis, P123 (4.0 g) was dissolved in 150 mL of water and 20 mL of conc. HCl in a 250 mL glass jar. The resulting mixture was stirred at 40 °C for 16 hr. Tetraethylorthosilicate (TEOS, 9.2 mL, 8.6 g, 41.3 mmol) was then added and the solution stirred for 20 hr at 40 °C. The resulting powder was then hydrothermally treated under static conditions in the same flask for 48 hr at 80 °C. The solid was recovered by filtration and washed with water. The surfactant was removed by Soxhlet extraction with ethanol for 5 days. The powder was recovered and dried under vacuum. The sulfur loading was between 0.474 mmol S/g silicate and 1.05 mmol S/g silicate as determined by elemental analysis.

Surface modification of SBA-15 to generate SBA-15-NH_2

SBA-15 (1 g) was suspended in 20 mL of dry toluene and the flask was purged with argon. APTES (2.5 mL) was added and the resulting suspension stirred overnight at 80 °C in an argon atmosphere. The solution was then cooled and the solids collected by filtration washing with three portions of toluene and two portions of THF. The resultant powder was dried under vacuum and analyzed by nitrogen adsorption and elemental analysis. The amine loading was determined by elemental analysis to be between 1.91

mmol N/g silicate and 3.61 mmol N/g silicate corresponding to an amine spacing of 3.01-4.09 aminopropyl groups/nm^2.

Synthesis and Characterization of other SBA-15 Scavengers

SBA-15-**33** and SBA-15-**35** were prepared using the same method as SBA-15-NH_2, using **33** and **35** in place of APTES. After recovery elemental analysis revealed ligand loadings of 2.09 mmol/g and 1.69 mmol/g for SBA-15-**33** and SBA-15-**35** respectively.

Characterization of Commercially Available Scavengers

Commercial aminopropyl-functionalized amorphous silica has a loading of 1.0 mmol aminopropyl groups/g of silica or 1.83 aminopropyl groups/nm^2. The imidazole functionalized silica (SiO_2-**34**) has a loading of 1.0 mmol imidazole/g of silica while the diethylene-triamine functionalized silica (SiO_2-**35**) has a loading of 1.3 mmol ligand/g of silica. The polymer based PL EDA and PL DETA had ligand loadings of 3.21 mmol/g and 2.71 mmol/g, respectively.

Olefin Metathesis with Grubbs' First Generation Catalyst

In a typical olefin metathesis, diethyl-diallylmalonate (120 µL, 120 mg, 0.50 mmol) was dissolved in 100 mL of dry distilled DCM and the solution

degassed by bubbling argon through the solvent for 5 min. Bis(tricyclohexylphosphine) benzylidine ruthenium (IV) chloride (Grubbs' I, 20 mg, 0.025mmol, 5 mol%) was then added to the flask and the reaction was stirred at room temperature for 2 hr under argon. At the end of the reaction, the solvent was removed and hexamethylbenzene was added as an internal standard. Yields were calculated based on NMR. The crude oil was then subjected to the scavenging procedure as described below. ^{1}H NMR (400 MHz, $CDCl_3$): δ 5.60 (s, 2H), 4.19 (q, 4H, *J* = 7.1 Hz), 3.00 (s, 4H), 1.24 (t, 6H, *J* = 7.1 Hz).

Hydrogenation with Noyori's catalyst

p-Bromoacetophenone (400 mg, 2mmol), pota ssium tert-butoxide (5.12 mg, 0.046 mmol, 1.0 M solution in THF), dichloro[(S)-(-)-2,2'-bis(diphenylphosphine)-1,1'-binaphthyl][(1S, 2S)-diphenylethylenediamine] ruthenium (II) (2.01 mg, 0.002 mmol) and hexamethylbenzene (20.7 mg, 0.128 mmol) as an internal standard were combined in an autoclave inside a glove box. The autoclave was then pressurized to 150 psi of hydrogen and reacted at room temperature for 6 hr. The pressure was then released and an aliquot taken for NMR. The remaining oil was then subjected to the scavenging procedure. ^{1}H NMR (500 MHz, $CDCl_3$): δ 7.49 (d, 2H, *J* = 15 Hz), 7.27 (d, 2H, *J* = 15 Hz), 4.88 (m, 1H), 1.94 (d, 1H, OH, *J* = 7.5 Hz), 1.49 (d, 3H, *J* = 13 Hz).

Typical ruthenium scavenging procedure

The sample to be scavenged was dissolved in 10 mL of distilled water, THF or a 9:1 solution of water:THF. Approximately 100mg of the scavenger was added to the solution and the vial left to stir for 1 hr at room temperature. The solution was then filtered through a syringe filter to remove the scavenger. The filtrate volume was brought up to 25 mL in a volumetric flask and analyzed by ICPMS. The amount of ruthenium in μg/5 mg of product was calculated from the number obtained from ICPMS to determine the total amount of ruthenium present in μg. This number was then divided by the amount of product recovered divided by 5 (to account for the 5 mg). To convert this number to a weight ppm (as is often done in the literature) it is multiplied by 200 (eg. 1 μg/5 mg = 200 ppm).

6.3 Experimental Procedures from Chapter 3

Synthesis of SBA-15-SH sol-gel

The sol-gel procedure was adapted from Stucky *et al.*[1] In a typical synthesis, P123 (4.0 g) was dissolved in 150 mL of water and 20 mL of conc. HCl in a 250 mL glass jar. The resulting mixture was stirred at 40 °C for 16 hr. Tetraethylorthosilicate (TEOS, 8.6 mL, 8 g, 38.5 mmol) was then added and the solution stirred for 3 hr at 40 °C. Finally, mercaptopropyltrimethoxysilane (MPTMS, 0.5 mL, 0.525 g, 2.8 mmol, 6.8 mol%) was added and the reaction stirred for 19 hr at 40 °C. The resulting powder was then hydrothermally treated under static conditions in the same flask for 48 hr at 80 °C. The solid was recovered by filtration and washed with water. The surfactant was removed by Soxhlet extraction with ethanol for 5 days. The powder was recovered and dried under vacuum. The sulfur loading was between 0.474 mmol S/g silicate and 1.05 mmol S/g silicate as determined by elemental analysis.

Synthesis of SBA-15-SH-Pd (Catalyst)

In a typical procedure, $Pd(OAc)_2$ (114.77 mg, 0.511 mmol) was dissolved in 75 mL of THF and stirred under an argon atmosphere for 15 min. SBA-15-SH (1.5157 g, 1.03 mmol S) was then added to the solution and stirred under argon for 1 hr at room temperature. The powder was filtered using a sintered glass funnel and washed with THF. The catalyst was then

collected in a vial and dried under vacuum overnight. The filtrate was collected and sent for ICPMS analysis to determine palladium content. Residual palladium in the filtrate was found to be <0.03% of the initially added Pd.

Grafting of Mercaptopropyl Trimethoxy Silane on SBA-15

SBA-15-SH (500 mg) was suspended in 25 mL of toluene in a round bottom flask. MPTMS (0.2 mL, 1.07 mmol) was added and the flask fitted with a Dean-Stark apparatus. The solution was refluxed for 17 h in an inert atmosphere. The powder was collected by filtration and washed with methanol, acetone and ethyl ether. The solid was then soxhlet extracted with 1:1 ethyl ether: dichloromethane for 24 h. The powder was then dried under vacuum for 16 h to remove any residual solvent.

Grafting of Trimethylsilyl Chloride on SBA-15-SH

SBA-15-SH (1.0 g) was suspended in 30 mL of toluene in a round bottom flask. Trimethylsilyl chloride (3.25 mL, 25.6 mmol) was added followed by pyridine (2.05 mL, 25.5 mmol). The flask was fitted with a condenser and the solution heated to 105 °C for 18 h. The powder was recovered by filtration and washed with ethyl ether and hot ethanol. The powder was then dried under vacuum for 16 h to remove any residual solvent.

Grafting of Dimethylsilyl Dichloride on SBA-15-SH

SBA-15-SH (1.5 g) was suspended in 45 mL of toluene in a round bottom flask. Dichlorodimethyl silane (4.65 mL, 38.6 mmol) was added followed by pyridine (3.10 mL, 38.5 mmol). The flask was fitted with a condenser and the solution heated to 105 °C for 4 h. The powder was recovered by filtration and washed with ethyl ether and hot ethanol. The material was then soxhlet extracted with ethanol for 24 h. The powder was then dried under vacuum for 16 h to remove any residual solvent.

Grafting of Diphenylsilyl Dichloride on SBA-15-SH

SBA-15-SH (2.0 g) was suspended in 60 mL of toluene in a round bottom flask. Dichlorodiphenyl silane (4.0 mL, 19.0 mmol) was added followed by pyridine (10 mL, 124 mmol). The flask was fitted with a condenser and the solution heated to 105 °C for 4 h. The powder was recovered by filtration and washed with ethyl ether and hot ethanol. The material was then soxhlet extracted with ethanol for 24 h. The powder was then dried under vacuum for 16 h to remove any residual solvent.

Synthesis of Phenyl pinacol borane (PhBpin)

Phenyl boronic acid (3.7 g, 30.0 mmol) and pinacol (4.0 g, 33.8 mmol) were dissolved in 100 mL of benzene and heated to 60 °C for 1 hr. The

solvent was then removed in vacuo and the resulting oil purified by column chromatography using an automated flash chromatography system. The solvent system used was 2% EtOAc in hexanes for 1 column volumes (CV), 2% to 10% EtOAc linear ramp over 10 CV and 5 CV at 10% EtOAc/ 90% hexanes. 5.8 g (28.6 mmol, 95 % yield) of phenyl pinacol borane was recovered. ^{1}H NMR (400 MHz, $CDCl_3$): δ 7.83 (d, 2H, *J* = 8.8 Hz), 7.48 (t, 1H, *J* = 8.8 Hz), 7.39 (t, 2H, *J* = 8.8 Hz), 1.37 (s, 12H).

General procedure for the Suzuki-Miyaura coupling reaction

p-Bromoacetophenone (50 mg, 0.25 mmol), phenyl boronic pinacolate (PhBpin, 75 mg, 0.375 mmol), potassium carbonate (70 mg, 0.50 mmol), SBA-15-SH-Pd (1 mol% Pd) and 1,4-dimethoxybenzene (35 mg, 0.253 mmol) as internal standard were combined in a round bottomed flask with a stir bar and flushed with argon. DMF (2.5 mL) and distilled water (0.125 mL) were added via syringe. The reaction was heated at 80 °C with stirring, reaction progress was monitored by GC-FID.

Suzuki Coupling Catalyst Turnover Number

p-Bromoacetophenone (2.49 g, 12.5 mmol), PhBpin (3.49 g, 17.1 mmol), potassium carbonate (3.42 g, 24.7 mmol), SBA-15-SH-Pd (0.00915 mol% Pd) and 1,4-dimethoxybenzene (882 mg, 6.38 mmol) as internal

standard were combined in a round bottomed flask with a stir bar and flushed with argon. DMF (25 mL) and distilled water (1.25 mL) were added via syringe. The reaction was heated to 80 °C with stirring, reaction progress was monitored by GC-FID.

General Procedure for Sonogashira Coupling

p-Bromoacetophenone (100 mg, 0.50 mmol), sodium acetate (83 mg, 1.01 mmol), SBA-15-SH-Pd (1 mol% Pd) and 1,4-dimethoxybenzene (33 mg, 0.239 mmol) as internal standard were combined in a test tube with a stir bar, fitted with a septum and flushed with argon. Phenylacetylene (77.5 mg, 0.76 mmol) was dissolved in DMF (5 mL) and added to the solid reagents. Distilled water (0.25 mL) was added via syringe. The reaction was heated to 100 °C with stirring, reaction progress was monitored by GC-FID.

Synthesis of 2-Furyl pinacol borane

2-Furyl boronic acid (1.1 g, 10 mmol) and pinacol (1.8 g, 15.2 mmol) were dissolved in benzene. The flask was fitted with a Dean-Stark apparatus and the solution was refluxed for 5 hr. The solvent was removed and the crude oil was purified by automated silica chromatography (solvent system: 3 % EtOAc in hexanes for 1 column volume (CV), 3 % to 15 % EtOAc over 10 CV and 15 % EtOAc for 3 CV). This afforded 1.2 g (6.2 mmol, 62 % yield) of

2-furyl pinacol borane. The spectra obtained matched those found in the literature[2]. ^{1}H NMR (400 MHz, $CDCl_3$): δ 7.66 (s, 1H), 7.09 (d, 1H, *J* = 3.2 Hz), 6.46 (d, 1H, *J* = 3.2 Hz), 1.35 (s, 12H).

Synthesis of 3-iodoindazole

This synthesis was adapted from Rault *et al.*[3] Indazole (1.0 g, 8.6 mmol) was dissolved in 50 mL of DMF, degassed by bubbling argon through the liquid for 10 min. Iodine (4.3 g, 17.1 mmol) was added to the solution followed by potassium hydroxide (1.9 g, 33.4 mmol). The resulting solution was stirred at room temperature for 2.5 hr. The residual iodine was quenched by addition of a saturated solution of sodium sulfite until the colour had disappeared. The liquid was poured into a separatory funnel containing 150 mL of a saturated sodium bicarbonate solution. Ethyl ether (150 mL) was added and the layers separated. The organic layer was set aside and the aqueous layer was washed with two portions of ethyl ether. The combined organics were then washed with two portions of saturated sodium bocarbonate, dried with magnesium sulfate and concentrated to dryness. This afforded 2.0 g (8.4 mmol, 98% yield) of 3-iodoindazole. The spectra obtained matched those reported in the literature[3]. ^{1}H NMR (400MHz, $CDCl_3$): δ 7.45 - 7.57 (m, 3H), 7.25 - 7.28 (m, 1H). TOF^+: MH^+ = 244.96 m/Z.

Synthesis of N-benzyl-3-iodoindazole

This procedure was adapted from Rault *et al.*[3] 3-Iodoindazole (1.3 g, 5.2 mmol) was dissolved in 15 mL of dry THF and cooled to 0 °C in an ice bath. Potassium tert-butoxide (7.5 mmol, 7.5 mL, 1 M solution in THF) was added and the resulting solution stirred for 1 hr at 0 °C. Benzyl bromide (650 µL, 5.5 mmol) was then added slowly and the solution allowed to warm to room temperature. After 4 hr at room temperature, the solvent was removed and the residue dissolved in ethyl acetate. The solvent was washed with brine, dried with magnesium sulfate and concentrated to dryness. The resulting oil was purified by automated silica chromatography (solvent conditions 5% EtOAc in hexanes for 1 CV, 5 % to 20 % EtOAc over 10 CV and finally 20 % EtOAc for 3 CV), 1.7 g (5.16 mmol, 98 % yield) of N-benzyl-3-iodoindazole was recovered. The spectra obtained matched those reported in the literature[3]. ^{1}H NMR (300 MHz, $CDCl_3$): δ 7.52 (d, 1H, J = 9 Hz), 7.40 (t, 1H, J = 7.8 Hz), 7.15 - 7.36 (m, 7H), 5.63 (s, 2H). TOF^+: MH^+ = 335.00 m/Z.

Synthesis of N-benzyl-3-(2-furyl)-indazole

N-benzyl-3-iodoindazole (149.2 mg, 0.45 mmol), potassium carbonate (141.6 mg, 1.02 mmol), SBA-15-SH-Pd (22.11 mg, 0.0055 mmol Pd, 1 mol%) and hexamethylbenzene (40.9 mg, 0.252 mmol, internal standard) were combined in a dry test tube. 2-furyl pinacol borane (143.1 mg, 0.74 mmol) was dissolved in 5 mL of DMF and added to the test tube. The reaction was

then placed in a preheated oil bath at 80 °C and stirred for 16 hr. After cooling the reaction to room temperature, the catalyst was filtered of by passing it through a syringe filter. The reaction was then diluted to 25 mL with EtOAc in a volumetric flask and a sample taken for ICPMS analysis of residual palladium. The solvent was then removed and the residue taken up in ethyl ether, the solvent was washed with brine and the organic layer set aside. The aqueous layer was washed with a further two portions of ethyl ether. The combined organic layers were then washed with two portions of brine, dried with magnesium sulfate and concentrated to dryness. The crude oil was purified on an automated silica chromatography system (Solvent system: 2 % EtOAc in hexanes for 1 CV, 2 % to 10 % EtOAc over 10 CV followed by 10 % EtOAc in hexanes for 3 CV) 71.6 mg (0.26 mmol, 58 % yield) of N-benzyl-3-(2-furyl)-indazole was recovered. The spectra obtained matched those reported in the literature[3]. ^{1}H NMR (300MHz, $CDCl_3$): δ 8.13 (d, 1H, J = 9.3 Hz), 7.63 (s, 1H), 7.15 - 7.45 (m, 8H), 6.96 (d, 1H, *J* = 5.1 Hz), 6.60 (t, 1H, *J* = 3 Hz), 5.68 (s, 2H). TOF^+: MH^+ = 275.12 m/Z.

Synthesis of 4-(3-methoxyphenyl)-but-3-en-2-one

This procedure was developed from Evans *et al.*[4] m-Anisaldehyde (610 µL, 5.0 mmol) was dissolved in 10 mL of acetone in a round bottomed flask. In a separate flask sodium hydroxide (448.0 mg, 11.2 mmol) was dissolved in 10 mL of water. The base solution was then added to the acetone solution

and the reaction was stirred at room temperature. After 1 hr the reaction was diluted with 20 mL of ethyl ether and the layers separated. The organic layer was washed with two portions of brine, dried with magnesium sulfate and concentrated to dryness. The crude material was subjected to a silica column with 40 % EtOAc in hexanes, 861.3 mg (4.89 mmol, 98 % yield) of 4-(3-methoxyphenyl)-but-3-en-2-one was recovered. The spectra obtained matched those reported in the literature[4]. ^{1}H NMR (300 MHz, $CDCl_3$): δ 7.50 (d, 1H, *J* = 18.6 Hz), 7.34 (t, 1H, *J* = 9 Hz), 7.16 (d, 1H, *J* = 8.1 Hz), 7.08 (s, 1H), 6.99 (d, 1H, *J* = 6.3 Hz), 6.73 (d, 1H, *J* = 18.6 Hz), 3.86 (s, 3H), 2.40 (s, 3H).

Synthesis of 4-(3-methoxyphenyl)-2-butanone

This synthesis was derived from Hagiwara and Uda[5]. 4-(3-methoxyphenyl)-but-3-en-2-one (861.3 mg, 4.89 mmol) was dissolved in 10 mL of absolute ethanol in a 250 mL hydrogenation bottle. Palladium on carbon (93.7 mg, 5 % Pd, 0.044 mmol Pd) was added to the bottle. The solvent was purged by bubbling argon through the liquid for 15 min. The bottle was then loaded onto a Parr hydrogenator. The vessel was charged and purged three times with hydrogen before being charged to 20 psig of hydrogen and refilling as needed to maintain pressure in the bottle. After 20 hr, the pressure was released and the palladium on carbon was removed by filtration through a pad of celite. The filtrate was concentrated to dryness and

the crude oil was purified by automated silica chromatography (solvent system: 5 % EtOAc in hexanes for 1 CV, 5 % to 20 % EtOAc over 10 CV and 20 % EtOAc for 3 CV). 524.2 mg (2.9 mmol, 60 % yield) of 4-(3-methoxyphenyl)-2-butanone was obtained. The spectra obtained matched those reported in the literature[5]. ^{1}H NMR (300 MHz, $CDCl_3$): δ 7.22 (t, 1H, J = 8.2 Hz), 6.68 - 6.87 (m, 3H), 3.81 (s, 3H), 2.91 (t, 2H, J = 8.7 Hz), 2.79 (t, 2H, J = 8.7 Hz), 2.12 (s, 3H).

Synthesis of 4-(2-iodo-5-methoxyphenyl)-2-butanone

This synthesis was adapted from Carson *et al.*[6] 4-(3-methoxyphenyl)-2-butanone (524.2 mg, 2.9 mmol) was dissolved in 10 mL of acetic acid. Iodine (747.0 mg, 2.9 mmol) was added to the solution followed by silver acetate (484.1 mg, 2.9 mmol). A white precipitate formed when the silver acetate was added. After stirring at room temperature for 3 hr, the AgI was removed by filtration and washed with acetic acid. Ethyl ether was added and the layers were separated. The organic layer was washed with water, 2 M NaOH, saturated sodium thiosulfite and brine. The organic layer was then dried with magnesium sulfate and concentrated to dryness. The crude oil was purified by automated silica chromatography (solvent system: 10 % EtOAc in hexanes for 1 CV, 10 % to 40 % EtOAc over 10 CV and 40 % EtOAc for 3 CV). After chromatography 650.6 mg (2.14 mmol, 74 % yield) of 4-(2-iodo-5-methoxyphenyl)-2-butanone was recovered. The spectra obtained matched

those reported in the literature[6]. ^{1}H NMR (300 MHz, $CDCl_3$): δ 7.68 (d, 1H, *J* = 9.9 Hz), 6.83 (d, 1H, *J* = 3 Hz), 6.52 (dd, 1H, *J* = 9.9, 3 Hz), 3.77 (s, 3H), 2.95 (t, 2H, *J* = 6.5 Hz), 2.74 (t, 2H, *J* = 6.5 Hz), 2.18 (s, 3H).

Synthesis of 4-[5-methoxy-2-(2-phenylethynyl)-phenyl]-2-butanone

4-(2-iodo-5-methoxyphenyl)-2-butanone (162.9 mg, 0.54 mmol), sodium acetate (82.0 mg, 1.08 mmol), SBA-15-SH-Pd (25.0 mg, 0.0063 mmol Pd, 1 mol%) and hexamethylbenzene (44.4 mg, 0.27 mmol, internal standard) were combined in a test tube fitted with a septum and purged with argon. DMF (5 mL) and water (0.25 mL) were added to the tube followed by phenyl acetylene (85 µL, 0.77 mmol). The reaction was then placed in a preheated oil bath at 80 °C and stirred for 18 hr. After cooling the reaction to room temperature, the catalyst was filtered of by passing it through a syringe filter. The reaction was then diluted to 25 mL with EtOAc in a volumetric flask and a sample taken for ICPMS analysis of residual palladium. The solvent was then removed and the residue taken up in ethyl ether, the solvent was washed with brine and the organic layer set aside. The aqueous layer was washed with a further two portions of ethyl ether. The combined organic layers were then washed with two portions of brine, dried with magnesium sulfate and concentrated to dryness. The crude oil was purified on an automated silica chromatography system (Solvent system: 10 % EtOAc in hexanes for 1 CV, 10 % to 40 % EtOAc over 10 CV followed by 40 % EtOAc in hexanes for 3

CV). This afforded 114.1 mg (0.41 mmol, 75 % yield) of 4-[5-methoxy-2-(2-phenylethynyl)-phenyl]-2-butanone. The spectra obtained matched those reported in the literature[6]. ^{1}H NMR (400 MHz, $CDCl_3$): δ 7.51 (d, 2H, *J* = 8 Hz), 7.46 (d, 1H, *J* = 10.8 Hz), 7.30 - 7.42 (m, 3H), 6.81 (s, 1H), 6.76 (d, 1H, *J* = 10.8 Hz), 3.83 (s, 3H), 3.13 (t, 2H, *J* = 10.4 Hz), 2.87 (t, 2H, *J* = 10.4 Hz), 2.17 (s, 3H).

Synthesis of 4-Trifluoromethoxyphenyl Pinacol Borane

p-Trifluoromethyoxyphenyl boronic acid (1.06 g, 5.16 mmol) and pinacol (891 mg, 7.54 mmol) were dissolved in benzene (30 mL). The solution was heated to 60 °C for 1 hr. The solvent was then evaporated and the crude oil purified by automated silica chromatography (Solvent system: 4 % EtOAc in hexanes for 1 CV, 4 % to 20 % EtOAc over 10 CV followed by 20 % EtOAc in hexanes for 3 CV). 1.33 g (4.62 mmol, 90 % yield) of pure 4-trifluoromethoxyphenyl pinacol borane was recovered. This molecule is now commercially available. ^{1}H NMR (400 MHz, $CDCl_3$): δ 7.85 (d, 2H, *J* = 10 Hz), 7.21 (d, 2H, *J* = 10 Hz), 1.37 (s, 12H).

Synthesis of 5-cyano-2-fluoro-4'-trifluoromethoxy-biphenyl (ABT-100)

3-Bromo-4-fluorobenzonitrile (110 mg, 0.55 mmol), 4-trifluoromethoxyphenyl pinacol borane (292 mg, 1.01 mmol), potassium

carbonate (188 mg, 1.36 mmol) and SBA-15-SH-Pd (21 mg, 0.0053 mmol, 1.0 mol %) were combined in a test tube fitted with a septum. The tube was purged with a flow of argon for 5 min. DMF (5 mL) and water (0.25 mL) were added to the tube and the reaction placed in a pre-heated oil bath at 80 °C. The reaction was stirred for 16 hr. The solution was poured into brine and extracted with three portions of ethyl ether. The combined organic layers were washed with two portions of brine, dried with magnesium sulfate, filtered and concentrated. The boronic ester co-elutes with the product so the crude mixture was dissolved in THF (10 mL) with sodium hydroxide (56.5 mg) and hydrogen peroxide (1 mL, 30 w/w%). This was stirred for 2 hr. The solution was then poured into brine and washed with three portions of ethyl ether. The combined organics were dried with magnesium sulfate, filtered and concentrated. The crude oil was purified by automated silica chromatography (Solvent system: 3 % EtOAc in hexanes for 1 CV, 3 % to 15 % EtOAc over 10 CV followed by 15 % EtOAc in hexanes for 3 CV). This afforded ABT-100 (125 mg, 0.45 mmol, 81 % yield). The spectra obtained matched those found in the literature[7]. ^{1}H NMR (400 MHz, $CDCl_3$): δ 7.77 (d, 1H, *J* = 7.5 Hz), 7.67 – 7.71 (m, 1H), 7.57 (d, 2H, *J* = 8.6 Hz), 7.35 (d, 2H, *J* = 8.6 Hz), 7.30 (d, 1H, *J* = 7.5 Hz).

Hydrogenation of Diphenylacetylene

Diphenylacetylene (447.7 mg, 2.5 mmol) and SBA-15-SH-Pd (10 mg, 0.04 mmol, 1.6 mol%) were dissolved in 30 mL of methanol in a 250 mL Parr shaker bottle. If quinoline is used as a catalyst poison one drop is added at this time. The solvent was degassed by bubbling argon through the solution for 15 min. The atmosphere in the bottle was changed to hydrogen by charging and evacuating three times. Finally the bottle was charged to 20 psig H_2 and the reaction shaken for 5 hr on a Parr hydrogenator. The catalyst was then removed by filtration and washed with methanol. The solvent was evaporated and 17.6 mg (0.13 mmol) of p-dimethoxybenzene was added as an internal standard. All yields are taken determined by NMR. ^{1}H NMR ($CDCl_3$): δ 7.21, (trans stilbene), 6.62 (cis stilbene), 2.95 (diphenylethane).

Heterogeneity Tests: Polyvinylpyridine/ Polystyrene

4-Bromoacetophenone (98.9mg, 0.50 mmol), phenyl pinacol borane (156 mg, 0.76 mmol), potassium carbonate (138 mg, 1.0 mmol), SBA-15-SH-Pd (14.8 mg, 0.005 mmol, 1 mol %), p-dimethoxybenzene (43.6 mg, 0.32 mmol, internal standard) and polyvinylpyridine (157 mg, 1.5 mmol N, 300 N/Pd) or polystyrene (163 mg) were combined in a test tube. DMF (5 mL) and water (0.25 mL) were added and the tube placed in a pre-heated oil bath at 80 °C for 24 hr. The reaction progress was monitored by GC at various intervals.

Heterogeneity Tests: Quadrapure TU

4-Bromoacetophenone (101 mg, 0.51 mmol), phenyl pinacol borane (158 mg, 0.77 mmol), potassium carbonate (142 mg, 1.03 mmol), SBA-15-SH-Pd (14.4 mg, 0.0049 mmol, 1.0 mol %), p-dimethoxybenzene (32.9 mg, 0.24 mmol, internal standard) and Quadrapure TU (55.5 mg, 0.011 mmol Pd capacity) were combined in a test tube in either an air or argon atmosphere. DMF (5 mL) and water (0.25 mL) or water (5 mL) alone were added and the tube placed in a pre-heated oil bath at 80 °C for 24 hr. The reaction progress was monitored by GC at various intervals.

Heterogeneity Tests: PL Thiourea MP

4-Bromoacetophenone (100 mg, 0.50 mmol), phenyl pinacol borane (155 mg, 0.76 mmol), potassium carbonate (139 mg, 1.01 mmol), SBA-15-SH-Pd (14.5 mg, 0.0049 mmol, 1.0 mol %), p-dimethoxybenzene (32.5 mg, 0.24 mmol, internal standard) and PL-thiourea MP (47.6 mg, 0.050 mmol thiourea) were combined in a test tube. DMF (5 mL) and water (0.25 mL) were added and the tube placed in a pre-heated oil bath at 80 °C for 24 hr. The reaction progress was monitored by GC at various intervals.

Heterogeneity Tests: Three Phase Test

4-Bromoacetophenone (53.1 mg, 0.27 mmol), phenyl pinacol borane (48.4 mg, 0.40 mmol), potassium carbonate (68.8 mg, 0.50 mmol), SBA-15-SH-Pd (8.2 mg, 0.0028 mmol, 1.0 mol %) and the immobilized aryl halide (256.9 mg) were combined in a test tube in either an air or argon atmosphere. DMF (2.5 mL) and water (0.13 mL) or water (2.5 mL) alone was added and the reaction placed in a pre-heated oil bath at 80 °C for 5 hr or 20 hr. The solids were then recovered by filtration and washed with ethyl acetate and dichloromethane. The filtrate was evaporated and p-dimethoxybenzene (24.7 mg, 0.18 mmol) was added as an internal standard for GC.

To hydrolyze the amide, a solution of potassium hydroxide (1.71 g, 30.4 mmol) in ethanol (10 mL) and water (5 mL) was prepared. The recovered solids were added to the solution and heated at 90 °C for 72 hr. The solution was then neutralized with 2M hydrochloric acid and extracted with dichloromethane and ethyl acetate. The combined organics were dried with magnesium sulfate and concentrated. The residue was dissolved in a 1:1 mixture of $CDCl_3$ and D_6-DMSO for NMR analysis. ^{1}H NMR (400 MHz, $CDCl_3$/D_6-DMSO): δ 8.03 (d, 2H, *J* = 9.6 Hz, 4-bromobenzoic acid), 7.84 (d, 2H, *J* = 6.8 Hz, 4-phenylbenzoic acid), 7.80 (d, 2H, *J* = 6.8 Hz, 4-phenylbenzoic acid)7.76 (d, 2H, *J* = 9.6 Hz, 4-bromobenzoic acid).

Suzuki Coupling Recycling Studies

Recycling studies were carried out using the same procedure but scaled up to use 50 or 100 mg of SBA-15-SH-Pd. After each cycle the supernatant was collected by filtration and analyzed by ICPMS for palladium content. The catalyst was then washed with copious amounts of EtOAc (~200 mL) and water to remove residual organics and salts. For the next recycle, the recovered catalyst was weighed and the amounts of reagents calculated based on 1 mol% Pd (assuming >99% Pd retention, confirmed by ICPMS).

6.4 Experimental Procedures from Chapter 4

X-ray Photoelectron Spectroscopy of SBA-15-SH-Pd Catalysts and Related Palladium and Sulfur Compounds

XPS measurements were performed using a Thermo Instruments Microlab 310F surface analysis system (Hastings, UK) under ultrahigh vacuum conditions and using a Mg Kα X-ray source (1253.6eV) at 10 kV anode potential and 10 mA emission current. Scans were acquired at fixed analyzer transmission (FAT) mode at a pass energy of 20 eV. All spectra were calibrated to the C 1s line at 285.0 eV; minor charging effects were observed. Spectra were background-subtracted using a Shirley fit algorithm and using a Powell peak-fitting algorithm within the spectrometer software. Catalyst samples and Pd compounds were prepared in powder form, and spread on Cu tape attached to the XPS sample holder. Air sensitive Pd(0) samples were prepared in a glove box and transferred immediately to the XPS loading chamber.

6.5 Experimental Procedures from Chapter 5

Synthesis of 2,4-Dibromonapthylamine

This synthesis was adapted from Newman, Sankaran and Olson[8]. Bromine (22 mL, 440 mmol) was dissolved in 200 mL of acetic acid. The solution was cooled to 0 °C in an ice bath. 1-Naphthylamine (28.2 g, 197 mmol) was dissolved in 100 mL of acetic acid and added slowly to the solution of bromine. After the addition of the naphthylamine a precipitate formed solidifying the solution, a further 100 mL of acetic acid was added. The reaction was then heated to 60 °C for 15 min. The precipitate was collected by filtration and washed with acetic acid. The solid was suspended in 1 M NaOH (colour change from green to purple) and the powder recovered by filtration, washing with lots of water. The crude solid was recrystallized from ethanol affording 41.7 g (138 mmol, 70 % yield) of 2,4-dibromonaphthylamine. The spectra obtained matched those reported in the literature[8]. ^{1}H NMR (300 MHz, $CDCl_3$): δ 8.19 (d, 1H, J = 8.4 Hz), 7.83 (d, 2H, J = 10.8 Hz), 7.64 (t, 1H, J = 8.4 Hz), 7.56 (t, 1H, J = 8.4 Hz).

Synthesis of 4-Bromonaphth[1,2-d][1,2,3]oxadiazole

This procedure was derived from Newman, Sankaran and Olson[8]. 2,4-Dibromonaphthylamine (10.0 g, 33.3 mmol) was dissolved in a mixture of acetic acid (150 mL) and propionic acid (25 mL). The solution was cooled to 0 °C in an ice bath and the sodium nitrite (2.7 g, 39.3 mmol) was then added

slowly over one minute. The reaction was stirred for 10 min in the ice bath and then poured into 200 mL of ice water. The solution was quickly filtered as the tar produced would gum up the filter paper. The filtrate was then added to 3 L of water and the product precipitated out over 30 min. Collection by filtration afforded 5.6 g (22.4 mmol, 67 % yield) of 4-bromonaphth[1,2-d][1,2,3]oxadiazole. As in the literature preparation[8] this product was carried forward with out further purification or characterization.

Synthesis of 4-Bromo-2-naphthol

This procedure was adapted from Newman, Sankaran and Olson[8]. 4-Bromonaphth[1,2-d][1,2,3]oxadiazole (4.5 g, 18.1 mmol) was dissolved in ethanol (90 mL) and cooled to 0 °C in an ice bath. Sodium borohydride (692.0 mg, 18.2 mmol) was added slowly and the solution bubbled vigorously. The solution was stirred for 3 hr at 0 °C ensuring the the gas evolution was complete. The reaction was then poured into a solution of water (500 mL) and hydrochloric acid (5 mL) to quench any remaining borohydride. 2 M sodium hydroxide was added to the solution until the pH was basic. The product was then extracted with dichloromethane. The aqueous layer was then acidified with 2 M hydrochloric acid and washed twice with ethyl ether. The organics were combined and washed twice with brine, dried with magnesium sulfate and concentrated to dryness. 4.0 g (18.0 mmol, 99 % yield) of 4-bromo-2-naphthol was recovered. The spectra obtained matched those reported in the

literature[8]. ^{1}H NMR (400MHz, $CDCl_3$): δ 8.15 (d, 1H, *J* = 12 Hz), 7.66 (d, 1H, *J* = 16.8 Hz), 7.39 - 7.55 (m, 3H), 7.15 (s, 1H).

Synthesis of 4,4'-Dibromo-1,1'-binaphth-2,2'-diol

This synthesis was derived from Chow and Ng[9]. In a round bottomed flask, 4-bromo-2-naphthol (4.5 g, 20.3 mmol) was dissolved in 125 mL of dry dichloromethane. Copper (II) chloro hydroxo tetramethyl ethylene diamine complex (942.6 mg, 2.03 mmol, 10 mol%) was added slowly to the solution. The reaction was stirred open to air at room temperature for 4 hr. The solution was diluted with dichloromethane and washed with three portions of saturated ammonium chloride to remove the copper. The organics were dried with magnesium sulfate and concentrated to dryness to afford 3.8 g (8.57 mmol, 85 % yield) of 4,4'-dibromo-1,1'-binaphth-2,2'-diol. The spectra obtained matched those reported in the literature[9]. ^{1}H NMR (300 MHz, $CDCl_3$): δ 8.29 (d, 2H, *J* = 11.4 Hz), 7.78 (s, 2H), 7.50 (t, 2H, *J* = 11.4 Hz), 7.36 (t, 2H, *J* = 5.7 Hz), 7.14 (d, 2H, *J* = 5.7 Hz).

Synthesis of 4,4'-Dibromo-2,2'-dimethoxymethyl-1,1'-binaphth-2,2'-diol

Sodium hydride (475.2 mg, 19.8 mmol) was dissolved in 30 mL of dry THF. 4,4'-dibromo-1,1'-binaphth-2,2'-diol (2.9 g, 6.63 mmol) was dissolved in 50 mL of dry THF and added to the solution of sodium hydride. The reaction

was stirred for 30 min under argon. Methoxymethyl chloride (1.13 mL, 14.9 mmol) was then added and the reaction stirred for 4 hr. The solution was diluted with ethyl ether and washed with water. The aqueous layer was then further extracted with ethyl ether and the organic layers combined. The organic layer was then washed with brine, dried with magnesium sulfate and concentrated to dryness. The crude material was purified on an automated silica chromatography system (solvent conditions: 4 % EtOAc in hexanes for 1 CV, 4 % to 16 % EtOAc over 10 CV and 16 % EtOAc for 3 CV). 2.2 g (4.1 mmol, 62 %) of 4,4'-Dibromo-2,2'-dimethoxymethyl-1,1'-binaphth-2,2'-diol was recovered after the column. ^{1}H NMR (400 MHz, $CDCl_3$): δ 8.26 (d, 2H, *J* = 15.2 Hz), 7.93 (s, 2H), 7.46 (t, 2H, *J* = 11.2 Hz), 7.24 - 7.35 (m, 2H), 7.15 (d, 2H, *J* = 11.2 Hz), 5.09 (d, 2H, *J* = 11.2 Hz), 4.99 (d, 2H, *J* = 11.2 Hz), 3.19 (s, 6H). ^{13}C NMR (100 MHz, $CDCl_3$): δ 152.26, 134.40, 127.90, 126.67, 125.70, 125.46, 123.64, 121.18, 120.38, 95.07, 55.93.

Synthesis of 4-Bromo-2-methoxy-naphthalene

4-Bromo-2-naphthol (3.5 g, 15.8 mmol) was dissolved in acetone (150 mL) in a round bottomed flask. Potassium carbonate (4.4 g, 31.8 mmol) and methyl iodide (3 mL, 48.2 mmol) were added. The flask was fitted with a reflux condenser and heated to reflux for 18 hr. Upon cooling, the solvent was removed and the residue dissolved in ethyl ether. 2 M Hydrochloric acid was added to the flask (careful lots of bubbling occurs). The layers were separated

and the organic layers washed with brine, dried with magnesium sulfate and concentrated to dryness. The crude material was purified on an automated silica chromatography system (solvent conditions: 5 % EtOAc in hexanes for 1 CV, 5 % to 20 % EtOAc over 10 CV and 20 % EtOAc for 3 CV). 3.1 g (12.9 mmol, 82 % yield) of 4-bromo-2-methoxynaphthylene was recovered. The spectra obtained matched those found in the literature[10]. ^{1}H NMR (400 MHz, $CDCl_3$): δ 8.15 (d, 1H, *J* = 11.6 Hz), 7.74 (d, 1H, *J* = 11.2 Hz), 7.52 (d, 1H, *J* = 3.6 Hz), 7.47 (t, 2H, *J* = 11.6 Hz), 7.14 (d, 1H, *J* = 3.6 Hz), 3.93 (s, 3H).

Attempted synthesis of 4,4'-Dibromo-2,2'-dimethoxy-1,1'-binaphthyl

In a round bottomed flask, 4-bromo-2-methoxynaphthylene (3.1 g, 12.9 mmol) was dissolved in 100 mL of dry dichloromethane. Copper (II) chloro hydroxo tetramethyl ethylene diamine complex (604.4 mg, 1.3 mmol, 10 mol%) was added and the solution stirred open to air for 4 hr. The reaction was diluted with dichloromethane and washed with two portions of saturated ammonium chloride to remove the copper. The organic layer was dried with magnesium sulfate and concentrated to dryness. A crude ^{1}H NMR indicated that no coupling had taken place and only starting material had been recovered.

Synthesis of 4,4'-Dibromo-2,2'-dimethoxy-1,1'-binaphthyl

In a round bottomed flask, 4,4'-Dibromo-1,1'-binaphth-2,2'-diol (2.8 g, 6.3 mmol) was dissolved in acetone (100 mL). Potassium carbonate (4.0 g, 28.7 mmol) and methyl iodide (1.8 mL, 28.9 mmol) and the solution refluxed for 18 hr. Upon cooling the solvent was removed and the residue dissolved in ethyl ether. The flask was rinsed with 2 M hydrochloric acid (caution excessive bubbling) and the two layers separated. The organic layer was washed with brine, dried with magnesium sulfate and concentrated to dryness. The crude material was then purified on a silica column with 20 % EtOAc in hexanes. The material was insoluble in the chromatography solvent so it was dry loaded on silica. 2.5 g (5.24 mmol, 83 % yield) of 4,4'-dibromo-2,2'-dimethoxy-1,1'-binaphthyl was obtained. The spectra obtained matched those found in the literature[9]. ^{1}H NMR (500 MHz, $CDCl_3$): δ 8.26 (d, 2H, *J* = 9 Hz), 7.79 (s, 2H), 7.45 (t, 2H, *J* = 9 Hz), 7.24 - 7.32 (m, 2H), 7.11 (d, 2H, *J* = 15 Hz), 3.78 (s, 6H).

Synthesis of 4,4'-Bis(triethoxysilyl)-2,2'-dimethoxy-1,1'-binaphthyl

In a flame-dried round bottomed flask, 4,4'-dibromo-2,2'-dimethoxy binaphthyl (487.4 mg, 1.03 mmol) was dissolved in dry THF (10 mL). This solution was cooled to -88 °C in an isopropanol-liquid nitrogen bath for 30 min. n-Butyl lithium (2.62 mL, 2.2 mmol, 0.84 M solution in hexanes) was

added slowly with a colour change from yellow to blue-green. After stirring for another 30 min, chloro triethoxysilane (430 µL, 2.19 mmol) was added. The cold bath was removed and the solution allowed to warm up to room temperature over night. The solution was then diluted with ethyl ether and washed with three portions of brine. The organic layer was dried with magnesium sulfate and concentrated to dryness. The crude oil was purified on a silica column, solvent conditions 15 % EtOAc in hexanes. 88.3 mg (0.138 mmol, 13 % yield) of 4,4'-bis(triethoxysilyl)-2,2'-dimethoxy-1,1'-binaphthyl was recovered. This product was recovered cleanly once and only proton NMR was obtained. Attempts to repeat the synthesis failed. ^{1}H NMR (400 MHz, $CDCl_3$): δ 8.38 (d, 2H, *J* = 8.4 Hz), 8.01 (s, 2H), 7.39 (td, 2H, *J* = 8.4, 1.2 Hz), 7.22 (td, 2H, *J* = 6.6, 1.2 Hz), 7.13 (d, 2H, *J* = 8.4 Hz), 4.05 (q, 12H, *J* = 7.0 Hz), 3.81 (s, 6H), 1.37 (t, 18H, *J* = 7.0 Hz).

Synthesis of 3-Bromophenyl(diphenyl)phosphine oxide

This material was prepared using a synthesis adapted from Lustenberger and Diederich[11]. m-Dibromobenzene (1.2 mL, 2.34 g, 9.93 mmol) was dissolved in 40 mL of freshly refluxed THF and cooled to -88 °C in an isopropanol/ liquid nitrogen bath. n-Butyl lithium (10.66 mmol, 1.05 eq) was added drop wise and the solution stirred for 45 min to complete the lithium halogen exchange. Chlorodiphenylphoshine (900 µL, 1.11g, 5.01 mmol) was then added drop wise and the solution stirred overnight warming to room

temperature. The THF was then removed by rotary evaporation and the residue dissolved in 40 mL of DCM and cooled to 0 °C in an ice bath. Hydrogen peroxide (30 % aqueous solution, 30 mL, 290 mmol) was added and the solution stirred for 4 hr at 0 °C. The solution was diluted with water and the layers separated. The organic layer was washed with saturated sodium sulfite, dried with magnesium sulfate and concentrated. The crude oil was purified by column chromatography using an automated flash chromatography system. The solvent system used was 2 % EtOAc / 98 % hexanes for one column volume, 2-10 % EtOAc linear ramp over ten column volumes and finally five column volumes at 10 % EtOAc/ 90 % hexanes. This afforded 3.36 g (9.42 mmol, 95%) of 3-bromophenyl(diphenyl)phosphine oxide. The spectra obtained matched those reported in the literature[11]. ^{1}H NMR (500MHz, $CDCl_3$): δ 7.85 (d, 1H, *J* = 13.3 Hz), 7.64 – 7.74 (m, 5H), 7.56 – 7.64 (m, 3H), 7.47 – 7.56 (m, 4H), 7.36 (dt, 1H, *J* = 4.0, 8.8 Hz). ^{13}C NMR (125MHz, $CDCl_3$): δ 135.47, 135.13, 135.04, 132.66, 132.50, 132.43, 131.01, 130.93, 130.60, 130.50, 129.13, 129.04. ^{31}P NMR (135 MHz, $CDCl_3$): δ 29.05.

Synthesis of 3-Iodophenyl(diphenyl)phosphine oxide

This procedure was adapted from Klapars and Buchwald[12]. 3-Bromophenyl(diphenyl)phosphine oxide (356.2 mg, 0.997 mmol), copper (I) iodide (17.3 mg, 0.0908 mmol, 9 mol%) and sodium iodide (303.9 mg, 2.03 mmol, 2 eq) were combined in a dry schlenk tube under argon. N,N'-

dimethylethylenediamine (10 μL, 0.138 mmol, 13.8 mol%) was added followed by 1 mL of dioxane. The septum was changed for a glass stopper and the tube was heated to 110 °C for 23 hr. Upon cooling, 5 mL of ammonium hydroxide (30% aqueous solution) was added to remove the copper. The tube was then washed with water and poured into a seperatory funnel. The aqueous layer was washed with three portions of DCM. The organics were dried with magnesium sulfate and concentrated to afford 392.0 mg (0.970 mmol, 97%) of product. ^{1}H NMR (500MHz, $CDCl_3$): δ 8.06 (d, 1H, *J* = 14.4 Hz), 7.90 (d, 1H, *J* = 8.8 Hz), 7.63 – 7.72 (m, 5H), 7.54 – 7.63 (m, 2H), 7.46 – 7.54 (m, 4H), 7.17 – 7.25 (m, 1H). ^{13}C NMR (125MHz, $CDCl_3$): δ 136.26, 132.55, 132.40, 132.30, 131.62, 131.40, 131.31, 130.50, 130.38, 129.03, 128.90, 95.23. ^{31}P NMR (135 MHz, $CDCl_3$): δ 28.64.

Synthesis of 2,2'-Bis(diphenylphosphino)-1,1'-binapthyl oxide (BINAPO)

This procedure was derived from Lemaire *et al.*[13] 2,2'-Bis(diphenylphosphino)-1,1'-binaphthalene (BINAP, 4.99 g, 8.01 mmol) was dissolved in 150 mL of DCM and cooled to 0 °C in an ice bath. Hydrogen peroxide (30 % aqueous solution, 30 mL, 290 mmol) was added to the solution and reacted for 4 hr at 0 °C. The reaction was halted by the addition of 100 mL of water and the layers separated. The organic layer was washes with a saturated solution of sodium sulfite, dried with magnesium sulfate and concentrated to give the product (5.20 g, 7.94 mmol, 99%). The BINAPO was

used without further purification. The spectra obtained matched those reported in the literature[13]. ^{1}H NMR (500 MHz, $CDCl_3$): δ 7.88 (dd, 2H, *J* = 8, 3.5 Hz), 7.84 (d, 2H, *J* = 7.5 Hz), 7.73 (dd, 4H, *J* = 11, 6.5 Hz), 7.35 – 7.94 (m, 12H), 7.22 – 7.32 (m, 8H), 6.79 – 6.86 (m, 4H). ^{31}P NMR (135 MHz, $CDCl_3$): δ 29.48.

Synthesis of 4,4'-Dibromo-2,2'-Bis(diphenylphosphino)-1,1'-binaphthyl oxide

This material was prepared using a synthesis from Lemaire *et al.*[13] BINAPO (1.31 g, 2.00 mmol) was taken up in 40 mL of DCM. Pyridine (200 µL, 196 mg, 2.48 mmol) was added followed by bromine (1 mL, 320 mg, 2.01 mmol). The reaction was stirred at room temperature for 20 hr. The residual bromine was quenched by addition of a saturated solution of sodium sulfite, the organic layer was then washed with saturated sodium bicarbonate and brine. The DCM was then removed and the residue resubjected to the bromination conditions. Upon work up the organic layer was dried with magnesium sulfate and concentrated. The crude product was purified by automated flash chromatography system. The solvent system used was 22% EtOAc/ 78% hexanes for one column volume, 22-90% EtOAc linear ramp over ten column volumes and finally five column volumes at 90% EtOAc/ 10% hexanes. This afforded 1.02 g (1.26 mmol, 63 %) of the desired product. The spectra obtained matched those reported in the literature[13]. ^{1}H NMR (500

MHz, $CDCl_3$): δ 8.24 (d, 2H, *J* = 8.5 Hz), 7.75 (d, 2H, *J* = 5.5 Hz), 7.68 (dd, 4H, *J* = 12, 7.5 Hz), 7.49 (t, 2H, *J* = 7.5 Hz), 7.38 - 7.45 (m, 8H), 7.25 - 7.33 (m, 8H), 6.89 (t, 2H, *J* = 8 Hz), 6.82 (d, 2H, *J* = 8.5 Hz). ^{31}P NMR (135MHz, $CDCl_3$): δ 28.26.

Synthesis of 4,4'-Diiodo-2,2'-Bis(diphenylphosphino)-1,1'-binaphthyl oxide via an Aromatic Finkelstein Reaction

This material was prepared using a modified synthesis from Klapars and Buchwald[12]. 4,4'-dibromoBINAPO (324.3 mg, 0.399 mmol), copper (I) iodide (84.5 mg, 0.444 mmol, 1.1 eq) and sodium iodide (598.9 mg, 4.00 mmol, 10 eq) were combined in a dry schlenk tube under argon. N,N'-dimethylethylenediamine (100 µL, 1.43 mmol, 3.6 eq) was added followed by 1 mL of dioxane. The flask was then heated at 110 °C for 3 days. 10 mL of ammonium hydroxide (30% aqueous solution) was added to chelate copper. The tube was washed with 10 mL of water and the two aqueous layers were then washed with three portions of DCM. The organic layer was dried with magnesium sulfate and concentrated. The resulting product was a mixture of diiodo, dibromo and iodo/bromo species. The crude reaction product was then treated with a further batch of copper (I) iodide (83.3 mg, 0.438 mmol, 1.1 eq), sodium iodide (599.3 mg, 4.00 mmol, 10 eq) and N,N'-dimethylethylenediamine (100 µL, 1.43 mmol, 3.6 eq) in 1 mL of dioxane for 3 days at 110 °C. After the same work up, 288.7 mg was recovered and purified

by column chromatography using an automated flash chromatography system. The solvent system used was 22% EtOAc/ 78% hexanes for one column volume, 22-90% EtOAc linear ramp over ten column volumes and finally five column volumes at 90% EtOAc/ 10% hexanes. This afforded 75.0 mg (0.083 mmol, 21%) pure 4,4'-diiodoBINAPO. This molecule was synthesized only once due to the difficulty of synthesis, thus we chose to pursue alternate routes and only proton and phosphorous spectra were obtained. ^{1}H NMR (500 MHz, $CDCl_3$): δ 8.08 (d, 2H, *J* = 8.5 Hz), 8.04 (dd, 2H, *J* = 6.5, 3 Hz), 7.62 – 7.78 (m, 6H), 7.39 - 7.50 (m, 8H), 7.27 - 7.30 (m, 8H), 6.86 (m, 2H), 6.79 (m, 2H). ^{31}P NMR (135 MHz, $CDCl_3$): δ 28.69.

Synthesis of 5,5'-Diiodo-2,2'-Bis(diphenylphosphino)-1,1'-binaphthyl oxide

This procedure was modified from Olah *et al.*[14] Triflic anhydride (750 µL, 1.26 g, 4.46 mmol) was dissolved in 10 mL of acetonitrile and cooled to 0 °C in an ice bath. 75 µL of water (4.17 mmol) was then added to form triflic acid followed by 2,2'-Bis(diphenylphosphino)-1,1'-binapthyl oxide (655 mg, 1.0 mmol) and finally N-iodosuccinimide (675 mg, 3.0 mmol). The ice bath was then removed and the reaction stirred at room temperature for 20hr. The solvent was removed in vacuo and the residue dissolved in DCM. The organic solvent was washed with saturated Na_2SO_3 and 2M NaOH. The organic layer was then dried with $MgSO_4$ and concentrated to dryness. The material was

then suspended in THF and the solid recovered by filtration. The powder was well washed with THF to remove any impurities. An off white solid was recovered from filtration (734 mg, 0.81 mmol, 81%). ^{1}H NMR (500MHz, $CDCl_3$): δ 8.18 (d, 2H, *J* = 8.6 Hz), 7.97 (d, 2H, *J* = 7.2 Hz), 7.73 (dd, 4H, *J* = 11.7, 7.9 Hz), 7.54 (dd, 2H, *J* = 11.0, 9.3 Hz), 7.41 (m, 8H), 7.33 (m, 4H), 7.27 (m, 4H), 6.76 (d, 2H, *J* = 8.5 Hz), 6.51 (t, 2H, *J* = 7.7 Hz). ^{13}C NMR (125MHz, $CDCl_3$): δ 141.39, 139.44, 135.68, 134.82, 132.71, 132.25, 131.90, 130.36, 130.21, 129.81, 128.77, 128.46, 128.34, 127.26, 99.17. ^{31}P NMR (135 MHz, $CDCl_3$): δ 30.02. ES^+: MH^+ = 906.5 m/Z.

Synthesis of 5,5'-Bis(triethoxysilyl)-2,2'-Bis(diphenylphosphino)-1,1'-binaphthyl oxide

This procedure was adapted from Masuda *et al.*[15,16] Rhodium (I) cyclooctene chloride dimer (5.2 mg, 0.021 mmol, 7.6 mol %) and 5,5'-diiodoBINAPO (252.0 mg, 0.278 mmol) were combined in a small schlenk tube under argon. DMF (1 mL) stored over molecular sieves for dryness was added to the tube followed by triethylamine (230 µL, 1.65 mmol). This solution was heated to 80 °C in an oil bath for 15 min before the addition of triethoxysilane (200 µL, 1.09 mmol) using a syringe pump, the addition occurred over a period of 2 hr. The reaction was then stirred for 3 hr at 80 °C. The DMF was then removed under high vacuum overnight and the residue taken up in DCM. The liquid was passed through a plug of celite to remove

any residual rhodium. The eluent of the celite plug was then concentrated and taken up in DCM again to be passed through a plug of silica. The crude material recovered from the silica plug is then concentrated and purified by preparative thin layer chromatography using 3:2 THF: hexane as the eluting solvent. This gave 53.5 mg (0.055 mmol, 20 % yield) of 5,5'-bis(triethoxysilyl) BINAPO. ^{1}H NMR (400 MHz, $CDCl_3$): δ 8.37 (dd, 2H, *J* = 8.8, 2.0 Hz) 7.79 (dd, 2H, *J* = 6.6, 1.0 Hz), 7.74 (dd, 4H, *J* = 12.2, 7.0 Hz), 7.46 (dd, 2H, *J* = 11.6, 8.8 Hz), 7.38 - 7.41 (m, 12H), 7.18 (td, 4H, *J* = 7.6, 2.4 Hz), 6.72 (d, 2H, *J* = 8 Hz), 6.63 (dd, 2H, *J* = 8.4, 6.8 Hz), 3.96 (q, 12H, *J* = 7.0 Hz), 1.31 (t, 18H, *J* = 7.0 Hz). ^{13}C NMR (100MHz, $CDCl_3$): δ 138.11, 137.49, 132.82, 132.71, 132.34, 132.26, 131.41, 131.09, 130.32, 129.04, 128.45, 128.32, 128.10, 127.98, 124.99, 59.22, 18.58. ^{31}P NMR (135 MHz, $CDCl_3$): δ 28.50.

Synthesis of 15 % BINAPO/ 85 % Biphenyl Periodic Mesoporous Organosilicate

This procedure was adapted from Crudden *et al.*[17] Brij 76 (395.6 mg) surfactant was dissolved in 11.3 g of water and 858 mg of concentrated hydrochloric acid at 60 °C for 1 hr in a propylene jar (Nalgene). Sodium chloride (1.2 g) was added and the solution kept at 60 °C for a further 3 hr. 5,5'-Bis(triethyoxysilyl) BINAPO (156.2 mg, 0.16 mmol) and 4,4'-bis(triethoxysilyl) biphenyl (456.7 mg, 0.85 mmol) were combined in a separate flask and dissolved in absolute ethanol (477 mg). The silyl monomer

solution was added to the surfactant solution and immediately a white precipitate formed. This solution was stirred for 20 hr at 60 °C. The temperature was then increased to 80 °C for a static aging of 24 hr. The solid was then recovered by filtration and washed with plenty of water. The surfactant was removed from the pores by soxhlet extraction with 1 % concentrated hydrochloric acid in ethanol for 4 days.

Synthesis of 15 % BINAPO/ 85 % TEOS Periodic Mesoporous Organosilicate (BINAPO-BiPh PMO)

This procedure was derived from Crudden *et al.*[17] Brij 76 (145 mg) surfactant was dissolved in 4.16 g of water and 314 mg of concentrated hydrochloric acid at 60 °C for 1 hr in a propylene jar. Sodium chloride (427 mg) was then added and the solution stirred at 60 °C for a further 3 hr. 5,5'-Bis(triethoxysilyl) BINAPO (56.7 mg) and tetraethylorthosilicate (142 mg) were combined and dissolved in ethanol (173 mg). This solution was then added to the surfactant solution and a white precipitate formed immediately. The silicate was stirred for 20 hr at 60 °C. The temperature was then increased to 80 °C and the material statically aged for 24 hr. The powder was recovered by filtration and washed with water. The surfactant was then removed by soxhlet extraction with 1 % concentrated hydrochloric acid in ethanol for 4 days. 155.5 mg of material was recovered.

Reduction of Triphenylphosphine Oxide: Screen of reductants

Triphenylphosphine oxide (50.53 mg, 0.18 mmol) was dissolved in toluene (1 mL) in a 20 mL vial. One of the reductants: sodium borohydride (71.85 mg, 1.90 mmol), trichlorosilane (60 µL, 0.59 mmol), phenylsilane (90 µL, 0.73 mmol), diisobutyl aluminum hydride (1.5 M, 0.6 mL, 0.90 mmol), lithium aluminum hydride (36.23 mg, 0.95 mmol), tributyl tin (250 µL, 0.93 mmol), borane (1 M, 2 mL, 2 mmol) or hydrazine (30 µL, 0.95 mmol) was added and the solution stirred at room temperature for 6 h then heated to 60 °C for 14 h. Samples were taken periodically to monitor the reduction by GC.

Attempted Reduction of Triphenylphosphine oxide: Methyl Iodide and Lithium Aluminum Hydride

This procedure was modified from Imamoto *et al.*[18] Triphenylphosphine oxide (49.85 mg, 0.18 mmol) was dissolved in dimethoxyethane (1 mL) in a 20 mL glass vial. Methyl iodide (30 µL, 0.48 mmol) was added and the reaction stirred at room temperature for 2 h. The reaction was then cooled to 0 °C in an ice bath and lithium aluminum hydride (36.13 mg, 0.95 mg) was added. This caused the solution to bubble vigorously. The solution was then stirred for a further 19 h. Samples were taken periodically to monitor the reduction by GC. No reduction was observed with these conditions.

Attempted Reduction of Triphenylphosphine oxide: DIBAL and Borane

This procedure was adapted from Busacca *et al.*[19] Triphenylphosphine oxide (49.89 mg, 0.18 mmol) was dissolved in borane-THF solution (1 M, 2 mL, 2 mmol BH_3) in a 20 mL vial. Diisobutyl aluminum hydride (1.5 M, 0.6 mL, 0.90 mmol) was then added and the solution stirred for 21 h. Samples were taken periodically to monitor the reduction by GC. No reduction was observed with these conditions.

Attempted Reduction of BINAPO PMO with Trichlorosilane

This procedure was developed from Shimada *et al.*[20] rac-BINAPO-BiPh PMO (176.3 mg) was suspended in toluene (30 mL) in a round bottom flask. Trichlorosilane (500 µL, 4.95 mmol) was added and the flask fitted with a condenser. The solution was heated to reflux for 3 h. The solid was recovered by filtration and washed with toluene and ethyl ether. No change in the P-C_{aryl} stretch was observed in the IR spectrum so the material was resuspended in toluene (30 mL) and trichlorosilane (500 µL, 4.95 mmol) for a further 48 h. Again the powder was recovered by filtration and washed with toluene and ethyl ether. IR and ^{31}P NMR demonstrate that little or no reduction occurred.

Attempted Reduction of BINAPO PMO with Phenylsilane

This procedure was adapted from Kant *et al.*[21] rac-BINAPO-BiPh PMO (54.8 mg) was suspended in phenyl silane (2 mL, 16.2 mmol) in a round bottom flask. The flask was fitted with a condenser and heated to reflux for 5 days. The powder was collected by filtration and washed with ethyl ether. IR and ^{31}P NMR demonstrate that little or no reduction occurred.

Protection of Surface Silanols in BINAPO PMO with Trimethylsilyl Chloride

rac-BINAPO-BiPh PMO (55.38 mg) was suspended in toluene (5 mL) in a round bottom flask. Trimethylsilyl chloride (200 µL, 1.58 mmol) and pyridine (120 µL, 1.49 mmol) were added and the flask fitted with a condenser. The solution was heated to 105 °C for 18 h. The powder was then collected by filtration and washed with ethyl ether and hot ethanol. rac-BINAPO-BiPh-TMS PMO (55.1 mg) was recovered.

Reduction of Protected BINAPO PMO

This procedure was adapted from McDonald *et al.*[22] rac-BINAPO-BiPh-TMS PMO (55.1 mg) was suspended in phenyl silane (2 mL, 16.2 mmol) in a round bottom flask. The flask was fitted with a condenser and heated to reflux

(119-121 °C). After 1 h, trichlorosilane (100 μL, 0.99 mmol) was added through the condenser. A further two portions of trichlorosilane was added after 3 and 16 h. The solution was stirred for an additional 8 h after the last addition of silane. The powder was then recovered by filtration and washed with dichloromethane, acetone and hot ethanol. rac-BINAP-BiPh-TMS PMO (55.6 mg) was recovered. ^{31}P NMR indicates that some of the phosphine oxides have been reduced however the major phosphorus species is the oxide. ^{31}P NMR (CP-MAS): δ 27.26, 14.92.

6.6 References

(1) Zhao, D.; Huo, Q.; Feng, J.; Chmelka, B.F.; Stucky, G.D. *J. Am. Chem. Soc.* **1998**, *120*, 6024.
(2) Melaimi, M.; Mathey, F.; Le Floch, P. *J. Organomet. Chem.* **2001**, *640*, 197.
(3) Collot, V.; Dallemagne, P.; Bovy, P.R.; Rault, S. *Tetrahedron* **1999**, *55*, 6917.
(4) Evans, D.A.; Gauchet-Prunet, J.A.; Carreira, E.M.; Charette, A. *J. Org. Chem.* **1991**, *56*, 741.
(5) Hagiwara, H.; Uda, H. *J. Chem. Soc. Perkin Trans. I* **1986**, 629.
(6) Carson, J.R.; Almond, H.R.; Brannan, M.D.; Carmosin, R.J.; Flaim, S.F.; Gill, A.; Gleason, M.M.; Keely, S.L.; Ludovici, D.W.; Pitis, P.M.; Rebarchak, M.C.; Villani, F.J. *J. Med. Chem.* **1988**, *31*, 630.
(7) Rozema, M.J.; Kruger, A.W.; Rohde, B.D.; Shelat, B.; Bhagavatula, L.; Tien, J.J.; Zhang, W.; Henry, R.F. *Tetrahedron* **2005**, *61*, 4419.
(8) Newman, M.S.; Sankaran, V.; Olson, D.R. *J. Am. Chem. Soc.* **1976**, *98*, 3237.
(9) Chow, H.F.; Ng, M.K. *Tetrahedron: Asymmetry* **1996**, *7*, 2251.
(10) Demirtas, I.; Erenler, R.; Cakmak, O. *J. Chem. Res. Synopses* **2002**, *10*, 524.
(11) Lustenberger, P.; Diederich, F. *Helv. Chim. Acta* **2000**, *83*, 2865.
(12) Klapars, A.; Buchwald, S.L. *J. Am. Chem. Soc.* **2002**, *124*, 14844.
(13) Berthod, M.; Saluzzo, C.; Mignani, G.; Lemaire, M. *Tetrahedron: Asymmetry* **2004**, *15*, 639.
(14) Olah, G.A.; Wang, Q.; Sandford, G.; Prakash, G.K.S. *J. Org. Chem.* **1993**, *58*, 3194.
(15) Murata, M.; Ishikura, M.; Nagata, M.; Watanabe, S.; Masuda, Y. *Org. Lett.* **2002**, *4*, 1843.
(16) Murata, M.; Yamasaki, H.; Ueta, T.; Nagata, M.; Ishikura, M.; Watanabe, S.; Masuda, Y. *Tetrahedron* **2007**, *63*, 4087.
(17) MacQuarrie, S.; Thompson, M.P.; Blanc, A.; Mosey, N.J.; Lemieux, R.P.; Crudden, C.M. *J. Am. Chem. Soc.* **2008**, *130*, 14099.
(18) Imamoto, T.; Kikuchi, S.I.; Miura, T.; Wada, Y. *Org. Lett.* **2001**, *3*, 87.
(19) Busacca, C.A.; Raju, R.; Grinberg, N.; Haddad, N.; James-Jones, P.; Lee, H.; Lorenz, J.C.; Saha, A.; Senanayake, C.H. *J. Org. Chem.* **2008**, *73*, 1524.
(20) Shimada, T.; Suda, M.; Nagano, T.; Kakiuchi, K. *J. Org. Chem.* **2005**, *70*, 10178.
(21) Kant, M.; Bischoff, S.; Siefken, R.; Grundemann, E.; Kockritz, A. *Eur. J. Org. Chem.* **2001**, 477.
(22) McDonald, A.R.; Muller, C.; Vogt, D.; van Klink, G.P.M.; van Koten, G. *Green Chem.* **2008**, *10*, 424.

Appendix A: Tables of XPS Data

Table A.1: Palladium XPS 3d5/2 and Auger MNN data

Entry	Sample	Ref	Pd $3d_{5/2}$/MNN XPS BE	Pd $3d_{5/2}$/MNN XAES KE	Pd $3d_{5/2}$/MNN α'
1	SiO_2-SH No Pd	1	-		-
2	SiO_2-SH-Pd 1:1 Unused	1	337.7	325.0	662.7
3	SiO_2-SH-Pd 2:1 Unused	1	337.9	324.2	662.1
4	SiO_2-SH-Pd 3:1 Unused	1	337.8	324.6	662.4
5	SiO_2-SH-Pd 4:1 Unused	1	337.9	324.7	662.6
6	SiO_2-SH-Pd Used 1x	1	337.4	325.2	662.7
7	SiO_2-SH-Pd Used 2x	1	337.4	325.7	663.1
8	SiO_2-SH-Pd Used 3x	1	337.4	325.8	663.2
9	SiO_2-SH-Pd Used 4x	1	337.8	325.0	662.9
10	SBA-15-SH-Pd (g) Unused	1	338.0	324.4	662.4
11	SBA-15-SH-Pd (g) Used 1x	1	337.5	325.3	662.8
12	SBA-15-SH-Pd (g) Used 2x	1	337.6	325.0	662.5
13	SBA-15-SH-Pd (g) Used 3x	1	337.5	325.2	662.7
14	SBA-15-SH-Pd (cc) Unused	1	337.7	324.8	662.5
15	SBA-15-SH-Pd (cc) Used 1x	1	337.5	326.9	664.3
16	SBA-15-SH-Pd (cc) Used 3x	1	337.3	325.5	662.8
17	Al-SBA-15-SH-Pd Unused	1	338.1	324.0	662.2
18	Al-SBA-15-SH-Pd Used 2x	1	337.4	325.5	662.8
19	Al-SBA-15-SH-Pd Used 3x	1	337.3	325.9	663.2
20	Al-SBA-15-SH-Pd Used 4x	1	337.3	325.4	662.7
21	Palladium (II) Acetate	1	338.8	324.8	663.6
22	Palladium (II) Oxide	1	338.1	327.5	665.6
23	Palladium (II) Sulfide	1	337.6	325.1	662.7
24	Palladium (II) Iodide	1	337.1	326.2	663.3
25	Palladium Powder	1	335.7	326.9	662.6
26		1	336.9	331.6	668.5
27	Palladium on Carbon	1	335.6	327.9	663.5
28		1	337.3	327.9	665.2
29	Palladium on Barium Sulfate	1	337.3	328.4	665.7
30	Tetrakis(triphenylphosphine) Palladium (0)	1	337.0	325.9	663.0
31	Bis(dibenzylideneacetone) Palladium (0)	1	337.1	325.9	663.1
32	Dodecanethiol SAM on Pd foil (substrate)	1	334.9	325.9	660.8
33	Dodecanethiol SAM on Pd foil (thiolated layer)	1	336.9	329.7	666.7

34	Palladium Metal	2	335.1	327.8	662.9
35	Palladium Metal	2	334.6	328.5	663.1
36	$Palladium_{25}$ $Magnesium_{75}$	3	336.2	326.4	662.6
37	$Palladium_{20}$ $Aluminum_{80}$	3	337.4	325.5	662.9
38	$Palladium_{50}$ $Silver_{30}$	4	334.6	328.8	663.4
39	$Palladium_{20}$ $Silver_{80}$	4	334.9	329.8	664.7
40	$Palladium_{10}$ $Silver_{90}$	4	334.9	329.7	664.6
41	$Palladium_{50}$ $Platinum_{50}$	4	334.6	327.5	662.1
42	$Palladium_{60}$ $Gold_{40}$	4	334.5	327.5	662.0
43	Palladium (II) Sulfate	2	338.7	324.8	663.5
44	Palladium (II) Acetoacetonato	2	338.1	324.9	663.0
45	Palladium (II) Nitrate	2	338.2	324.7	662.9
46	Palladium (II) Bis(cyanide)	2	338.7	323.7	662.4
47	Sodium tetrachloropalladate	2	338.0	323.4	661.4
48	Potassium tetrachloropalladate	2	337.9	323.1	661.0
49	Tetraammine Palladium (II) Chloride	2	338.4	323.8	662.2
50	Bis(cyclooctane) Palladium (II) Chloride	2	338.5	323.8	662.3
51	Bis(triphenylphosphine) Palladium (II) Chloride		338.0	323.6	661.6
52	Palladium (II) Chloride	2	338.0	325.2	663.2
53	Palladium (II) Bromide	2	337.7	324.9	662.6

Table A.2: Sulfur XPS 2p and Auger KLL data

Entry	Sample	Ref	XPS BE	S 2p/KLL XAES KE	α'
1	SiO_2-SH No Pd	1	164.6	2111.7	2276.3
2	SiO_2-SH-Pd 1:1 Unused	1	163.4	2114.0	2277.3
3	SiO_2-SH-Pd 2:1 Unused	1	163.5	2112.6	2276.2
4	SiO_2-SH-Pd 3:1 Unused	1	163.5	2113.7	2277.2
5	SiO_2-SH-Pd 4:1 Unused	1	163.9	2112.0	2275.8
6	SiO_2-SH-Pd Used 1x	1	163.2	2113.8	2276.9
7	SiO_2-SH-Pd Used 2x	1	162.7	2114.6	2277.3
8	SiO_2-SH-Pd Used 3x	1	162.5	2114.2	2276.7
9	SiO_2-SH-Pd Used 4x	1	162.7	2113.0	2275.7
10	SBA-15-SH-Pd (g) Unused	1	163.5	2112.9	2276.3
11	SBA-15-SH-Pd (g) Used 1x	1	163.3	2113.0	2276.3
12	SBA-15-SH-Pd (g) Used 2x	1	162.9	2113.9	2276.8
13	SBA-15-SH-Pd (g) Used 3x	1	163.1	2114.0	2277.1
14	SBA-15-SH-Pd (cc) Unused	1	163.4	2112.8	2276.2
15	SBA-15-SH-Pd (cc) Used 1x	1	163.4	2112.4	2275.7
16	SBA-15-SH-Pd (cc) Used 3x	1	162.9	2113.8	2276.7

17	Al-SBA-15-SH-Pd Unused	1	163.8	2112.3	2276.1
18	Al-SBA-15-SH-Pd Used 2x	1	163.2	2114.1	2277.4
19	Al-SBA-15-SH-Pd Used 3x	1	163.1	2113.4	2276.5
20	Al-SBA-15-SH-Pd Used 4x	1	162.7	2114.4	2277.1
21	Palladium on Barium Sulfate	1	169.6	2107.5	2277.2
22	Palladium (II) Sulfide	1	162.7	2115.6	2278.3
23	Dodecanethiol on Au foil	1	163.2	2114.8	2278.0
24	Dodecanethiol on Pd foil	1	162.6	2116.6	2279.2
25	Sulfur (elemental)	5	162.0	2117.2	2279.2
26	Sodium Sulfide	5	159.5	2117.3	2276.7
27	Potassium Sulfide	5	160.2	2117.9	2278.0
28	Iron (II) Sulfide	5	159.7	2121.1	2280.8
29	Nickel Sulfide	5	159.9	2121.0	2280.9
30	Nickel Sulfide		162.8	2116.1	2278.9
31	Copper (1) Sulfide	5	160.4	2119.2	2279.6
32	Zinc Sulfide	5	160.2	2118.3	2278.4
33	Molybdenum Sulfide (MoS_2)	5	160.4	2119.5	2279.9
34	Cadmium Sulfide	5	159.9	2118.7	2278.6
35	Antimony Sulfide (Sb_2S_3)	5	160.0	2120.1	2280.1
36	Mercury Sulfide	5	160.2	2119.3	2279.5
37	Lead Sulfide	5	158.8	2121.0	2279.8
38	Iron Arsenosulfide (FeAsS)	5	160.5	2120.2	2280.7
39	Silver Sulfide	5	159.6	2120.2	2279.8
40	Tungsten Sulfide (WS_2)	5	162.8	2115.6	2278.4
41	Nickel Tungstosulfide ($NiWS_2$)	5	162.6	2115.9	2278.5
42	Lithium Sulfate	5	167.4	2109.9	2277.3
43	Sodium Sulfate	5	167.7	2109.7	2277.3
44	Potassium Sulfate	5	168.1	2109.3	2277.4
45	Ammonium Sulfate	5	166.9	2110.7	2277.6
46	Berylium Sulfate	5	167.5	2110.2	2277.6
47	Magnesium Sulfate	5	167.5	2110.4	2277.9
48	Calcium Sulfate	5	167.0	2110.8	2277.8
49	Strontium Sulfate	5	167.3	2110.4	2277.7
50	Barium Sulfate	5	167.1	2111.0	2278.1
51	Aluminum Sulfate	5	167.4	2110.2	2277.6
52	Potassium Aluminum Sulfate	5	167.3	2110.4	2277.7
53	Ammonium Aluminum Sulfate	5	167.3	2110.4	2277.7
54	Manganese Sulfate	5	167.0	2111.4	2278.4
55	Iron (II) Sulfate	5	166.9	2111.4	2278.3
56	Iron (III) Sulfate	5	167.1	2111.3	2278.4
57	Ammonium Iron (II) Sulfate	5	167.0	2110.9	2277.9
58	Cobalt Sulfate	5	166.9	2111.7	2278.6
59	Nickel Sulfate	5	167.0	2111.5	2278.4
60	Copper Sulfate	5	167.1	2111.6	2278.6

61	Zinc Sulfate	5	167.8	2110.0	2277.8
62	Tin Sulfate	5	167.9	2110.1	2278.0
63	Mercury Sulfate	5	167.4	2110.7	2278.1
64	Ammonium Disulfate	5	167.1	2110.4	2277.5
65	Potassium Disulfate	5	167.4	2110.0	2277.4
66	Potassium Disulfate	5	167.1	2110.3	2277.4
67	Sodium Bisulfite	5	165.8	2111.5	2277.3
68	Sodium Sulfite	5	165.5	2111.6	2277.1
69	Sodium Thiosulfate (Na_2S-**S**O_3)	5	166.5	2111.7	2278.2
70	Sodium Thiosulfate (Na_2**S**-SO_3)	5	160.6	2116.4	2276.9
71	Ammonium Isothiocyanate	5	160.3	2115.7	2276.0
72	Diethylcarbamodithiolate $(C_2H_5)_2NCS_2$	5	159.7	2117.1	2276.8
73	Methionine	5	161.1	2115.1	2276.2
74	Cysteine	5	161.5	2116.2	2277.7
75	Sulfacetone	5	161.2	2116.0	2277.2
76	Octanethiol on Au	6	162.6	N/A	N/A
77	Dodecanethiol on Ag	6	161.9	N/A	N/A

Table A.3: Silicon XPS 2p data

Entry	Sample	Ref	Si 2p XPS BE
1	SiO_2-SH No Pd	1	104.5
2	SiO_2-SH-Pd 1:1 Unused	1	103.7
3	SiO_2-SH-Pd 2:1 Unused	1	103.6
4	SiO_2-SH-Pd Used 1x	1	103.2
5	SiO_2-SH-Pd Used 2x	1	103.1
6	SiO_2-SH-Pd Used 3x	1	103.0
7	SiO_2-SH-Pd Used 4x	1	103.4
8	SBA-15-SH-Pd (g) Unused	1	103.7
9	SBA-15-SH-Pd (g) Used 1x	1	103.4
10	SBA-15-SH-Pd (g) Used 2x	1	103.2
11	SBA-15-SH-Pd (g) Used 3x	1	103.3
12	SBA-15-SH-Pd (cc) Unused	1	103.1
13	SBA-15-SH-Pd (cc) Used 1x	1	103.3
14	SBA-15-SH-Pd (cc) Used 3x	1	103.0
15	Al-SBA-15-SH-Pd Unused	1	103.7
16	Al-SBA-15-SH-Pd Used 2x	1	103.2
17	Al-SBA-15-SH-Pd Used 3x	1	103.3
18	Al-SBA-15-SH-Pd Used 4x	1	102.8

References

(1) Measured in our study
(2) Wagner, C.D.; Gale, L.H.; Raymond, R.H. *Analytical Chemistry* **1979**, *51*, 466.
(3) Davies, M.; Weightman, P. *Phys. Rev. B* **1984**, *30*, 4183.
(4) Weightman, P.; Andrews P.T. *J. Phys. Chem.* **1980**, *20*, 83.
(5) Yu, X.R.; Liu, F.; Way, Z.Y.; Chen, Y. *J. Electron Spectros. Rel. Phenom.* **1990**, *50*, 159.
(6) Bensebaa, F.; Zhou, Y.; Deslandes, Y.; Kraus, E.; Ellis, T.H. *Surf. Sci.* **1998**, *405*, L472.

Appendix B: X-Ray Crystallographic Data for 5,5'-diiodoBINAPO

A crystal of the compound (colorless, block-shaped, size 0.30 x 0.24 x 0.10 mm) was mounted on a glass fiber with grease and cooled to -93 °C in a stream of nitrogen gas controlled with Cryostream Controller 700. Data collection was performed on a Bruker SMART APEX II X-ray diffractometer with graphite-monochromated Mo K_a radiation (λ = 0.71073 Å), operating at 50 kV and 30 mA over 2q ranges of 4.50 ~ 52.00º. No significant decay was observed during the data collection.

Data were processed on a PC using the Bruker AXS Crystal Structure Analysis Package:[1] Data collection: APEX2 (Bruker, 2006); cell refinement: SAINT (Bruker, 2005); data reduction: SAINT (Bruker, 2005); structure solution: XPREP (Bruker, 2005) and SHELXTL (Bruker, 2000); structure refinement: SHELXTL; molecular graphics: SHELXTL; publication materials: SHELXTL. Neutral atom scattering factors were taken from Cromer and Waber.[2] The crystal is monoclinic space group *C*2/c, based on the systematic absences, *E* statistics and successful refinement of the structure. The structure was solved by direct methods. Full-matrix least-square refinements minimizing the function $\sum w (F_o^2 - F_c^2)^2$ were applied to the compound. All non-hydrogen atoms were refined anisotropically. The H atom of the disordered $CHCl_3$ was located from difference Fourier map and refined isotropically. All of the other H atoms were placed in geometrically calculated positions with C-H = 0.95Å, and refined as riding atoms, with Uiso(H) = 1.2 Ueq.

Convergence to final R_1 = 0.0221 and wR_2 = 0.0569 for 4064 (I>2σ(I)) independent reflections, and R_1 = 0.0261 and wR_2 = 0.0591 for all 4532 (R(int) = 0.0167) independent reflections, with 294 parameters, were achieved.[3] The largest residual peak and hole to be 0.524 and – 0.531 e/Å^3, respectively. Crystallographic data, atomic coordinates and equivalent

isotropic displacement parameters, bond lengths and angles, anisotropic displacement parameters, hydrogen coordinates and isotropic displacement parameters, torsion angles are given in Table 1 to 6. The molecular structure and the cell packing are shown in Figures 1 and 2.

---

[1] Bruker AXS Crystal Structure Analysis Package:

Bruker (2000). SHELXTL. Version 6.14. Bruker AXS Inc., Madison, Wisconsin, USA.

Bruker (2005). XPREP. Version 2005/2. Bruker AXS Inc., Madison, Wisconsin, USA.

Bruker (2005). SAINT. Version 7.23A. Bruker AXS Inc., Madison,Wisconsin, USA.

Bruker (2006). APEX2. Version 2.0-2. Bruker AXS Inc., Madison, Wisconsin, USA.

[2] Cromer, D. T.; Waber, J. T. *International Tables for X-ray Crystallography*; Kynoch Press: Birmingham, UK, 1974; Vol. 4, Table 2.2 A.

[3] $R_1 = \sum | |Fo| - |Fc| | / \sum |Fo|$

$wR_2 = \{\sum [w (Fo^2 - Fc^2)^2] / \sum [w(Fo^2)^2]\}^{1/2}$

($w = 1 / [\sigma^2(Fo^2) + (0.0313P)^2 + 5.40P]$, where $P = [\text{Max} (Fo^2, 0) + 2Fc^2] / 3$)

Figure B.1. Molecular Structure (Displacement ellipsoids for non-H atoms are shown at the 50% probability level and H atoms are represented by circles of arbitrary size.)

a)

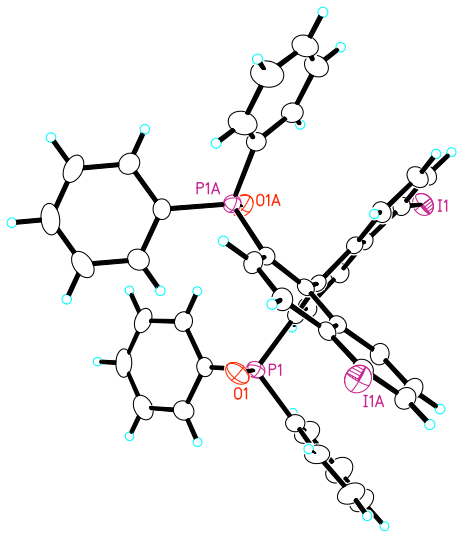

b)

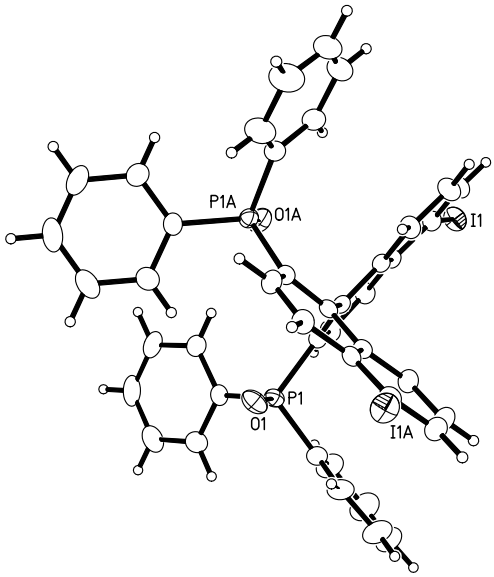

c)

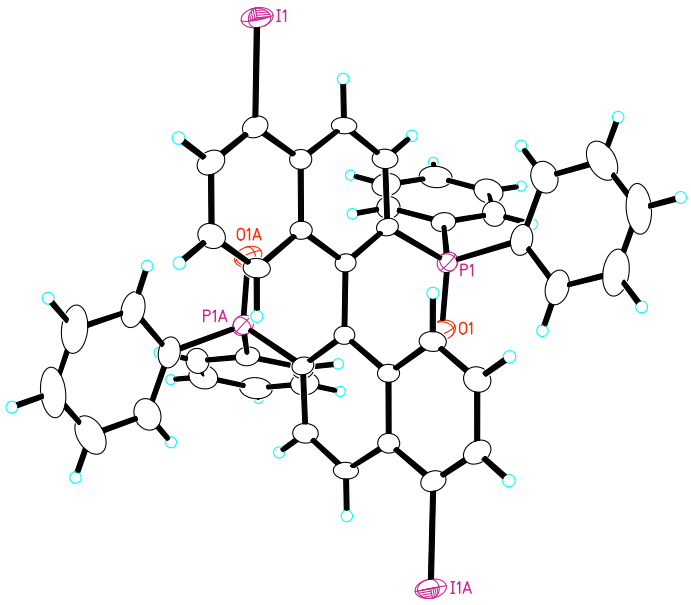

b)

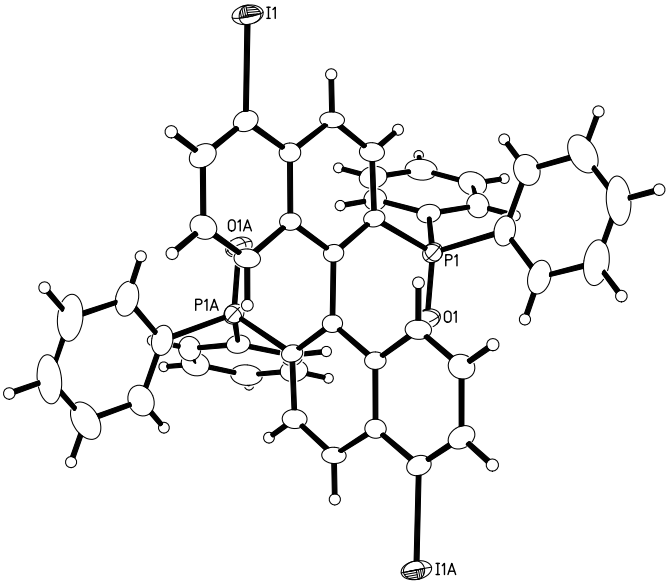

Figure B.2. Unit cell packing

a)

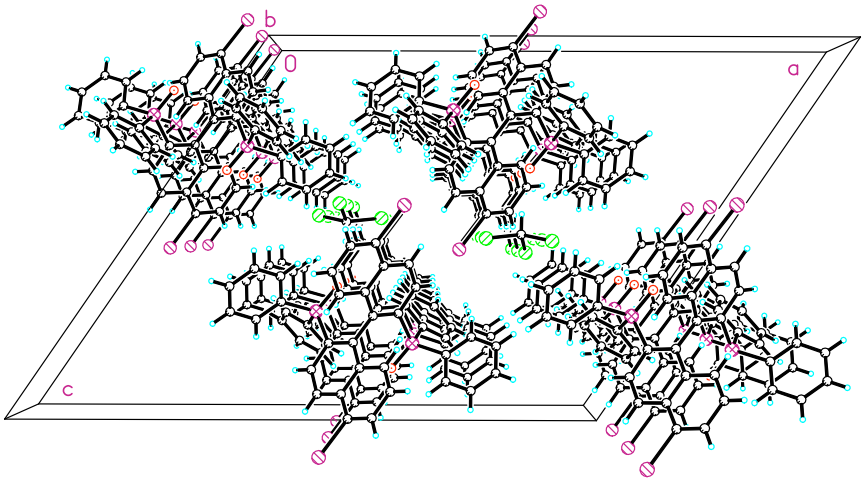

b)

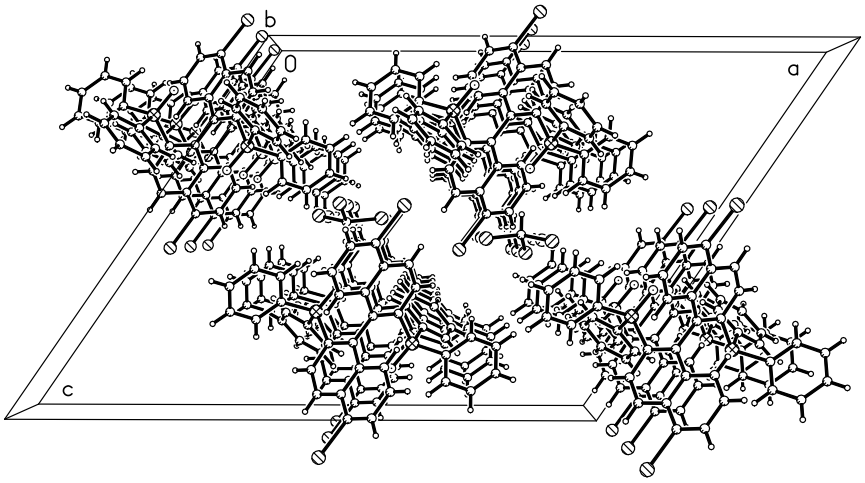

Table B.1. Crystal data and structure refinement for cc23

Identification code	cc23	
Empirical formula	C46 H32 Cl6 I2 O2 P2	
Formula weight	1145.16	
Temperature	180(2) K	
Wavelength	0.71073 Å	
Crystal system	Monoclinic	
Space group	C2/c	
Unit cell dimensions	a = 27.8693(3) Å	a= 90°.
	b = 9.17960(10) Å	b= 124.3460(10)°.
	c = 21.9637(3) Å	g = 90°.
Volume	4639.26(10) $Å^3$	
Z	4	
Density (calculated)	1.640 Mg/m^3	
Absorption coefficient	1.807 mm^{-1}	
F(000)	2248	
Crystal size	0.30 x 0.24 x 0.10 mm^3	
Theta range for data collection	2.25 to 26.00°.	
Index ranges	-34<=h<=34, -11<=k<=10, -27<=l<=20	
Reflections collected	11106	
Independent reflections	4532 [R(int) = 0.0167]	
Completeness to theta = 26.00°	99.6 %	
Absorption correction	Multi-scan	
Max. and min. transmission	0.8399 and 0.6177	
Refinement method	Full-matrix least-squares on F^2	
Data / restraints / parameters	4532 / 0 / 294	
Goodness-of-fit on F^2	1.027	
Final R indices [I>2sigma(I)]	R1 = 0.0221, wR2 = 0.0569	
R indices (all data)	R1 = 0.0261, wR2 = 0.0591	
Largest diff. peak and hole	0.524 and -0.531 e.$Å^{-3}$	

Table B.2. Atomic coordinates (x 10^4) and equivalent isotropic displacement parameters ($Å^2$x 10^3) for cc23. U(eq) is defined as one third of the trace of the orthogonalized U^{ij} tensor.

	x	y	z	U(eq)
I(1)	10689(1)	13218(1)	10549(1)	32(1)
P(1)	9038(1)	8984(1)	7101(1)	21(1)
O(1)	9099(1)	8860(2)	6474(1)	31(1)
C(1)	9603(1)	10054(2)	7873(1)	20(1)
C(2)	9988(1)	10919(2)	7832(1)	18(1)
C(3)	10371(1)	11888(2)	8428(1)	18(1)
C(4)	10747(1)	12841(2)	8381(1)	23(1)
C(5)	11099(1)	13791(2)	8939(1)	28(1)
C(6)	11089(1)	13841(2)	9571(1)	27(1)
C(7)	10730(1)	12927(2)	9630(1)	22(1)
C(8)	10361(1)	11915(2)	9069(1)	19(1)
C(9)	9980(1)	10951(2)	9105(1)	23(1)
C(10)	9614(1)	10070(2)	8530(1)	24(1)
C(11)	9037(1)	7239(2)	7476(1)	23(1)
C(12)	9562(1)	6587(2)	8007(1)	28(1)
C(13)	9568(1)	5183(3)	8240(1)	35(1)
C(14)	9056(1)	4422(3)	7946(1)	37(1)
C(15)	8534(1)	5051(3)	7412(1)	37(1)
C(16)	8522(1)	6459(3)	7174(1)	31(1)
C(17)	8376(1)	9907(2)	6847(1)	31(1)
C(18)	8163(1)	9917(3)	7288(2)	45(1)
C(19)	7678(1)	10740(4)	7082(2)	59(1)
C(20)	7406(1)	11561(3)	6442(2)	61(1)
C(21)	7609(1)	11543(3)	6006(2)	57(1)
C(22)	8092(1)	10716(3)	6201(1)	41(1)
C(23)	8520(1)	1622(3)	9846(2)	39(1)
Cl(1A)	9044(2)	2486(3)	9752(4)	71(1)
Cl(2A)	8227(5)	10(10)	9393(5)	96(2)
Cl(3A)	7979(2)	2773(6)	9690(3)	59(1)
Cl(1B)	8873(5)	2242(14)	9488(6)	105(3)
Cl(2B)	8211(9)	70(20)	9228(9)	81(3)

Cl(3B)	7948(4)	2954(11)	9554(7)	65(2)

Table B.3. Bond lengths [Å] and angles [°] for cc23.

I(1)-C(7)	2.101(2)
P(1)-O(1)	1.4831(15)
P(1)-C(11)	1.801(2)
P(1)-C(17)	1.809(2)
P(1)-C(1)	1.817(2)
C(1)-C(2)	1.378(3)
C(1)-C(10)	1.425(3)
C(2)-C(3)	1.438(3)
C(2)-C(2)#1	1.497(4)
C(3)-C(4)	1.414(3)
C(3)-C(8)	1.423(3)
C(4)-C(5)	1.367(3)
C(5)-C(6)	1.404(3)
C(6)-C(7)	1.367(3)
C(7)-C(8)	1.418(3)
C(8)-C(9)	1.418(3)
C(9)-C(10)	1.355(3)
C(11)-C(12)	1.390(3)
C(11)-C(16)	1.393(3)
C(12)-C(13)	1.384(3)
C(13)-C(14)	1.380(4)
C(14)-C(15)	1.379(4)
C(15)-C(16)	1.387(3)
C(17)-C(22)	1.387(3)
C(17)-C(18)	1.392(4)
C(18)-C(19)	1.383(4)
C(19)-C(20)	1.384(5)
C(20)-C(21)	1.361(5)
C(21)-C(22)	1.386(4)
C(23)-Cl(1B)	1.669(9)
C(23)-Cl(3A)	1.709(5)
C(23)-Cl(2A)	1.711(9)
C(23)-Cl(1A)	1.774(4)
C(23)-Cl(2B)	1.811(18)

C(23)-Cl(3B)	1.815(10)

O(1)-P(1)-C(11)	112.76(10)
O(1)-P(1)-C(17)	112.27(10)
C(11)-P(1)-C(17)	107.03(10)
O(1)-P(1)-C(1)	114.54(9)
C(11)-P(1)-C(1)	106.18(9)
C(17)-P(1)-C(1)	103.30(10)
C(2)-C(1)-C(10)	119.11(18)
C(2)-C(1)-P(1)	123.15(14)
C(10)-C(1)-P(1)	117.57(15)
C(1)-C(2)-C(3)	120.11(17)
C(1)-C(2)-C(2)#1	121.92(17)
C(3)-C(2)-C(2)#1	117.95(17)
C(4)-C(3)-C(8)	119.35(18)
C(4)-C(3)-C(2)	121.04(17)
C(8)-C(3)-C(2)	119.60(17)
C(5)-C(4)-C(3)	121.04(19)
C(4)-C(5)-C(6)	120.2(2)
C(7)-C(6)-C(5)	119.81(19)
C(6)-C(7)-C(8)	122.03(18)
C(6)-C(7)-I(1)	116.94(15)
C(8)-C(7)-I(1)	120.79(15)
C(7)-C(8)-C(9)	124.03(18)
C(7)-C(8)-C(3)	117.54(18)
C(9)-C(8)-C(3)	118.42(18)
C(10)-C(9)-C(8)	120.90(18)
C(9)-C(10)-C(1)	121.73(19)
C(12)-C(11)-C(16)	119.5(2)
C(12)-C(11)-P(1)	119.54(17)
C(16)-C(11)-P(1)	120.47(17)
C(13)-C(12)-C(11)	119.9(2)
C(14)-C(13)-C(12)	120.4(2)
C(15)-C(14)-C(13)	120.1(2)
C(14)-C(15)-C(16)	120.1(2)
C(15)-C(16)-C(11)	120.0(2)

C(22)-C(17)-C(18)	119.1(2)
C(22)-C(17)-P(1)	117.43(19)
C(18)-C(17)-P(1)	123.30(19)
C(19)-C(18)-C(17)	119.8(3)
C(18)-C(19)-C(20)	120.3(3)
C(21)-C(20)-C(19)	120.1(3)
C(20)-C(21)-C(22)	120.4(3)
C(21)-C(22)-C(17)	120.2(3)
Cl(1B)-C(23)-Cl(3A)	112.5(4)
Cl(1B)-C(23)-Cl(2A)	103.6(8)
Cl(3A)-C(23)-Cl(2A)	109.9(4)
Cl(1B)-C(23)-Cl(1A)	18.0(3)
Cl(3A)-C(23)-Cl(1A)	113.0(3)
Cl(2A)-C(23)-Cl(1A)	118.2(5)
Cl(1B)-C(23)-Cl(2B)	94.1(10)
Cl(3A)-C(23)-Cl(2B)	110.0(7)
Cl(2A)-C(23)-Cl(2B)	10.7(10)
Cl(1A)-C(23)-Cl(2B)	109.8(8)
Cl(1B)-C(23)-Cl(3B)	103.8(5)
Cl(3A)-C(23)-Cl(3B)	9.4(6)
Cl(2A)-C(23)-Cl(3B)	110.0(5)
Cl(1A)-C(23)-Cl(3B)	105.9(4)
Cl(2B)-C(23)-Cl(3B)	108.2(7)

Symmetry transformations used to generate equivalent atoms:

#1 -x+2,y,-z+3/2

Table B.4. Anisotropic displacement parameters ($Å^2 x\ 10^3$)for cc23. The anisotropic displacement factor exponent takes the form: $-2p^2[\ h^2a^{*2}U^{11} + ... + 2\ h\ k\ a^*\ b^*\ U^{12}\ ]$

	U^{11}	U^{22}	U^{33}	U^{23}	U^{13}	U^{12}
I(1)	41(1)	37(1)	22(1)	-7(1)	21(1)	-5(1)
P(1)	21(1)	23(1)	18(1)	0(1)	10(1)	-3(1)
O(1)	35(1)	36(1)	20(1)	-5(1)	15(1)	-11(1)
C(1)	21(1)	20(1)	18(1)	1(1)	11(1)	1(1)
C(2)	19(1)	19(1)	15(1)	3(1)	10(1)	4(1)
C(3)	20(1)	20(1)	16(1)	2(1)	11(1)	3(1)
C(4)	30(1)	24(1)	22(1)	0(1)	18(1)	-2(1)
C(5)	31(1)	29(1)	30(1)	-2(1)	21(1)	-8(1)
C(6)	29(1)	25(1)	22(1)	-5(1)	12(1)	-4(1)
C(7)	26(1)	24(1)	15(1)	0(1)	11(1)	3(1)
C(8)	21(1)	18(1)	17(1)	3(1)	11(1)	4(1)
C(9)	30(1)	27(1)	19(1)	2(1)	18(1)	0(1)
C(10)	29(1)	24(1)	24(1)	2(1)	18(1)	-4(1)
C(11)	28(1)	20(1)	22(1)	-1(1)	16(1)	-1(1)
C(12)	30(1)	28(1)	26(1)	-2(1)	16(1)	3(1)
C(13)	47(2)	28(1)	31(1)	5(1)	24(1)	14(1)
C(14)	65(2)	21(1)	41(1)	1(1)	40(1)	3(1)
C(15)	47(2)	29(1)	45(1)	-7(1)	32(1)	-13(1)
C(16)	29(1)	31(1)	33(1)	-1(1)	17(1)	-4(1)
C(17)	22(1)	25(1)	35(1)	1(1)	10(1)	-1(1)
C(18)	35(1)	50(2)	49(2)	5(1)	23(1)	9(1)
C(19)	43(2)	61(2)	78(2)	1(2)	38(2)	11(2)
C(20)	30(2)	40(2)	93(3)	7(2)	23(2)	7(1)
C(21)	31(2)	43(2)	70(2)	22(2)	12(2)	6(1)
C(22)	26(1)	37(1)	42(1)	11(1)	9(1)	-2(1)
C(23)	45(2)	36(1)	30(1)	2(1)	17(1)	2(1)
Cl(1A)	72(2)	68(2)	107(3)	-2(1)	70(2)	-4(1)
Cl(2A)	128(3)	35(1)	63(4)	-12(2)	17(3)	7(1)
Cl(3A)	44(1)	55(2)	78(2)	-8(1)	34(2)	4(1)
Cl(1B)	82(4)	179(7)	76(4)	-19(4)	58(3)	-43(4)
Cl(2B)	98(4)	51(5)	43(5)	-23(4)	9(3)	4(3)

Cl(3B)	28(2)	26(2)	88(5)	-1(2)	1(2)	-3(1)

Table B.5. Hydrogen coordinates (x 10^4) and isotropic displacement parameters ($Å^2$x 10^3) for cc23.

	x	y	z	U(eq)
H(4A)	10755	12820	7955	28
H(5A)	11350	14419	8899	34
H(6A)	11331	14509	9956	32
H(9A)	9981	10924	9538	27
H(10A)	9359	9447	8565	29
H(12A)	9916	7105	8209	34
H(13A)	9927	4741	8605	42
H(14A)	9062	3462	8113	45
H(15A)	8182	4521	7206	44
H(16A)	8162	6891	6805	37
H(18A)	8351	9361	7729	53
H(19A)	7531	10741	7380	71
H(20A)	7077	12138	6307	73
H(21A)	7419	12101	5564	69
H(22A)	8229	10703	5891	49
H(23)	8730(12)	1410(30)	10345(16)	40(7)

Table B.6. Torsion angles [°] for cc23.

O(1)-P(1)-C(1)-C(2)	12.3(2)
C(11)-P(1)-C(1)-C(2)	137.42(17)
C(17)-P(1)-C(1)-C(2)	-110.12(18)
O(1)-P(1)-C(1)-C(10)	-172.41(15)
C(11)-P(1)-C(1)-C(10)	-47.28(18)
C(17)-P(1)-C(1)-C(10)	65.18(18)
C(10)-C(1)-C(2)-C(3)	-3.7(3)
P(1)-C(1)-C(2)-C(3)	171.50(14)
C(10)-C(1)-C(2)-C(2)#1	177.98(18)
P(1)-C(1)-C(2)-C(2)#1	-6.8(3)
C(1)-C(2)-C(3)-C(4)	-176.58(19)
C(2)#1-C(2)-C(3)-C(4)	1.8(3)
C(1)-C(2)-C(3)-C(8)	1.9(3)
C(2)#1-C(2)-C(3)-C(8)	-179.77(17)
C(8)-C(3)-C(4)-C(5)	-0.4(3)
C(2)-C(3)-C(4)-C(5)	178.1(2)
C(3)-C(4)-C(5)-C(6)	-0.4(3)
C(4)-C(5)-C(6)-C(7)	0.6(3)
C(5)-C(6)-C(7)-C(8)	-0.1(3)
C(5)-C(6)-C(7)-I(1)	-174.43(17)
C(6)-C(7)-C(8)-C(9)	-179.6(2)
I(1)-C(7)-C(8)-C(9)	-5.5(3)
C(6)-C(7)-C(8)-C(3)	-0.6(3)
I(1)-C(7)-C(8)-C(3)	173.51(14)
C(4)-C(3)-C(8)-C(7)	0.8(3)
C(2)-C(3)-C(8)-C(7)	-177.65(17)
C(4)-C(3)-C(8)-C(9)	179.90(18)
C(2)-C(3)-C(8)-C(9)	1.4(3)
C(7)-C(8)-C(9)-C(10)	176.2(2)
C(3)-C(8)-C(9)-C(10)	-2.8(3)
C(8)-C(9)-C(10)-C(1)	1.0(3)
C(2)-C(1)-C(10)-C(9)	2.4(3)
P(1)-C(1)-C(10)-C(9)	-173.14(17)
O(1)-P(1)-C(11)-C(12)	85.57(18)

C(17)-P(1)-C(11)-C(12)	-150.49(17)
C(1)-P(1)-C(11)-C(12)	-40.64(19)
O(1)-P(1)-C(11)-C(16)	-86.30(19)
C(17)-P(1)-C(11)-C(16)	37.6(2)
C(1)-P(1)-C(11)-C(16)	147.48(17)
C(16)-C(11)-C(12)-C(13)	-1.2(3)
P(1)-C(11)-C(12)-C(13)	-173.15(17)
C(11)-C(12)-C(13)-C(14)	0.3(3)
C(12)-C(13)-C(14)-C(15)	0.6(3)
C(13)-C(14)-C(15)-C(16)	-0.8(4)
C(14)-C(15)-C(16)-C(11)	-0.1(4)
C(12)-C(11)-C(16)-C(15)	1.1(3)
P(1)-C(11)-C(16)-C(15)	172.95(18)
O(1)-P(1)-C(17)-C(22)	-16.9(2)
C(11)-P(1)-C(17)-C(22)	-141.18(19)
C(1)-P(1)-C(17)-C(22)	107.0(2)
O(1)-P(1)-C(17)-C(18)	167.3(2)
C(11)-P(1)-C(17)-C(18)	43.0(2)
C(1)-P(1)-C(17)-C(18)	-68.8(2)
C(22)-C(17)-C(18)-C(19)	-0.6(4)
P(1)-C(17)-C(18)-C(19)	175.1(2)
C(17)-C(18)-C(19)-C(20)	-0.5(5)
C(18)-C(19)-C(20)-C(21)	1.1(5)
C(19)-C(20)-C(21)-C(22)	-0.6(5)
C(20)-C(21)-C(22)-C(17)	-0.5(4)
C(18)-C(17)-C(22)-C(21)	1.1(4)
P(1)-C(17)-C(22)-C(21)	-174.8(2)

Symmetry transformations used to generate equivalent atoms:

#1 -x+2,y,-z+3/2